



ScuDo
Scuola di Dottorato ~ Doctoral School
WHAT YOU ARE, TAKES YOU FAR

Doctoral Dissertation
Doctoral Program in Structural Engineering (30th Cycle)

Numerical models for the robustness assessment of reinforced concrete framed buildings

By

Dario La Mazza

Supervisors:

Prof. Luca Giordano, Supervisor
Ph. D. Paolo Castaldo, Co-Supervisor

Doctoral Examination Committee:

Prof.ssa Beatrice Belletti, Referee, Università degli Studi di Parma
Prof. Gabriele Bertagnoli, Politecnico di Torino
Prof. Rosario Ceravolo, Politecnico di Torino
Prof. Matteo Colombo, Referee, Politecnico di Milano
Prof. Antonino Recupero, Università degli Studi di Messina

Politecnico di Torino
2018

Declaration

I hereby declare that, the contents and organization of this dissertation constitute my own original work and does not compromise in any way the rights of third parties, including those relating to the security of personal data.

Dario La Mazza

2018

* This dissertation is presented in partial fulfillment of the requirements for **Ph.D. degree** in the Graduate School of Politecnico di Torino (ScuDo).

*I would like to dedicate this thesis to my aunts Margherita and Maria,
who loved me more than a son*

Acknowledgements

The writing of this dissertation would not have been possible without the support and guidance of very special people, whom I wish to thank.

I would like to thank Prof. Giuseppe Lacidogna for its coordinating activities of the XXX cycle of the Ph.D. course in Structural Engineering.

I am deeply indebted to my supervisor, Prof. Luca Giordano, whose expertise, guidance and support have encouraged me to work on a very interesting topic. And to my co-supervisor Ph.D. Paolo Castaldo who helped me with his sage advices.

I am grateful to Prof. Mancini whose precious teachings have been a source of inspiration for me. He kindly integrated me in his working group, giving me the opportunity to grow and to improve myself within a stimulating environment.

I am thankful to Ph.D. Gabriele Bertagnoli and Dr. Diego Gino, for our joint projects and for the time we spent together on research activities, they have constantly supported my work with their ideas.

I would also like to thank all the research group members and my colleagues: Costanza, Fabio, Isabella, Marzia and Paola, it was a pleasure to work together, sharing ideas and taking inspiration from our discussions.

A special thanks to my soul mate and life companion Serena, who has always believed in me, encouraging me to do even better and supporting me every time I was in difficulties. And to my family for their love, support and comprehension over these years, they have always been there for me. All this would not have been possible without their help.

Abstract

Cast in situ reinforced concrete frame is one of the most common options for civil buildings. Although earliest common usages of this solution date back to second half of 19th century, research activity is constantly developing to investigate several aspects, especially about nonlinear behaviour of reinforced concrete structures.

Structural robustness of buildings is actually one of the key issues faced by the international scientific community. This expression is used to indicate a desirable property of a structure that allows it to withstand an accidental event, preventing progressive and/or disproportionate collapse.

Interest in this topic has been growing rapidly after the collapse of Ronan Point Apartment Tower in Newham, East London, in 1968, when a gas explosion destroyed a loadbearing concrete panel causing the collapse of an entire corner of the building and killing four peoples.

Although the issue of progressive collapse of multi-storey frames has been widely studied in the last decades, according to the literature review, the actual structural response following a localised failure has not yet been fully understood. Besides, many design guidelines for preventing progressive collapse denote a lack of adequate theoretical supports.

Several technics have been developed to evaluate the response after an accidental situation. In Europe, EN1991-1-7 has introduced the notional removal

design strategy. This approach establishes that a building should be checked to ensure that upon the notional removal of each column or each beam supporting a column, or any nominal section of load-bearing wall, one at a time in each storey of the building, the structure remains stable exhibiting only localised failure.

Currently one of the main solutions to ensure robustness consists in tying together structural members by using continuous reinforcement. In this context, the designer is required to evaluate the global structural response, then the role played by the floor-system becomes crucial. Unfortunately, to consider the contribution of the floor system in the post-failure behaviour involves longer times for modelling and analyses.

The study here presented is articulated through several points. The initial intent is to develop simplified models of the floor-system able to simulate its behaviour, to obtain accurate results through a more efficient modelling. Different numerical models will be presented. These will focus on distinct simplification levels, depending on the finite elements adopted. The codes used for nonlinear numerical analyses have been previously tested and validated on experimental tests on 2D and 3D specimens and both static and dynamic analyses.

The second aim is to evaluate the effectiveness of different floor-system typologies on the global behaviour of reinforced concrete frames. Two typical reinforced concrete solutions are tested: the first exploits a bidirectional slab, while the second adopts monodirectional joists and a collaborating slab.

To compare the results, a structure with features common to most of the reinforced concrete buildings has been chosen as reference test. The considered scenarios involve the removal of four distinct columns: two internal ones with different boundary conditions, an edge element and a corner one, all the columns are placed at the ground floor level.

The third aim is to evaluate the influence of several parameters on global response, to identify their possible influence on the phenomenon and to highlight which among these have a determining impact on the structural response. The factors investigated are: primary beams depth, columns depth, presence of bracing systems, continuous reinforcement amount and seismic detailing.

The achieved results provide precise information on the overall structural behaviour, highlighting the key role played by certain factors such as the percentage of continuous reinforcement in the beams and the importance of seismic detailing. At the same time the analyses have highlighted the marginal influence exerted by other parameters like the stiffening contribution given by a bracing system or stiffer columns, whose effects may be considered negligible.

Contents

1. Introduction.....	1
1.1 Background.....	1
1.2 Aims and Objectives.....	5
2. Literature Review	7
2.1 Introduction	7
2.2 Reinforced concrete framed structures	7
2.3 Structural robustness, progressive and disproportionate collapse	8
2.4 Current provisions for structural robustness.....	9
2.4.1 Eurocodes.....	9
2.4.1.1 Requirements for Class 2b framed structures	16
2.4.1.2 Notional element removal according EN 1991-1-7	20
2.4.2 American Society of Civil Engineering (ASCE 7-05).....	21
2.4.3 General Services Administration (GSA) Unified Facilities Criteria UFC 4-023-03	22
2.5 Experimental studies on progressive collapse of RC buildings	27
2.5.1 Progressive collapse of a 2D beam-column assembly under a column removal scenario	27
2.5.2 Progressive collapse of 3D beam-column and beam-column-slab substructures	34
2.5.3 Discussion of the results	40
2.6 Numerical studies on progressive collapse of RC buildings	42
2.6.1 Izzuddin, 2007	42

2.6.2 Qian, 2015.....	44
2.6.3 Petrone et al., 2016	50
3. Software validation	54
3.1 Introduction	54
3.2 TNO Diana v.10.1	55
3.3 SeismoStruct 2016.....	65
3.3.1 Nonlinear static analysis validation	66
3.3.2 Nonlinear dynamic analysis validation.....	72
4. Numerical Studies on Simplified Models.....	80
4.1 Introduction	80
4.2 Response of 2D beam-column assemblies under a column removal scenario.....	81
4.2.1 Influence of distributed loads applied on the beams.....	81
4.2.2 Structural response after sudden dynamic column removal	84
4.3 Floor system simplified numerical models.....	87
4.3.1 Simplified model EB1	88
4.3.2 Simplified model EB2	90
4.3.3 Simplified model EB3	92
4.3.4 Simplified model SPR	94
5. 3D Complete Models - Design and Finite Element Modelling	99
5.1 Introduction	99
5.2 3D building design	100
5.3 3D building design including seismic action.....	106
5.4 Description of nonlinear static time-history analyses.....	108
5.4.1 Collapse scenarios.....	109
5.4.2 Finite element modelling – Floor system: slab.....	113
5.4.3 Finite element modelling – Floor system: Joists with collaborating slab.....	118

5.4.4 The compatibility torsion issue.....	123
6. Analysis of the Results	125
6.1 Introduction	125
6.2 Collapse scenario 1 analysis	127
6.2.1 Collapse scenario 1 – Floor system: Slab	128
6.2.2 Collapse scenario 1 – Floor system: Joists with collaborating slab	132
6.3 Collapse scenario 2 analysis	138
6.3.1 Collapse scenario 2 – Floor system: slab.....	139
6.3.2 Collapse scenario 2 – Floor system: joist with collaborating slab	142
6.4 Collapse scenario 3 analysis	148
6.4.1 Collapse scenario 3 – Floor system: slab.....	149
6.4.2 Collapse scenario 3 – Floor systems: joists with collaborating slab	152
6.5 Collapse scenario 4 analysis	158
6.5.1 Collapse scenario 4 – Floor system: slab.....	159
6.5.2 Collapse scenario 4 – Floor system: joists with collaborating slab	163
7. Conclusions and Recommendations for Future Works	169
7.1 Introduction	169
7.2 Finite element software validation and calibration.....	170
7.3 Simplified numerical models to consider slab contribution	171
7.4 Simplified numerical models to consider slab contribution	172
7.5 Recommendations for future works	174
8. References.....	176
9. Appendix A.....	
10. Appendix B	
11. Appendix C	

List of Figures

Figure 1: Ronan Point collapse	2
Figure 2: Alfred P. Murrah Building collapse	4
Figure 3: World Trade Center collapse	4
Figure 4: Failure modes of Ronan Point collapse (PCA, 1975).....	9
Figure 5: Strategies for accidental design situations (Way, 2011).....	12
Figure 6: Categorization of consequences classes (Way, 2011)	14
Figure 7: Building classes and solution strategies (CEN, 2006).....	15
Figure 8: Ties for accidental actions (CEN, 2004).....	17
Figure 9: Recommended limit of admissible damage (Way, 2011).....	21
Figure 10: Tie forces in a framed structure (Dod, 2013)	23
Figure 11: Loads transfer mechanisms: (a) arching action, (b) plastic hinge formation, and (c) catenary action (Lew, 2011).....	26
Figure 12: Details of IMF specimen (Lew, 2011).....	30
Figure 13: Details of SMF specimen (Lew, 2011).....	30
Figure 14: View of SMF specimen (Lew, 2011)	31
Figure 15: Instrument layouts for INC-inclinometer, ENC-position transducer, LC-load cell, other sensors are LVDTs (Lew, 2011).....	31
Figure 16: Vertical load versus vertical deflections of IMF specimen at (a) $\frac{1}{4}$ span of beams, (b) mid-span of beams, (c) $\frac{3}{4}$ span of beams, and (d) centre column (Lew, 2011)	32
Figure 17: Vertical load versus vertical displacements of SMF specimen at (a) $\frac{1}{4}$ span of beams, (b) mid-span of beams, (c) $\frac{3}{4}$ span of beams, and (d) centre column (Lew, 2011)	33
Figure 18: Plan layout of the prototype building (Qian, 2015).....	34
Figure 19: Details of specimen S1 (Qian, 2015).....	35
Figure 20: Specimens ready for testing (Qian, 2015)	37
Figure 21: Comparison of the load–displacement relationship of test specimens: (a) specimen P1; (b) specimen P2; (c) specimen T1; (d) specimen T2; (e) specimen S1; (f) specimen S2 (Qian, 2015).....	39

Figure 22: Schematic of CCA/CMA mechanism (Qian, 2014)	41
Figure 23: Schematic of TCA/TMA mechanism (Qian, 2014).....	41
Figure 24: Multi-storey building subject to sudden column loss (Izzuddin, 2007)	43
Figure 25: Sub-structural levels for progressive collapse assessment (Izzuddin, 2007)	43
Figure 26: Comparison of the load–displacement relationship of test specimens: (a) specimen P1; (b) specimen P2; (c) specimen T1; (d) specimen T2; (e) specimen S1; (f) specimen S2 (Qian, 2015).....	45
Figure 27: Influence of boundary conditions applied on the beam ends: (a) load–displacement curve; (b) horizontal movement plotted against vertical displacement (Qian, 2015)	46
Figure 28: Influence of beam longitudinal reinforcement ratio on the response of test specimens: (a) specimen T2; (b) specimen S2 (Qian, 2015).....	47
Figure 29: Slab effects on RC buildings with varying beam longitudinal reinforcement ratio (Qian, 2015).....	47
Figure 30: Influence of beam depth on the response of RC frames: (a) specimen T2; (b) specimen S2 (Qian, 2015).....	48
Figure 31: Slab effects on buildings with varying beam depths (Qian, 2015)	48
Figure 32: Influence of slab reinforcement ratio on the response of bare frames and beam–slab frames (Qian, 2015).....	49
Figure 33: Slab effects on RC buildings with varying slab reinforcement ratio (Qian, 2015)	49
Figure 34: Influence of slab thickness on the response of bare frames and beam–slab frames (Qian, 2015)	49
Figure 35: Slab effects on RC buildings with varying slab thicknesses (Qian, 2015)	50
Figure 36: Plan view of the prototype frame (Petrone, 2016).....	51
Figure 37: Beam grids to replace floor slabs: (a) beams in both directions, (b) beams in short direction, (c) mixed configuration, and (d) Case (a) with added diagonals (Petrone, 2016).....	52

Figure 38: Diana finite elements and interpolant functions: a) CL9BE, b) CL18B, c) CQ40S	56
Figure 39: Shell-beam elements coupling	57
Figure 40: Structural portion of specimens S1 and S2 modelled in DIANA..	58
Figure 41: Concrete behaviour according to CEB-FIP Model Code 90 (Graph not in scale)	59
Figure 42: Restraint device and tension/compression load cell (Qian, 2015).	60
Figure 43: Constraint system adopted to simulate the actual boundary conditions	61
Figure 44: Views of the finite element models: a) Specimen P1, b) Specimen P2, c) Specimen T1, d) Specimen T2, e) Specimen S1, f) Specimen S2	62
Figure 45: Comparison between experimental and numerical results: a) Specimen P1, b) Specimen P2, c) Specimen T1, d) Specimen T2, d) Specimen S1, e) Specimen S2	63
Figure 46: Deformed shapes of the finite element models: a) Specimen P2, b) Specimen T1 and c) Specimen S1	64
Figure 47: Vertical layout of the specimen with cross section details and instrumentation arrangement	66
Figure 48: Layout of SeismoStruct finite element model with cross section discretization	67
Figure 49: Concrete constitutive law proposed by Mander	68
Figure 50: Concrete constitutive law proposed by Chang and Mander	68
Figure 51: Steel bilinear constitutive law	69
Figure 52: Comparison between numerical results and experimental data.....	70
Figure 53: Strain-displacement and stress-displacement curves for the beam reinforcements near the external column (a, b) and near the central column removed (c, d)	72
Figure 54: Specimen layout with cross section details (Pham, 2017).....	73
Figure 55: Test setup (Pham, 2017)	74
Figure 56: Loading system and quick release device (Pham, 2017).....	75

Figure 57: Finite element model adopted for nonlinear dynamic analyses validation.....	76
Figure 58: Comparison between experimental data and numerical results.....	78
Figure 59: Influence of the applied loads on the beams.....	83
Figure 60: Results obtained with nonlinear dynamic analyses	85
Figure 61: EB1 - Slab discretization and beam elements cross section.....	89
Figure 62: EB1 - Force-Displacement curves	90
Figure 63: EB2 - Slab discretization and beam elements cross section.....	91
Figure 64: EB2 - Force-Displacement curves	92
Figure 65: EB3 - Slab discretization and beam elements cross section.....	93
Figure 66: EB3 - Force-Displacement curves	94
Figure 67: Discretization adopted to evaluate the stiffness of the springs	96
Figure 68: Numerical model SPR	96
Figure 69: SPR - Slab discretization and beam elements cross section.....	97
Figure 70: SPR - Force-Displacement curves	98
Figure 71: Plan layout of the building.....	100
Figure 72: Longitudinal elevation of the building	101
Figure 73: Transverse elevation of the building.....	101
Figure 74: 3D finite element model developed with SAP2000	103
Figure 75: Cross section of the primary external beams.....	104
Figure 76: Cross section of the primary internal beams.....	104
Figure 77: Cross section of the secondary external beams	104
Figure 78: Cross section of the secondary internal beams	104
Figure 79: Cross section of the columns	105
Figure 80: Cross section of the slab	105
Figure 81: Cross section of the primary external beams.....	105
Figure 82: Cross section of the primary internal beams.....	105
Figure 83: Cross section of the secondary beams	106

Figure 84: Cross section of the columns	106
Figure 85: Cross section of the floor system.....	106
Figure 86: Elastic response spectrum and design spectrum.....	107
Figure 87: Layout of the collapse scenarios.....	109
Figure 88: Cross-section of a primary spandrel beam.....	115
Figure 89: Cross-section of a primary internal beam.....	116
Figure 90: Cross-section of a secondary spandrel beam	116
Figure 91: Cross-section of a secondary internal beam	116
Figure 92: Cross-section of the slab.....	116
Figure 93: Cross-section of a column	117
Figure 94: Plan layout of the equivalent girder.....	117
Figure 95: SeismoStruct slab model extrapolated from the 3D building.....	118
Figure 96: Cross-section of a primary spandrel beam.....	120
Figure 97: Cross-section of a primary internal beam.....	121
Figure 98: Cross-section of a secondary spandrel beam	121
Figure 99: Cross-section of the macro joist	121
Figure 100: Cross-section of a column	122
Figure 101: Plan layout of the equivalent girder.....	122
Figure 102: SeismoStruct floor system model adopted for 3D buildings.....	123
Figure 103: Example of compatibility torsion (Pillai, 2007)	124
Figure 104: Bracing systems position	126
Figure 105: Collapse scenario 1	127
Figure 106: Collapse scenario 1 - Reference test.....	128
Figure 107: Collapse scenario 1 - Influence of primary beams depth	130
Figure 108: Collapse scenario 1 – Influence of columns depth	130
Figure 109: Collapse scenario 1 - Influence of bracings.....	131
Figure 110: Collapse scenario 1 - Reference test.....	133
Figure 111: Collapse scenario 1 – Influence of primary beams depth.....	134

Figure 112: Collapse scenario 1 – Influence of columns depth	134
Figure 113: Collapse scenario 1 – Influence of bracing system	135
Figure 114: Collapse scenario 1 - Influence of minimum tying	136
Figure 115: Collapse scenario 1 - Influence of continuous reinforcement ...	137
Figure 116: Collapse scenario 1 - Influence of seismic detailing	137
Figure 117: Collapse scenario 2	138
Figure 118: Collapse scenario 2 - Reference test	139
Figure 119: Collapse scenario 2 - Influence of primary beams depth	140
Figure 120: Collapse scenario 2 – Influence of columns depth	141
Figure 121: Collapse scenario 2 – Influence of bracing system	142
Figure 122: Collapse scenario 2 – Reference test	143
Figure 123: Collapse scenario 2 – Influence of primary beams depth.....	144
Figure 124: Collapse scenario 2 - Influence of beams depth	144
Figure 125: Collapse scenario 2 - Influence of bracings system.....	145
Figure 126: Collapse scenario 2 - Influence of minimum tying	146
Figure 127: Collapse scenario 2 - Influence of continuous reinforcement ...	147
Figure 128: Collapse scenario 2 - Influence of seismic detailing	147
Figure 129: Collapse scenario 3	148
Figure 130: Collapse scenario 3 - Reference test.....	149
Figure 131: Collapse scenario 3 - Influence of primary beams depth	150
Figure 132: Collapse scenario 3 - Influence of columns depth.....	151
Figure 133: Collapse scenario 3 - Influence of bracing systems.....	151
Figure 134: Collapse scenario 3 - Reference test.....	153
Figure 135: Collapse scenario 3 - Influence of primary beam depths	154
Figure 136: Collapse scenario 3 - Influence of columns depth.....	154
Figure 137: Collapse scenario 3 - Influence of bracing systems.....	155
Figure 138: Collapse scenario 3 - Influence of minimum tying	156
Figure 139: Collapse scenario 3 - Influence of continuous reinforcement ...	157

Figure 140: Collapse scenario 3 - Influence of seismic detailing.....	157
Figure 141: Collapse scenario 4.....	159
Figure 142: Collapse scenario 4 - Reference test.....	159
Figure 143: Collapse scenario 4 - Influence of primary beams depth	161
Figure 144: Collapse scenario 4 - Influence of columns depth.....	161
Figure 145: Collapse scenario 4 - Influence of bracing systems.....	162
Figure 146: Collapse scenario 4 - Reference test.....	163
Figure 147: Collapse scenario 4 - Influence of primary beams depth	164
Figure 148: Collapse scenario 4 - Influence of columns depth.....	164
Figure 149: Collapse scenario 4 - Influence of bracing systems.....	165
Figure 150: Collapse scenario 4 - Influence of minimum tying	166
Figure 151: Collapse scenario 4 - Influence of continuous reinforcement ...	167
Figure 152: Collapse scenario 4 - Influences of seismic detailing.....	167

List of Tables

Table 1: Average compressive and tensile strengths of concrete.....	28
Table 2: Average mechanical properties of reinforcing bars	28
Table 3: Specimen properties.....	35
Table 4: Specimen properties.....	36
Table 5: Properties of reinforcing steel	36
Table 6: Test results	39
Table 7: Test comparison	40
Table 8: Stiffness adopted for nonlinear springs.....	61
Table 9: Configuration of the tests.....	69

Table 10: Specimens parameters and material properties	73
Table 11: Distributed load applied for each test in addition to the self-weight	81
Table 12: Distributed loads applied for each numerical simulation	85
Table 13: Nonlinear dynamic analyses results	87
Table 14: Material parameters	101
Table 15: Spectra parameters	107
Table 16: Modal periods, frequencies and participation factors	107
Table 17: Collapse scenario 1 (Slab) – Summary of the results	132
Table 18: Collapse scenario 1 (Joists + Collaborating Slab) – Summary of the results	138
Table 19: Collapse scenario 2 (Slab) – Summary of the results	142
Table 20: Collapse scenario 2 (Joists + Collaborating slab) – Summary of the results	148
Table 21: Collapse scenario 3 (Slab) – Summary of the results	152
Table 22: Collapse scenario 3 (Joists + Collaborating slab) – Summary of the results	158
Table 23: Collapse scenario 4 (Slab) – Summary of the results	162
Table 20: Collapse scenario 4 (Joists + Collaborating slab) – Summary of the results	168

Chapter 1

Introduction

1.1 Background

Cast in situ reinforced concrete frame is one of the most common options for civil buildings with spans between 4m and 12m. Since the first patents and initial applications, this material has undergone a deep evolution becoming one of the most widely used in the world for the construction of a wide range of structures. By combining the excellent tensile behaviour of steel bars and the compressive one of concrete, a high-performance material is obtained, the use of which represents in many cases the most cost-effective solution. The vertical elements (column) and the horizontal ones (beams) transfer both the horizontal and vertical loads to the foundations. In these structures, generally also the floor system is built by using cast in situ reinforced concrete elements, exploiting unidirectional solutions (e.g. joists with collaborating slab), or a bidirectional one (e.g. bidirectional slab).

In the early development of reinforced concrete frames, only the gravity and wind loads were considered while the abnormal loads such as those caused by an explosion or impact were rarely included in the design. Therefore, most of the structures do not have any specific provisions to withstand accidental actions.

In civil engineering, the expression structural robustness is used to indicate a desirable property of a structure that allows it to resist against an accidental event, preventing a progressive and/or disproportionate collapse. Although these terms are sometimes improperly used as synonyms, the former can be defined as one that

affects more structural elements connected, which collapse one after the other as happens, as an example, with the dominoes. The concept of disproportionate collapse instead, is closely related to the event that caused it: because of an exceptional event the structure can be damaged, but damage must be proportional to the cause that produced it. Furthermore, if progressive collapse occurs it does not necessarily result in disproportionate collapse.

According to EN 1991-1-7 - Actions on structures. General actions. Accidental actions: “Robustness is the ability of a structure to withstand events like fire, explosions, impact or the consequences of human error, without being damaged to an extent disproportionate to the original cause” (CEN, 2006). Accidental design situations are defined in BS EN 1990 - Basis of structural design. This document defines accidental actions like: “Design situations involving exceptional conditions of the structure or its exposure, including fire, explosion, impact or local failure” (CEN, 2002).

Structural robustness of buildings is actually one of the major issues faced by the international scientific community. Interest in this topic has been growing rapidly since the 1970s, following the collapse of the Ronan Point Apartment Tower in Newham, East London, in 1968 (see Figure 1) (Saunders, 1968; Longinow, 1998).

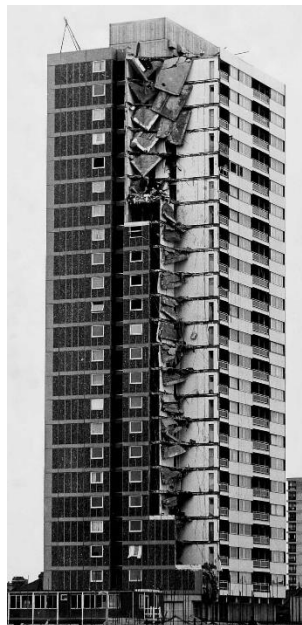


Figure 1: Ronan Point collapse

A gas explosion on the 18th floor of the 22-story Ronan Point apartment tower destroyed part of the reinforced concrete loadbearing wall at a corner of the building. The failure caused the collapse of the block placed above the eighteenth floor. The weight of this part of the building as it fell caused the collapse of the remaining portion of the south-east corner placed below, killing four people and injuring 17. The inquiries established that the pressure caused by the explosion was in the normal range for a gas explosion (Saunders, 1968; Pearson, 2005); the initial structural damage was mainly due to its design and it was not the result of any deficiencies in the workmanship or in the erection on site (Merola, 2009). Furthermore, the inquiries highlighted a lack of provisions for general structural integrity in existing building codes.

After this event, the British Standards started to incorporate provisions to deal with the problem of progressive collapse (Starossek, 2007; Ned, 2008). The U.K. building regulation established that, to avoid disproportionate collapse, all buildings must be designed by tying together structural elements, adding redundant members, and providing sufficient strength to obtain ductile elements capable of redistributing loads (Ellingwood, 2007). The Fifth Amendment of British Standard has introduced two important concepts for the first time: “Key Element Design” and “Alternate Load Path”. These two concepts have been employed by the current British Standards and many other International Codes (Merola, 2009).

A study conducted by Longinow and Ellingwood (Longinow, 1998) found that in the decade after the Ronan Point collapse, over 300 engineering articles and reports were published on this issue. In the following years this event led to changes in the structural standards and codes adopted in several countries like United Kingdom and Europe in general, the United States, and Canada. The adoption of new design criteria, together with the absence of significant disproportionate collapses led to a gradual reduction of the research about this issue. However, in the last decades, especially following the collapses of the Murrah Building in Oklahoma City in 1995 (see Figure 2) and of the World Trade Centre in New York in 2001 (see Figure 3), the research activities have seen a renewal (Canisius, 2011).



Figure 2: Alfred P. Murrah Building collapse



Figure 3: World Trade Center collapse

After these events U.S. government agencies (GSA, 2003; DoD, 2005; Dod, 2013), have published a series of document containing the design requirements for preventing progressive collapse, focusing mainly on two approaches, an indirect one defined as Tie Force method (TF) and direct one defined as Alternate Load Path method (ALP) (British Standard, 1997; DoD, 2005; Dod, 2013; CEN, 2006).

The efforts made by international scientific community have allowed not only to improve the current knowledge about accidental conditions including severe malicious attacks, abnormal loads and human errors, but also to develop specific strategies to study the response of a building after an accidental event, to evaluate the structural robustness and to design robust structures. Nevertheless, at present there is neither a uniform theory of robustness and progressive collapse, nor agreement on terminology.

Although the issue of progressive collapse of multi-storey frames has been widely studied in the last decades, according to the literature review, the research about the influence of the floor system on the global structural response is rather limited (Bao, 2017). In addition, many design guidelines for preventing progressive collapse denote a lack of adequate theoretical supports.

1.2 Aims and Objectives

The provision of horizontal and vertical tyings is one of the most used solutions to ensure the structural robustness of a building. The Annex A of EN 1991-1-7 introduces an alternative to this procedure. This solution, defined as “Notional removal design strategy”, establishes that the building should be checked to ensure that, upon the notional removal of each supporting column and each beam supporting a column, or any nominal section of load-bearing wall, one at a time in each storey of the building, the structure remains stable and that any local damage does not exceed a certain limit (CEN, 2006).

Following this strategy more specific damage scenarios are considered, whereby the designer is required to assess the area of the damage, i.e. the building’s ability to localise damage. However, the notional removal design strategy is still somewhat prescriptive because the chosen damage scenarios involve the removal of only one supporting member (beam, column or wall) at a time.

In this context, the designer is required to evaluate the global response of the structure, then the role played by the floor-system becomes crucial, as demonstrated

by Bao (Bao, 2017), therefore this contribution cannot be neglected. However, the floor-system modelling involves significant computational burdens, this means longer times for modelling and analyses.

Then the initial aim of this work is to find simplified models for the floor-system able to simulate its behaviour to obtain accurate results through a more efficient modelling. Distinct numerical models will be presented. These will focus on various simplification levels, depending on the finite elements adopted. The codes adopted for the nonlinear numerical analyses have been previously tested and validated on experimental tests available in the literature.

Once reliable simplified models have been identified, the second aim is to evaluate the effectiveness of different floor-system typologies on reinforced concrete frames. To make possible a comparison, a structural solution, having standard features for a cast in situ reinforced concrete frame, has been identified as reference.

The objectives of present study can be summarised as follow:

- To assess the reliability of commercial nonlinear finite element codes in the evaluation of the structural response after an element removal;
- To identify effective solutions to simplify the floor-system modelling;
- To evaluate the influence of the floor-system in the response of reinforced concrete frame structures;
- To find and highlight possible leading factors in the global structural response.

Although this approach is suggested by one of the main codes at European level, and this design method proved to work effectively, the actual response of the structure after the localised failures has not yet been fully understood.

Chapter 2

Literature Review

2.1 Introduction

In this chapter is presented a review about progressive and disproportionate collapse, structural robustness, experimental and numerical analyses of the progressive collapse resistance of reinforced concrete structures. Paragraph 2.2 contains a brief description of RC frame structures. Section 2.3 reports the definition of progressive collapse and the factors that affect structural robustness. Paragraph 2.4 reports current provisions for structural robustness, focusing on European and American standards. Through experimental and FE studies conducted in the last decade, the efficiency of the current tie force method is discussed in section 2.5. While the most recent experimental and FE studies on progressive collapse in RC structures with extensive discussion are presented in sections 2.6 and 2.7, respectively. A review of analytical approach to define progressive collapse resistance of RC structure is discussed in section 2.8. Finally, section 2.9 reports a summary of the literature review.

2.2 Reinforced concrete framed structures

Concrete frame structures represent one of the most common structural typologies in the world. This type of building consists of a frame in which the horizontal members are called beams, and vertical members are called columns. The floor system is generally represented by a bidirectional solution realised with a concrete slab, or a monodirectional system formed by RC joists and a collaborating slab. The loads acting on the slab are transferred to the beams and then to the columns that transmit the actions to the foundations. Column are the primary load-bearing element of the building: the failure of a beam or slab in fact usually affects only one floor, while if a column collapses the damage can generally interest a larger portion of the structure.

Normally, the frames are designed to withstand both vertical and horizontal loads, but in some cases the skeleton made by beams and columns is stiffened against horizontal actions by means of shear walls and/or concrete cores (e.g. elevator shaft, stairwell).

2.3 Structural robustness, progressive and disproportionate collapse

In structural engineering, the term robustness has a precise definition, according to EN 1991-1-7 - Actions on structures. General actions. Accidental actions “*Robustness is the ability of a structure to withstand events like fire, explosions, impact or the consequences of human error, without being damaged to an extent disproportionate to the original cause*”. Accidental design situations are defined in BS EN 1990 – Basis of structural design: “*Accidental design situations are design situations involving exceptional conditions of the structure or its exposure, including fire, explosion, impact or local failure*”. A structure is then defined as robust if it does not show a collapse, neither progressive nor disproportionate, as a result of an accidental action.

Disproportionate and progressive collapse are often used as interchangeably definitions but in general a progressive collapse identifies the spread from the initial failure of one or a few localised structural elements to a larger structural portion, while a disproportionate collapse indicates that the consequence of an event is far greater than expected. (Way, 2011; Meacham, 2006). If progressive collapse occurs it does not necessarily result in a disproportionate one, although often this is true. As an example, the Ronan Point collapse is a case in which a progressive collapse did result in a disproportionate one, see Figure 4.

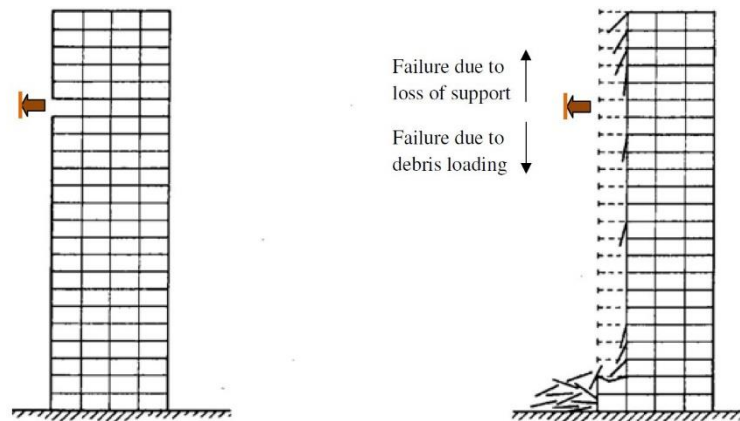


Figure 4: Failure modes of Ronan Point collapse (PCA, 1975)

Other definitions for progressive collapse are given in the standard defined by the American Society of Civil Engineering (ASCE): “*the spread of an initial local failure from element to element resulting, eventually, in collapse of an entire structure or disproportionately large part of it*” (ASCE 7-05, 2006). This definition is also used by the American Department of Defence (DoD, 2005), while the General Services Administration (GSA, 2003) defines progressive collapse as “*a situation where local failure of a primary structural component leads to the collapse of adjoining members which, in turn, leads to additional collapse, hence the total damage is disproportionate to the original cause*”.

2.4 Current provisions for structural robustness

Since the Ronan Point collapse, standards and codes have attempted to deal with the issue of structural robustness. Generally, the followed approach was an indirect one based on prescriptive provisions. The main aim of the codes was to enhance the overall integrity by means of the prescription of tyings between the structural elements. In the following sections are discussed the regulations adopted by main structural codes to prevent progressive collapse.

2.4.1 Eurocodes

These documents represent the reference for structural design for the European Union members, each country in addition can adopt supplementary documents defined as National Annex.

EN 1990 – Basis of structural design can be considered as the core document, as it defines the principles and the requirements for safety, serviceability and durability of structures.

About structural robustness, EN 1990 states that: “*A structure shall be designed and executed in such a way it will not be damaged by events such as: explosion, impact, and the consequences of human errors, to an extent disproportionate to the original cause*”.

Potential damage shall be avoided or limited by an appropriate choice of one or more of the following:

- Avoiding, eliminating or reducing the hazards to which the structure can be subjected;
- Selecting a structural form which has low sensitivity to the hazards considered;
- Selecting a structural form and design that can withstand adequately the accidental removal of an individual member or a limited part of the structure;
- Avoiding as far as possible structural systems that can collapse without warning;
- Tying the structural members together.

Eurocodes introduce the concept of accidental design situation (e.g. fire, explosion, impact, etc...) defining a specific load combination. The accidental combination of actions is used by the designer to verify the robustness of a structure, particularly with the notional removal and key element methods. This equation, given in paragraph 6.4.3.3 of EN 1990, is reported in the following:

$$\sum_{j \geq 1} G_{k,j} + A_d + \Psi_{1,1} Q_{k,1} + \sum_{i \geq 1} \Psi_{2,i} Q_{k,i} \quad (1)$$

Where:

“+” implies “to be combined with”, Σ implies “the combined effect of”, $G_{k,j}$ are the characteristic values of the permanent actions, A_d is the design value of the accidental action, $Q_{k,1}$ is the characteristic value of the leading variable action, $Q_{k,i}$ are the characteristic values of the other variable actions, $\Psi_{1,1}$ is the factor for the frequent value of the leading variable action $Q_{k,1}$, $\Psi_{2,i}$ are the factors for the quasi-permanent value of the i-th variable action $Q_{k,i}$.

EN 1991-1-7 - Actions on structures. General actions. Accidental actions provides strategies and rules to withstand accidental actions.

Eurocodes accept the localised failure due to accidental actions provided this does not compromise the stability of the whole structure, the overall load-bearing and the resistance of the structure is maintained. The minimum period that most buildings need to survive following an accident should be that period needed to facilitate the safe evacuation and rescue of personnel from the building and its surroundings (i.e. the emergency measures). Longer periods of survival might be required for buildings used for handling hazardous materials, provision of essential services, or for national security reasons.

It should be noted that EN 1991-1-7 does not specifically deal with accidental actions caused by external explosions and terrorist activities, or the residual stability of buildings or other civil engineering works damaged by seismic action or fire.

About design strategies, EN 1991-1-7 identify two generic types:

- Strategies based on identified accidental actions;
- Strategies based on unidentified accidental actions.

These solutions are illustrated in Figure 3.1 of BS EN 1991-1-7, reproduced here in Figure 5.

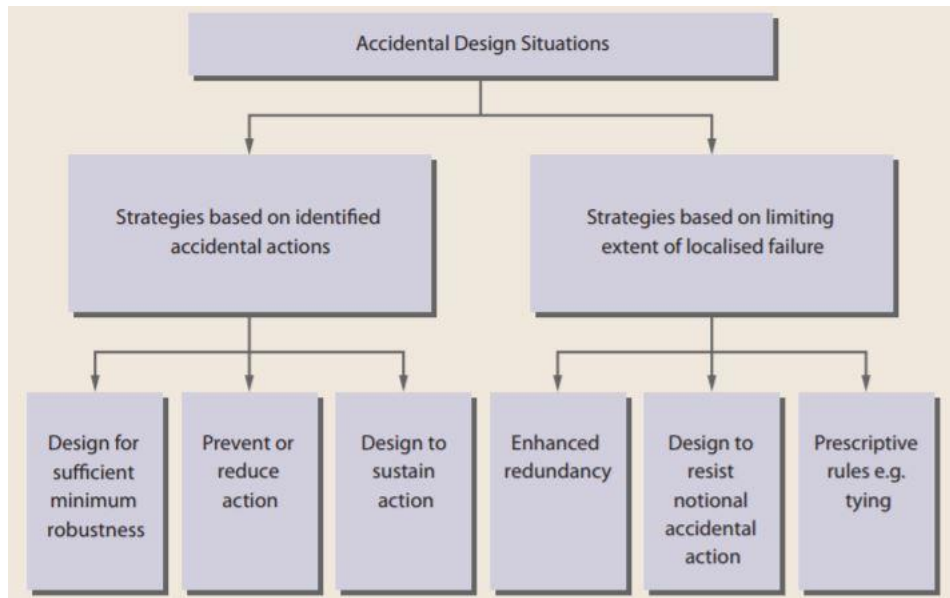


Figure 5: Strategies for accidental design situations (Way, 2011)

If the accidental actions are not specified, the strategies defined are based on the limitation of the extent of localised failure. This kind of solution might provide adequate robustness against the accidental actions not specifically covered by EN 1991-1-7 defined before. According to this document the mitigation should be reached by adopting one or more of the following approaches:

- Designing key elements, on which the stability of the structure depends, to sustain the effects of a model of accidental action A_d ;
- Designing the structure so that in the event of a localised failure (e.g. failure of a single member) the stability of the whole structure or of a significant part of it would not be endangered;
- Applying prescriptive design/detailing rules that provide acceptable robustness for the structure (e.g. three-dimensional tying for additional integrity, or a minimum level of ductility of structural members subject to impact).

If the accidental actions are specified, EN 1991-1-7 establishes that measures should be taken to mitigate the risk of accidental actions. These solutions can include one or more of the following strategies:

- By preventing the occurrence of the action;
- By protecting the structure against the effects of the accidental action;

- By ensuring that the structure has sufficient robustness, by adopting one or more of the following approaches:
 - By designing certain components of the structure upon which stability depends as key elements;
 - By designing structural members, and selecting materials, to have sufficient ductility, capable of absorbing significant strain energy without rupture;
 - By incorporating sufficient redundancy in the structure to facilitate the transfer of actions to alternative load paths following an accidental event;

EN 1991-1-7 defines the strategies for accidental design situations based on the consequences associated to a hypothetical failure of the building. Four different consequence classes (CC) are defined i.e. CC1, CC2a, CC2b and CC3. The requirements are progressively more stringent from CC1 to CC3.

The building classification is a simplification of a complex risk-based building classification system which consider:

- The number of people at risk;
- The location of the structure and its height;
- The perception in society of damage to the structure;
- The type of load and likelihood that the load will occur at the same time as a large number of people being present within or near the structure;
- The structural type and nature of the material.

Figure 6 illustrates the scheme adopted in EN 1997-1-7 to classify the buildings.

CONSEQUENCES CLASS	BUILDING TYPE AND OCCUPANCY
1 Low consequences of failure	Single occupancy houses not exceeding 4 storeys. Agricultural buildings. Buildings into which people rarely go, provided no part of the building is closer to another building, or area where people do go, than a distance of 1.5 times the building height.
2a (Lower risk group) Medium consequences of failure	5 storey single occupancy houses. Hotels not exceeding 4 storeys. Flats, apartments and other residential buildings not exceeding 4 storeys. Offices not exceeding 4 storeys. Industrial buildings not exceeding 3 storeys. Retailing premises not exceeding 3 storeys of less than 1000 m ² floor area in each storey. Single storey educational buildings. All buildings not exceeding two storeys to which the public are admitted and which contain floor areas not exceeding 2000 m ² at each storey.
2b (Upper risk group) Medium consequences of failure	Hotels, flats, apartments and other residential buildings greater than 4 storeys but not exceeding 15 storeys. Educational buildings greater than single storey but not exceeding 15 storeys. Retailing premises greater than 3 storeys but not exceeding 15 storeys. Hospitals not exceeding 3 storeys. Offices greater than 4 storeys but not exceeding 15 storeys. All buildings to which the public are admitted and which contain floor areas exceeding 2000 m ² but not exceeding 5000 m ² at each storey. Car parking not exceeding 6 storeys.
3 High consequences of failure	All buildings defined above as Class 2 Lower and Upper Consequences Class that exceed the limits on area and number of storeys. All buildings to which members of the public are admitted in significant numbers. Stadia accommodating more than 5000 spectators. Buildings containing hazardous substances and /or processes.

Figure 6: Categorization of consequences classes (Way, 2011)

Figure 7 summarizes the solution strategies for each class.

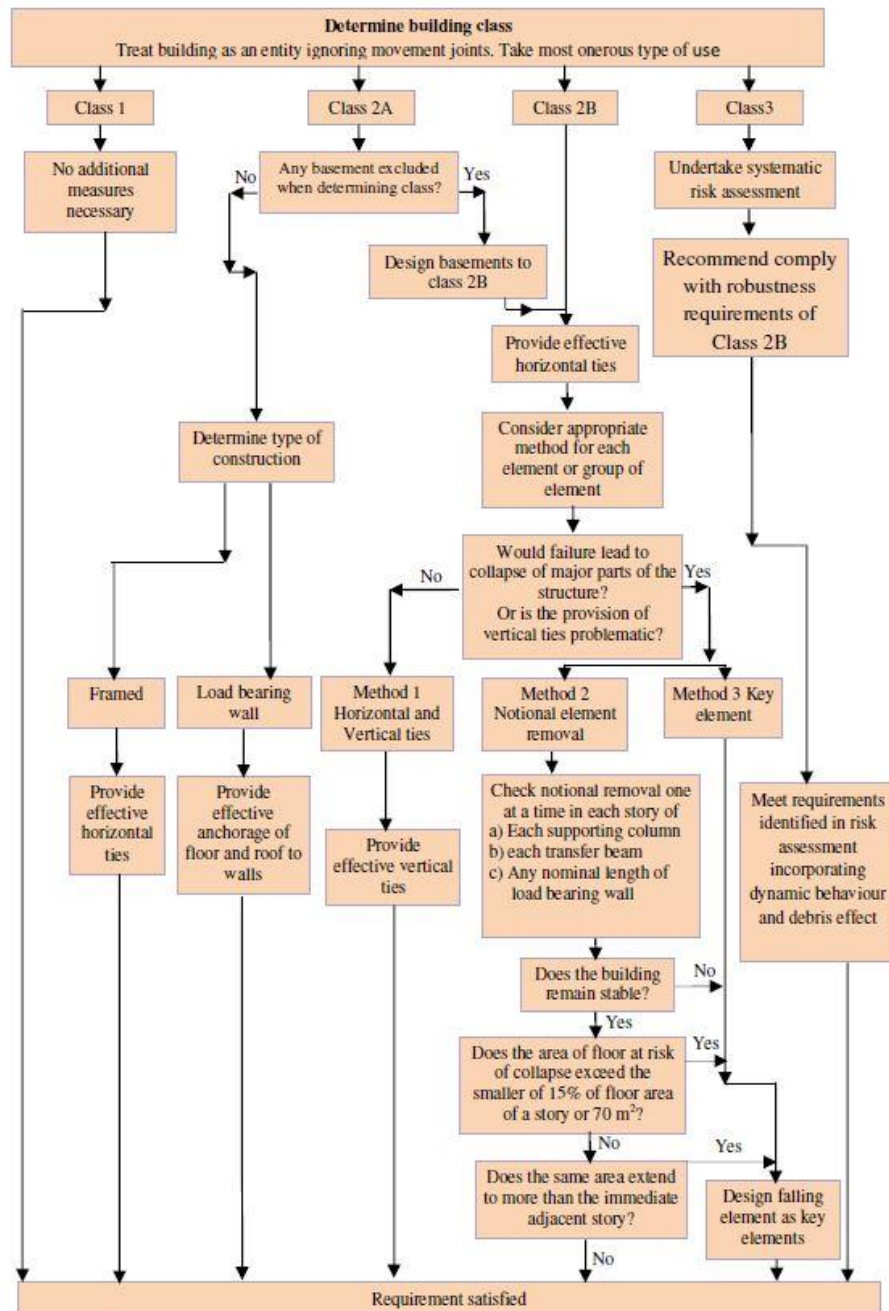


Figure 7: Building classes and solution strategies (CEN, 2006)

2.4.1.1 Requirements for Class 2b framed structures

In this section will be presented the requirements to be satisfied for Class 2b frame structures, as these are more stringent than those of previous classes, while class 3 buildings require the development of a risk analysis that is outside the scope of this work.

The section A.4 of Annex A of EN 1991-1-7 defines the requirements for Class 2b buildings, stating that these structures require additional provisions in addition to the ones defined for Class 1 buildings. About this class, EN 1991-1-7 states that “Provided a building has been designed and constructed in accordance with the rules given in EN 1990 to EN 1999 for satisfying stability in normal use, no further specific consideration is necessary with regard to accidental actions from unidentified causes”. Hence, for reinforced concrete frame structures must be adopted the requirements defined in section 9.10 of EN 1992-1-1 - Design of concrete structures - Part 1-1: General rules and rules for buildings (CEN, 2004). This document establishes that if the structures are not designed to withstand accidental actions shall have a suitable tying system, to prevent progressive collapse by providing alternative load paths after local damage. In particular, the following ties should be provided:

- Peripheral ties:

At each floor and roof level an effectively continuous peripheral tie within 1,2 m from the edge should be provided. The ties should can resist a tensile force:

$$F_{tie,per} = l_i \cdot q_1 \leq q_2 \quad (2)$$

Where:

$F_{tie,per}$ tie force, l_i length of the end-span, values of q_1 and q_2 for use in a Country may be found in its National Annex. The recommended value of q_1 is 10 kN/m and of q_2 is 70 kN. In addition, structures with internal edges (e.g. atriums, courtyards, etc.) should have peripheral ties in the same way as external edges which shall be fully anchored.

- Internal ties:

These ties should be at each floor and roof level in two directions approximately at right angles. They should be effectively continuous throughout their length and should be anchored to the peripheral ties at each end, unless continuing as horizontal ties to columns or walls.

The internal ties may, in whole or in part, be spread evenly in the slabs or may be grouped at or in beams, walls or other appropriate positions.

In each direction, internal ties should resist a design value of tensile force

Values of $F_{tie,int}$ for use in a Country may be found in its National Annex. The recommended value is 20 kN/m.

In floors without screeds where ties cannot be distributed across the span direction, the transverse ties may be grouped along the beam lines. In this case the minimum force on an internal beam line is:

$$F_{tie,int} = (l_1 + l_2)/2 \cdot q_3 \leq q_4 \quad (3)$$

Where:

l_1 , l_2 are the span lengths (in m) of the floor slabs on either side of the beam (see Figure 8), q_3 and q_4 for use in a Country may be found in its National Annex. The recommended value of q_3 is 20 kN/m and of q_4 is 70 kN.

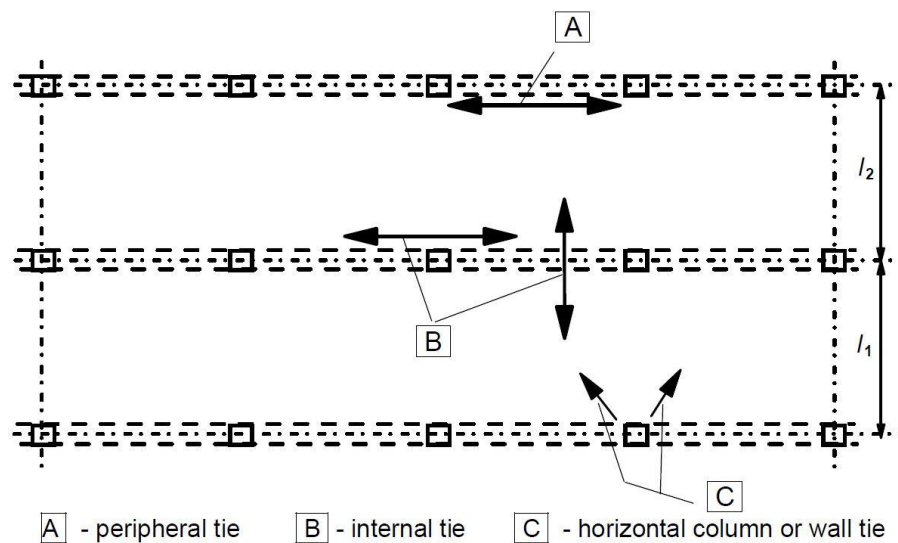


Figure 8: Ties for accidental actions (CEN, 2004)

- Horizontal column or wall ties:

Edge columns and walls should be tied horizontally to the structure at each floor and roof level. The ties should be capable of resisting a tensile force $f_{tie,fac}$ per metre of the façade. For columns the force need not exceed $F_{tie,col}$.

Values of $f_{tie,fac}$ and $F_{tie,col}$ for use in a Country may be found in its National Annex. The recommended value of $f_{tie,fac}$ is 20 kN/m and of $F_{tie,col}$ is 150 kN.

Corner columns should be tied in two directions, steel provided for the peripheral tie may be used as the horizontal tie in this case.

- Where required, vertical ties, particularly in panel buildings:

In panel buildings of 5 storeys or more, vertical ties should be provided in columns and/or walls to limit the damage of collapse of a floor in the case of accidental loss of the column or wall below. These ties should form part of a bridging system to span over the damaged area.

Normally, continuous vertical ties should be provided from the lowest to the highest level, capable of carrying the load in the accidental design situation, acting on the floor above the column/wall accidentally lost. Other solutions e.g. based on the diaphragm action of remaining wall elements and/or on membrane action in floors, may be used if equilibrium and sufficient deformation capacity can be verified.

Where a column or wall is supported at its lowest level by an element other than a foundation (e.g. beam or flat slab) accidental loss of this element should be considered in the design and a suitable alternative load path should be provided.

These are the requirements to be satisfied for Class 1 buildings. For Class 2b frame structures EN 1991-1-7 states that:

- Horizontal ties should be provided around the perimeter of each floor and roof level and internally in two right angle directions to tie the column and wall elements securely to the structure of the building. The ties should be continuous and be arranged as closely as practicable to the edges of floors and lines or columns and walls. At least 30 % of the ties should be located within the close vicinity of the grid lines of the columns and the walls.

Each continuous tie, including its end connections, should resist a design tensile load of T_i for the accidental limit state in the case of internal ties, and T_p , in the case of perimeter ties, equal to the following values:

$$T_i = \max(0.8(g_k + \Psi q_k)sL ; 75kN) \quad (4)$$

$$T_p = \max(0.4(g_k + \Psi q_k)sL ; 75kN) \quad (5)$$

Where:

s is the spacing of ties, L is the span of the tie, Ψ is the relevant factor in the expression for combination of action effects for the accidental design situation (Ψ_1 or Ψ_2 in accordance with expression (6.11 b) of EN 1990).

- For vertical ties: each column and wall should be tied continuously from the foundations to the roof level. In the case of framed buildings (e.g. steel or reinforced concrete structures) the columns and wall carrying vertical actions should resist an accidental design tensile force equal to the largest design vertical permanent and variable load reaction applied to the column from any one storey. Such accidental design loading should not be assumed to act simultaneously with permanent and variable actions that may be acting on the structure.

As an alternative to the provision of these ties:

- The building should be checked to ensure that upon the notional removal of each supporting column and each beam supporting a column, or any nominal section of load-bearing wall (one at a time in each storey of the building) the building remains stable and that any local damage does not exceed a certain limit. Where the notional removal of such columns and sections of walls would result in an extent of damage in excess of the agreed limit, or other such limit specified, then such elements should be designed as a "key element".

A "key element" should sustain an accidental design action of A_d applied in horizontal and vertical directions (in one direction at a time) to the member and any attached components having regard to the ultimate strength of such components and their connections. Such accidental design loading should be applied in accordance with expression (6.11b) of EN 1990 and may be a concentrated or distributed load. The recommended value of A_d for building structures is 34 kN/m².

Hence Eurocodes suggest the following approaches:

- Tying;
- Notional removal;
- Key element.

The designer can mix methods within the same structure i.e. building may generally satisfy the tie requirements, but if there are some areas that do not

satisfy the tying, the designer can apply the notional removal method or the key element approach to deal with robustness requirements.

2.4.1.2 Notional element removal according EN 1991-1-7

As this is the approach adopted to carry out the numerical analysis developed in this work, it will be discussed in detail:

The notional removal design strategy for robustness in BS EN 1991-1-7, A.4 is presented as an alternative to the provision of horizontal and vertical tying. The benefits of this design strategy are that instead of following prescriptive rules (e.g. tying), more specific damage scenarios are considered, whereby the designer is required to assess the area of the damage, i.e. the building's ability to localise damage. The notional removal design strategy is still somewhat prescriptive in that the damage scenarios that the designer is required to assess involve the removal of one supporting member (beam or column) at a time. The notional removal design strategy will generally only be successful for small column spacings. In practical terms, the advantage is that if the structure has reasonably small beam spans and if the structure is well interconnected, then notional removal offers the designer an opportunity for satisfying robustness rules with an acceptance of local damage. This can be useful if for some reason it is not possible to comply fully with tying rules.

The requirements of the notional removal design strategy as defined in A.4 of BS EN 1991-1-7 are given below.

1. Each supporting member should be notionally removed one at a time to ensure that the limit of admissible local damage is not exceeded and that the building remains stable.
2. For notional removal, a supporting member is a column section (a length between adjacent storeys) or a beam supporting one or more columns.
3. The limit of admissible local damage recommended in BS EN 1991-1-7, Annex A, is:

$$\min(15\% \text{ of floor area ; } 100\text{m}^2) \quad (6)$$

In each two adjacent storeys (see Figure 9)

Upon the notional removal of any single member, the structure must remain stable as a whole.

4. If the notional removal of any supporting element would result in the collapse of an area greater than the admissible local damage that element should be designed as a key element.
5. If the notional removal of any supporting element would result in the building being unstable that element should be designed as a key element.

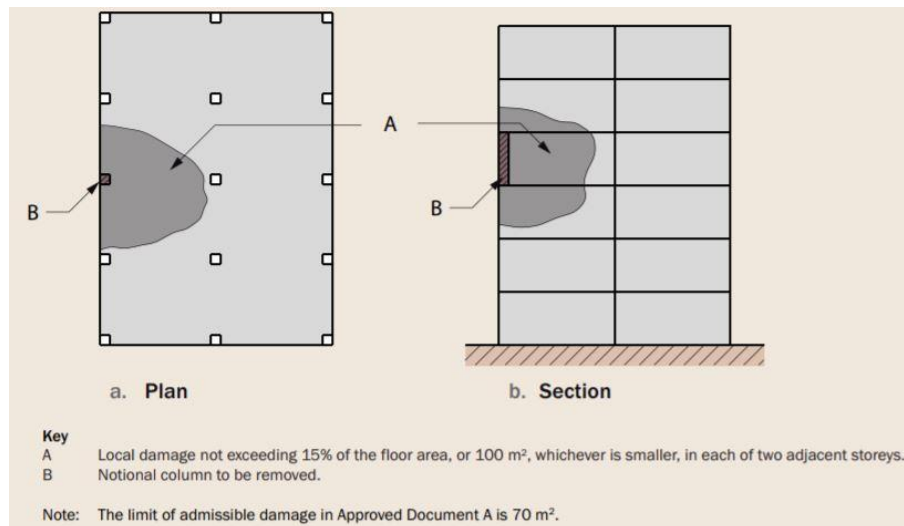


Figure 9: Recommended limit of admissible damage (Way, 2011)

The designer is required to determine the amount of structural damage after the notional removal. For the case of a column being notionally removed, all the beams supported by the column are assumed to collapse and all the floor slabs supported by the collapsed beams are assumed to collapse. To ensure the damage does not spread down the building, the floor below the damaged area should be checked to ensure that it does not collapse due to the debris. At the same time, to ensure the damage does not spread up the building, the floors above the removed column should be checked to determine whether they can bridge over the damaged area.

2.4.2 American Society of Civil Engineering (ASCE 7-05)

The American Society of Civil Engineering mainly focuses on a threat-independent approach. To withstand progressive collapse the designer is addressed to enhance the redundancy and the development of alternate load paths. ASCE 7-05 defines two possible methods:

-
- **Direct design method:** the resistance against progressive collapse is considered explicitly by means of two approaches:
 - Alternate Load Path method: by providing alternate load paths to bridge over localized damage and prevents progressive collapse;
 - Specific Local Resistance method: by defining key elements that do not have to collapse after an accidental event.

According to this standard, the load combinations for extraordinary events is reported in the following. Then after the element removal, the damaged structure should bear a load equal to:

$$Q = (0.9 \text{ or } 1.2)D + (0.5L + 0.25S_n) + 0.2W \quad (7)$$

Where:

D is the dead load, L is the live load, S_n is the snow load and W is the wind load.

- **Indirect design method:** is a prescriptive approach in which the minimum levels of strength, continuity, and ductility are provided.

According to this standard, the elements placed in the area above the column removed should bear a load equal to:

$$G_{LD} = \Omega_{LD}(1.2D + 0.5L \text{ or } 0.2S) \quad (8)$$

While the elements placed in the area away from the removed column should bear a load equal to:

$$G = 1.2D + 0.5L \text{ or } 0.2S \quad (9)$$

Where:

Ω_{LD} is a load increase factor, D is the dead load, L is the live load, S is the snow load and W is the wind load.

2.4.3 General Services Administration (GSA) Unified Facilities Criteria UFC 4-023-03

According to this document all the buildings with three levels or more should be designed for structural robustness. Furthermore, establishes distinct levels of

resistance to progressive collapse, according to the Occupancy Category. Three possible strategies are defined:

- **Tie force Method (TF):** this is an indirect approach based on the provision of minimum levels of continuity, ductility and redundancy by specifying the minimum strength needed to tie the whole structure.

Although TF is similar to the method defined in the Eurocode, the tie force requirement is significantly greater than this code. With this approach, the whole structure is mechanically tied together using four different typologies of ties i.e. internal longitudinal, transverse longitudinal, peripheral and vertical ones (see Figure 10). Tie forces can be provided by the existing structural elements that have been designed using conventional design methods to carry the standard loads imposed upon the structure.

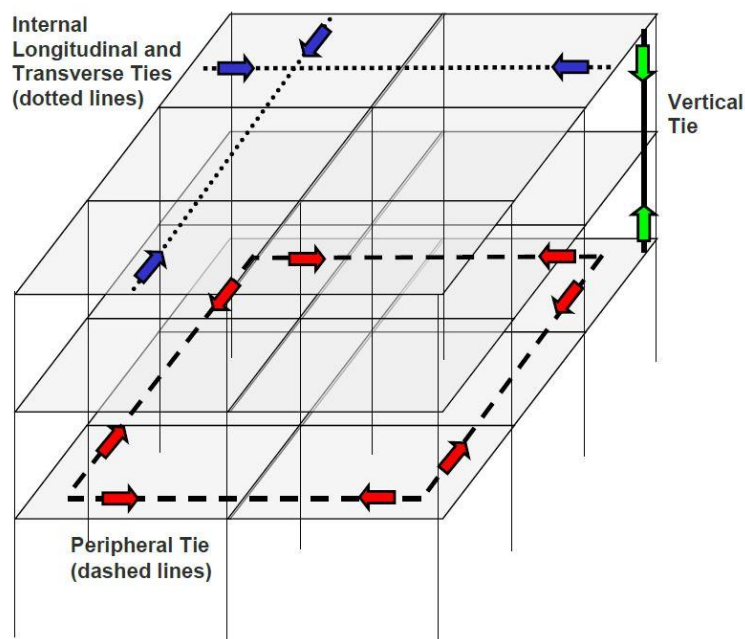


Figure 10: Tie forces in a framed structure (Dod, 2013)

This method is applicable if the framed structures have at least four bays in both directions.

To determine the required tie strength, the designer should consider the floor load given by the following equation:

$$w_F = 1.2D + 0.5L \quad (10)$$

Where:

w_F is the floor load, D is the dead load and L is the live load.

About longitudinal and transverse internal ties, the required tie strength is given by:

$$F_l = 3w_FL_1 \quad (11)$$

Where:

L_1 is the greater of the distances between the centres of the columns supporting any two adjacent floor spaces in the direction under consideration.

About peripheral ties, the required strength is given by:

$$F_p = 6w_FL_1L_p + 3W_c \quad (12)$$

Where:

L_1 for peripheral ties at the edge of the building is the greater of the distances between the centres of the columns, at the perimeter of the building in the direction under consideration, while for peripheral ties at openings is the length of the bay in which the opening is located, in the direction under consideration; h_w is the clear story height and L_p is 1m.

About vertical ties the designer can use the columns to carry the required vertical tie strength. Each column shall be tied continuously from the roof level down to the first column above the foundation.

- **Alternate Load Path Method (AP):** through which structures should be capable to bridge over removed elements. The designer may use the AP method to determine if the structure can bridge over the damaged element after it has been notionally removed.

UFC document defines three typologies of analysis:

- Linear static: it considers the material as linear-elastic, it allows only small deformations and the loads are applied statically;
- Nonlinear static: it considers both geometry and material nonlinearity and the loads are applied statically;

- **Nonlinear dynamic:** it considers both geometry and material nonlinearity and the loads are applied dynamically.

Under normal conditions, the load is transferred from the application point to the foundations through pre-determined load paths. After the failure of one element due to an accidental load, the structure can find an alternate load paths to bridge the damaged area, preventing progressive collapse. The new paths can be found exploiting tying, catenary action of the beams and diaphragm action of the floor plans.

One of the aims of the present study is to assess if the catenary action can be activated in frame structures. Hence this mechanism will be discussed in greater detail.

- **Catenary Action Mechanism:** In RC structures, in presence of large deformations (e.g. due to the loss of a column), catenary and membrane action can withstand gravity loads through the development of tensile force in the remaining elements, that will work as ties.

The activation of this mechanism requires an adequate amount of continue reinforcement in the beams and a sufficient ductility of these elements to satisfy the deformational demand of the damaged structure.

In reinforced concrete frames, the development of this mechanism can be explained in this way: after the column loss, the beams located near the damaged area undergo increasing vertical displacements, and consequently increasing rotations to find an equilibrium configuration. If the elements involved have sufficient rotational capacity, it is noteworthy that the structural response evolves through three distinct phases. The first one is characterized by the development of minor flexural cracks in the beams. This is an arching action stage, in which compressive arching forces developed due to horizontal restraint at the beam ends, provide additional stiffness and load-carrying capacity; a plastic hinging stage, in which due to the increasing rotation of the beams, the flexural bending causes the tensile yielding of the reinforcing bars, and the concrete softening and crushing in compression, causing a reduction in load-carrying capacity; the third stage is characterized by the catenary action, in which tensile catenary forces are activated supplying additional load-carrying capacity. While beam-end rotations continued to increase during the third stage, the overall load carrying capacity of the assembly was dominated by the development of

catenary action, which prevented a further drop in load. These mechanisms are summarised in Figure 11.

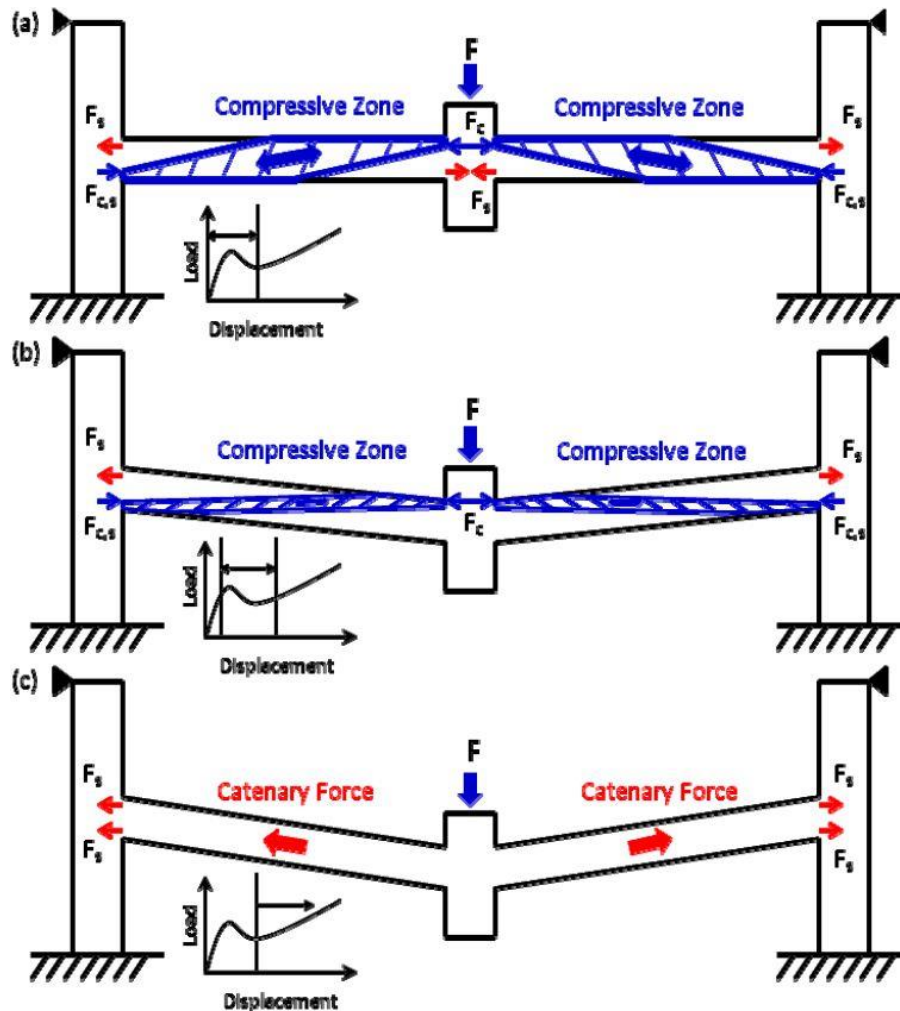


Figure 11: Loads transfer mechanisms: (a) arching action, (b) plastic hinge formation, and (c) catenary action (Lew, 2011)

- **Enhanced Local Resistance Method:** in which the capacity of columns is increased to insure a ductile failure mechanism when the elements are loaded laterally. For this reason, the element should be designed to avoid the failure in shear prior of the development of the maximum flexural strength.

2.5 Experimental studies on progressive collapse of RC buildings

In recent decades, the research about progressive collapse has made considerable progresses, however due to the complexity of the issue, experimental studies on reinforced concrete frame structures are limited. The main limits are represented by the availability of suitable equipment and by the costs involved in studies. Most of the studies focused on the two-dimensional behaviour of limited structural portions (e.g. beam-column assemblies), generally neglecting the effects due to three-dimensional behaviour and the contribution offered by the slab. In this section will be resumed two notable studies: the first one conducted by Lew et al. in 2011 on real scale beam-column reinforced concrete assemblies, the second one conducted by Qian et al. in 2014 on one-quarter scaled beam-column and beam-column-slab substructures.

2.5.1 Progressive collapse of a 2D beam-column assembly under a column removal scenario

Part of the work described in this section was also previously published by Lew et al. in 2011 (Lew, 2011).

The National Institute of Standards and Technology (NIST) carried out a comprehensive analytical and experimental research program to study the vulnerability of multi-story building structures to disproportionate collapse. This work presents an experimental study, conducted in 2011, on two reinforced concrete beam-column assemblies, each comprising three columns and two beams. These substructures represent portions of the structural framing system of two ten-story reinforced concrete frame buildings. The design of these two prototype buildings was based on:

- International Code Council (ICC), 2003 International Building Code (ICC, 2003);
- American Society of Civil Engineers (ASCE) Standard 7-02, Minimum Design Loads for Buildings and Other Structures (ASCE, 2002);
- American Concrete Institute (ACI), Building Code Requirements for Structural Concrete (ACI 318-02) and Commentary (ACI 318R-02) (ACI, 2002).

In particular, one building was designed for Seismic Design Category C (SDC C) while the other for Seismic Design Category D (SDC D). The beam-column assemblies were taken from the exterior moment-resisting frames of these buildings. The assembly from the SDC C building was part of an intermediate moment frame (IMF) and the assembly from the SDC D building was part of a special moment frame (SMF). The full-scale test assemblies were subjected to monotonically increasing vertical displacement of the centre column to simulate a column removal scenario.

Table 1 and Table 2 show the average compressive and tensile strengths of concrete and the mechanical properties of reinforcing bars used for the test. As shown in Figure 12 and Figure 13, all beam longitudinal bars were anchored at the exterior beam-column joints by means of mechanical anchorage to simulate continuity of the longitudinal bars in the real frame. The footings for the end columns were designed to simulate two fully restrained joints. The top of the end columns was restrained from horizontal movement by a two-roller fixture, while the other degrees of freedom were allowed.

Table 1: Average compressive and tensile strengths of concrete

Specimen	Compressive Strength		Split-Cylinder Tensile Strength
	psi (MPa)		psi (MPa)
	Footings	Beams and Columns	Beams and Columns
IMF	5700 (39)	4700 (32)	450 (3.1)
SMF	5300 (37)	5200(36)	420 (2.9)

Table 2: Average mechanical properties of reinforcing bars

Heat	Bar size	Yield Strength	Ultimate Strength	Rupture Strain
		ksi (MPa)	ksi (MPa)	
A ¹	#8	69 (476)	94 (648)	21%
B ²	#9	67 (462)	93 (641)	18%
C ³	#9	70 (483)	100 (690)	17%

D ⁴	#10	73 (503)	106 (731)	16%
E ⁵	#4	76 (524)	103 (710)	14%
F ⁶	#4	79 (545)	98 (676)	15%

¹ Top bars in beam of IMF specimen and all beam reinforcement in SMF specimen

² Bottom bars in beam of IMF specimen

³ Vertical bars in columns of IMF specimen

⁴ Vertical bars in columns of SMF specimen

⁵ Ties and stirrups in IMF specimen

⁶ Ties and stirrups in SMF specimen

To apply the load to the centre column were used four hydraulic jacks placed below the strong floor of the laboratory; the load was transferred to the specimen using four post-tensioning rods anchored to a steel plate that transferred the load at the top of the column. The test was performed under displacement control at a rate of approximately 25 mm/min. The use of four different hydraulic jacks to apply the load enabled control of any possible in-plane rotation of the centre column in the advanced loading stages; while out-of-plane movement of the assembly was restrained by four steel channels fixed to the floor. Furthermore, pulling down the beam with jacks, rather than pushing it from a support above, minimized the tendency for lateral movement of the beam. Figure 14 shows a view of SMF specimen.

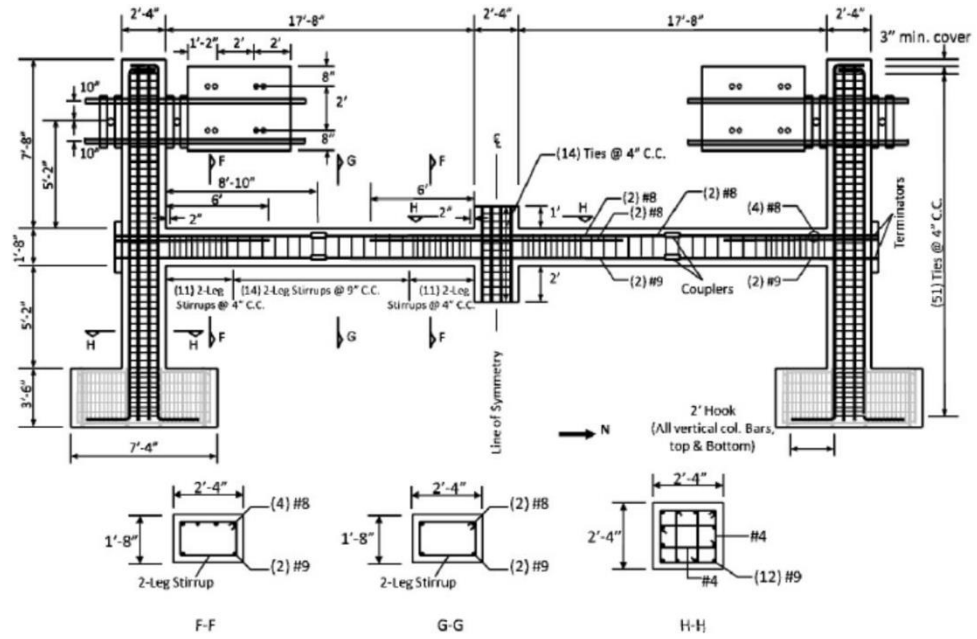


Figure 12: Details of IMF specimen (Lew, 2011)

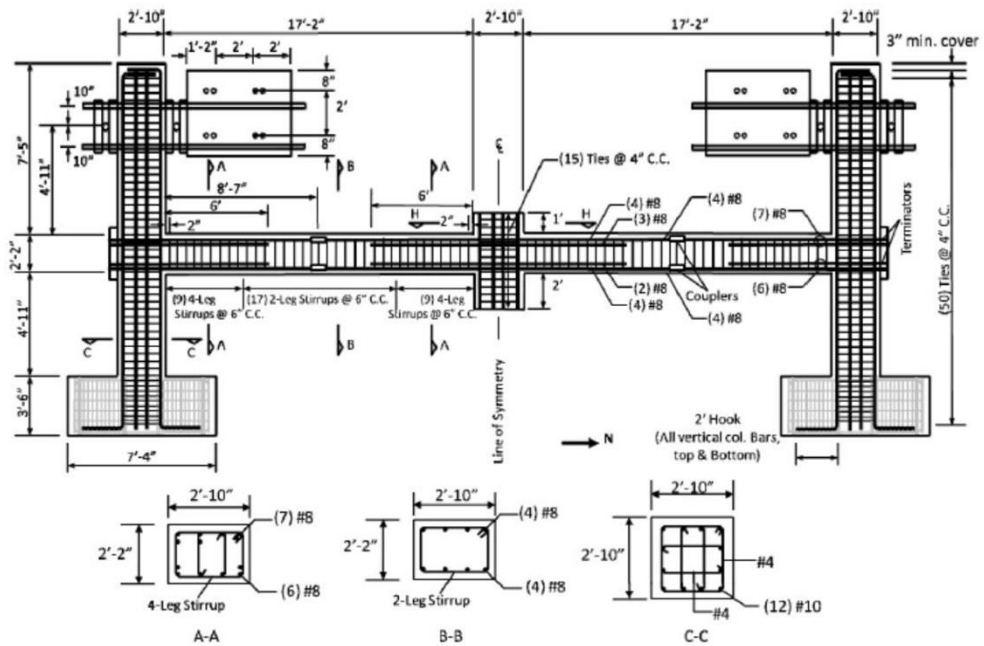


Figure 13: Details of SMF specimen (Lew, 2011)

observed. This behaviour is due to the restraint to horizontal movements of the beams provided by the end columns, which induced the development of arching action in the beams.

A significant reduction of the beam stiffness was observed instead in both specimens because of the yielding of the beam bottom reinforcing bars near the centre column and the top reinforcing bars near the end columns. As a result, while the rate of vertical displacement of the centre column remained constant, the load level increased gradually at a lower rate. For the IMF specimen, Figure 16 shows that the load reached a peak value of 296 kN with a corresponding centre column displacement of about 127 mm, while Figure 17 shows that for the SMF specimen the load reached a peak value of 903 kN with a corresponding centre column displacement of about 112 mm.

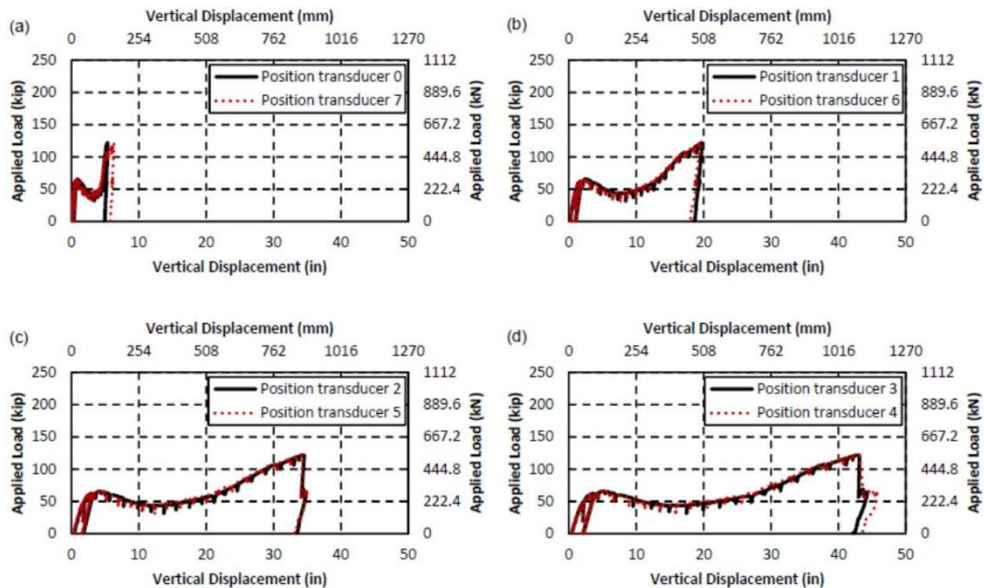


Figure 16: Vertical load versus vertical deflections of IMF specimen at (a) $\frac{1}{4}$ span of beams, (b) mid-span of beams, (c) $\frac{3}{4}$ span of beams, and (d) centre column (Lew, 2011)

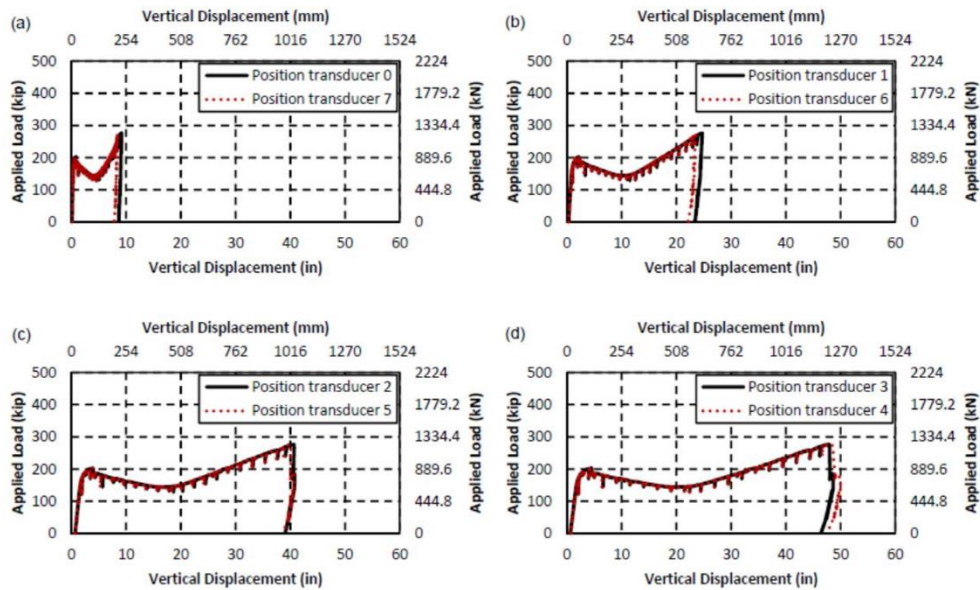


Figure 17: Vertical load versus vertical displacements of SMF specimen at (a) $\frac{1}{4}$ span of beams, (b) mid-span of beams, (c) $\frac{3}{4}$ span of beams, and (d) centre column (Lew, 2011)

For both specimens, after reaching the initial peak load, there was a softening phase in which the load began to drop with increasing vertical displacement of the centre column. When the vertical displacement of the centre column exceeded the depth of the beam, the load started to increase again. The recovery of bearing capacity was possible due to the development of the catenary action in the beams as full-depth cracks developed. This mechanism was highlighted by the observation of tensile strains in both top and bottom reinforcing bars at mid-span of the beams.

At the last stage, both specimens failed due to fracture of beam-bottom reinforcing bars near the centre column at an ultimate load greater than the initial peak load reported above. The ultimate load of the IMF specimen was 547 kN, with a corresponding centre column displacement of 1092 mm, while the ultimate load of the SMF specimen was 1232 kN, with a corresponding centre column displacement of 1219 mm.

Comparing the ultimate load reached by the specimens, SMF has shown an increase of bearing capacity of +125% if compared to ultimate load of IMF specimen. However, also this assembly has shown a good response exceeding the initial peak load of +85%, while the ultimate load of the SMF specimen exceeded the initial peak load by a factor of only +36%.

2.5.2 Progressive collapse of 3D beam-column and beam-column-slab substructures

Part of the work described in this section was also previously published by Qian et al. in 2015 (Qian, 2015).

In 2015, a research group from Nanyang Technological University of Singapore developed a series of experimental test on one-quarter scaled 3D reinforced concrete assemblies to evaluate their response after a column removal (Qian, 2015). Previous studies evaluated the reliability of reinforced concrete structures to resist progressive collapse and the effective reliability of resisting mechanisms like compressive arch action (CAA) and tensile catenary action (TCA) in RC beams. However, generally these studies referred to 2D planar frames or sub-frames disregarding 3D or slab effects.

Although the extent of 3D effects is different for buildings designed with varying dimensions and reinforcement properties, the work proposed by Qian is a reference point for the evaluation of these contributes to resist progressive collapse.

Two prototype buildings were designed, in accordance with ACI Committee 318-08, and tested to carry out an assessment of the reliability of CAA and TCA developed in RC beams and CMA and TMA developed in RC slabs for preventing collapse of RC buildings. Table 3 and Table 4 summarize the properties of the specimens: models S1 and S2 are directly scaled down from prototype buildings, while specimens T1 and T2 respectively have similar beams to S1 and S2 but without RC slab. Figure 18 shows the portion selected for the tests, Figure 19 shows the layout of specimen S1.

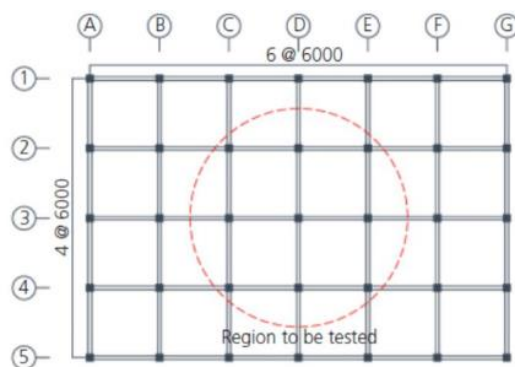


Figure 18: Plan layout of the prototype building (Qian, 2015)

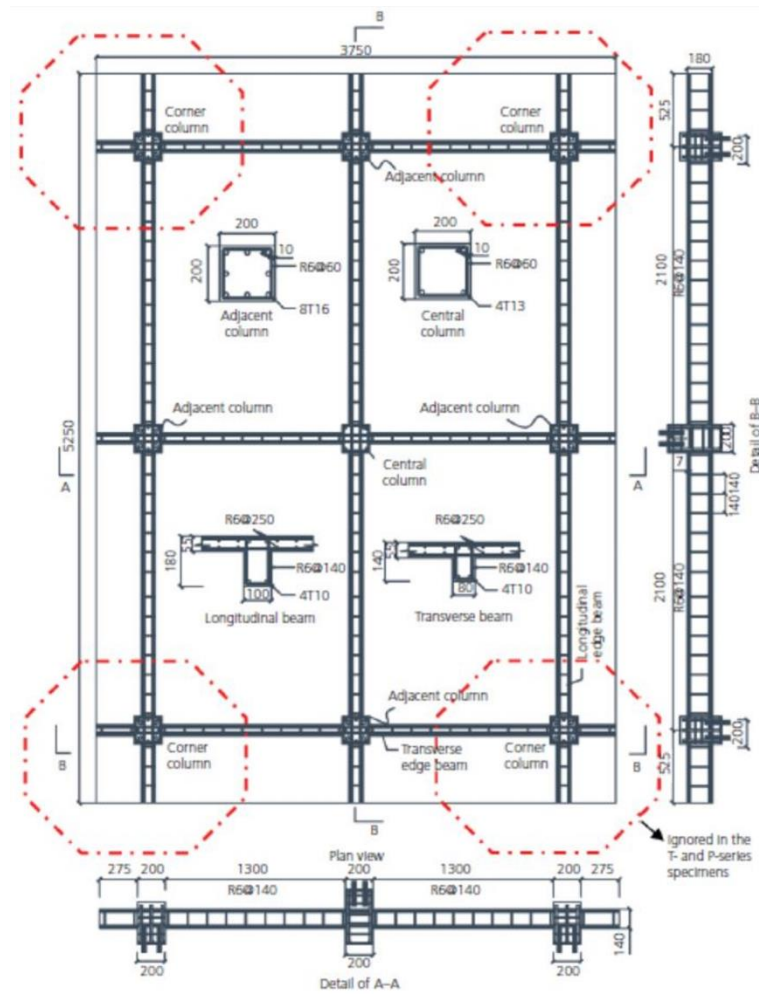


Figure 19: Details of specimen S1 (Qian, 2015)

About the materials, the measured average concrete compressive strengths at 28d after casting are 20, 21, 22, 23, 23 and 23MPa for P1, P2, T1, T2, S1 and S2, respectively. Table 5 summarizes the steel reinforcements properties.

Table 3: Specimen properties

Test ID	Elements		Longitudinal rebar		
	Beam-T	Beam-L	Column-I	Beam-T	Beam-L
P1	Type1*	NA	4T13	4T10	NA
P2	NA	Type2*	4T13	NA	4T10
T1	Type1*	Type2*	4T13	4T10	4T10

T2	Type1*	Type1*	4T13	4T10	4T10
S1	Type1*	Type2*	4T13	4T10	4T10
S2	Type1*	Type1*	4T13	4T10	4T10

*Type 1: clear span = 1300 mm, cross-section = 140x80 mm²; Type 2: clear span = 1900 mm, cross-section = 180x100 mm². T10 = deformed bar of 10 mm diameter; Beam-L = longitudinal beam; Beam-T = transverse beam; Column-I = interior column.

Table 4: Specimen properties

Test ID	Transverse reinforcement ratio			Slab reinforcement ratio	
	Joint	Beam-T	Beam-L	Top	Bottom
P1	R6@60	R6@140	NA	NA	NA
P2	R6@60	NA	R6@140	NA	NA
T1	R6@60	R6@140	R6@140	NA	NA
T2	R6@60	R6@140	R6@140	NA	NA
S1	R6@60	R6@140	R6@140	0.25%	0.25%
S2	R6@60	R6@140	R6@140	0.25%	0.25%

Table 5: Properties of reinforcing steel

Types*	Yield strength	Yield strain	Ultimate strength	Elongation ratio
	MPa	x10-6	MPa	%
T10	437	2273	568	13.1
T13	535	2605	611	11.6
T16	529	2663	608	14.3
R6	355	1910	465	17.5

*R6 = plain round bar of 6 mm diameter; T10 = deformed bar of 10 mm diameter; T13 = deformed bar of 13 mm diameter; T16 = deformed bar of 16 mm diameter.

Figure 20 shows the test setup for specimens S1 (on the left) and T1 (on the right). The constraints that in the actual structure are represented by the columns are reproduced by means of eight strong steel supports. To simulate the loss of centre column caused by extreme events, the authors have used a hydraulic jack which apply vertical displacement at the centre column to achieve a push-down loading regime. To ensure that the applied load was vertical, and the failure of the specimens was symmetric the authors have designed a steel assembly placed beneath the hydraulic jack. For P-series and T-series specimens, only two and four supports were respectively used to apply fixed conditions to adjacent columns.

As regard the instrumentation: linear variable deformation transducers (LVDTs) and line transducers were installed to monitor the evolution of the deformation. Strain gauges were also mounted on the steel bars before casting.

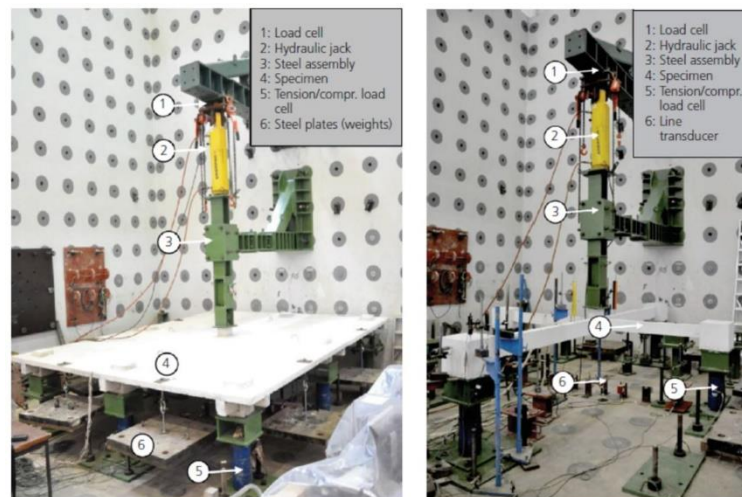


Figure 20: Specimens ready for testing (Qian, 2015)

At the end of the test, in specimen S1, authors have observed flexural elliptical cracks at the top face of the slab and concrete crushing at the top slab near the centre column. The deformation was mainly concentrated in the centre of the slab (enclosed by the outermost elliptical crack), while limited deformation and damage were observed in the outer region.

Two zones can be highlighted: an inner region with large deformation defined as “tensile net”, and an outer region called “compressive ring”. In addition, authors observed severe cracking in the bottom region of beams as well as slabs and the fracture of a rebar in correspondence of the centre column–slab interface. Punching

shear failure was detected in the centre column–slab connection and severe detachment between slabs and beams was also observed.

Specimen S2 exhibited a behaviour similar to S1, but circular cracks were detected at the top face and concrete crushing was observed at the compressive ring at the end of the test.

Specimens T1 and T2 had shown plastic hinges at the beam ends, accompanied by flexural cracks and concrete crushing. Rebar fracture also occurred at the interior column-beam interfaces. Unexpectedly, severe shear damage was observed at one of the transverse beams. According to the authors, this may be due to initial deficiencies concentrated in that region before testing. However, the shear failure did not stop the development of tensile catenary action in the beams.

Specimens P1 and P2, have shown failure modes similar to the longitudinal and transverse beams of T1, respectively.

Figure 21 shows the load-displacement curves for each test. It can be noted that the first peak load exceeded the yield loads significantly, this was due to CAA and CMA developed in beams or slabs. The ratios of first peak load to yield load were 1.33, 1.38, 1.40, 1.33, 1.44 and 1.37 for specimens P1, P2, T1, T2, S1 and S2, respectively. After the flexural peak, all specimens shown a softening phase due to the formation of plastic hinges followed by a re-increase of load resistance. For the S-series of specimens, the load re-ascending was observed at about 1.2 times the slab thickness. However, for P-series and T-series tests, this phenomenon was observed at about 1.0 times the beam depth. The ultimate load capacity due to development of TCA and TMA could increase the first peak load by 47%, 64%, 18%, 41%, 47% and 34% for specimens P1, P2, T1, T2, S1 and S2, respectively. To quantify the 3D effects, the test results from T-series tests were compared with the ones of P-series tests. It was found that 3D effects excluding slab contribution could increase the first crack load, yield load, initial stiffness, first peak load and ultimate load capacity by up to 88%, 100%, 127%, 109% and 68%, respectively. Comparing the test results of S-series with P-series indicated that 3D effects including slab contribution could increase the first crack load, yield load, initial stiffness, first peak load and ultimate load capacity up by 450%, 246%, 244%, 259% and 260%, respectively. Table 6 summarizes the measured results.

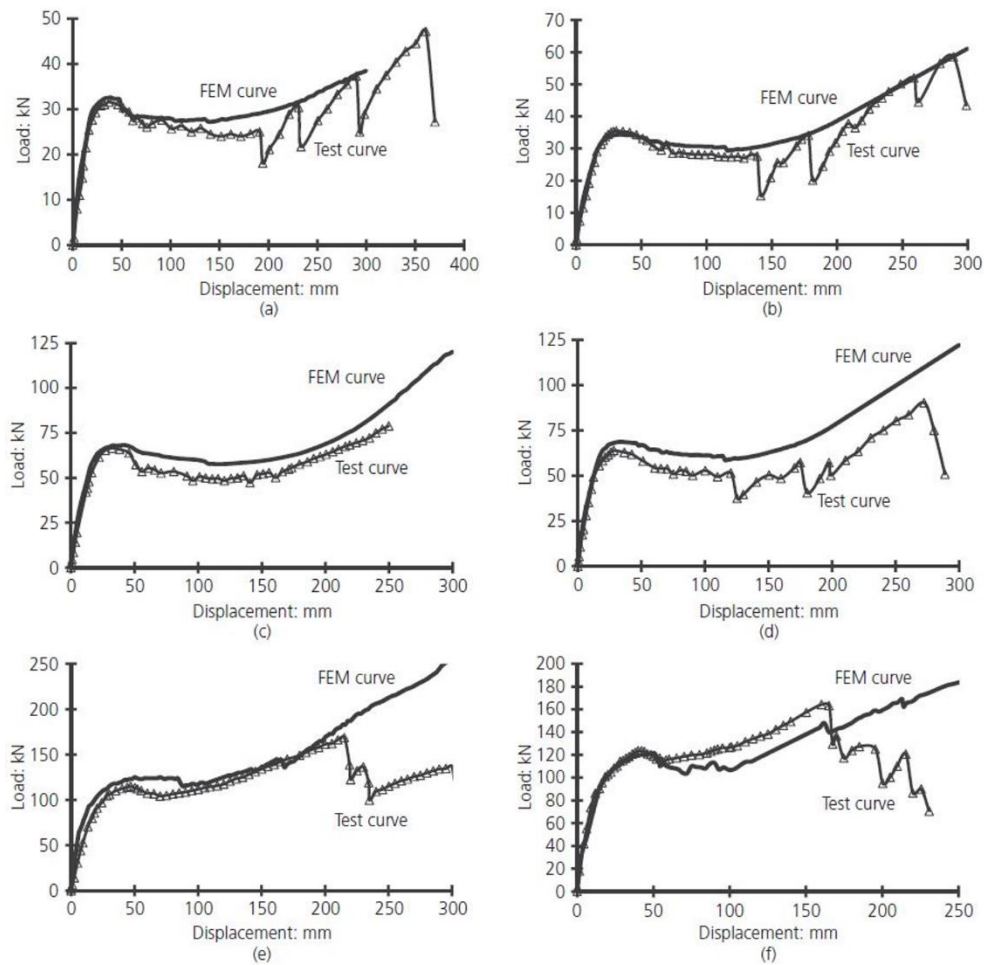


Figure 21: Comparison of the load–displacement relationship of test specimens: (a) specimen P1; (b) specimen P2; (c) specimen T1; (d) specimen T2; (e) specimen S1; (f) specimen S2 (Qian, 2015)

Table 6: Test results

Test	F_{cr}^*	F_y^*	Initial stiffness	F_u^*	F_t^*	F_u/F_y	F_t/F_u
	kN	kN		kN/mm	kN	kN	-
P1	8	24	1.5	32	47	1.33	1.47
P2	11	26	1.8	36	59	1.38	1.64
T1	15	48	3.4	67	79	1.40	1.18
T2	18	48	3.9	64	90	1.33	1.41
S1	44	80	4.8	115	169	1.44	1.47

S2 56 90 6.2 123 165 1.37 1.34

* F_{cr} , F_y , F_u and F_t represent the first cracking load, yield load, the first peak load and ultimate load capacity due to tensile catenary or tensile membrane actions, respectively.

Table 7: Test comparison

Ratio	F_{cr}^*	F_y^*	Initial stiffness	F_u^*	F_t^*
T1/P1	1.88	2.00	2.27	2.09	1.68
T2/P2	1.64	1.85	2.17	1.78	1.53
S1/P1	5.50	3.33	3.2	3.59	3.60
S2/P2	5.09	3.46	3.44	3.42	2.80

In conclusion, Qian et al. found that by considering 3D effects, excluding slab contribution, could increase the yield load of the 2D bare-frame by 100.0%. However, by considering also the slab contribution it is possible to increase the yield load of the 2D bare-frame by 246.2%. Compressive arch action could increase the yield load of beams assemblies by 40%, while tensile catenary action could increase the yield load by 126.9%. For beam–slab assemblies, the compressive arch action and compressive membrane action could increase their yield load by 44%, while tensile catenary action and tensile membrane action could increase the yield load by 111.3%.

2.5.3 Discussion of the results

The most of experimental tests developed to investigate progressive collapse of RC frame buildings have shown that if the structure has sufficient ductility, several resisting mechanisms can be developed before to reach the collapse. These include, compressive arch action/compressive membrane action (CAA/CMA) and tensile catenary action/tensile membrane action (TCA/TMA).

The studies presented hereinbefore have demonstrated that if the edges of slabs or beams are restrained against lateral movement by stiff boundary elements (e.g. represented surrounding structural portions that are not damaged), horizontal compressive force or thrust are induced in the slab/beam.

This is due to the slab or beam deflection, which changes the geometry causing the outward displacement of slab or beam and react against the stiff boundary elements.

The induced compressive force enhances the flexural load of slab/beam through moment-axial force interaction. Figure 22 shows a schematic of the CCA/CMA resisting mechanism. Generally, the compressive forces developed in this phase produce stresses in reinforcement smaller than the yielding value. Therefore, this mechanism produces an increase of flexural capacities of the beam or slab.

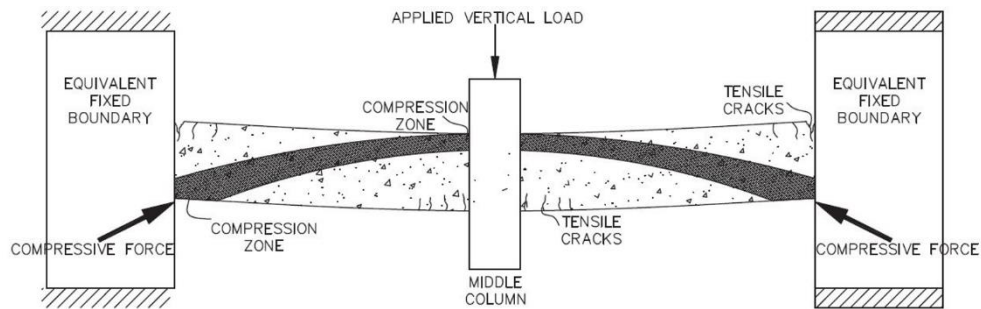


Figure 22: Schematic of CCA/CMA mechanism (Qian, 2014)

Increasing the vertical displacement, concrete crushing becomes severe, and flexural cracks may interest the whole thickness of beam or slab. Then the load is mainly carried by the continuous reinforcement present along the elements acting as a tensile net or chain action. The catenary force development is evidenced by tensile strains in both top and bottom reinforcing bars at mid-span of the beams. Figure 23 shows a schematic of the TAA/TMA resisting mechanism.

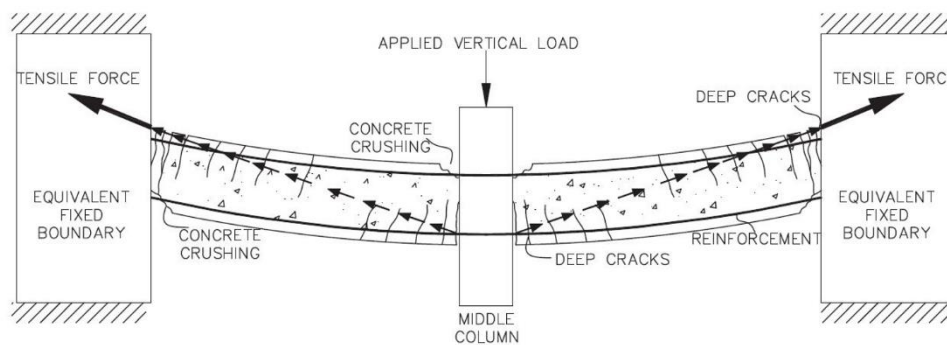


Figure 23: Schematic of TCA/TMA mechanism (Qian, 2014)

The experimental studies have shown that in most cases the failure is due to bars fracture near the column removed. Furthermore, the boundary conditions as well as the geometry of the structure have significantly effects on the structural response. This makes it difficult to generalize to provide effective design guidance. For this reason, a large experimental program would be needed to investigate the phenomenon in a more in-depth way. Actually, to address this lack of data, a solution is to combine experimental results with parametric numerical studies.

2.6 Numerical studies on progressive collapse of RC buildings

In designing robust structures, a valuable help for the designer is given by the possibility to carry out numerical analyses. The resistant mechanisms to withstand progressive collapse, discussed in the previous paragraph, produce a non-linear structural behaviour often associated with dynamic effects. Numerical analyses to be developed to properly simulate these aspects are rather complex and need to be carried out by an expert designer. Due to the importance of the consequences of progressive collapse, the analyses need to be reliable, and capable to provide accurate information about the actual structural behaviour. Thus, to develop efficient and reliable methods significant efforts have been made by the scientific community in the last decades. Below are briefly some of the obtained results regarding progressive collapse analyses.

2.6.1 Izzuddin, 2007

Part of the work described in this section was also previously published by Izzuddin in 2007 (Izzuddin, 2007).

Izzuddin in 2007 proposed an assessment framework based on three main stages (Izzuddin, 2007):

1. Evaluation of nonlinear static response of the damaged structure under gravity loading;
2. Simplified dynamic assessment to establish the maximum dynamic response under sudden column loss;
3. Ductility assessment of the connections.

This procedure may be applied at the overall structural level (Figure 24) and, importantly, at various substructural levels (Figure 25).

As an example, the structure shown in Figure 24 can be simplified by applying appropriate boundary conditions to represent the interaction with the surrounding structure (Figure 25a). If the surrounding columns are capable to withstand the redistributed load, is possible a further simplification considering only the floors above the column removed where deformation is concentrated (Figure 25b). Moreover, if the floors are identical in terms of structure and loading, the axial force in the columns immediately above the lost column becomes negligible, and a reduced model consisting of a single floor system may be considered (Figure 25c).

Finally, if the designer ignores the planar effects offered by the floor slab, may be considered only the beams converging in the affected node (Figure 25d). However, this approach has a drawback represented by the requirement of separate analyses for different column removal scenarios because the boundary conditions change every time.

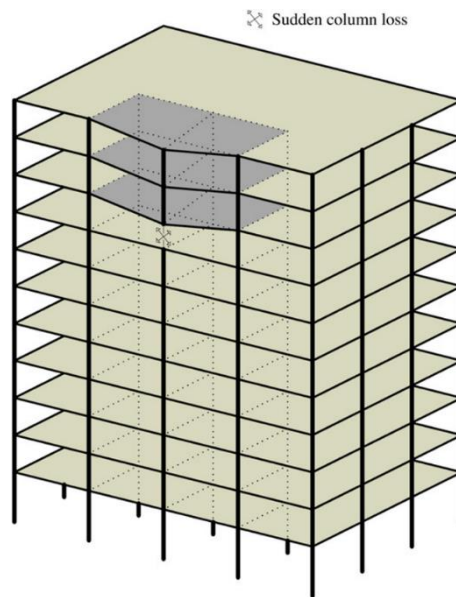


Figure 24: Multi-storey building subject to sudden column loss (Izzuddin, 2007)

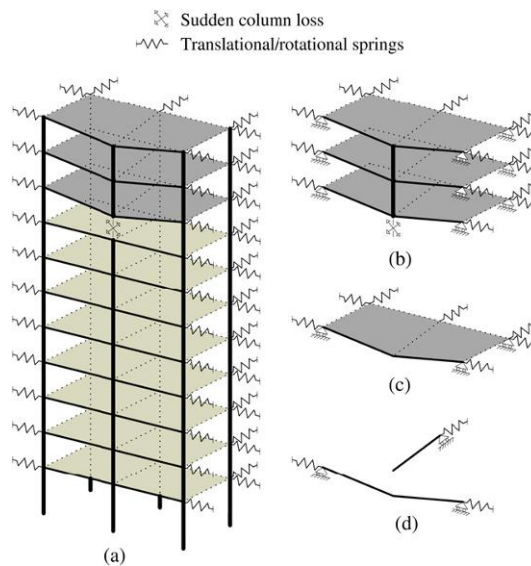


Figure 25: Sub-structural levels for progressive collapse assessment (Izzuddin, 2007)

2.6.2 Qian, 2015

Part of the work described in this section was also previously published by Qian et al. in 2015 (Qian, 2015).

Qian in 2015 developed a parametric study, complementary to the experimental one presented hereinbefore, to evaluate the influences of critical parameter individuated during the experimental tests (Qian, 2015). Several finite element analyses were developed to study the effects related by:

1. Influences on the first peak load (FPL) and ultimate load capacity (ULC);
2. Influences on the extent of slab effects.

The variables ‘BL’, ‘BD’, ‘SR’ and ‘ST’ reported in the following represent beam reinforcement ratio, beam depth, slab reinforcement ratio and slab thickness, respectively.

For this study specimens T2 and S2 were taken as control specimens. The analyses were carried out using the software DIANA (DIANA, 2008), beams and columns were modelled with 20-node brick elements, while the slabs were modelled with 8-node shell elements. The constitutive law adopted for concrete was the total rotating crack model, a 3D extension of the model proposed by Selby and Vecchio (Selby, 1993). The response of concrete in compression was modelled with a parabolic compressive softening model. It should be noted that a parabolic compressive softening model defined by Li et al. (Li, 2011) was used. In the tension part, conventional linear softening stress–strain based on fracture energy was adopted. The beam longitudinal reinforcing bars were modelled by using truss elements. The bond–slip between the reinforcement element and the surrounding concrete element was considered by adopting line interface element. The bond–slip model suggested by CEB–FIP model code 1990 (CEB, 1993) was used in this numerical study.

To verify the reliability of finite element models, authors developed a calibration procedure based on the comparison of load–displacement curves of test specimens and the simulated ones. As shown in Figure 26, FEMs were able to simulate the initial stiffness, yield strength and first peak load. For large displacement behaviour (TCA or TMA), FEMs could also reproduce the general trends. However, they could not predict the ultimate displacement and failure of the specimens properly. This was mainly because the elements, which had reached their failure criteria were not removed from the model. In these FEAs, the authors

assumed the specimens had failed when the ultimate displacement had reached double that of the short span.

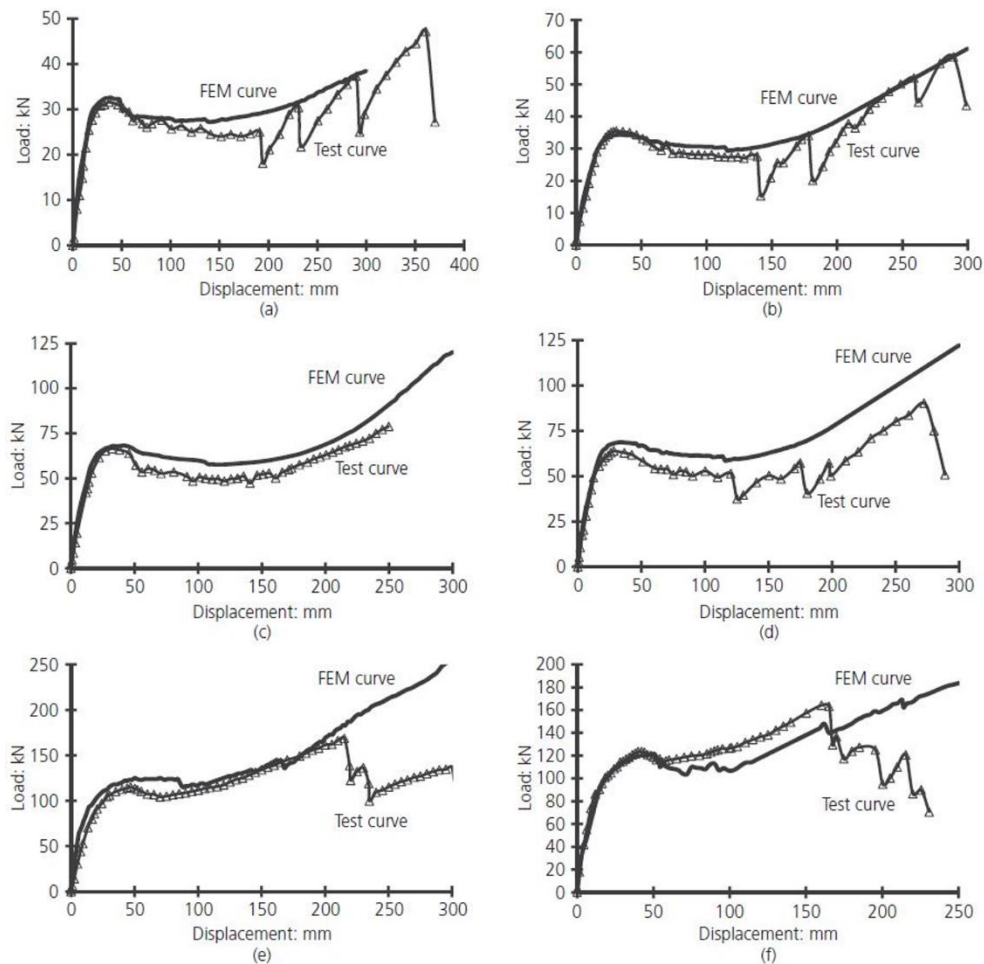


Figure 26: Comparison of the load–displacement relationship of test specimens: (a) specimen P1; (b) specimen P2; (c) specimen T1; (d) specimen T2; (e) specimen S1; (f) specimen S2 (Qian, 2015)

To quantify the influence of boundary conditions on the development of compressive membrane action and catenary membrane action, authors developed a sensitivity study comparing the effects of three configurations. The comparison reported in Figure 27a shows that the FEMs with equivalent fixed boundary conditions would slightly over-estimate CAA, but could predict the TCA developed in the beams well. Comparing the FEMs with pin supports with the results of FEM with realistic boundary conditions, it was found that the pin supports simplification could simulate the CAA accurately, whereas it would underestimate TCA

significantly. Figure 27b shows the relationships of horizontal movement plotted against vertical displacement of adjacent joints from FEMs with different boundary conditions. Similar maximum outward displacements (negative values) and maximum inward displacements (positive values) were obtained from the FEMs with equivalent fixed conditions or realistic boundary conditions.

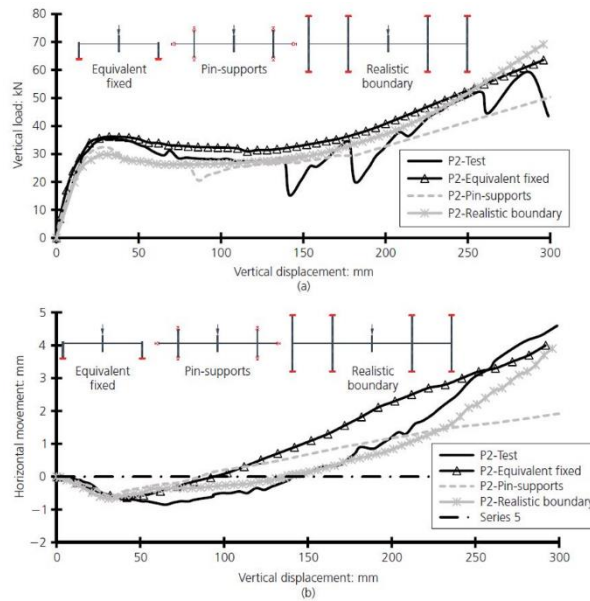


Figure 27: Influence of boundary conditions applied on the beam ends: (a) load–displacement curve; (b) horizontal movement plotted against vertical displacement (Qian, 2015)

Figure 28 shows the influence of the reinforcement ratio. For both the specimens, an increase of the beam longitudinal reinforcement improved the global behaviour in terms of initial stiffness, yield strength, FPL and ULC. However, observing the failure of beam–slab specimen S2, it can be noted that high longitudinal reinforcement ratio produces a more brittle performance. This was mainly due to concrete crushing in the compressive zone. By comparing these two series of specimens, it was found that the extents of slab effects on FPL and ULC decreased with increase of the beam longitudinal reinforcement ratio (Figure 29).

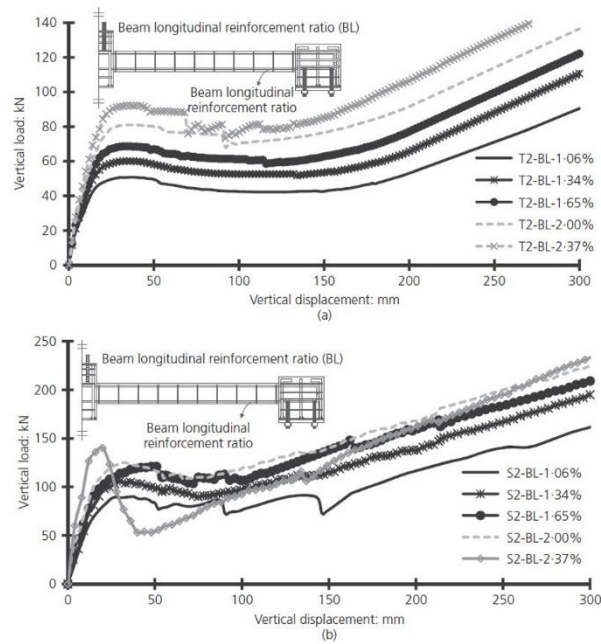


Figure 28: Influence of beam longitudinal reinforcement ratio on the response of test specimens: (a) specimen T2; (b) specimen S2 (Qian, 2015)

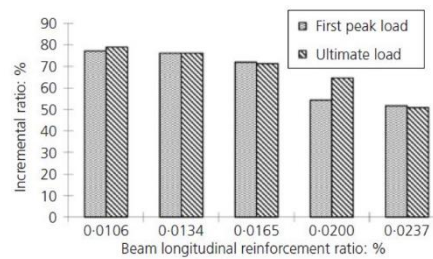


Figure 29: Slab effects on RC buildings with varying beam longitudinal reinforcement ratio (Qian, 2015)

As shown in Figure 30, for both the specimens, the increase of beam depth enhanced the initial stiffness and the yield strength. However, the force enhancement factor, defined as the ratio of FPL to yield strength, decreased with an increase of beam depth. Moreover, as shown in the figure, similar ULC was obtained even when the beam depth increased significantly.

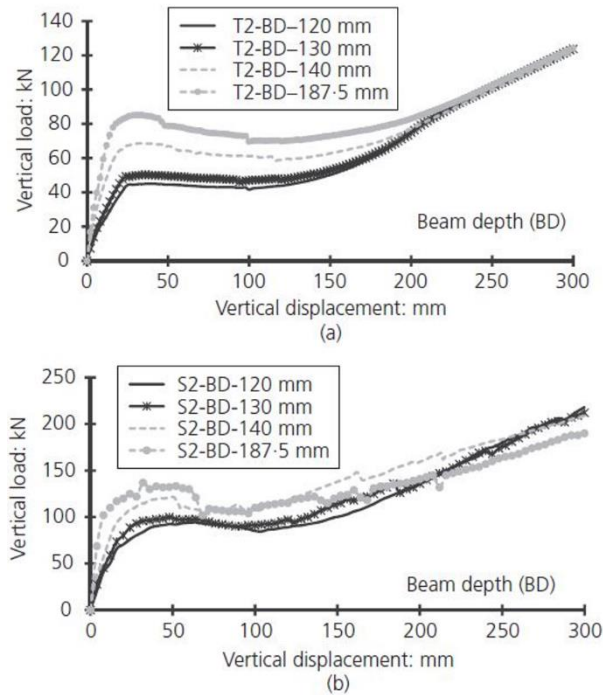


Figure 30: Influence of beam depth on the response of RC frames: (a) specimen T2; (b) specimen S2 (Qian, 2015)

The results reported in Figure 31 shown that the influence of slab effect decreased with the increase of beam longitudinal reinforcement.

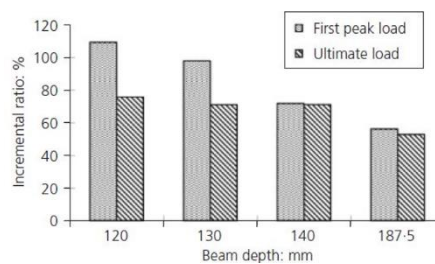


Figure 31: Slab effects on buildings with varying beam depths (Qian, 2015)

About the influence of slab reinforcement ratio on the response of beam–slab specimen S2. As shown in Figure 32, greater amount of reinforcement ratio increased the tensile membrane action, while it did not affect the compressive membrane action.

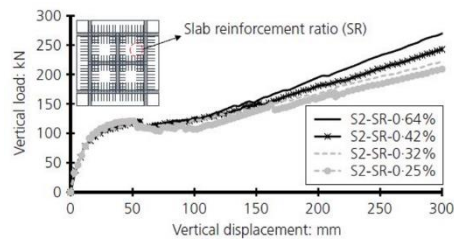


Figure 32: Influence of slab reinforcement ratio on the response of bare frames and beam–slab frames (Qian, 2015)

Figure 33 illustrates that greater percentages of slab reinforcement increased the ULC significantly, while no clear effects were seen on the FPL of the frame.

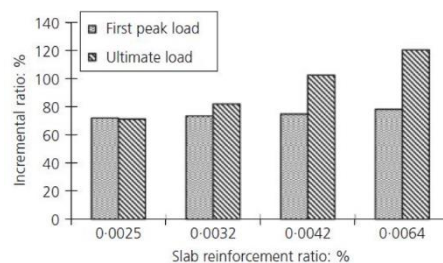


Figure 33: Slab effects on RC buildings with varying slab reinforcement ratio (Qian, 2015)

Figure 34 shows the effects of slab thickness on the response of beam–slab specimen S2. It can be noted that the FPL improved increasing slab thickness, while at the same time the ULC decreased. This was mainly due to the improving of compressive membrane action. However, the specimen with thinner slab was prone to deform and to form steel net at the large displacement stage.

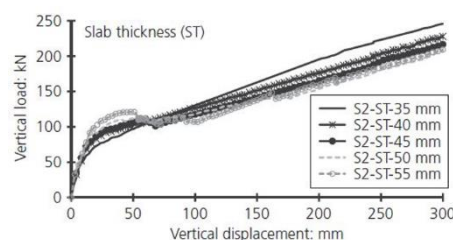


Figure 34: Influence of slab thickness on the response of bare frames and beam–slab frames (Qian, 2015)

The FPL improved significantly increasing the slab thickness, as shown in Figure 35. However, the extent of slab effects on ULC decreased with the increase of slab thickness.

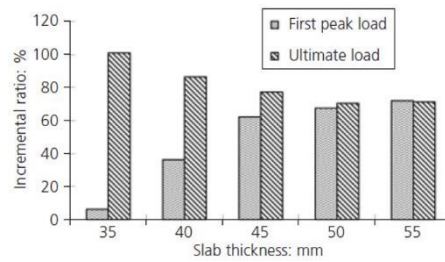


Figure 35: Slab effects on RC buildings with varying slab thicknesses (Qian, 2015)

2.6.3 Petrone et al., 2016

Part of the work described in this section was also previously published by Petrone et al. in 2016 (Petrone, 2016).

In 2016, Petrone developed a study about modelling of RC frame structures, to offer useful guidelines on simulation of these structures in the context of progressive collapse and alternate load path method (ALP) (Petrone, 2016). For this purpose, authors used a concrete moment resisting building frame (Figure 36) having plan dimensions 45m x 30m and story height equal to 4.6m for the 1st floor and 3.7m for the remaining floors. The study was developed with and without the incorporation of floor slabs to highlight the contributes provided by the floor system. The analyses were carried out using the software LS-DYNA (Hallquist, 2007). Primary beams and columns were modelled using Hughes–Liu elements with multiple integration points along the length and cross section integration by means of fibre discretization at integration points, while slabs were represented as layered shells with smeared reinforcement. Both material and geometrical nonlinearities, including damage and fracture, were considered.

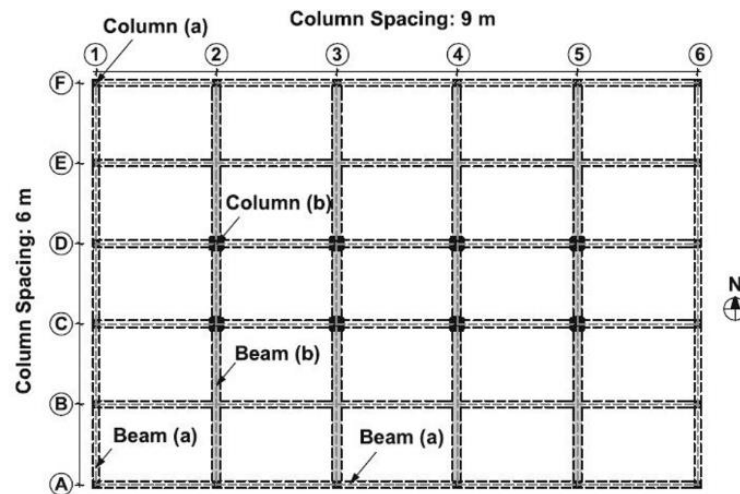


Figure 36: Plan view of the prototype frame (Petrone, 2016)

Authors underline the importance to carry out sensitivity studies with varying mesh sizes and integration points and examining the distribution of deformations and forces in critical element to achieve a reasonable balance between accuracy and computational efficiency. Another factor to be considered is the element discretization, since beams are deemed to be critical for the evaluation of the structural behaviour in response to the sudden loss of a vertical element. In addition, this aspect influences the length of the plastic hinge zones, whose formation is crucial for the development of catenary effect (Yi, 2008; Yi, 2014; Li, 2014).

To model the slabs directly not only allows to consider their contribution in the global structural response, but also permit to define more realistic alternate load path. Obviously, this is not possible in those models that does not consider explicitly the presence of the floor system. In their study, Petrone et al. have developed a sensitivity study about the gravity load distribution after a column removal comparing the results obtained considering or disregarding the presence of the slab. Authors found that the frame model with loads applied on the beams considerably overestimates the deflection of beams. Similar considerations can be done for vertical displacement. This was attributed to two factors: firstly, to distribute the gravity loads directly on the beams led to a concentration of loads in the plastic hinge zones and consequently to very large displacements after column removal, secondly, unlike models which incorporate slabs, frame models were unable to adequately account for alternate load paths and force redistribution after sudden column removals.

This study faced also the issue of slab modelling in finite element analyses. Efficient slab models are not commonly available in structural analysis software thereby prompting engineers and researchers to seek alternative schemes using available beam models. Previous studies (Nurhuda, 2004; Tian, 2012) have identified some configurations of beam grids suitable for the analysis of RC flat-plate structures. Sasani (Sasani, 2011) used a two-directional grid of beams (similar to Figure 37a) with modified torsional properties and an effective width to capture nonlinear effects in the slab region and reported satisfactory results. To verify the efficiency and accuracy of alternative modelling methods to simulate the contribution of slabs in progressive collapse analysis, the nonlinear response of some simplified grid beam models under gravity loads and column removal scenarios was investigated. The validity of four different grid beam configurations, as depicted in Figure 37, was verified by comparing their responses with the one obtained with a model that simulates the slab using layered shell elements with nonlinear material properties, considered as the exact solution.

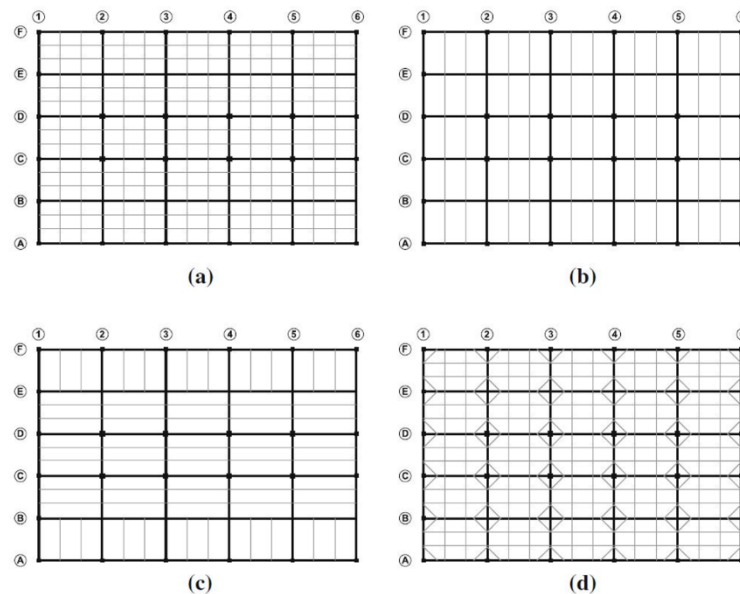


Figure 37: Beam grids to replace floor slabs: (a) beams in both directions, (b) beams in short direction, (c) mixed configuration, and (d) Case (a) with added diagonals (Petrone, 2016)

The configuration (a) had two-way grid beams, the authors tested the cases of 1, 3, 5, and 7 evenly distributed girders for each panel. In all cases grid beams were assigned the same depth and the same reinforcement ratio as the slab. Compared to the “exact” model defined above, the two-way grid beam model produced acceptable results in terms of axial forces under gravity loads, however the errors

in peak displacements ranged from 10 to 25 % (in the region of the missing column lines) and even larger errors were noted in predicting shear forces in the beams. Both the configurations (b) and (c) represented an attempt in redistributing loads on the main beams based on the column configuration and expected load transfer and both these configurations were evaluated for 3, 5 and 7 grid beams. The second configuration was that of one-way grid beams, along the short direction. When tested under gravity loads, this configuration with 7 grid beams in each panel gave acceptable approximations of both resultant forces and displacements. However, when evaluated for the scenario involving a column removal, the errors were significant (with displacements being overestimated by a factor of 3 or more). Likewise, the third configuration, wherein one-way grid beams run in the short direction in the exterior panels and in the long direction in the interior panels, was also unsatisfactory in predicting either displacements or internal forces to an acceptable degree. The configuration (d) was a modification of the configuration (a), where elastic diagonals were added at the corners of the panels. The overall arrangement of the grid beams was conceived with the idea of reproducing in each panel the distribution of bending moments and the formation of yield lines observed in slab panels. Though this configuration provided the best estimates of displacement, the model was incapable of reproducing correct internal forces. This part of the study demonstrated the difficulty in simulating true slab effects using a grid of beams. While calibrating the stiffness properties of the beams to produce acceptable results under gravity loads appeared feasible, the task of recalibrating the models for each successive column removal made this approach unreliable and unfeasible.

Chapter 3

Software validation

3.1 Introduction

The research activity was based on the use of different finite element software, widely diffused in the structural scientific field. These codes simulate the structural behaviour evolution, by considering the nonlinear response of the damaged structure. As mentioned in previous sections, one of the most common strategies to assess the structural robustness of a building is the notional element removal. This technique presents several advantages, including that of being scenario-independent. Following this approach, generally the designer assumes that, whatever is the cause of the damage, the effect is the loss of a main structural element. In particular, Eurocode 1 part 1-7 states that the check of the structural stability must be carried out by removing, one at a time, each column and/or each beam supporting a column.

Under these conditions it is evident that the element removal implies a drastic change in the static scheme, especially in the region adjacent to the damaged area. The only way for the structure to withstand the external loads, is to exploits all the resistance resources available. This means to activate complex mechanisms whose effects generally, on the safety side, the designer does not consider in the design phase but which can be exploited in ultimate conditions. To do this, the structure must satisfy several requirements, in terms of ductility, hyperstaticity, presence of continuous reinforcement in the beams, etc...

That described above, it is useful to understand the complexity of the issues and the difficulties encountered by software in simulating the structural behaviour evolution. To study the phenomenon, it should be referred to finite element codes able to develop nonlinear analyses considering both the material inelasticity and the geometric nonlinearity. It should also be emphasized that in the study of these issues, the dynamic aspect is of particular relevance, for this reason in some cases it is necessary to refer to nonlinear dynamic analyses.

The complexity of the analyses to be carried out therefore requires a validation and calibration procedure of the software used. For this purpose, several experimental tests, available in literature and considered suitable to be numerically implemented, were chosen and simulated. The validated software were: SeismoStruct 2016 (Seismosoft, 2016) and DIANA v.10.1 (DIANA, 2016). The following paragraphs presents the results of the validation procedure.

3.2 TNO Diana v.10.1

This software was used in a first phase to evaluate the influence that the floor systems (e.g. concrete slab) have on the overall structural behaviour.

To develop a finite element model which considers the slab contribution is an onerous operation from the analytical point of view. This choice implies an exponential increase of the number of elements used to discretize the structure, resulting in rather long analysis times, including pre-processing and post-processing.

Once the role played by these elements has been evaluated, different simplified models have been proposed and tested to identify workable solutions able to properly reproduce the slab contribution and, at the same time, to limit the computational costs resulting from this choice.

For this purpose, it was chosen to use the software DIANA v.10.1 through which nonlinear static analyses were developed, using both beam that shell elements.

The validation was carried out by using the results of the research carried out by Qian (Qian, 2015) previously described in paragraph 2.6.2. This work summarises the results of a study on the contribution offered by slabs in the assessment of the robustness of a reinforced concrete building, after the failure of a column. In particular, the authors carried out several experimental tests on 1/4 scale whose results, in terms of load-displacement diagrams, were compared to the ones obtained by means of several FEM simulations carried out by the same authors by using DIANA software. However, such models have been developed by using shell elements to model the slabs and brick elements for the beams. Although the obtained results are rather accurate, they are not applicable to complete building models due to the associated computational burdens.

For this reason, simplified models have been developed, in particular the elements used are the following:

- Beam elements “CL9BE” to model the beams in P-series tests;
- Beam elements “CL18B” to model the beams in T-series and S-series tests;
- Shell elements “CQ40S” to model the slab in S-series tests.

Figure 38 shows an illustration of the elements and the respective interpolant functions.

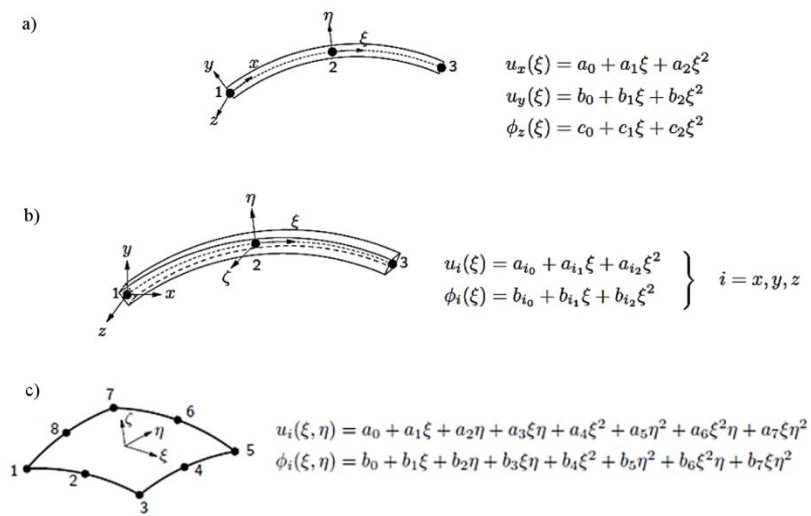


Figure 38: Diana finite elements and interpolant functions: a) CL9BE, b) CL18B, c) CQ40S

The selected beam elements are class-III elements, based on an isoparametric formulation which assumes that displacements and rotations of the beam axis normals are independent and are interpolated from the nodal displacements and rotations. The overall response of the elements is obtained numerically integrating over their cross-section and along their axis. These elements are based on Mindlin-Reissner theory, and consider the shear deformations through the thickness of the element. The stiffness matrix will then consist of two contributions, one related to bending moment and another related to shear.

The elements are curved, which means that they have a number of nodes greater than two (in this case three) and the interpolating functions are second order ones or higher.

The shell elements are also curved and represent a degeneration of the three-dimensional elements, assuming the following assumptions:

- The normals to the mean surface remain straight even after the deformation (but not necessarily normal to it);
- Shear deformation is calculated according the Mindlin-Reissner theory;
- The normal stresses at the mean surface are null.

The coupling between shell and beam elements has been solved as follow: having the slab and the beam distinct centroids, it was chosen to represent both the elements at the level of the mean surface of the slab, by associating to the beam elements a rigid link simulating the eccentricity between the centroids, as shown in Figure 39. In this way it was considered a perfect bond between the beam and the slab. The eccentricity adopted allows to properly consider the actual mechanical properties of the elements, simulating the plane section conservation principle.

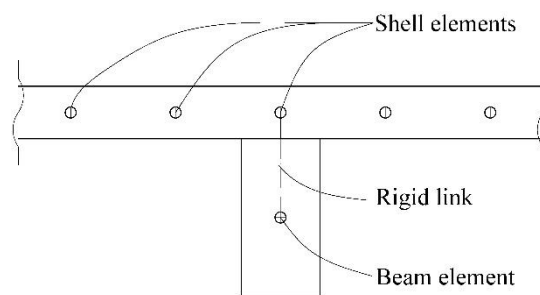


Figure 39: Shell-beam elements coupling

In addition, for S1 and S2 models, it was exploited the double symmetry of the specimens by modelling only one quarter of the structure, appropriately restraining the symmetry axes. In particular by preventing rotations and horizontal displacements along the axes of symmetry (u_x and ϕ_y for symmetry axis A shown in Figure 40, u_y and ϕ_x for symmetry axis B shown in Figure 40). In this way it was possible to reduce the mesh element size without excessively increasing the analysis time.

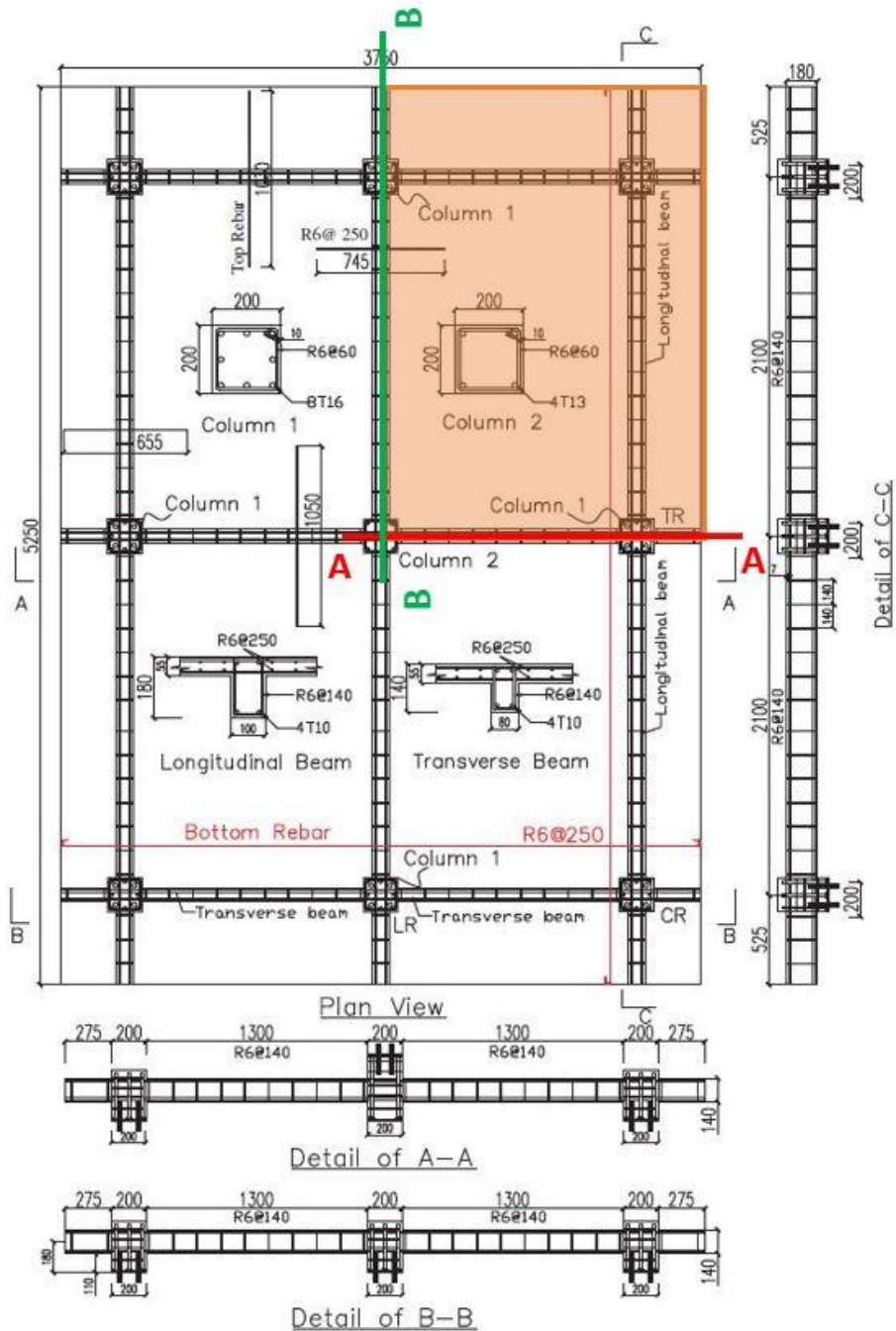


Figure 40: Structural portion of specimens S1 and S2 modelled in DIANA

About the materials, concrete behaviour was simulated considering the following hypotheses: the compressive behaviour was defined by Model Code 1990 (CEB, 1993) and shown in Figure 40; the response under tensile stresses was considered as linear elastic up to the reaching of the maximum stress allowed f_t ; after

this point the stress-strain relation was simulated with a linear softening branch. In particular, the tension softening law adopted for the concrete subjected to tension is the one defined by the CEB-FIP Model Code 1990 (CEB, 1993). The tensile concrete behaviour in the post-cracking phase was defined on the basis of the evaluation of the Mode-I fracture energy G_f^I and the definition of crack bandwidth h . For beam elements the default crack bandwidth was the length of the element, calculated as V/A where V was the volume of the element and A was the average cross-sectional area of the beam. The combinations of a small Mode-I fracture energy G_f^I and a large crack bandwidth h may lead to a decreased tensile strength f_t , in this case the software shown a warning that allowed to check the accuracy of the procedure. The software allowed also to overwrite the crack bandwidth to avoid an excessive reduction of the tensile strength. The fracture was given by:

$$G_f = G_{f0} \cdot \left(\frac{f_{cm}}{f_{cm0}} \right)^{0.7} \quad (13)$$

Where:

$f_{cm0} = 10$ MPa, $f_{cm} = 25$ MPa, G_{f0} is defined as a function of the maximum aggregate size, in particular in this case the maximum aggregate size was 16 mm, then $G_{f0} = 30 \text{ J/m}^2$. Considering these values, G_f was considered equal to:

$$G_f = 30 \cdot \left(\frac{25}{10} \right)^{0.7} = 57 \text{ J/m}^2 \approx 0.06 \text{ N/mm} \quad (14)$$

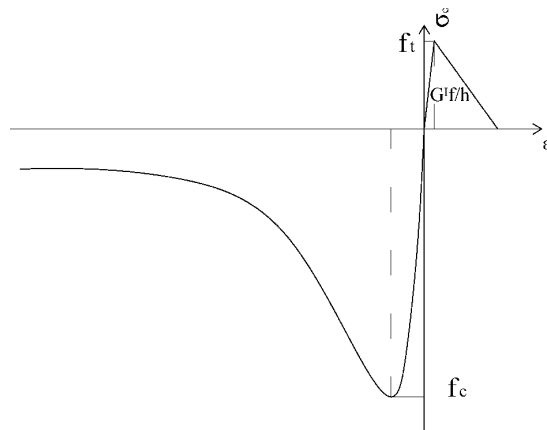


Figure 41: Concrete behaviour according to CEB-FIP Model Code 90 (Graph not in scale)

The cracking behaviour was modelled according to the total strain rotating crack model (Vecchio, 1986), in which the stress-strain relations are evaluated in

the principal directions of the strain vector. This approach is well suited for reinforced concrete structures. The basic concept of the Total Strain crack models is that the stress is evaluated in the directions which are given by the crack directions. The only status parameters are the maximum tensile and compressive principal strains that are ever reached in the integration point.

About the steel reinforcements, it was considered a perfect bond between concrete and steel bars, assuming that the concrete and reinforcements detailing (e.g. anchorage length l_{bd} , reinforcement hooks, concrete confinement, etc...) allows to consider a perfect bond between the materials. The constitutive law adopted for the bars was a bilinear one with a hardening branch, it was defined in accordance with the experimental data reported by the authors. The criterion adopted to combine the stresses was the one defined by Von Mises.

During the validation phase, specific attention was paid to the definition of the boundary conditions. Figure reports a zoom of the devices adopted to restrain the specimens including the tension/compression load cell.

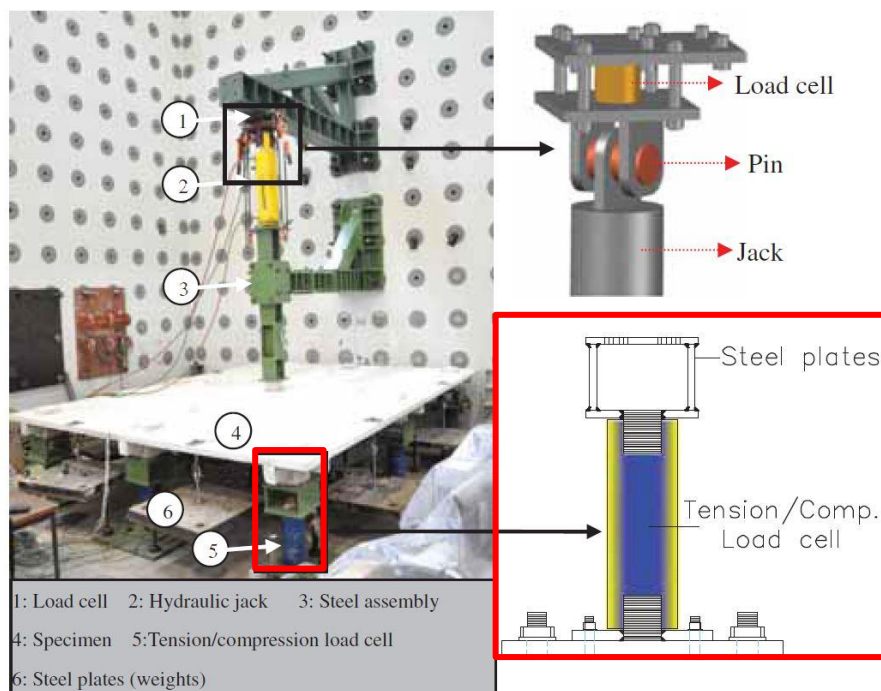


Figure 42: Restraint device and tension/compression load cell (Qian, 2015)

By analysing the experimental data, it was chosen to develop the restraint device shown in Figure 43:

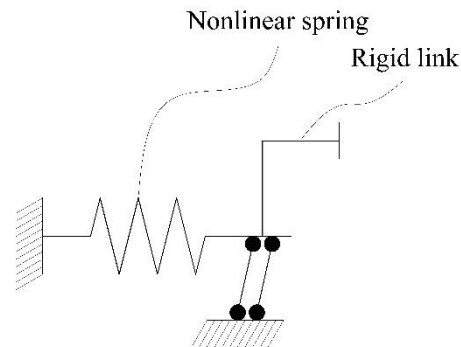


Figure 43: Constraint system adopted to simulate the actual boundary conditions

This device is based on the coupling between a full restraint and a double pendulum by means of a nonlinear elastic spring having different behaviour in compression and tension. The double pendulum in turn is connected to structure by means of a rigid link simulating the eccentricity between centroids of the elements and the point of application of the restraint (the strong floor of the laboratory). The nonlinear spring was set to be stiffer in compression (comparable to a perfect bond) and more deformable in tension (depending on the type of connected elements). This choice is due to the non-perfect behaviour of this kind of constraints subjected to increasing tensile stresses. The calibration of the spring was based on the experimental results provided by Qian et al. In conclusion the system adopted completely prevents the rotations and the translation in vertical direction, leaving certain margins to the horizontal displacements, particularly those associated with traction stresses. Table 8 shows the stiffness values adopted for nonlinear springs.

Table 8: Stiffness adopted for nonlinear springs

Element	Stiffness [N/mm]	
	Compression	Tension
Longitudinal beam	3.0E+08	3.0E+03
Transversal beam	3.0E+08	3.0E+03

Figure 44 reports different views of the finite element models. The mesh size is variable for the models but is in the range between 3 and 5 cm, both for beam and shell elements. The mesh independence was evaluated before of the development of the analyses.

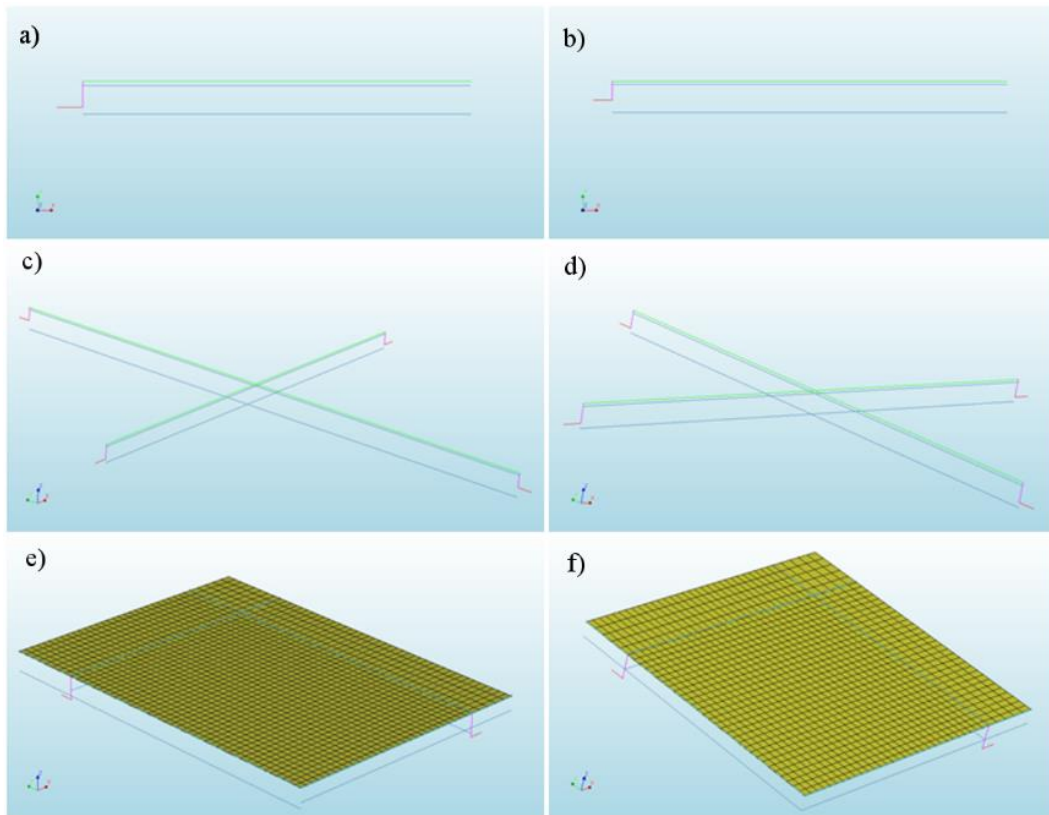


Figure 44: Views of the finite element models: a) Specimen P1, b) Specimen P2, c) Specimen T1, d) Specimen T2, e) Specimen S1, f) Specimen S2

The analyses were carried out considering both the material inelasticity and the geometric nonlinearity, including the large displacements effects. The tests were conducted by applying a linear vertical displacement in the midspan of the specimens. The load was applied through 60 identical load steps. After a calibration procedure it was chosen to apply the displacement with steps of 5mm, the analyses end if within a predefined number of iterations, at each degree of freedom of the structure, the value of the displacement is greater than the tolerance specified. The convergence criterion is based on the displacements control, in particular it was defined a tolerance of $2E-02$. The iteration method is the one defined by Newton-Raphson. Finally, it was checked the ultimate strain in the materials in order to stop the analyses if one of the materials exceeded this parameter. During the tests the trend of the total vertical reaction was monitored, in order to compare these values with the experimental results on the basis of Load-Displacement curves. Figure 45

shows the results obtained through numerical simulations, while Figure 46 illustrates, as an example, the deformed shapes of three models.

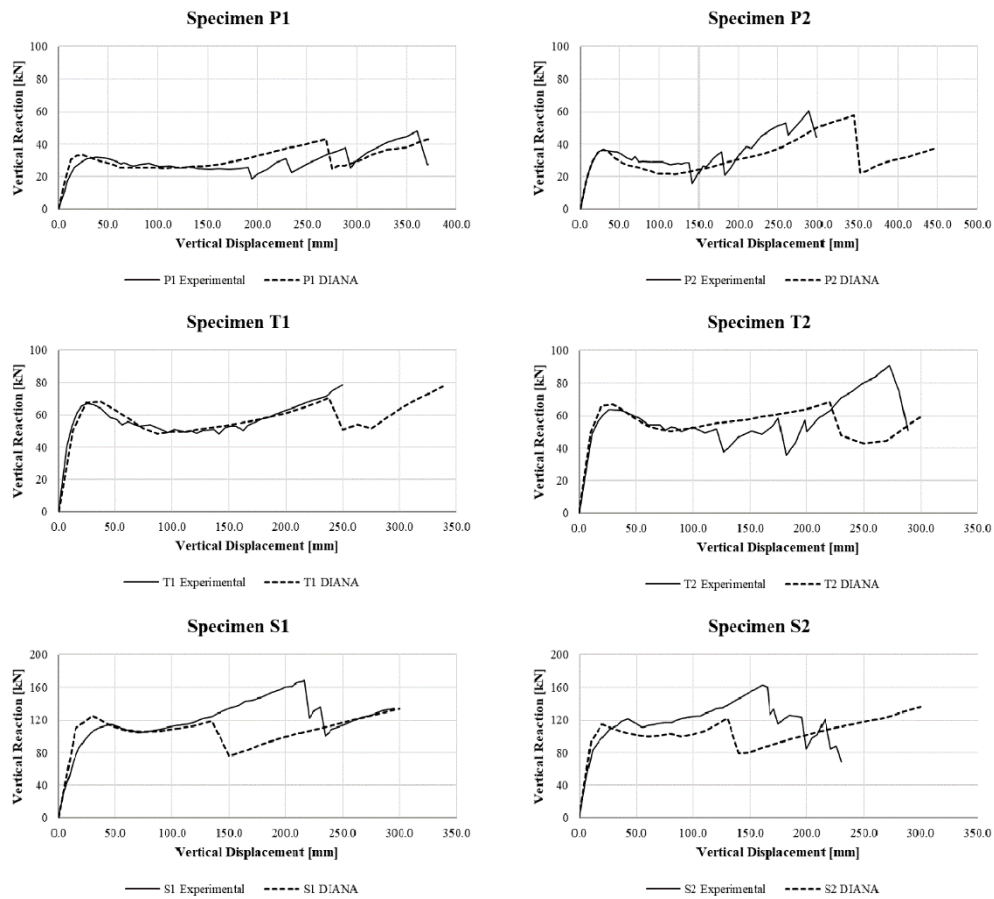


Figure 45: Comparison between experimental and numerical results: a) Specimen P1, b) Specimen P2, c) Specimen T1, d) Specimen T2, d) Specimen S1, e) Specimen S2

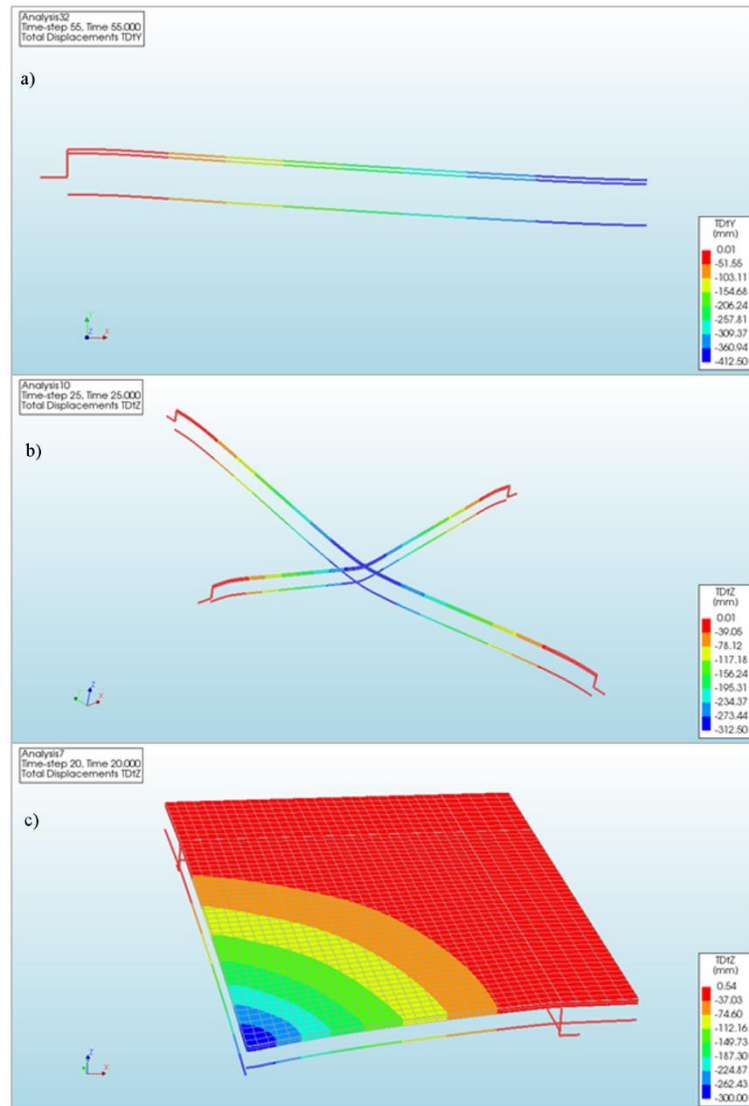


Figure 46: Deformed shapes of the finite element models: a) Specimen P2, b) Specimen T1 and c) Specimen S1

The analyses performed showed a good correspondence between experimental data and numerical results. In detail, it can be noticed that the models were able to simulate appreciably the first part of the curve, both as regards the stiffness of the specimens and the flexural peak.

The models showed a good response also in the second part of the analyses, characterized by the yielding of the beam reinforcements in top regions placed near the external columns and in the bottom region near the central column (in correspondence of the application point of the vertical displacement). The software

was able to replicate also the subsequent softening phase, recorded experimentally. For higher vertical displacements, it should be noted that the models were capable to simulate the increase of the bearing capacity due to the catenary action.

In general, the models were able to accurately predict the ultimate load, especially for P1, P2, T1 and S1 specimens. However, there was a greater difficulty in predicting the corresponding vertical displacements. It is noted that in the presence of large displacements, the analyses showed a certain gap if compared with the experimental data. The numerical models seem to anticipate the experimental response, this condition was evident observing the results obtained for P1, T2, S1 and S2 specimens.

It should be noted that the numerical models of P1, S1 and S2 specimens, although they capture the flexural peak loads, they are not able to correctly reproduce the progressive softening that occurs experimentally. This behaviour is due to a diffused cracking of the specimens that the numerical models can reproduce only partially. This cracking is also due to a spatial variability of the concrete strength that the numerical models cannot reproduce.

In conclusion it can be stated that DIANA models were able simulate the experimental behaviour with a high degree of approximation. Therefore, the validation procedure was successfully completed.

3.3 SeismoStruct 2016

Part of the work described in this section was also previously published by Bertagnoli et al. in 2016 (Bertagnoli, 2016a).

SeismoStruct is a finite element software for structural analysis, able to predict the behaviour in large displacements of three-dimensional framed structures subjected to both static and dynamic loads, by considering both geometric nonlinearity and material inelasticity. The validation of this software therefore involved both static and dynamic tests.

3.3.1 Nonlinear static analysis validation

The validation of nonlinear static analyses was carried out by referring to the test previously described in section 2.5.1. Figure 47 shows the vertical layout of the specimen with cross section details and instrumentation arrangement.

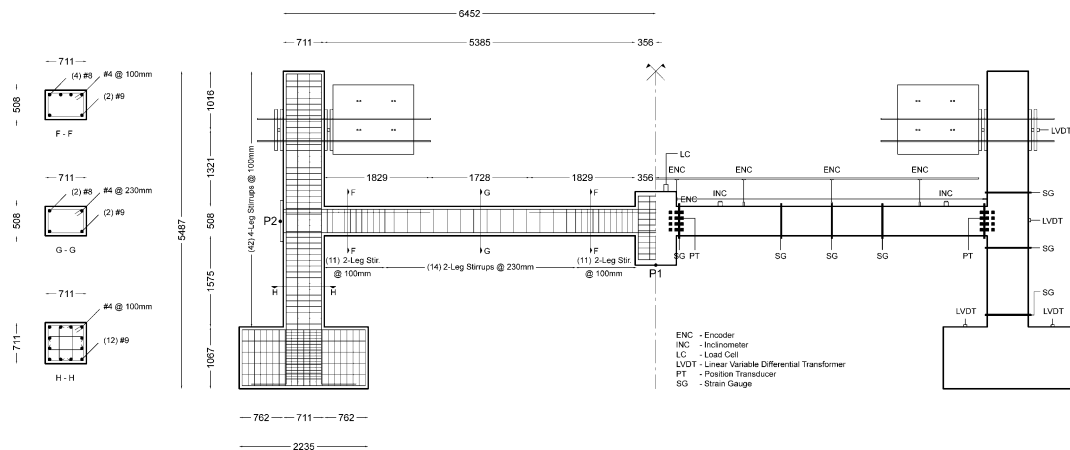


Figure 47: Vertical layout of the specimen with cross section details and instrumentation

SeismoStruct models were characterized by force-based fibre beam elements named “infrmFB” (Spacone, 1996; Neuenhofer, 1997) to represent beams and columns. These elements, able to capture the inelastic behaviour along their entire length, exploited cross section integration with each integration point assigned to a discretized cross-sectional geometry component defined as “fibre”; the sectional stress-strain state was obtained through the integration of the nonlinear uniaxial material response of the individual fibres in which the section was subdivided, considering the spread of inelasticity along the member length and across the section depth. After a software calibration procedure, the fibres number for each section and the number of integration sections for each element were set as follow: 150 for the former, and 5 for the latter.

This choice was suggested by the possibility to consider both the geometrical and mechanical nonlinearities. The formers include large displacements or rotations and large independent deformations relative to the element's chord, also known as “P-Delta” effects (Correia, 2006); the manners are implicitly considered by associating at each fibre, in which the section is discretized, the constitutive law chosen for the specific material. Figure 48 shows a layout of the finite element model with cross section discretization.

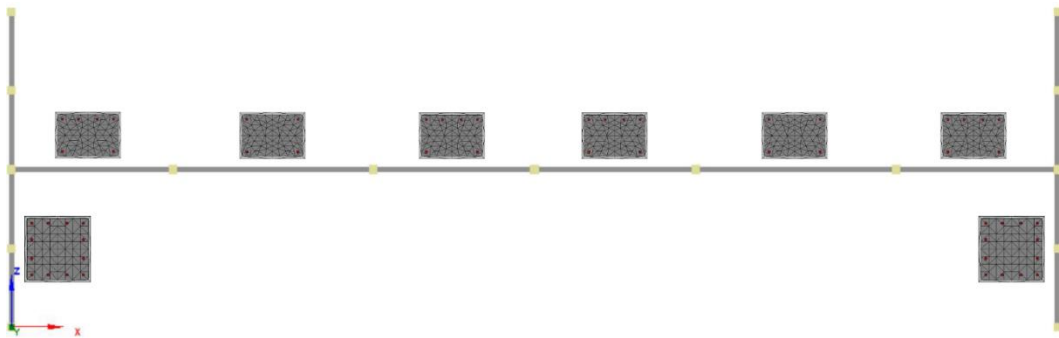


Figure 48: Layout of SeismoStruct finite element model with cross section discretization

About the materials, Figure 49 and Figure 50 show the concrete constitutive laws adopted. Two different concrete models available in the software's library were tested: the first one was suggested by Mander (Mander, 1988), while the second one was the concrete complete model proposed by Chang and Mander (Chang, 1994). The steel adopted for reinforcements exploited a uniaxial bi-linear model with a hardening branch, as shown in Figure 51.

As mentioned previously, SeismoStruct models exploited one-dimensional elements, therefore the concrete confinement was considered indirectly modifying concrete parameters. As it is known, the confinement changes considerably the compressive behaviour of concrete, for this reason it was chosen to test different confinement levels to evaluate the difference in terms of structural response. Table 9 shows the confinement level adopted for each model. About the cracking behaviour, all the models considered the smeared crack approach.

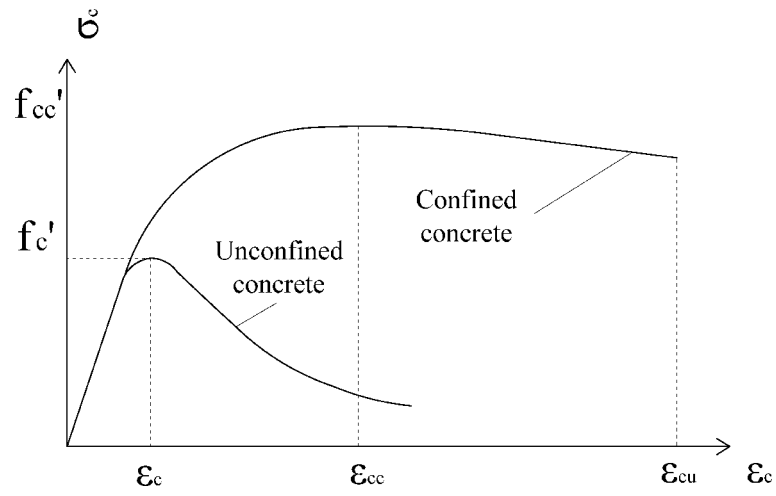


Figure 49: Concrete constitutive law proposed by Mander

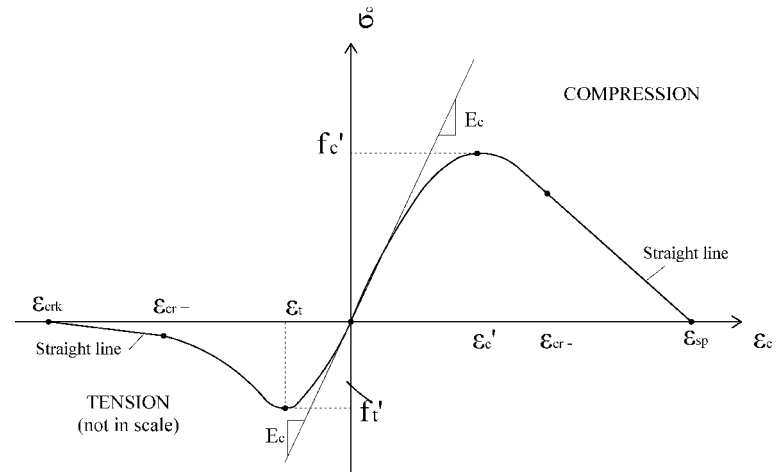


Figure 50: Concrete constitutive law proposed by Chang and Mander

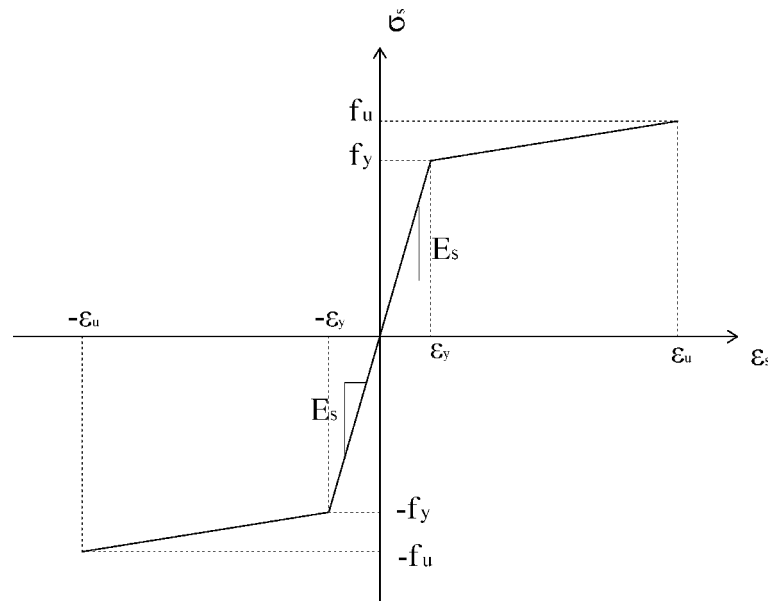


Figure 51: Steel bilinear constitutive law

Table 9: Configuration of the tests

ID	Constitutive law	Confinement level	ID	Constitutive law	Confinement level
MA1	Mander	MRV ¹	CM1	Chang-Mander	CMRV ²
MA2	Mander	1.1·MRV	CM2	Chang-Mander	1.1·CMRV
MA3	Mander	0.9·MRV	CM3	Chang-Mander	0.9·CMRV

^{1,2} MRV and CMRV are respectively the reference values calculated according to Mander's and Chang-Mander's formulations

The static nonlinear analyses were carried out by dividing the test in 120 steps, each loading step corresponded to an increase of the displacement of 10 mm. The solver used the Skyline method which provided better numerical stability, despite being slower. The convergence criterion was based on displacements/rotations.

The structural response was investigated by monitoring the following parameters as a function of the displacement of the central point (P1 shown in Figure 47): the applied load by the jacks and the horizontal displacement of the left end of the beam (Point P2 shown in Figure 47). Figure 52a and Figure 52b shows the results obtained, compared with the experimental data.

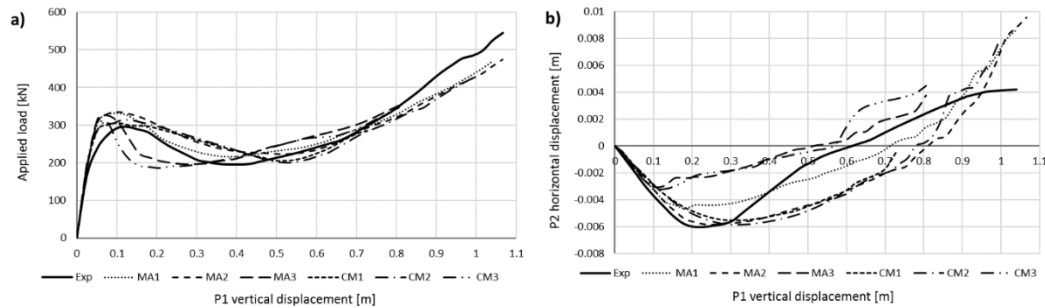


Figure 52: Comparison between numerical results and experimental data

The experimental behaviour in the initial loading phase can be considered linear elastic until the reaching of about 70% of the flexural peak. An interesting consideration can be done about the displacement of point P2: in this stage in fact a negative variation of this parameter (thus point P2 is directed towards the outside) can be observed. Monitoring the axial force, it can be found that the beams are in compression. This condition is due to cracking that causes an increase of the beam length, partially prevented by the presence of the end columns. The numerical models developed can simulate this phase with a good approximation; however, they are all stiffer than the experimental frame. There is in fact a loss of accuracy in the actual progressive cracking.

Increasing the displacement, the experimental measurements highlighted the overcoming of the yielding strain of the bars in the zones close to columns and in particular: in the top region of beams near lateral columns, because of the negative bending moment, and in the bottom region of beams near the central column, due to the positive bending moment. Considering SeismoStruct results: the maximum flexural load was better approximated by CM1 (+4%), while the corresponding MA1 showed a greater gap (+12.5%) between numerical and experimental results. Up to this point, the confinement did not influence the results significantly.

By applying increasing displacements, the specimen showed a post-peak behaviour characterized by an initial softening phase, followed by a second stage marked by the increase of the applied force. Clearly in this stage, the slope of Force-Displacement curve, which can be interpreted as a measure of the system stiffness, was lower; cross-section performances were being degraded progressively due to cracking and localized steel yielding. The recovery of bearing capacity was due to the “catenary action” arisen in the beams, as confirmed by the trend of the horizontal displacement which was negative until reaching a vertical displacement of about 0.50m and become positive because of the catenary action.

Focusing on the trend of the applied force, it can be noted that, for subsequent vertical displacements, initially the load decreased until the horizontal displacement of point P2 went close to 0m; monitoring the axial force, in this step beam compression decreased progressively. Then, when the displacement became positive, the axial force in the beams switched to tension and the applied load increased. At this stage, the change from the flexural to the tie-behaviour was observed; this trend remained up to the failure reached in correspondence of a vertical displacement of about 1.10m. About the numerical results: MA1 model matched better the evolution of the applied force in function of the vertical displacement of point P1, while CM1 model showed a greater stiffness reduction than the experimental one. Unlike the previous step, results were influenced by the concrete confinement: a reduced softening effect was related to higher confinement levels and vice versa. As regards the trend of the horizontal displacement of point P2, no model was able to properly reproduce the different phases of the post-peak behaviour. This could be explained by the fact that all the models referred to a smeared cracking approach, hence they were not able to capture completely the localised damaging occurred experimentally (e.g. few cracks with significant opening). About SeismoStruct models it can be observed that MA1 curve changed the displacement trend at the correct load level but was not able to reach the maximum value. Vice versa CM1 model reached the maximum value but was not able to change the trend at the correct load level. In this case the confinement played a significant role.

In the last phase, considering the behaviour shown in Figure 52a all the SeismoStruct theoretical curves were very close together and in general underestimated the experimental load values. However, the overall behaviour was still reproduced with a good approximation, unlike what shown in Figure 52b where all the curves were very different from each other and in any case, were far from the experimental one. It is important to highlight that, to exploit the catenary action, the strain reinforcements reached very high values. In this case, the ultimate strain of the steel greatly influenced the results.

By analysing the trend of the strains/stresses in reinforcements for increasing vertical displacements, up to about 65cm it can be noted that the equilibrium was guaranteed by means of the beam rotation that causes the increase of the strains in the materials as shown in Figure 53. After this point, the most stressed sections were no longer able to rotate further as the external fibres reached the ultimate strain. It therefore happened that, for further vertical displacements, the increase of load-

bearing capacity was obtained by extending the length of the zones affected by the plasticization.

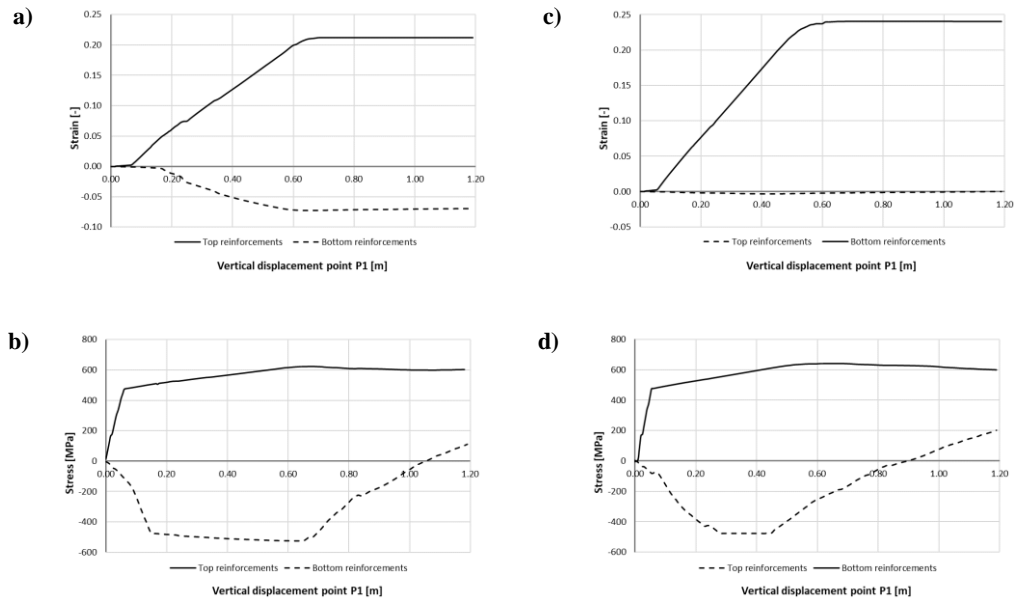


Figure 53: Strain-displacement and stress-displacement curves for the beam reinforcements near the external column (a, b) and near the central column removed (c, d)

Summarising the results obtained from the different numerical models in this step, it can be observed that SeismoStruct models were able to replicate correctly the experimental behaviour by means of nonlinear static analyses. Hence the validation was successfully completed.

3.3.2 Nonlinear dynamic analysis validation

The validation of nonlinear static analyses was carried out by referring to the experimental tests developed by Pham and Tan in 2017 at Nanyang Technological University, Singapore (Pham, 2017).

Specimens consisted in a portion of an actual 2D frame. In particular they were double span beam-column assemblies composed by: external columns, main beams (including two portions of them placed beyond the columns to replicate the actual continuity of the reinforcements at the nodes and to apply boundary conditions closer to the actual ones) and a middle joint in correspondence of the central column, which was the one to simulate the dynamic removal. Figure 54 shows a layout of the specimen:

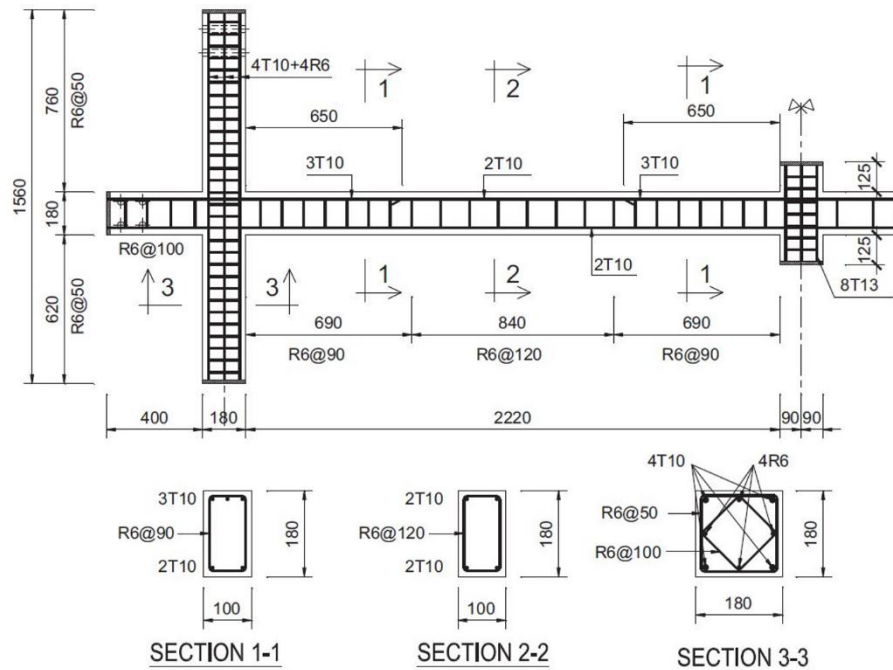


Figure 54: Specimen layout with cross section details (Pham, 2017)

Specimens were realized with a concrete having a cylinder strength of 35 MPa, about reinforcements: high strength deformed bars were used for longitudinal reinforcements while the stirrups were realized with mild steel round bars. Table 10 summarises the specimens' parameters and the material properties.

Table 10: Specimens parameters and material properties

Specimen	Concrete cylinder strength (MPa)	Applied load (kN)
FD1/1	35	20
FD1/2	35	29
FD2	35	34

Reinforcement	Diameter (mm)	Yield strength f_y (MPa)	Elastic modulus (GPa)	Tensile strength f_u (MPa)	Ultimate strain (%)
R6	6	352	220	539	19.2
T10	10	554	196	653	11.5
T13	13	535	188	615	8.5

As shown in Figure 54, the beams were reinforced with continuous bottom bars along the double span, while top reinforcements were reduced at curtailment points

located at 650 mm from the edges of the column. The length of the columns and of the external beams were chosen to coincide with the contra-flexural points of the complete 2D frame, this solution allowed to simulate the actual boundary conditions by means of the use of pinned supports and horizontal restraints. Figure 55 shows the test setup:

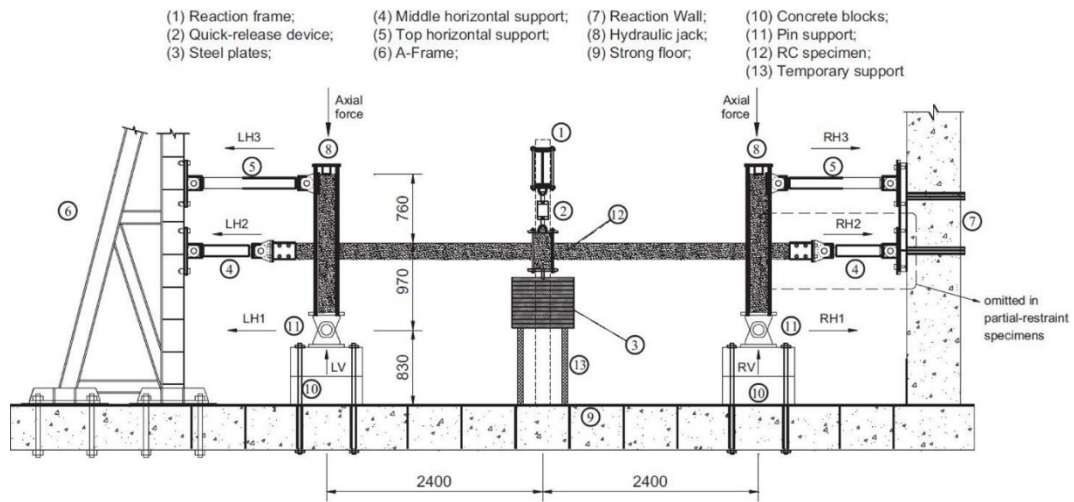


Figure 55: Test setup (Pham, 2017)

As illustrated in Figure 55, the external columns were preloaded by using steel rods and hydraulic jacks, to simulate the axial force acting in the actual frame, coming from the gravity loads due to the above floors.

A different system was used to apply the load to central column. In this case in fact, to evaluate the dynamic effects produced by the sudden column removal, the applied load was simulated by means of steel plates placed on a temporary support and linked to a quick release device. Figure 56 shows the loading system and a detail of the quick release device.

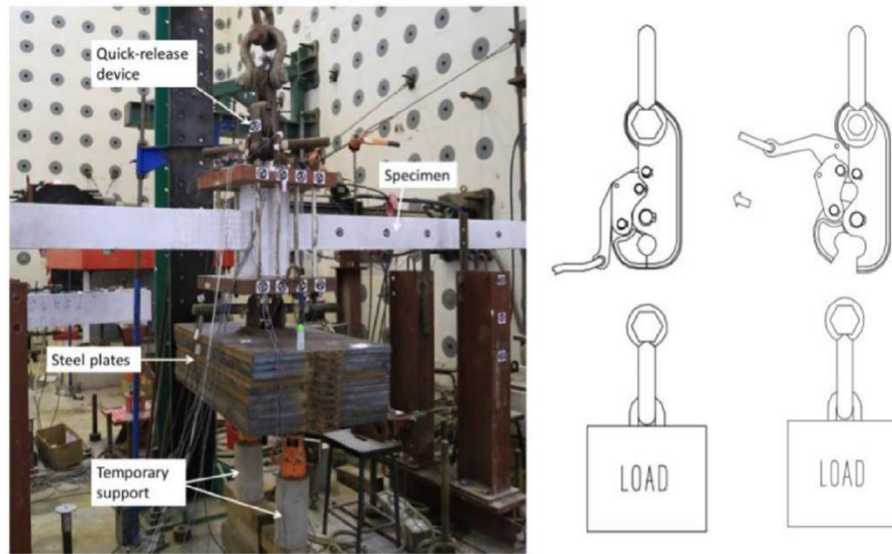


Figure 56: Loading system and quick release device (Pham, 2017)

It should be noted that FD1 specimen was tested dynamically twice: the first release characterised by an applied load of 20 kN, caused only limited damages (e.g. minor cracks in the bottom region of the beams near the central column and in the top region near the external columns). The second release had an applied load of 29 kN, this caused large vertical deflections, developing the catenary action in the beams and fracturing a beam bottom rebar near the central column. About FD2 specimen, this was loaded once, because the applied load of 34 kN caused the collapse of the specimen hitting the strong floor of the laboratory.

About the instrumentation, the reactions were measured by means of load pins and horizontal load cells, while linear variable displacement transducers LVDTs and line transducers were installed along the beams to record displacements and deformations. The dynamic data were recorded with a sampling rate of 1000 Hz, to measure the in-plane displacements were used two additional slow-motion cameras able to capture the deflection of marked points at a rate of 240 fps.

The finite element models built to simulate the experimental behaviour used “InfrmFB” elements, they were the same adopted in the previous case. After a software calibration procedure, the fibres number for each section and the number of integration sections for each element were set as follow: 150 for the former, and 5 for the latter.

About the materials, Figure 49 and Figure 50 show the constitutive laws adopted for concrete and steel respectively: the concrete complete model proposed by Chang and Mander (Chang, 1994) and the uniaxial bi-linear model with hardening branch for steel.

The dynamic nonlinear analyses were carried out by dividing the total duration of the test of 4s in 1600 steps, then the time step was of 0.0025s. The solver used the Skyline method which provided better numerical stability, despite being slower. The convergence criterion was based on displacements/rotations. Finally, having to use a direct numeric integration technique to solve the system of motion equations, the Hilber-Hughes-Taylor algorithm was chosen.

In the finite element analyses the dynamic release of the load was simulated by means of a temporary element that connected the load application point to a fully restrained node. Following this solution, at time t_0 the applied external load was transferred to the strong floor through the temporary support. At time t_1 this element was suddenly deactivated, activating the free-fall dynamic test and transferring the external load directly to the beams. Figure 57 shows a view the finite element model.

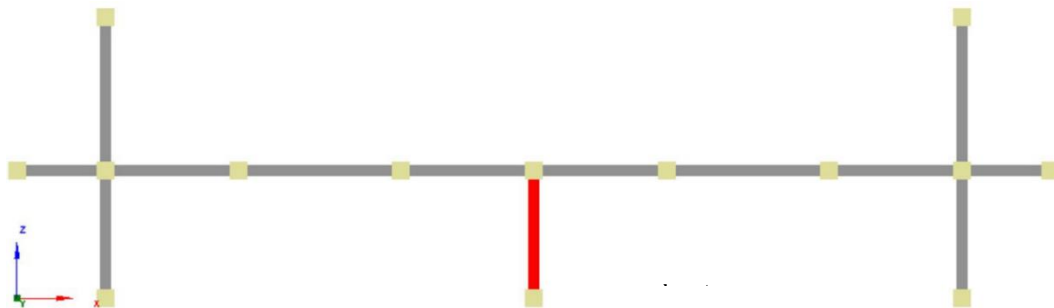


Figure 57: Finite element model adopted for nonlinear dynamic analyses validation

The structural response was investigated by monitoring the following parameters in function of the time: the displacement of the middle joint, the total vertical reaction and the total horizontal reaction of the left side of the specimen. Figures 55a-f show the results obtained, compared with the experimental data.

The experimental behaviour can be summarized as follow: after the removing of the temporary support, the system exhibited an initial increasing vertical displacement up to the reaching of an equilibrium configuration. Once this

condition was found, the frame oscillated until the inherent damping of the structure reduced the oscillations up to zero.

Depending on the magnitude of the applied load, the equilibrium condition was reached for progressively larger displacements and at different time: about 1.0s for FD1 and 0.8s for FD2 as shown in Figure 58a and Figure 58b. However, the FD2 specimen collapsed hitting the strong floor, then this result cannot be considered as effective.

The trend graphed in Figure 58c and Figure 58d highlights that, after an initial transition phase in which the specimen was deforming progressively, the total vertical reaction showed big amplitude oscillations around the equilibrium condition.

The loads applied in both FD1 and FD2 cases produced a bending moment greater than the flexural capacity of the double-span beams, then plastic hinges developed at the end of these elements causing their rotation to find an equilibrium condition by means of the exploitation of catenary action. An evidence of this was given by the trend of horizontal reaction. Observing the graphs of Figure 58e and Figure 58f it can be noted that after the initial transition phase in which the beams were in compression, the axial force switched to tension activating the catenary action.

The numerical analyses performed did not consider the damping. This choice was made after a preliminary study in which several types of damping were tested: proportional to the stiffness, proportional to the mass and Rayleigh-damping. All the tested solutions shown that the vertical displacement at which the equilibrium was reached, was considerably smaller if compared with the solution without damping, which in turn found an equilibrium position for lower vertical displacements with respect to the experimental results. Considering also that in this kind of studies the part of the analysis of greatest interest is the first, until the equilibrium condition is reached, and that in these cases most of the dissipative phenomena are energetic due to the plasticization of the sections, it was chosen to not apply a damping to the model.

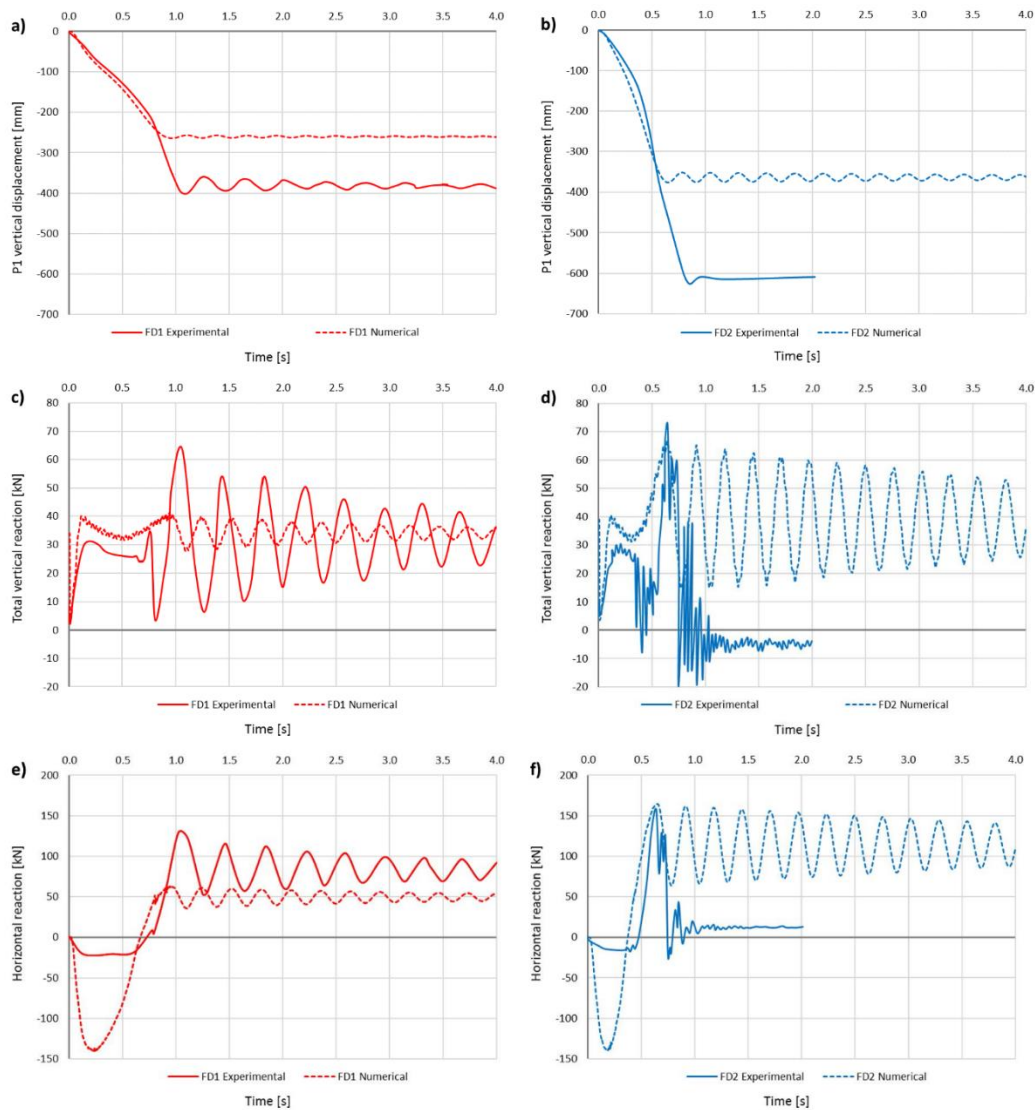


Figure 58: Comparison between experimental data and numerical results

By analysing the numerical results, it can be noted that FD1 and FD2 models were able to replicate with good approximation the first phase of the analyses. Considering the behaviour of FD1 specimen, was reached for a vertical displacement of the middle joint equal to about 25 cm which represents the 60% of the value recorded during the test (40 cm). A similar behaviour was obtained with the FD2 specimen with an equilibrium condition reached for a vertical displacement of about 36.5 cm. However, in this case it was not possible to compare directly the numerical results with the experimental data due to the premature failure of the specimen.

By comparing the trend of the total vertical reaction, FD1 numerical results well approximated the initial transition phase, with an overestimation of +33% of the experimental reaction, in the second phase instead the fem model exhibited a slight oscillation (between 28 and 40 kN in the first cycles) respect to the experimental one (between 7 and 65 kN in the first cycles), this was related to the fact that the equilibrium state was achieved for a smaller displacement in the numerical simulation. FD2 specimen also showed a good approximation of the first phase in which a comparison was possible.

Finally, by comparing the trend of the horizontal reaction it should be highlighted that numerical models were able to capture the overall behaviour characterised by a first compressive phase and the subsequent development of the catenary action. However, FD1 fem model showed an important overestimation of the initial compressive phase with a peak value of about 140 kN against the corresponding value of 20 kN measured experimentally, this difference become less evident in the tensile phase where in the first cycles the numerical model exhibited an oscillation between 35 and 60 kN, while the experimental data report oscillations between 60 and 120 kN. Similar considerations can be done for FD2 model.

In conclusion, it can be stated that, although the uncertainties associated with this kind of analyses were greater if compared with the ones nonlinear static analyses the complexity associated with nonlinear dynamic analysis, the results obtained from the numerical models represented an acceptable approximation of the experimental behaviour. It should be noted, however, that the degree of uncertainty associated with this kind of analysis was greater than the static case. The models were able to capture global behaviour with an acceptable approximation; their use can therefore be allowed to perform qualitative assessments of structural response. The validation procedure was successfully completed.

Chapter 4

Numerical Studies on Simplified Models

4.1 Introduction

The development of experimental campaigns to study the mechanisms involved in the structural robustness of reinforced concrete buildings constitutes an expensive operation. In addition, as suggested by previous studies (Qian, 2015), the structural behaviour varies significantly, especially in the case of 3D structures, depending on several structural characteristics (e.g. span length, geometry of structural elements, reinforcements amount, floor system type, etc...). Therefore, it is difficult to find general conclusions based on experimental results, unless reference is made to large-scale experimental campaigns. In this context, finite element modelling becomes essential to broaden the experimental knowledge.

In this chapter, several finite element models were developed and analysed. Initially the study concerned the behaviour of two-dimensional structural assemblies, easier to study and useful to understand the development of different resistant mechanisms.

In a second phase, the study focused on assessing the contribution provided by floor systems. Initially, simple models were examined to progressively get to more complex systems whose behaviour better simulates the actual one.

However, to consider the presence of the floor system, requires a large number of finite elements to be used, this choice involves very long analysis times and difficulties in model management. For this reason, it has been launched a parallel study to evaluate the possibility of exploiting alternative solutions to simulate the presence of the floor system without excessively complicate the models.

4.2 Response of 2D beam-column assemblies under a column removal scenario

Part of the work described in this section was also previously published by Bertagnoli et al. in 2016 (Bertagnoli, 2016b).

The response of a 2D beam-column assembly under a column removal scenario has already been partially studied in the previous chapter. In this section are included the analyses considering further aspects such as the presence of distributed loads acting on the beams and the dynamic removal of the column. The concrete beam column assembly chosen as reference test is the one designed by NIST researchers, previously described in section 2.5.1 and used for the validation of SeismoStruct software. The numerical simulations shown in this section were developed with SeismoStruct.

4.2.1 Influence of distributed loads applied on the beams

The purpose of this section is to evaluate how the presence and the magnitude of an external load applied to the beam can change the behaviour described in sections 2.5.1 and 3.3.1.

According to the main structural codes, the element removal represents an accidental situation. This means that in general, the structure should be checked considering also the loads imposed by the accidental combination. In particular, the beams are loaded by the permanent actions, to which it should be added a percentage of variable loads.

In this study the effect of four different distributed load levels is evaluated. It should be noted that these loads are applied with constant magnitude for all the duration of the test, the nonlinear behaviour is due to the vertical displacement of the central column. Table 11 summarises tests characteristics.

Table 11: Distributed load applied for each test in addition to the self-weight

ID Case	Distributed load applied	Ratio respect to CS Case
AS ¹	0.00 kN/m	0.00
BS	18.25 kN/m	0.50

CS	36.50 kN/m	1.00
DS	46.00 kN/m	1.26
ES	54.75 kN/m	1.50

¹As Case represents the MA1 model seen in paragraph 3.3.1.

AS case represents the MA1 model (tested in section 3.3.1) which is used as reference model in the assessment of the influence of the applied loads. The magnitude assigned to CS case was calculated by the authors to simulate the load acting on beams in accidental combination. BS and ES cases represents respectively an underestimation and an overestimation of the load applied in CS case. Finally, the load applied in DS case is the maximum that allows to find an equilibrium configuration exploiting the flexural resources of the beams, as it will be described in detail hereinafter.

Results from each model are shown in Figure 59a, Figure 59b and Figure 59c. The “Variation of vertical reaction” reported on the vertical axis of Figure 59a represents the variation of vertical reaction at central column due to only vertical imposed displacement of point P1. Therefore, these values do not consider the reaction due to the applied load (corresponding to a vertical displacement of the point P1, equal to 0 m). Figure 56c shows instead, on vertical axis, the trend of the “Total vertical reaction” in correspondence of the central column which includes, in addition to the reaction due to vertical imposed displacement, the external distributed load contributions.

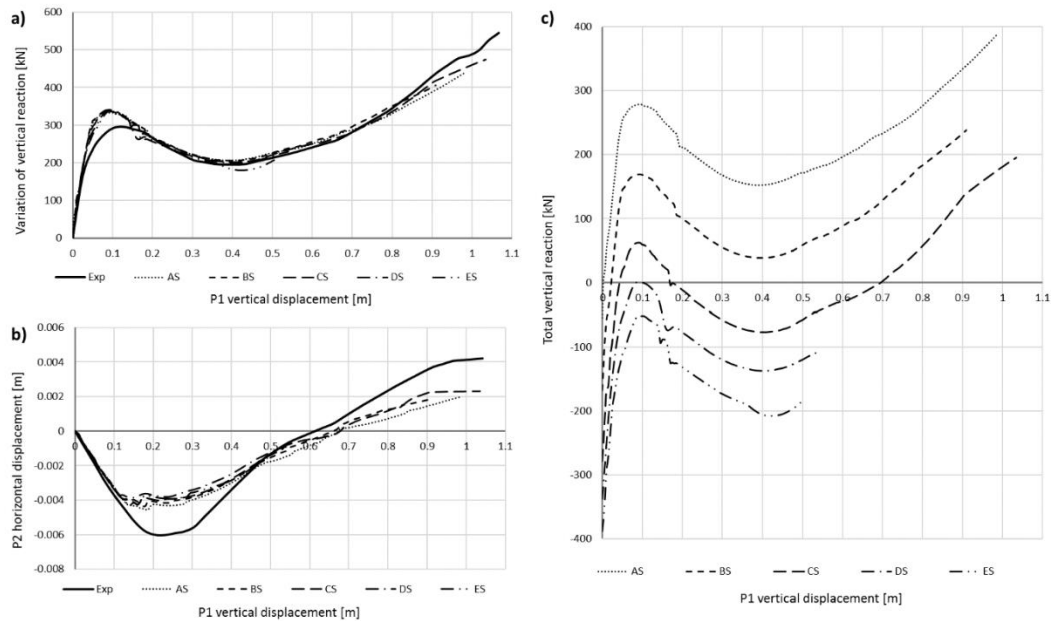


Figure 59: Influence of the applied loads on the beams

Overlaying the curves (Figure 59a and Figure 59b) it is possible to highlight that, up to the CS case, the value of the applied distributed load does not influence significantly the global behaviour. However, for high loading levels (DS and ES cases) it can be noted that the analyses end at a relatively small vertical displacement of point P1 (about 0.5m) if compared to the other cases. This is an important consideration, because the horizontal displacement of point P2 at this moment is still negative, which means that beams are still in compression, and then the catenary action does not occur. However, in DS case the system can reach an equilibrium configuration exploiting the flexural strength available, while in ES case the flexural bearing capacity is not sufficient to ensure the equilibrium, thus it would be necessary to exploit the catenary action. However, the analysis does not find a convergence and then is stopped before that this mechanism is activated, therefore the system seems to be unable to develop it because of the high-level load applied.

Figure 59c shows the evolution of the total reaction of the central column, considering the applied loads and the displacement of the column itself. When the curves intersect the horizontal axis, the system reaches an equilibrium configuration without applying a reaction to the point P1. The portions above the horizontal axis can be interpreted as an extra resistance resource of the system, which can be exploit, as an example, to counteract the dynamic effects of the column removal,

that are not considered in these analyses. On the other hand, if the curve occupies only the region below the horizontal axis, it is not possible to reach an equilibrium condition after removing the central column. When the column is removed, depending on the applied loads, the curves can intersect the horizontal axis one or more times, which means that several equilibrium configurations are possible. In particular, for small displacement values, the equilibrium is achieved due to the system ability to transfer the loads through compressive and flexural mechanisms. On the opposite, for higher displacements, the equilibrium is possible only exploiting the catenary action.

From Figure 59c, it is evident that increasing the distributed load applied to beams, compressive and flexural mechanisms are not sufficient to guarantee an equilibrium configuration. The catenary action becomes the only solution to transfer the load avoiding the collapse. However, to activate this behaviour, beams must have large rotational capacity in the zones near the end columns, this means that the beams ductility plays a fundamental role. It must be emphasized that the maximum load that the structure can withstand considering a static removal of the column corresponds to the DS case.

4.2.2 Structural response after sudden dynamic column removal

In the previous section the column removal was simulated by applying an increasing displacement and performing nonlinear static analyses. This condition can be considered realistic for the cases in which there is a progressive reduction of the bearing capacity of the element (e.g., in case of fire). Moreover, many accidental events involve a sudden removal of a structural element (e.g., impacts or explosions). For this reason, in this paragraph the behaviour was studied by means of nonlinear dynamic analyses.

With reference to the numerical simulations, at time t_0 in correspondence of the central column there is an element simulating the initial conditions in which the column is still present. In this phase, the self-weight and the distributed applied loads are considered. At time t_1 the central column is deactivated, then the loads are forced to follow an alternative load-path exploiting the resistance resources of the beams.

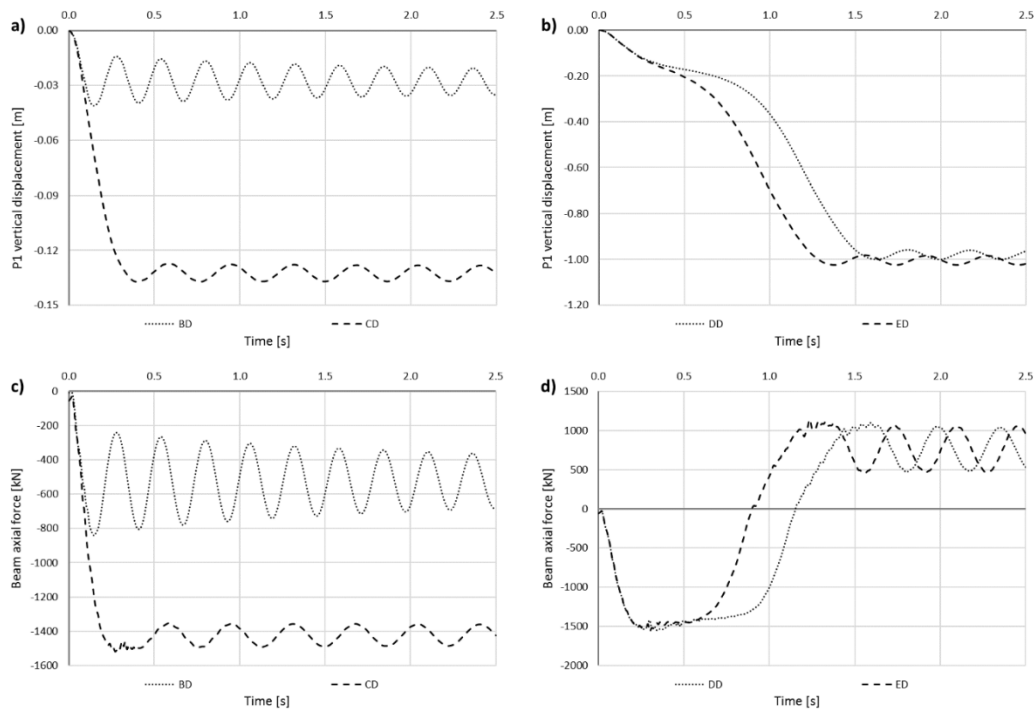
Following an approach similar to the one adopted for the second stage, various loads were applied to the system in order to highlight the differences with regard to the global behaviour. Table 12 summarizes the layout of the numerical simulations:

Table 12: Distributed loads applied for each numerical simulation

ID Case	Distributed load applied
BD	18.25 kN/m
CD	36.50 kN/m
DD	37.40 kN/m
ED	38.00 kN/m

BD and CD cases were the nonlinear dynamic analyses performed considering the same applied loads used in BS and CS cases described in section 4.2.1. DD and ED cases were selected as the first load level for which the system exhibits the catenary action (DD case) and the maximum distributed load considered by the software to carry out the analysis (ED case).

Figure 60a and Figure 60b show the vertical displacement of the point P1 as a function of time. DD and ED cases are shown separately because the relating displacements are considerably larger than those associated with the other cases. Figure 60c and Figure 60d show the trend of the axial force in the beam, allowing thus to appreciate the development of the catenary action.

**Figure 60:** Results obtained with nonlinear dynamic analyses

It can be noted that in general, after the removing of the central column, the system exhibited an initial increasing vertical displacement up to the reaching of an equilibrium configuration. Once this condition was found, the frame oscillated until the inherent damping of the structure reduced the oscillations up to zero.

Depending on the magnitude of the applied load, the equilibrium condition was reached for progressively larger displacements and at different time (about 0.1-0.25s for cases BD and CD, against 1.25-1.50s for cases DD and ED). This is an important consideration because the displacement level significantly changes the mechanism that allows the beams to transfer loads.

As shown in Figure 60a and Figure 60b in fact, for BD and CD cases, the equilibrium condition was reached with relatively small vertical displacements compared to the ones found in DD and ED cases. In fact, the distributed loads applied in DD and ED cases produced a bending moment greater than the flexural capacity of the beams, by developing plastic hinges at the end of these elements causing their rotation to find an equilibrium condition by means of the exploitation of different resisting mechanism. An evidence of this was given by the trend of the axial force in the beams it can be observed that for BD and CD cases, beams were in compression for the whole test, while for DD and ED cases the axial force switched from compression to tension before that the equilibrium was reached, highlighting the development of the catenary action. This can be understood as follows: in BD and CD cases, the loads transfer was ensured by the compressive arch action resources (CAA) of the beams); in DD and ED cases on the contrary, the system was forced to exploit the catenary action (CA) to withstand the external loads.

The analyses point out how a minor increase in the load can drastically change the system response. As mentioned before, the value of 36.5kN/m was estimated as the load acting on beams in accidental combination but was sufficient an increase of only 2.5% of the load applied (37.4kN) to switch the behaviour from a flexural one to a catenary action based one. If the beams did not have a sufficient rotational capacity the system became unable to transfer the load exploiting only the flexural resources.

Another consideration to be emphasized is that the maximum load for which the system reached the equilibrium in dynamic conditions was 38kN/m, which represents an increase of only 4.1% respect to the load applied in accidental combination. Then, according to the numerical simulations developed, by

considering the dynamic effect, the resistance resources were very limited because a minimum increase in the load applied was sufficient to change the global behaviour and/or prevent the reaching of the equilibrium.

By comparing the maximum loads that the frame can withstand, it must be highlighted that the value reached in static conditions was 21% greater than the one obtained with the dynamic analyses.

Table 13 summarizes the results achieved with the nonlinear dynamic analyses.

Table 13: Nonlinear dynamic analyses results

ID Case	Distributed load applied [kN/m]	P1 vertical displacement [m]	Beam axial force range [kN]	Load carrying type
BD	18.25	-0.028	-840 / -9 ²	CAA
CD	36.50	-0.132	-1521 / -31 ²	CAA
DD	37.40	-0.980	-1548 / +1100	CA
ED	38.00	-1.003	-1570 / +1141	CA

¹ Average value of the oscillations around the equilibrium position; ² Values reached before the column removal

4.3 Floor system simplified numerical models

One of the aims of this work is to identify possible simplified solutions to model adequately the floor plans. This makes the analyses more performing and reduces pre- and post-processing phases. The models were developed by using as reference the specimen S1, previously described in section 2.5.2. The numerical simulations shown in this section were developed with Diana 10.1.

The setup of the analyses is the same previously described in section 2.5.2, so it has not been reported here again. Two distinct levels of simplification have been studied. To simulate the slab contribution the solution tested exploit respectively:

- Equivalent beam elements in longitudinal and transverse direction. In this case the structure was modelled by considering equivalent T-shape beams with a cross section given by the rectangular beam itself and a top flange represented by the collaborating slab. This discretization was done both in

longitudinal that in transverse direction, thus obtaining a girder of equivalent beams as shown in Figures 61, 63 and 65.

Three different cases were studied:

- An initial model, named “EB1”, considering only the slab portions collaborating with primary beams;
 - An evolution of the previous model, named “EB2”, considering an intermediate equivalent beam;
 - A further evolution of the previous models, named “EB3”, considering three intermediate elements in both directions.
- Nonlinear springs simulating the equivalent beams. This solution, named “SPR”, represents a further simplification of the previous one. The idea was to avoid modelling the equivalent beams by replacing them with springs having a stiffness equivalent to the flexural inertia of the corresponding element.

All the models had a mesh size variable in the range 3÷5 mm, both for beam and shell elements. The mesh independence was evaluated before of the development of the analyses.

4.3.1 Simplified model EB1

This model considered only the slab portions collaborating (including the reinforcements) with the beams. On the safety side it was assumed that in each direction the width of the collaborating slab was equal to a quarter of the span. Figure 61 shows the slab subdivision and the cross section of beam elements adopted for model EB1.

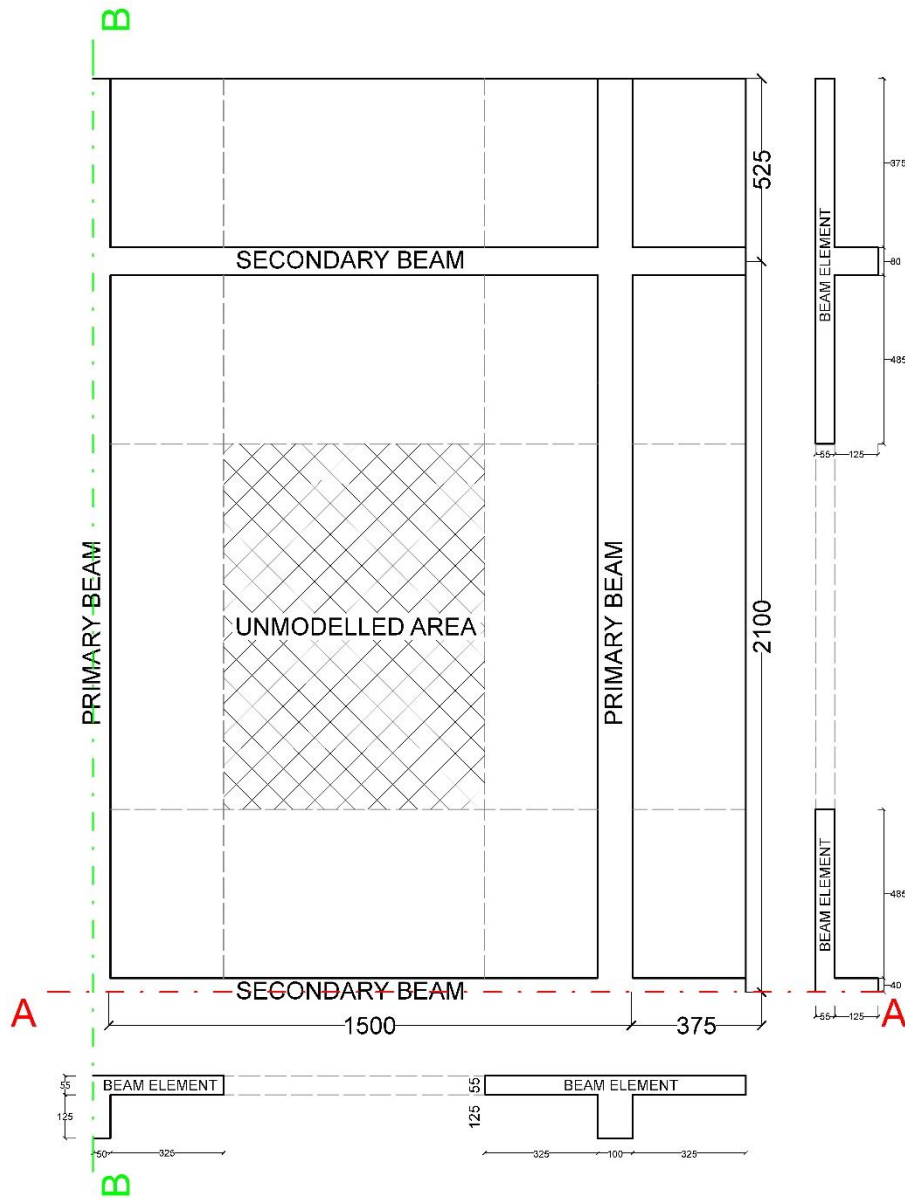


Figure 61: EB1 - Slab discretization and beam elements cross section

Figure 62 reports the Force-Displacement curve obtained. The comparison was made both with the experimental results that those obtained with the shell elements.

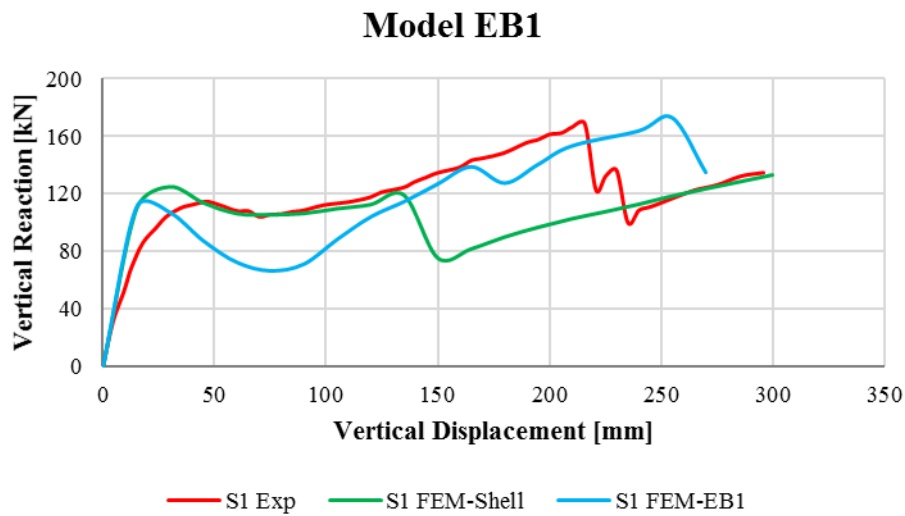


Figure 62: EB1 - Force-Displacement curves

By comparing the results, it can be noted that in the first phase the behaviour was the same of the FEM-Shell, both the models in fact overestimated the uncracked stiffness, losing accuracy in simulating progressive cracking, however the flexural peak was well captured. About the softening phase, FEM-EB1 was not able to reproduce properly the experimental behaviour. Although there was an improvement of the results for displacement between about 17 and 22 cm, the model, unlike the FEM-Shell, was not able to correctly reproduce the last phase of the analysis. The model was able to globally reproduce the experimental behaviour, however, since this was a quite simplified model, it was decided to evaluate the response by introducing a more accurate discretization.

4.3.2 Simplified model EB2

This model represented a first evolution of the EB1. In this case a further beam element in both longitudinal and transverse directions was implemented. Figure 63 shows the slab subdivision and the cross section of beam elements adopted for model EB2.

Model EB2

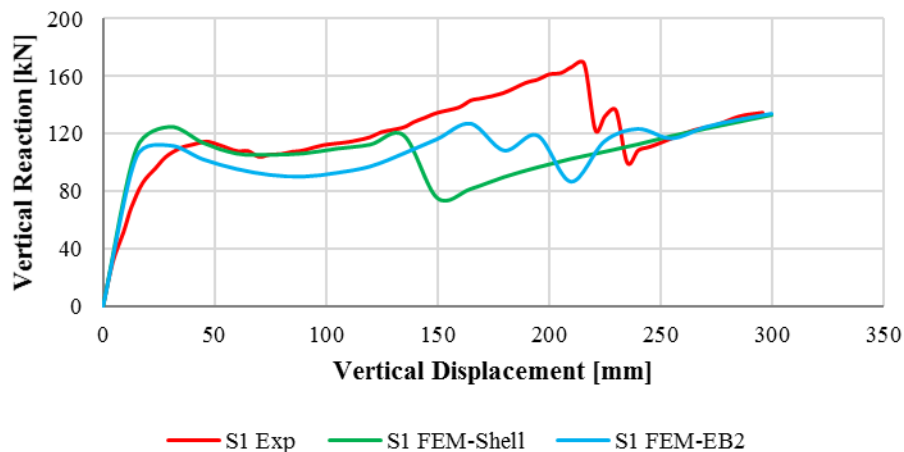


Figure 64: EB2 - Force-Displacement curves

By comparing the results, it can be noted that in the first phase the behaviour is the same of the EB1, therefore the additional element in both directions did not significantly improve the behaviour. However, it can be noted a clear improvement in reproducing both the softening phase, that the last stage of the analysis.

4.3.3 Simplified model EB3

Based on the results obtained with EB2 model, it was decided to test a second evolution. EB3 model in fact exploits a more refined discretization with an additional element in both directions. Figure 65 shows the slab subdivision and the cross section of beam elements adopted for model EB3.

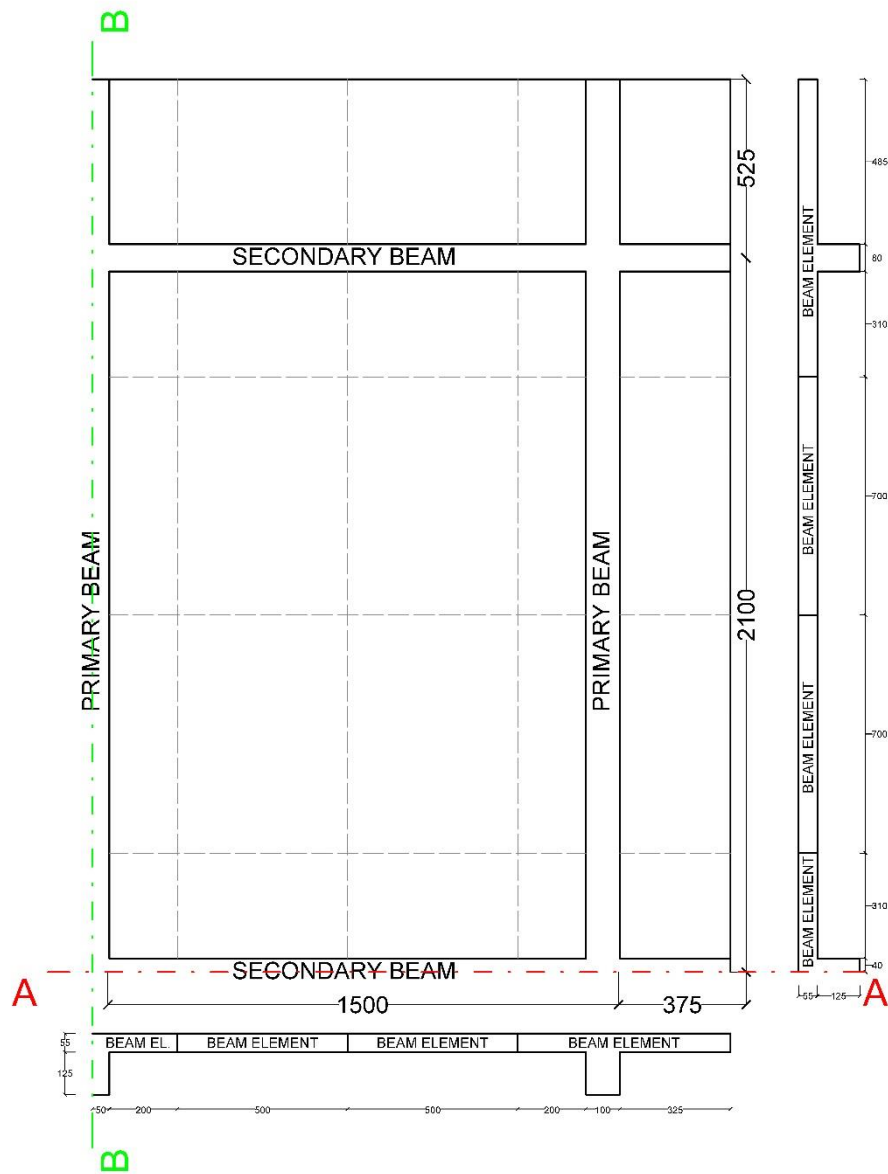


Figure 65: EB3 - Slab discretization and beam elements cross section

Figure 66 reports the Force-Displacement curve obtained. The comparison was made both with the experimental results that those obtained with the shell elements.

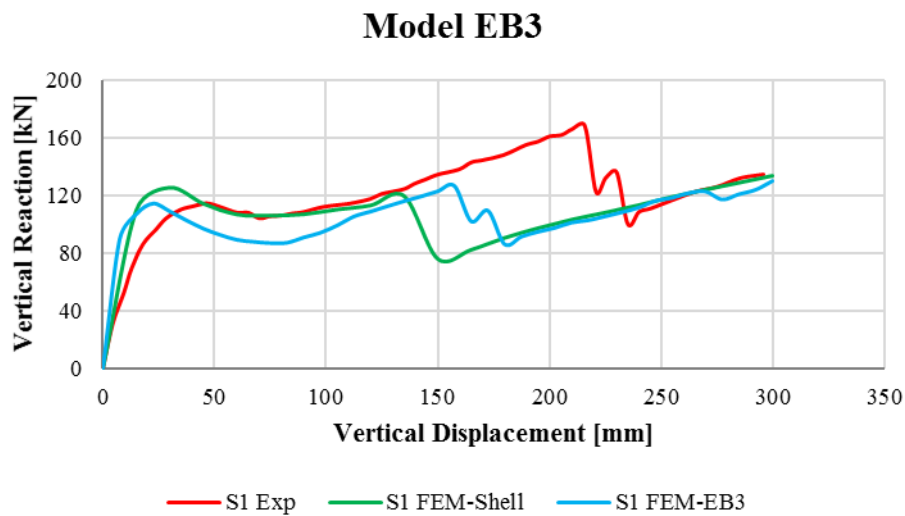


Figure 66: EB3 - Force-Displacement curves

By comparing the results, it can be noted that both the initial and the softening phases were reproduced with the same approximation of the EB2 model, therefore the additional element in both directions did not significantly improve the behaviour. However, it can be noted a clear improvement in reproducing the last stage of the analysis.

The outcomes achieved with this discretization constitutes a crucial result. It can be argued that, in a global analysis, it was sufficient to subdivide each floor field by using at least 2 elements per side to properly consider the contribution offered by the floor system. Based on these results, it was chosen the discretization level to be used to simulate the system plan in the 3D models described in subsequent chapters.

4.3.4 Simplified model SPR

This model represents a further simplification, different from the ones tested up to now. In fact, the equivalent beams have been replaced by elastic springs.

Figure 69 shows a discretization of the specimen S1 based on the results achieved by simplified model EB3 which was the most performing among those developed in the previous stage. It should be noted that while the EB3 model reproduced only 1/4 of the structure (exploiting the double symmetry as mentioned in Section X), the SPR model simulated the whole structure.

This model represented a further simplification, different from the ones tested up to now. In fact, the equivalent beams were replaced by elastic springs.

The idea was to replace the equivalent beams of model EB3 with some springs each of which had a stiffness equal to the flexural one of the corresponding equivalent beam replaced.

The stiffness of each spring was evaluated by considering the equivalent beam as simply supported and by applying a fictitious force in the midspan. Once the displacement was measured, the stiffness was calculated by reversing the following formula:

$$d = \frac{F \cdot L^3}{48 \cdot E \cdot I} \rightarrow K = \frac{48 \cdot E \cdot I}{L^3} \quad (13)$$

Where:

d is the displacement, F is the applied force, L is the span length, E is the elastic modulus, I is the moment of inertia and K is the flexural stiffness. Considering the structure described in section 2.5.2 the following stiffnesses were calculated as follows:

For springs applied on transverse beams:

$$K_T = \frac{48 \cdot 28960 \cdot \left(\frac{500 \cdot 55^3}{12}\right)}{4200^3} = 130 \text{ N/mm} \quad (14)$$

For springs applied on longitudinal beams:

$$K_L = \frac{48 \cdot 28960 \cdot \left(\frac{700 \cdot 55^3}{12}\right)}{3000^3} = 500 \text{ N/mm} \quad (15)$$

The stiffness should be calculated by considering the contribution of five forces, as in each direction, in addition to the force applied by the orthogonal beam (in black in Figure 67), there would be also those of the equivalent beams (in dashed green and blue in Figure 67).

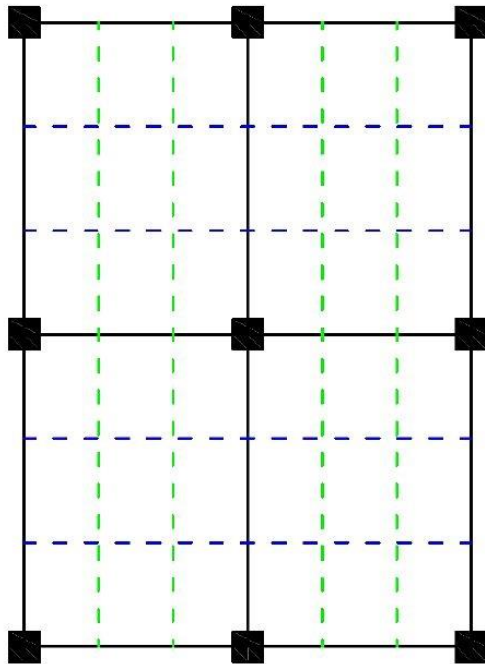


Figure 67: Discretization adopted to evaluate the stiffness of the springs

Therefore, in this case we would have to add the contributions of 5 forces to calculate the total displacement (being in the linear elastic field it can be applied the superposition principle). However, as demonstrate in a separate study, the forces transmitted by the other beams (the dashed green and blue) were rather small and closer to the restraints, so for the sake of greater simplification it was chosen to disregard these contributions. Figure 69 shows the slab subdivision and the cross section of beam elements adopted for model SPR. Figure 68 shows a view of the FEM SPR.

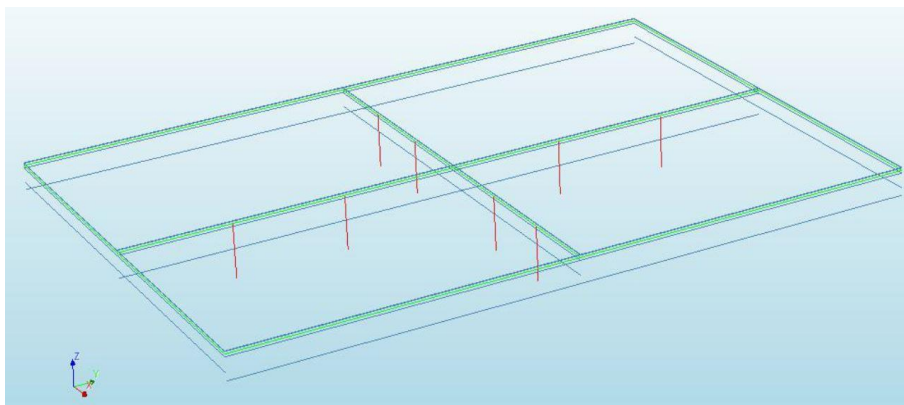


Figure 68: Numerical model SPR

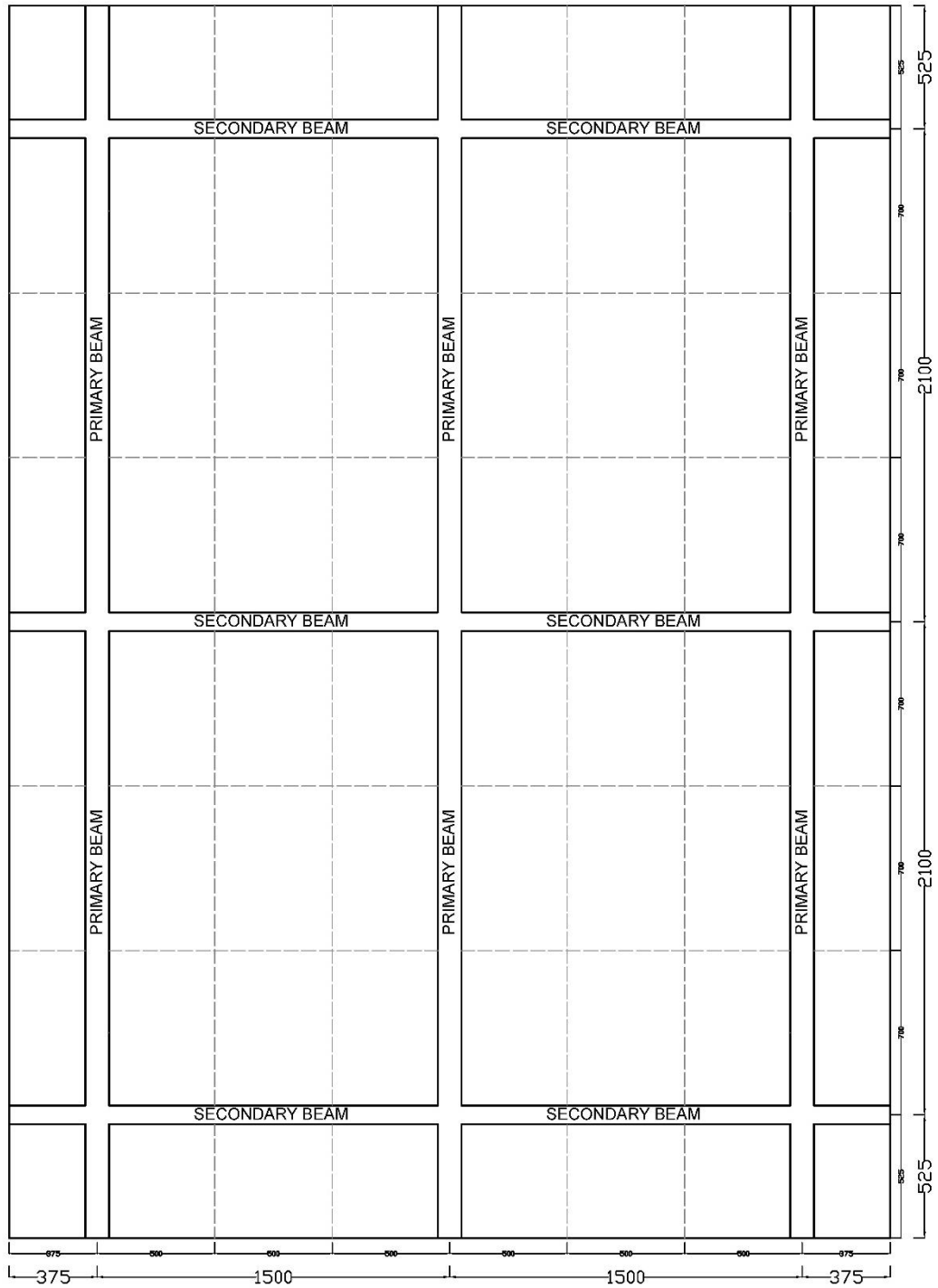


Figure 69: SPR - Slab discretization and beam elements cross section

Figure 70 reports the Force-Displacement curve obtained. The comparison was made both with the experimental results that those obtained with the shell elements.

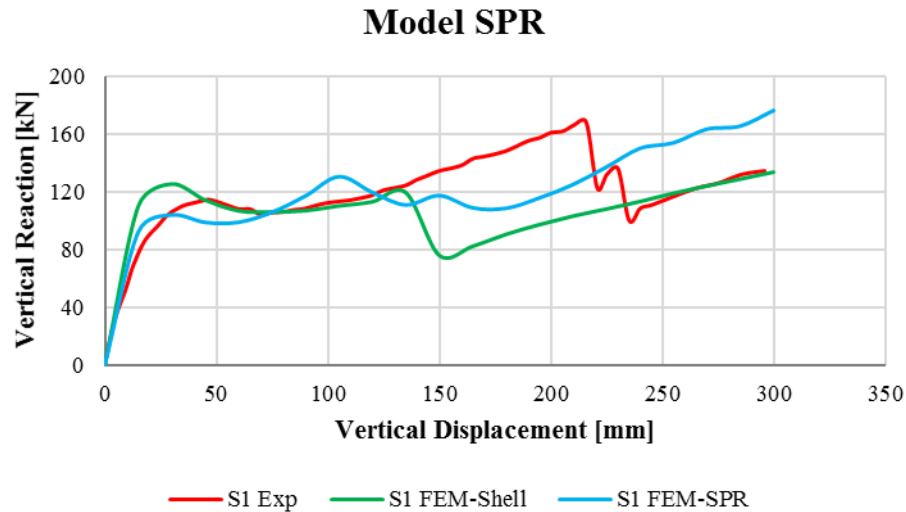


Figure 70: SPR - Force-Displacement curves

By comparing the results, it can be noted an improvement in reproducing the initial phase up to the reaching of the flexural peak. The model well simulated also the beginning of the softening phase. However, for imposed displacements greater than 5 cm, it can be noted a loss of accuracy of the results. Probably this was due to the linear behaviour of the springs used in the analysis.

In conclusion it can be stated that the proposed simplifications provide good approximations of experimental results and therefore are suitable to be implemented within more complex models used to evaluate the structural response globally. By comparing the degree of complexity of each model with the approximation achieved it can be stated that the best results are obtained from the EB3 model, whose discretization was then chosen as a reference for the simulations made in the following.

Chapter 5

3D Complete Models - Design and Finite Element Modelling

5.1 Introduction

This chapter illustrates the results of a detailed study on the behaviour of 3D reinforced concrete frames subjected to a column removal.

The structure examined was chosen by considering characteristics comparable with most of the reinforced concrete frame buildings (in terms of span length, number of floors, structural elements design, construction details, etc...). Therefore, the results obtained can be taken as reference for similar buildings.

This study aims to determine if the column removal can lead to the structural collapse, and to evaluate the better solutions which can be adopted to avoid progressive and/or disproportionate collapse.

Several nonlinear static analyses are developed, considering different scenarios: the removed elements are identified among those located at the ground floor, but in distinct positions (e.g. internal columns, edge columns, corner columns) because it is not known a priori, what configurations can lead to higher damages.

The analyses cover several aspects, including the role played by different type of floor system, the amount of continuous reinforcement in the beams, the primary beams depth, the columns depth, the presence of bracing systems, the amount of continuous reinforcement and finally the role played by seismic detailing.

5.2 3D building design

Part of the work described in this section was also previously published by La Mazza et al. in 2017 (La Mazza, 2017).

The building had a rectangular shape, with planar dimensions of 48m in longitudinal direction and 20m in transverse direction. In elevation, the structure was composed by four levels, the first of which had a height of 5m, while the others measure 3.5m. The reinforced concrete structure consisted of five longitudinal frames each of which had six spans of 8m long and seven transverse frames with four spans 5m long.

About the floor system, two different solutions were considered: the first one characterised by a predominantly monodirectional reinforced concrete slab, while the second one involved reinforced concrete unidirectional joists and a collaborating slab. Figure 71 shows the plan layout of the building, while Figure 72 and Figure 73 show the longitudinal and transverse elevation respectively.

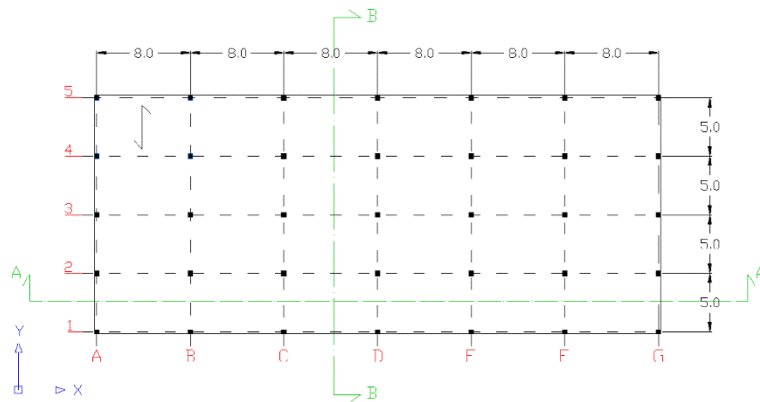


Figure 71: Plan layout of the building

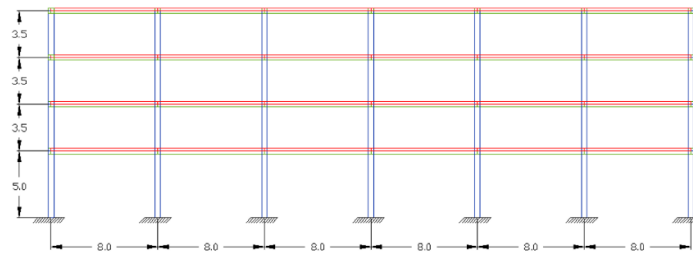


Figure 72: Longitudinal elevation of the building

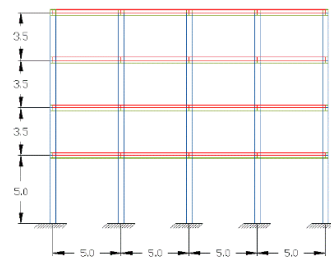


Figure 73: Transverse elevation of the building

The structure was designed at the ultimate limit states by considering the contribution of permanent and variable vertical loads, wind and snow actions, and the effects of constructive imperfections according to Eurocodes prescriptions. At this stage the seismic action was not considered. Further details on the design are given below. Appendix A reports structural drawings of the building.

- **Materials:**

Table 14 summarises the characteristics of the materials adopted.

Table 14: Material parameters

Concrete C30/37		Steel B450C	
f_{ck}	30 N/mm ²	f_{yk}	450 N/mm ²
R_{ck}	37 N/mm ²	f_{tk}	540 N/mm ²
f_{cm}	38 N/mm ²	E_s	200000 N/mm ²
f_{ctm}	2.9 N/mm ²	ν	0.3
E_{cm}	32800 N/mm ²	γ	78 kN/m ³
ν	0.2		
γ	24 kN/m ³		

The characteristic values have been scaled to the design ones through the partial factors provided by the Eurocodes: $\gamma_c = 1.5$ for concrete and $\gamma_s = 1.15$ for steel.

- **Loads:**

- **Self-weight G_{k1} :** calculated according to the geometry of the elements and the specific weight of the materials;
- **Superimposed dead load G_{k2} :** 3 kN/m² including concrete subfloor, paving, plaster and partition walls;
- **External cladding load G_{k3} :** 10 kN/m applied to external beams, except for the roofing ones;
- **Variable loads Q_{k1} :** 2 kN/m² defined according to the EN 1991-1-1 (CEN, 2004), for Category A buildings (domestic, residential areas) and applied at each floor level, including the roof one;
- **Wind loads Q_{k2} :** 1.75 kN/m² defined according to the EN 1991-1-4 (CEN, 2005), for a building built in Turin;
- **Snow loads Q_{k3} :** 1.25 kN/m² defined according to the EN 1991-1-3 (CEN, 2003), for a building built in Turin;
- **Global geometric imperfections:** evaluated according to the section 5.2 of EN 1992-1-1 (CEN, 2004).

The structural design was carried out by using the software SAP2000 (CSI, 2016). Figure 74 shows a view of the finite element model. The building was designed considering only the resisting contribution offered by the frames, in this phase in fact the presence of the floor system was disregarded on the safety side. However, horizontal constraints were introduced at each floor level to simulate the planar stiffness contribution given by the slab. For this reason, the floor system was designed separately considering the static scheme of continuous beam.

In the pre-dimensioning phase, on the safety side, the contribution of the collaborating slab defined in the section 5.3.2.1 of the EN 1992-1-1 was disregarded. However, it will be considered in the structural element design.

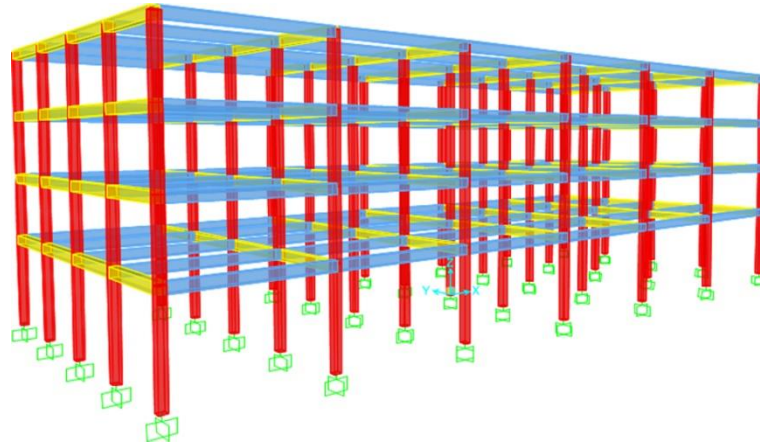


Figure 74: 3D finite element model developed with SAP2000

The structure was designed by considering the actions defined in accordance with the ultimate limit state combination defined in section 6.4 of EN 1990:

$$\sum_{j \geq 1} \gamma_{G,j} G_{k,j} + \gamma_P P + \gamma_{Q,1} Q_{k,1} + \sum_{i \geq 2} \gamma_{Q,i} \Psi_{0,i} Q_{k,i} \quad (16)$$

Where:

“+” implies “to be combined with”, Σ implies “the combined effect of”, $\gamma_{G,j}$ is the partial factor for the j-th permanent action, $G_{k,j}$ are the characteristic values of the permanent actions, γ_P is the partial factor for the prestressing action, P is the representative value of the prestressing action, $\gamma_{Q,i}$ is the partial factor for the i-th variable action, $Q_{k,1}$ is the characteristic value of the leading variable action, $Q_{k,i}$ is the characteristic value of the i-th variable action, $\Psi_{0,i}$ is the factor for the characteristic value of the i-th variable action $Q_{k,i}$.

According to EN 1990, the partial factors adopted are equal to: $\gamma_{G,j} = 1.35$ or 1.00 for permanent actions and $\gamma_{Q,i} = 1.50$ or 0.00 for variable actions.

Figure 75-Figure 80 show the cross-section details of the structural elements of the building with the reinforced concrete slab as floor system. Appendix A reports the complete structural drawings.

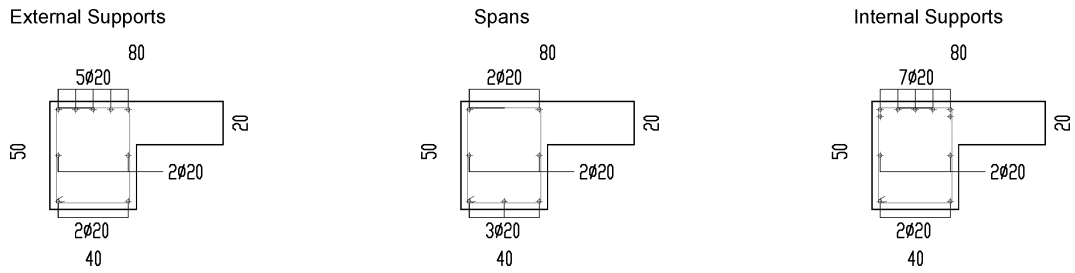


Figure 75: Cross section of the primary external beams

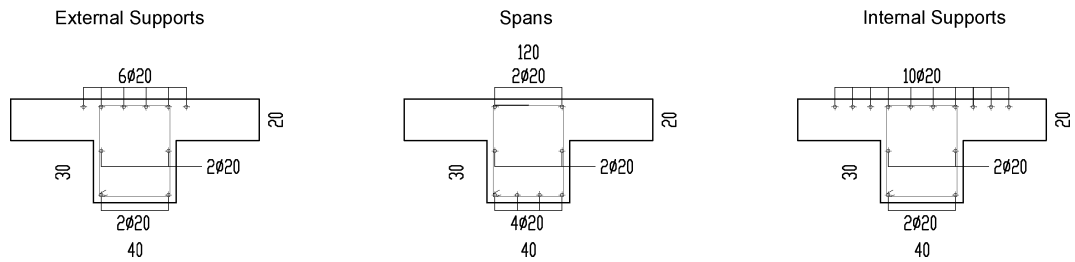


Figure 76: Cross section of the primary internal beams

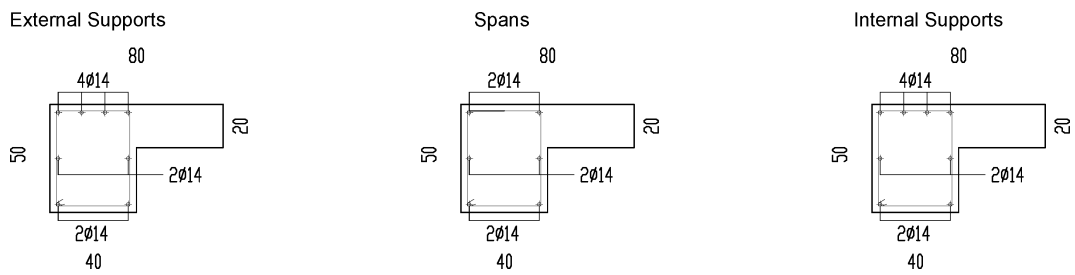


Figure 77: Cross section of the secondary external beams

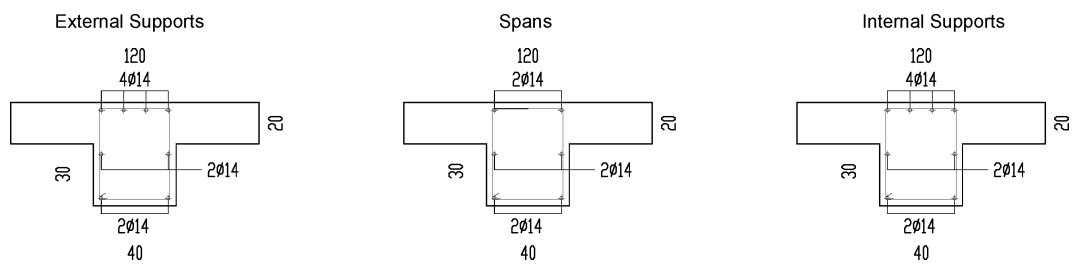


Figure 78: Cross section of the secondary internal beams

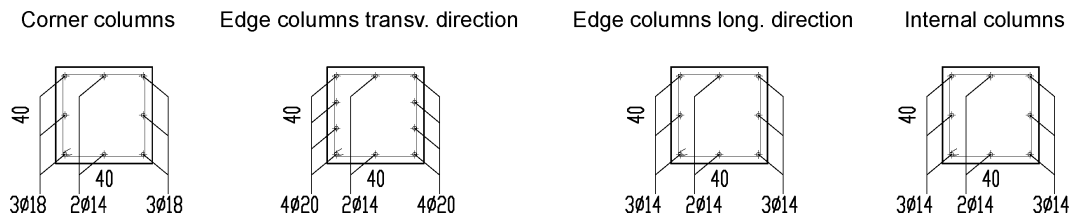


Figure 79: Cross section of the columns



Figure 80: Cross section of the slab

Figure 81-Figure 85 show the cross-section details of the elements of the structure which exploits the joists as floor system. Appendix B reports the complete structural drawings.

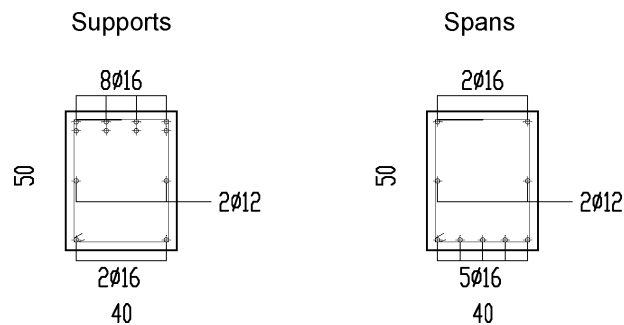


Figure 81: Cross section of the primary external beams

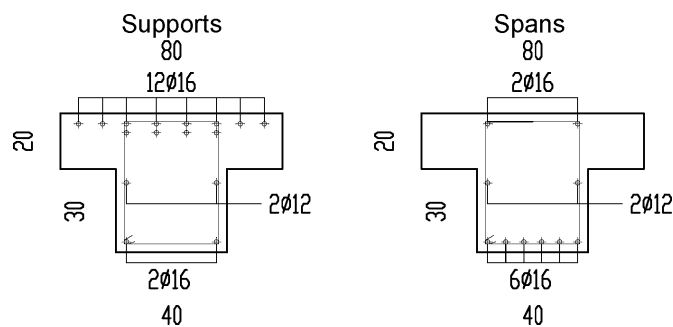


Figure 82: Cross section of the primary internal beams

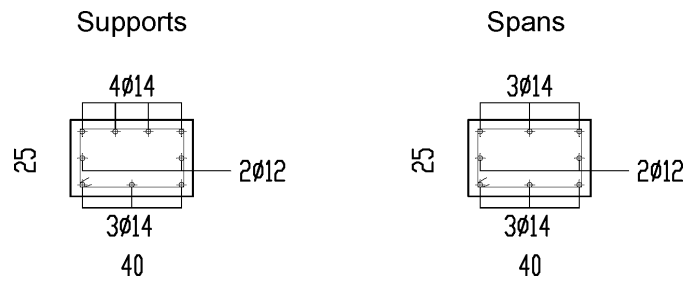


Figure 83: Cross section of the secondary beams

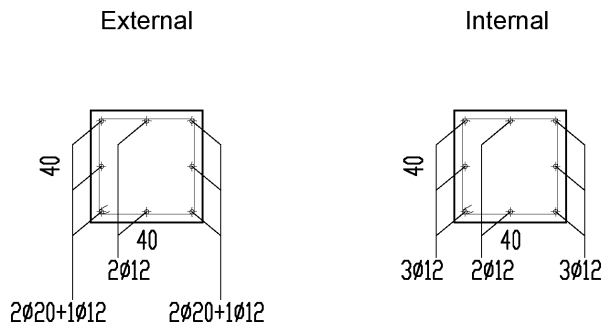


Figure 84: Cross section of the columns



Figure 85: Cross section of the floor system

5.3 3D building design including seismic action

This paragraph reports the assessment of the improvements achievable, in terms of structural robustness, by adopting seismic detailing.

For this scope, it was chosen to design the structure to withstand an earthquake. This section summarises the results of the seismic design of the building.

The structure considered is the one described in section 5.2 which exploits the floor system with joists and collaborating slab. In addition to the specifications mentioned above, the description of the seismic action used to design the structure is reported hereinafter.

It was chosen a peak ground acceleration (PGA) of 0.15g. This PGA is the limit value between seismic zones 2 and 3 defined by Italian National Annex of Eurocodes 8 (CEN, 2005b). In this way it was avoided at the same time both an oversizing of the elements due to high PGA, that a marginal role of the seismic design as a result of low levels of PGA. About the soil, it was assumed a ground type C. The behaviour factor q was set equal to 3.9, considering that the structural scheme is a frame designed for a medium ductility class. The damping ζ was considered equal to 5%. Table 15 summarizes the spectrum parameters. Figure 86 shows the elastic response spectrum and the design one.

Table 15: Spectrum parameters

Ag	Spectrum Type	Ground Type	Soil Factor	Tb	Tc	Td	Lower Bound Factor	Ductility Class	Behave Factor
-	-	-	-	Sec	Sec	Sec	-	-	-
0.15	1	C	1.15	0.2	0.6	2	0.2	DCM	3.9

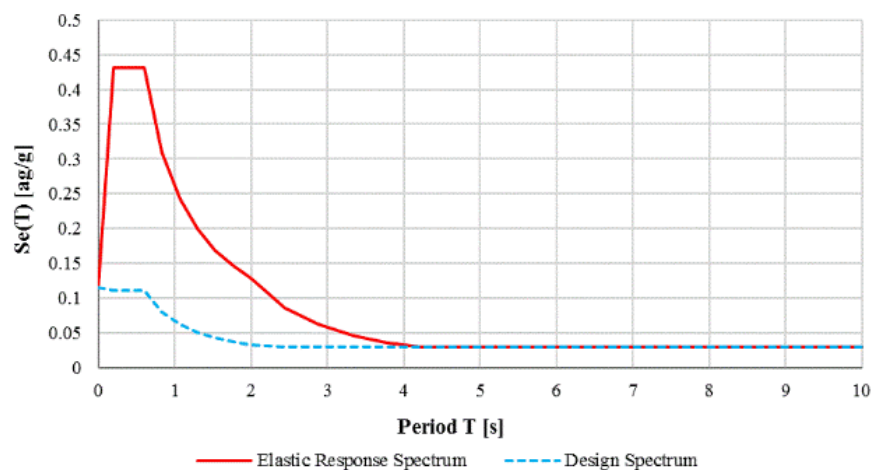


Figure 86: Elastic response spectrum and design spectrum

Seismic action was considered through a spectral response modal analysis; Table 16 summarises the periods and frequencies of the 12 eigenmodes of the structure with their respective modal participation factors in X and Y directions.

Table 16: Modal periods, frequencies and participation factors

Mode	Period	Frequency	UX	UY	SumUX	SumUY
-	s	Hz	%	%	%	%

1	1.70	0.59	0.00	87.00	0.00	87.00
2	1.26	0.79	0.00	0.00	0.00	87.00
3	0.92	1.09	92.42	0.00	92.42	87.00
4	0.48	2.10	0.00	10.18	92.42	97.18
5	0.37	2.71	0.00	0.00	92.42	97.18
6	0.28	3.59	6.30	0.00	98.72	97.18
7	0.22	4.52	0.00	2.42	98.72	99.60
8	0.18	5.54	0.00	0.00	98.72	99.60
9	0.15	6.79	1.10	0.00	99.83	99.60
10	0.13	7.75	0.00	0.40	99.83	100.00
11	0.11	9.15	0.00	0.00	99.83	100.00
12	0.10	10.24	0.17	0.00	100.00	100.00

The Square Root of Sum of Squares (SRSS) technique was used to combine the accelerations in X and Y directions, while the Complete Quadratic Combination (CQC) was used for the modal combination. By considering both the earthquake in X and Y directions and the sign of the additional torque moments, a total of 32 seismic combinations were applied.

Appendix C reports the structural drawings of the building.

5.4 Description of nonlinear static time-history analyses

Once the structure was designed, the column removal was simulated through nonlinear static time-history analyses. In this approach the loads were applied according to the loading function shown below:

$$P_i = \lambda_i(t) \cdot P_i^0 \quad (17)$$

Where:

$\lambda_i(t)$ is the loading factor;

P_i^0 is the nominal load.

The analyses were based on the displacement control of a user-determined node. At each step the loading factor $\lambda_i(t)$ was calculated by the software to apply a load P_i which produced a target displacement of the selected node. After a calibration procedure it was chosen to apply the displacement with steps of 10mm. The convergence criterion was based on displacement/rotation control, in particular

it was defined a tolerance of $5E-04$ m and $5E-04$ rad respectively. The analyses ended if within a predefined number of iterations, at each degree of freedom of the structure, the value of displacement/rotation was greater than the tolerance specified. In case of non-convergence, divergence of the solution or numerical instability, an automatic pitch control algorithm imposed a reduction of the load increment or of the time step before to restart the analysis from the last equilibrium point. Once this condition was obtained the software tried to automatically restore the loading factor defined by the user. If the solution diverged after the maximum iteration number and for the maximum reduction of the loading factor the analysis was stopped.

The iteration method is the one defined by Newton-Raphson. Finally, it was checked the ultimate strain in the materials in order to stop the analyses if one of the materials exceeded this parameter.

By means of this strategy, it was possible to capture response irregularities, to observe the softening branch of the post-peak response, and to obtain a smooth distribution of the points of the force-displacement curve.

5.4.1 Collapse scenarios

For both the models, different collapse scenarios were identified. All models consider that the removed columns were located at the ground floor. After a sensitivity analysis, four different configurations were chosen to be tested. Figure 87 shows the position of the removed elements:

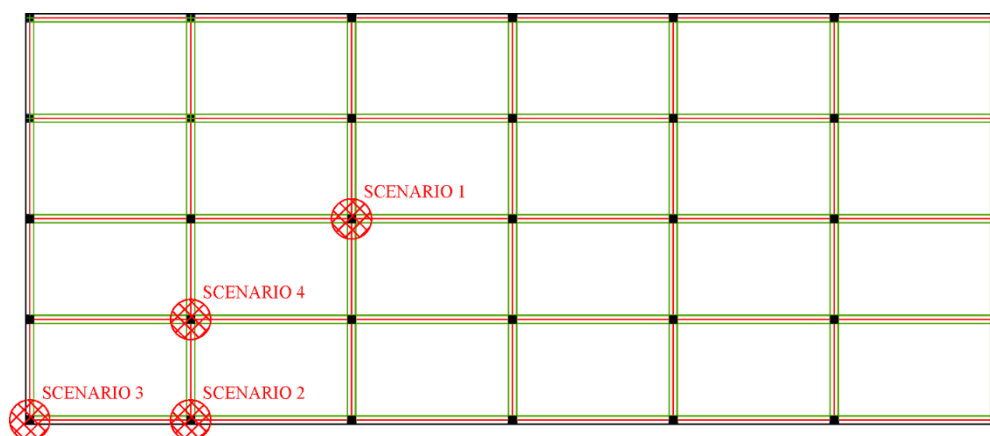


Figure 87: Layout of the collapse scenarios

Scenarios 1 and 4 regarded internal columns: the first was a situation in which the spans directly involved were located within the structure, whereas in the second case the damaged area involved one edge of the building, then the boundary conditions were different.

Scenarios 2 and 3 represented respectively a case in which the element removed was an edge column and a corner column. Typically, the last two were the most critical cases, in fact these elements were exposed to major risks of being involved in accidental situations. Furthermore, being connected to a small number of elements there was a smaller possibility to redistribute the loads or to find alternate load paths once the element collapsed.

The column removal represented an accidental situation, hence the load combination to be used to check the structure and to evaluate its response was the combination for accidental design situations, as defined in section 6.4.3.3 of EN 1990:

$$\sum_{j \geq 1} G_{k,j} + A_d + \Psi_{1,1} Q_{k,1} + \sum_{i \geq 1} \Psi_{2,i} Q_{k,i} \quad (15)$$

Where:

“+” implies “to be combined with”, Σ implies “the combined effect of”, $G_{k,j}$ are the characteristic values of the permanent actions, A_d is the design value of an accidental action, $Q_{k,1}$ is the characteristic value of the leading variable action, $Q_{k,i}$ are the characteristic values of the other variable actions, $\Psi_{1,1}$ is the factor for the frequent value of the leading variable action $Q_{k,1}$, $\Psi_{2,i}$ is the factors for the quasi-permanent value of the i -th variable action $Q_{k,i}$.

Before testing the configurations, it was checked that the minimum tie-requirements defined in section 9.10 of EN 1992-1-1 (and here reported in detail in section 2.4.1.1) were met:

- **Peripheral ties in longitudinal direction:**

$$T_p = \max(0.4(g_k + \Psi q_k)sL ; 75kN)$$

$$T_p = \max(0.4 \cdot (5 + 0.3 \cdot 3) \cdot 5 \cdot 8 ; 75kN) = 94.5 kN$$

The corresponding minimum area of continuous reinforcement was calculated by dividing this force by the characteristic yielding strength of the steel bars:

$$As_p = T_p / f_{yk} = 94.5 \cdot 10^3 / 450 = \mathbf{210 \text{ mm}^2}$$

The spandrel beams had respectively:

- Slab solution:

$$As_p = 6\Phi 20 = \mathbf{1884 \text{ mm}^2} \geq \mathbf{210 \text{ mm}^2}$$

- Joists solution:

$$As_p = 4\Phi 16 + 2\Phi 12 = \mathbf{1030 \text{ mm}^2} \geq \mathbf{210 \text{ mm}^2}$$

In both cases the requirement was amply complied.

- **Peripheral ties in transverse direction:**

$$T_p = \max(0.4(g_k + \Psi q_k)sL ; 75kN)$$

$$T_p = \max(0.4 \cdot (5 + 0.3 \cdot 3) \cdot 8 \cdot 5 ; 75kN) = \mathbf{94.5 \text{ kN}}$$

The corresponding minimum area of continuous reinforcement was calculated by dividing this force by the characteristic yielding strength of the steel bars:

$$As_p = T_p / f_{yk} = 94.5 \cdot 10^3 / 450 = \mathbf{210 \text{ mm}^2}$$

The spandrel beams had respectively:

- Slab solution:

$$As_p = 6\Phi 14 = \mathbf{924 \text{ mm}^2} \geq \mathbf{210 \text{ mm}^2}$$

- Joists solution:

$$As_p = 6\Phi 14 + 2\Phi 12 = \mathbf{1150 \text{ mm}^2} \geq \mathbf{210 \text{ mm}^2}$$

In both cases the requirement was amply complied.

- **Internal ties in longitudinal direction:**

$$T_i = \max(0.8(g_k + \Psi q_k)sL ; 75kN)$$

$$T_i = \max(0.8 \cdot (5 + 0.3 \cdot 3) \cdot 5 \cdot 8 ; 75kN) = \mathbf{189 \text{ kN}}$$

The corresponding minimum area of continuous reinforcement was calculated by dividing this force by the characteristic yielding strength of the steel bars:

$$As_i = T_i/f_{yk} = 189 \cdot 10^3/450 = \mathbf{420 \text{ mm}^2}$$

The elements had respectively:

- Slab solution:

▪ Beams:

$$As_i = 6\Phi 20 = \mathbf{1884 \text{ mm}^2} \geq \mathbf{420 \text{ mm}^2}$$

▪ Slab:

$$As_i = \Phi 8/15 \text{ sup and inf} = \mathbf{670 \text{ mm}^2/m} \geq \mathbf{420 \text{ mm}^2}$$

- Joists solution:

▪ Beams:

$$As_i = 4\Phi 16 + 2\Phi 12 = \mathbf{1030 \text{ mm}^2} \geq \mathbf{420 \text{ mm}^2}$$

In all cases the requirement was amply complied.

• **Internal ties in transverse direction:**

$$As_i = \max(0.8(g_k + \Psi q_k)sL ; 75kN)$$

$$As_i = \max(0.8 \cdot (5 + 0.3 \cdot 3) \cdot 8 \cdot 5 ; 75kN) = \mathbf{189 \text{ kN}}$$

The corresponding minimum area of continuous reinforcement was calculated by dividing this force by the characteristic yielding strength of the steel bars:

$$As_i = T_i/f_{yk} = 189 \cdot 10^3/450 = \mathbf{420 \text{ mm}^2}$$

The elements had respectively:

- Slab solution:

▪ Beams:

$$As_i = 6\Phi 14 = \mathbf{924 \text{ mm}^2} \geq \mathbf{420 \text{ mm}^2}$$

▪ Slab:

$$As_i = \Phi 10/15 \text{ sup and inf} = \mathbf{1047 \text{ mm}^2/m} \geq \mathbf{420 \text{ mm}^2}$$

- Joists solution:

▪ Beams:

$$As_i = 4\phi 16 + 2\phi 12 = 1030 \text{ mm}^2 \geq 420 \text{ mm}^2$$

▪ Joists:

$$As_i = 2\phi 12/50 = 452 \text{ mm}^2/m \geq 420 \text{ mm}^2$$

In all cases the requirement was amply complied.

• **Columns:**

$$T_c = (5 + 3) \cdot 5 \cdot 8 = 320 \text{ kN}$$

The corresponding minimum area of continuous reinforcement was calculated by dividing this force by the characteristic yielding strength of the steel bars:

$$As_c = T_c/f_{yk} = 320 \cdot 10^3/450 = 711 \text{ mm}^2$$

The columns had a minimum amount of continuous reinforcements respectively equal to:

- Slab solution:

$$As_c = 8\phi 14 = 1231 \text{ mm}^2 \geq 711 \text{ mm}^2$$

- Joists solution:

$$As_c = 8\phi 12 = 904 \text{ mm}^2 \geq 711 \text{ mm}^2$$

In both cases the requirement was amply complied.

5.4.2 Finite element modelling – Floor system: slab

In this section was described the necessary inputs to develop the finite element models used for the analyses.

• **Materials:**

- **Concrete C30/37:** The concrete behaviour was simulated by using the uniaxial nonlinear model with constant confinement suggested by Mander et al. in 1988 (Mander, 1998).

To define the model the input parameters were:

- Average cylindrical compressive strength:

$$f_{cm} = f_{ck} + 8 = 38 \text{ MPa}$$

- Average tensile strength:

$$f_{ctm} = 0.3 \cdot f_{ck}^{2/3} = 2.9 \text{ MPa}$$

- Young's modulus:

$$E_{cm} = 22000 \cdot \left(\frac{f_{cm}}{10}\right)^{0.3} = 32800 \text{ MPa}$$

- Strain related to the maximum compressive strength:

$$\varepsilon_c = 0.002 \text{ m/m}$$

- Specific weight:

$$\gamma_c = 24 \text{ kN/m}^3$$

The Poisson's coefficient was assumed by default equal to 0.2 for concrete.

- **Steel B450C:** The reinforcement behaviour was simulated by using a uniaxial bilinear law with a hardening branch. To define the material the user set the following parameters:

- Tensile strength:

$$f_y = 450 \text{ MPa}$$

- Young's modulus:

$$E_{sm} = 200000 \text{ MPa}$$

- Hardening parameter:

$$\mu = \frac{E_{sp}}{E_s} = \frac{(f_t - f_y)}{\left(\varepsilon_{ult} - \frac{f_y}{E_s}\right)} * \frac{1}{E_s} = 0,0062$$

- Ultimate strain (for maximum tensile stress or for buckling):

$$\varepsilon_{us} = 0.075 \text{ m/m}$$

- Specific weight:

$$\gamma_s = 78 \text{ kN/m}^3$$

- **Element cross sections:** in this modulus the user set the cross-section geometry, the materials used and, in case of reinforced concrete sections, the concrete cover and both the longitudinal and transverse reinforcements. Once the input parameters were defined, the software calculated all the properties (e.g. axial stiffness EA, bending stiffness EI, torsional stiffness

GJ, confinement factor, mass and weight of the section, etc...) needed to perform the analysis.

- **Structural nodes:** these include all the nodes connected to a structural element. At each node the software associates the degrees of freedom, defining the size of the stiffness matrix of the structure and of the forces/displacements vector.

In this model was placed a node in correspondence of each cross-section variation (including reinforcements), in this way each element had only one cross-section, regardless of the number of integration sections considered.

The number of structural nodes defined for this structure was 1255.

- **Structural elements:** the models use 3D inelastic beam-column elements with a force-based formulation named “infrmFB”. This choice was suggested by the possibility to consider both the geometrical and mechanical nonlinearities. These elements used cross section integration with each integration point assigned to a discretized cross-sectional geometry component defined as “fibre”; the sectional stress-strain state was obtained through the integration of the nonlinear uniaxial material response of the individual fibres in which the section was subdivided, by considering the spread of inelasticity along the member length and across the section depth.

The number of structural elements used for this structure was 2220.

Below are reported the details adopted for each structural element typology.

- **Primary spandrel beams:** these elements were modelled by considering 5 integration sections, each of which was discretized by using 200 fibres. Figure 88 shows a view of the cross section:

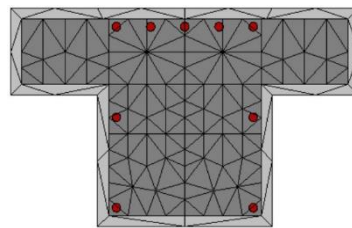


Figure 88: Cross-section of a primary spandrel beam

- **Primary internal beams:** these elements were modelled by considering 5 integration sections, each of which was discretized by using 200 fibres. Figure 89 shows a view of the cross section:

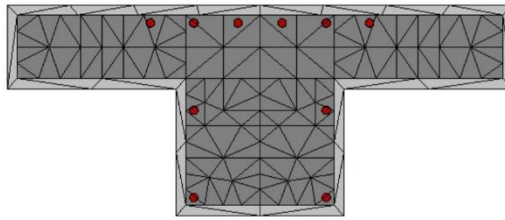


Figure 89: Cross-section of a primary internal beam

- **Secondary spandrel beams:** these elements were modelled by considering 5 integration sections, each of which was discretized by using 200 fibres. Figure 90 shows a view of the cross section:

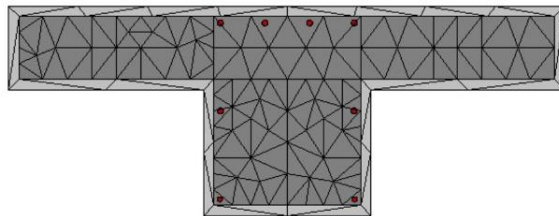


Figure 90: Cross-section of a secondary spandrel beam

- **Secondary internal beams:** these elements were modelled by considering 5 integration sections, each of which was discretized by using 200 fibres. Figure 91 shows a view of the cross section:

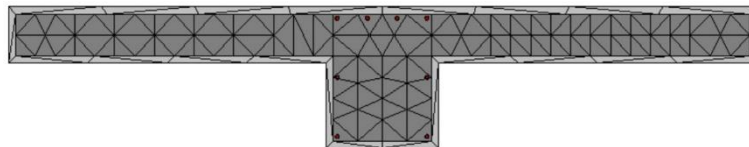


Figure 91: Cross-section of a secondary internal beam

- **Slab:** these elements were modelled considering 5 integration sections, each of which was discretized by using 200 fibres. Figure 92 shows a view of the cross section:



Figure 92: Cross-section of the slab

- **Columns:** these elements were modelled considering 5 integration sections, each of which was discretized by using 150 fibres. Figure 93 shows a view of the cross section.

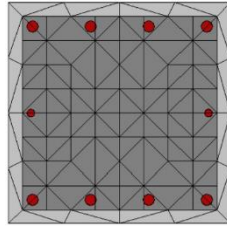


Figure 93: Cross-section of a column

Although the slab resistance contribution was omitted in the frame design, the 3D models adopted for nonlinear time-history analyses considered the presence of the floor system. The slab in fact, because of its in-plane stiffness, plays a crucial role in determining the overall structural response. Moreover, cannot be neglected its contribution in loads transferring.

Based on the results reported above in section 4.3, it was decided to model the slab through a two-dimensional girder. Each floor area between two primary and two secondary beams was thus divided into three parts per side by introducing equivalent beams having rectangular cross-section. Figure 94 illustrates a plan layout of the equivalent girder adopted.

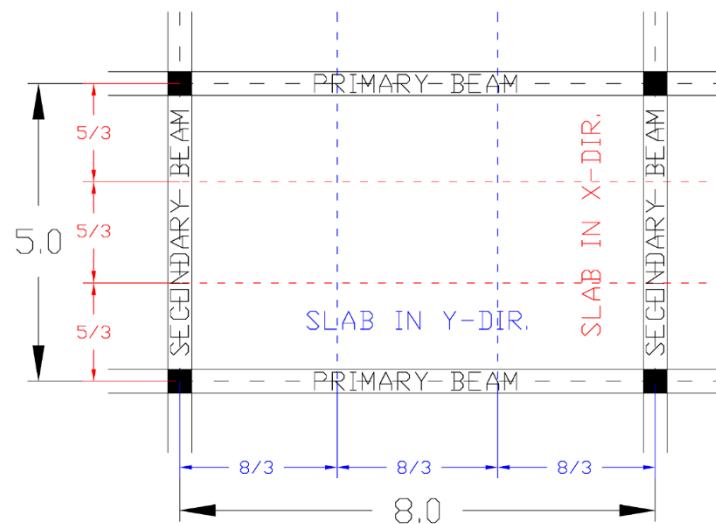


Figure 94: Plan layout of the equivalent girder

A density of 12 kN/m^3 was assigned to concrete slab to do not overestimate its weight. In this way it was possible to schematize a 2D element, through a system of 1D elements designed to have an equivalent global stiffness to the actual one.

Figure 95 shows a view of a floor, modelled as described above, extrapolated from the 3D global model.

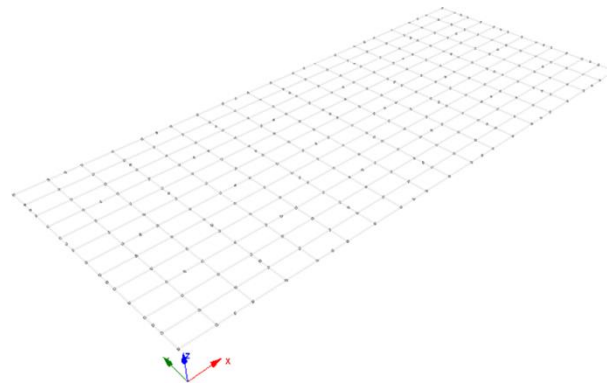


Figure 95: SeismoStruct slab model extrapolated from the 3D building

- **Boundary conditions:** these were defined by the external constraints applied to the structural nodes. In this model all the columns were fully restrained at the base, preventing the translations in x, y and z direction and the rotations around x, y and z axes.
- **Loads:** the loads applied were the ones defined according to the accidental combination previously described. The accidental action A_d was represented by a vertical downward increasing displacement applied in correspondence of the removed column to simulate its failure. This displacement was simulated by means of a static time-history load. This was a static load varying in pseudo-time domain based on the loading curve defined. The load magnitude at each step was calculated as the product between the nominal load value and the variable factor defined by the loading curve.

The analyses developed use a linear increasing loading curve, after a calibration procedure it was chosen to divide the time-history in steps of 0.01s.

5.4.3 Finite element modelling – Floor system: Joists with collaborating slab

In this section it was described the necessary inputs to develop the finite element models used for the analyses.

- **Materials:**

- **Concrete C30/37:** The concrete behaviour was simulated by using the uniaxial nonlinear model with constant confinement suggested by Mander et al. in 1988 (Mander, 1998).

To define the model the requested parameters were:

- Average cylindrical compressive strength:

$$f_{cm} = f_{ck} + 8 = 38 \text{ MPa}$$

- Average tensile strength:

$$f_{ctm} = 0.3 \cdot f_{ck}^{2/3} = 2.9 \text{ MPa}$$

- Young's modulus:

$$E_{cm} = 22000 \cdot \left(\frac{f_{cm}}{10}\right)^{0.3} = 32800 \text{ MPa}$$

- Strain related to the maximum compressive strength:

$$\varepsilon_c = 0.002 \text{ m/m}$$

- Specific weight:

$$\gamma_c = 24 \text{ kN/m}^3$$

The Poisson's coefficient was assumed by default equal to 0.2 for concrete.

- **Steel B450C:** The reinforcement behaviour was simulated by using a uniaxial bilinear law with a hardening branch. To define the material the user set the following parameters:

- Tensile strength:

$$f_y = 450 \text{ MPa}$$

- Young's modulus:

$$E_{sm} = 200000 \text{ MPa}$$

- Hardening parameter:

$$\mu = \frac{E_{sp}}{E_s} = \frac{(f_t - f_y)}{\left(\varepsilon_{ult} - \frac{f_y}{E_s}\right)} * \frac{1}{E_s} = 0,0062$$

- Ultimate strain (for maximum tensile stress or for buckling):

$$\varepsilon_{us} = 0.075 \text{ m/m}$$

- Specific weight:

$$\gamma_s = 78 \text{ kN/m}^3$$

- **Element cross sections:** in this modulus the user set the cross-section geometry, the materials used and, in case of reinforced concrete sections,

the concrete cover and the longitudinal and transverse reinforcements. Once the input parameters were defined by the user, the software calculated all the properties (e.g. axial stiffness EA, bending stiffness EI, torsional stiffness GJ, confinement factor, mass and weight of the section, etc...) needed to perform the analysis.

- **Structural nodes:** they include all the nodes connected to a structural element. At each node the software associated the degrees of freedom, defining the size of the stiffness matrix of the structure and of the forces/displacements vector.

In this model was placed a node in correspondence of each cross-section variation (including reinforcements), in this way each element had only one cross-section, regardless of the number of integration sections considered.

The number of structural nodes defined for this structure was 1735.

- **Structural elements:** the models exploited 3D inelastic beam-column elements with a force-based formulation named “infrmFB”. This choice was suggested by the possibility to consider both the geometrical and mechanical nonlinearities. These elements were force-based elements and use cross section integration with each integration point assigned to a discretized cross-sectional geometry component defined as “fibre”; the sectional stress-strain state was obtained through the integration of the nonlinear uniaxial material response of the individual fibres in which the section was subdivided, considering the spread of inelasticity along the member length and across the section depth.

The number of structural elements used for this structure was 2604.

Below were reported the details adopted for each structural element typology.

- **Primary spandrel beams:** these elements were modelled by considering 7 integration sections, each of which was discretized by using 600 fibres. Figure 96 shows a view of the cross section:

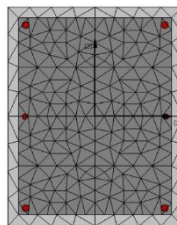


Figure 96: Cross-section of a primary spandrel beam

- **Primary internal beams:** these elements were modelled by considering 7 integration sections, each of which was discretized by using 600 fibres. Figure 97 shows a view of the cross section:

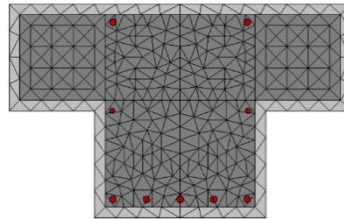


Figure 97: Cross-section of a primary internal beam

- **Secondary beams:** these elements were modelled by considering 5 integration sections, each of which was discretized by using 400 fibres. Figure 98 shows a view of the cross section:

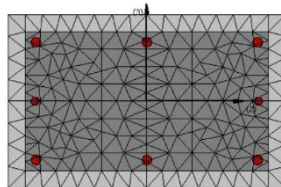


Figure 98: Cross-section of a secondary spandrel beam

- **Joists:** these elements were modelled by considering 3 integration sections, each of which was discretized by using 600 fibres. Figure 99 shows a view of the cross section:

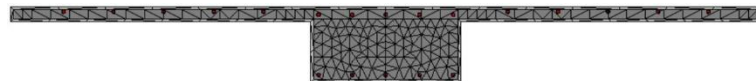


Figure 99: Cross-section of the macro joist

- **Columns:** these elements were modelled by considering 5 integration sections, each of which was discretized by using 500 fibres. Figure 100 shows a view of the cross section.

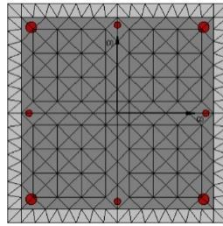


Figure 100: Cross-section of a column

Although the floor system resistance contribution was omitted in the frame design, the 3D models adopted for nonlinear time-history analyses consider the presence its presence. In fact, because of its in-plane stiffness, plays a crucial role in determining the overall structural response. Moreover, cannot be neglected its contribution in loads transferring.

Based on the results reported above in section 4.3, it was decided to model the floor system by using equivalent “macro-joists” each of them having the properties of 5 joists. Thus, for each span were used only 3 elements instead of 15. Figure 101 illustrates a plan layout of the equivalent girder adopted.

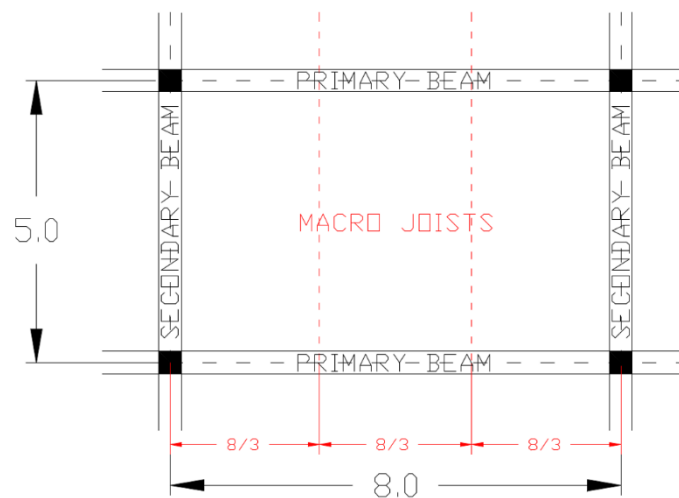


Figure 101: Plan layout of the equivalent girder

In this way it was possible to schematize a 2D element, through a system of 1D elements designed to have an equivalent global stiffness to the actual one. Figure 102 shows a view of a floor, modelled as described above, extrapolated from the 3D global model.

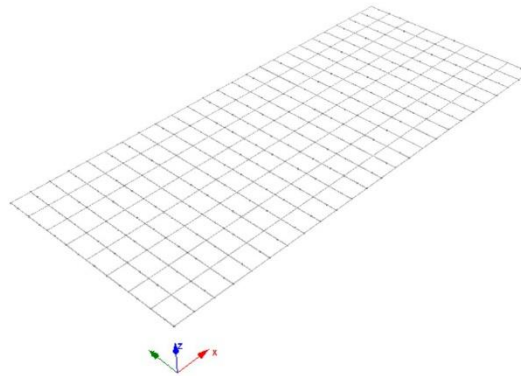


Figure 102: SeismoStruct floor system model adopted for 3D buildings

- **Boundary conditions:** these were defined by the external constraints applied to the structural nodes. In this model all the columns were fully restrained at the base, by preventing the translations in x, y and z direction and the rotations around x, y and z axes.
- **Loads:** the loads applied were the ones defined according the accidental combination previously described. The accidental action A_d was represented by a vertical downward increasing displacement applied in correspondence of the removed column to simulate its failure. This displacement was simulated by means of a static time-history load. This was a static load varying in pseudo-time domain based on the loading curve defined. The load magnitude at each step was calculated as the product between the nominal load value and the variable factor defined by the loading curve.

The analyses developed use a linear increasing loading curve, after a calibration procedure it was chosen to divide the time-history in steps of 0.01s.

5.4.4 The compatibility torsion issue

During the analysis it was noticed the occurrence of non-negligible torsional stresses in the beams. In particular it was a compatibility torsion induced by the bending moment of the elements adopted to replace the slab which were applied along the length of the member as shown in Figure 103.

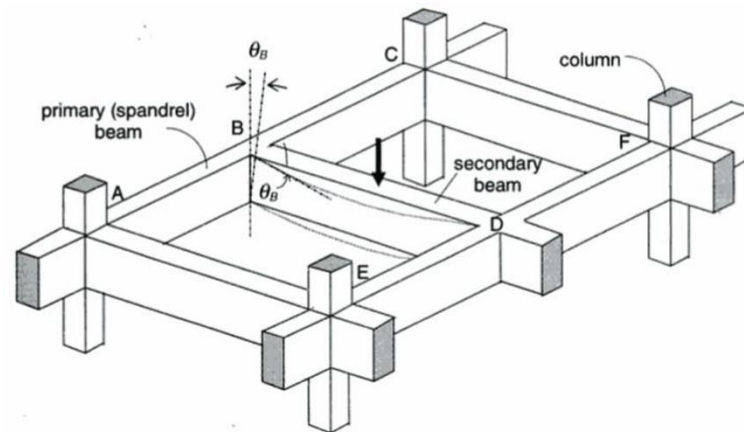


Figure 103: Example of compatibility torsion (Pillai, 2007)

These twisting moments are directly related to the torsional stiffness of the member that, in reinforced concrete member is drastically reduced by torsional cracking. It was therefore expected that such moments would be reduced rapidly after cracking, however the software was not able to properly reproduce this aspect. The problem could be resolved easily by modifying the torsional inertia fictitiously, however Seismostruct did not allow to modify directly this parameter, hence the problem was solved by introducing torsional releases at the ends of the beams. This has led to a global model with a reduced stiffness, but at the same time more conservative and overall closer to the actual behaviour.

Chapter 6

Analysis of the Results

6.1 Introduction

In this chapter are discussed the results obtained through FEM modelling. For each solution and each scenario described in the previous chapter, was evaluated and commented the influence of different parameters on the structural behaviour.

For each configuration was defined a reference test, represented by the frame designed for ultimate limit state (ULS) conditions, the other solutions constitute a variation of the reference one. In particular, it was evaluated the influence of the following factors:

- **Primary beam depth:** this parameter influences both local and global behaviour in various aspects. The beams were designed to develop a resisting bending moment regardless of their depth, so the higher beams have lower reinforcement percentages than the reference solution, while the lower ones have larger amounts of steel bars. The reference test was designed by considering a beam depth of 50cm, corresponding to a span-depth ratio L/h of 1/16. The alternative solutions have respectively a depth of 40cm (span-depth ratio equal to 1/20) and 65cm (span-depth ratio equal to 1/12).

A higher beam depth generally leads to higher ductility levels, the beams in fact can exhibit greater rotational capabilities before to collapse. However, at the same time smaller reinforcement amounts influence the response in the catenary action stage;

- **Column depth:** the column size influences several aspects, both in local that in global response. According to the results reported in the previous chapters, in the most advanced analysis stages, catenary action becomes the main resisting mechanism. As mentioned before, the development of this behaviour is clearly influenced by the characteristics of the beams, but also depends on the degree of constraint offered by the columns, in particular by the flexural stiffness of these elements. For this reason, it was chosen to vary

the column depth (i.e. in the direction of the primary frames). The reference test was designed by considering square columns 40x40cm. The alternative solution tested is characterised by rectangular columns 40x60 cm. This means that, disregarding the contribution of the reinforcements in the calculation of the moments of inertia, the alternative solution exploits columns with an inertia that is 3,375 times greater than the reference one;

- **Bracing system:** the reference building is a frame composed by beams and columns, however generally reinforced concrete structures are designed by considering also the presence of shear walls and/or concrete cores (e.g. stairwell, elevator shaft, etc...). These elements, in addition to provide a resisting contribution, primarily play a crucial role to stiffening the structure. This second aspect was considered, by introducing, in correspondence of each floor, some fictitious constraints simulating the action of the bracing system. Three distinct configurations were tested, Figure 104 shows the position of the bracings and the respective schematizations adopted;

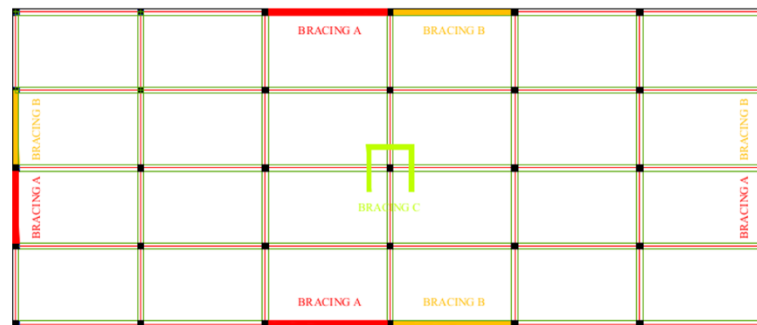


Figure 104: Bracing systems position

- **Eurocodes tying:** according the requirements defined in section 2.4.1.1, the minimum amount of reinforcements to be used is rather limited, then the reference models consider greater amounts of continuous reinforcement (deriving from ULS verifications) than the ones defined by the Eurocodes. Then it was chosen to evaluate the structural response by considering the minimum amount of tying calculated according to the Eurocodes provisions. Three distinct solutions have been considered: the minim tying defined by Eurocodes spread only between bottom bars, twice the Eurocodes amount spread between top and bottom bars, and finally twice the Eurocodes amount but spread only between bottom bars. The influence of this parameter was only tested on the models that use joists with collaborating slab as floor system.
- **Continuous reinforcement:** it was chosen to evaluate the structural response by considering continuous reinforcement on both primary beams

and secondary beams. Two solutions were tested for each scenario: in the manner the continuous reinforcement are only the bottom bars, in the latter both top and bottom bars are continuous. The influence of this parameter was only tested on the models that use joists with collaborating slab as floor system.

- **Seismic detailing:** Although the main structural regulations impose requirements about robustness, many structures are not designed with specific reference to this issue. However, these buildings have generally been designed to resist against an earthquake, in accordance the principles of the capacity design. In general, referring to reinforced concrete structures, this approach states that: dissipation zones must be designed to ensure good levels of ductility, continuous reinforcement must be arranged in the beams and the columns must be reinforced to prevent their collapse due to shear before of the formation of the dissipation zones in the beams (for bending moment and shear) and of the complete plasticization of themselves for bending moment. These details modify the behaviour also with regard to structural robustness. The influence of this parameter was only tested on the models that use joists with collaborating slab as floor system.

6.2 Collapse scenario 1 analysis

The collapse scenario 1 concerns the removal of an internal column, Figure 105 illustrates the position of the element.

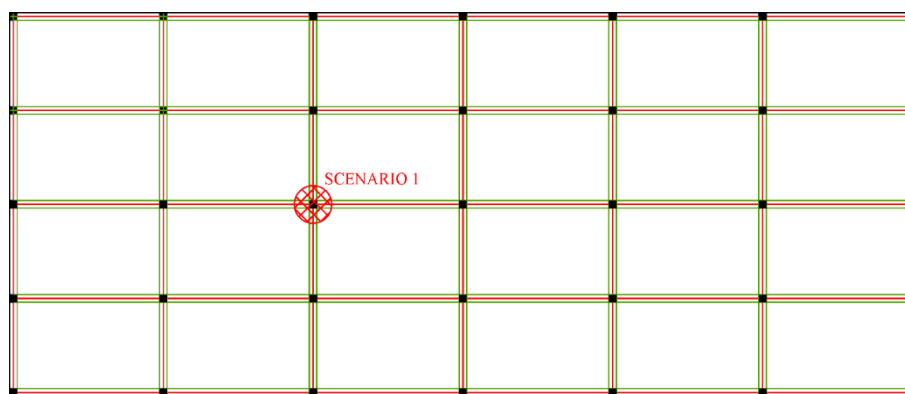


Figure 105: Collapse scenario 1

As mentioned, the column removal was simulated by imposing a vertical linearly increasing displacement of the node placed in correspondence of the top of the column removed.

6.2.1 Collapse scenario 1 – Floor system: Slab

Figure 106a shows the trend of the vertical reaction measured in correspondence of the column removed, for increasing vertical displacements. The evolution of this parameter in fact can be considered as a measure of the bearing capacity of the damaged structure.

For zero vertical displacement it can be observed a positive vertical reaction of about +500 kN which represents the axial force acting on the column before its removal. By progressively increasing the vertical displacement, the reaction decreases until it reaches a zero value, this condition physically identifies the vertical displacement which unloads the column and in this case is reached for a vertical displacement of about 2.5 cm.

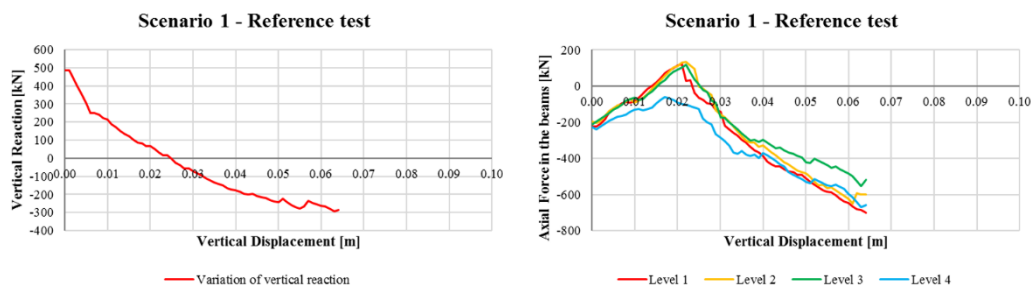


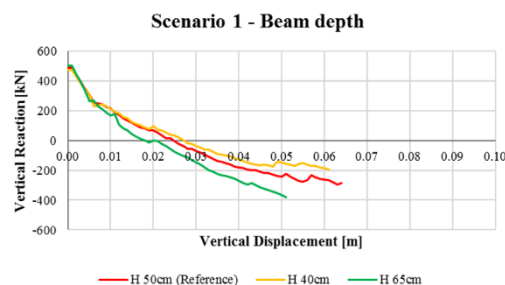
Figure 106: Collapse scenario 1 - Reference test

If the structure has additional resisting strength, the displacement can be furtherly increased. This causes the inversion of the sign of the reaction, hence the analysis proceeds until the ultimate load capacity is reached in one or more elements. The negative values achieved, about -300 kN for a vertical displacement of about 6.5 cm, can be interpreted as an extra-resistance resource exploitable by the damaged structure in accidental conditions. From a physical point of view, it can be explained as the need to apply a further external force, equal in modulus but opposite in sign respect to the measured reaction, to cause the structural collapse.

Based on the results previously reported in Chapter 4, it was monitored the trend of the axial force in the primary beams. The evolution of this parameter allows in fact to evaluate if the resistive mechanism changes from a predominantly flexural behaviour to a catenary one.

Simplified models highlighted that, if there is an appropriate amount of continuous reinforcement in the elements and if they have sufficient rotational capacity, increasing the vertical displacement the resisting mechanism switches from a flexural one to a tie one. In other words, by increasing the applied displacement, the beam zones close to the columns undergo a progressive plasticization. The beams, by means of their rotation, can transfer a portion of the vertical loads applied, exploiting the vertical component of the axial force transferred through the continuous reinforcements. Having this force in fact an inclination with respect to the horizontal axis (defined by the rotation of the beam necessary to withstand the vertical load), it will also have a horizontal component represented by a positive axial force in the beam. Figure 106b shows, the trend of the axial force in primary beam directly involved by the column removal (placed at level 1), and in the corresponding beams of the upper levels. It can be noted that at the beginning of the analysis all the beams are subjected to a negative axial force of about -200 kN, increasing the applied displacement the compression decreases progressively in all the elements. However, while the axial force of beams of levels 1, 2 and 3 switches to tension for imposed vertical displacement of the column between 1.5 ÷ 2.5 cm reaching a peak value of about +160 kN, the beam of level 4 remains in compression. By proceeding with the test all the beams return to compression, reaching maximum values between -510 ÷ -690 kN at the end of the analysis.

As mentioned, the influence of several parameters was tested to highlight the presence of possible decisive factors in the development of the structural response. Figure 107a shows the influence of different beam depths on the variation of vertical reaction, Figure 107b and Figure 107c show the trend of the axial force in the beams for both the solutions.



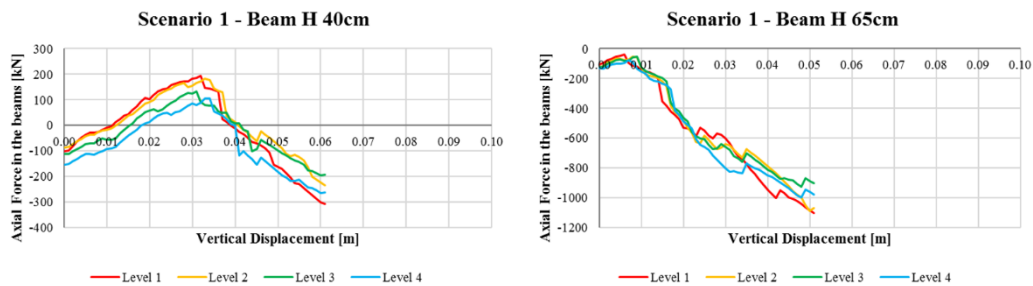


Figure 107: Collapse scenario 1 - Influence of primary beams depth

By comparing the curves reported in Figure 107a it can be noted that beams with great depth give better results in ultimate conditions than the standard test or the one with the highest span/depth ratio. In fact, although with this solution is reached a maximum displacement of 5 cm against the values of 6 cm reached with the other cases, the vertical reaction reached in ultimate condition is the highest if compared with the others, respectively -400 kN versus -250 kN for standard beams and -200 kN for beams with a depth of 40 cm.

By analysing the trend of the axial force in the beams it can be noted that the solution with H 40 cm beams shows a response close to the standard one, while with the solution with H 65 cm beams the elements remain in compression for all the analysis, reaching a maximum value of about -1100 kN. No appreciable differences of behaviour can be highlighted between the beams of the various levels.

Figure 108a shows the influence of a different column depth on the variation of vertical reaction, Figure 108b shows the trend of the axial force for H 60 cm columns solution.

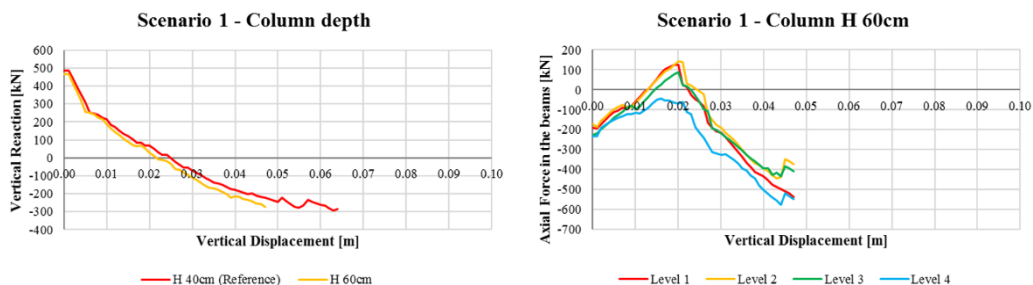


Figure 108: Collapse scenario 1 – Influence of columns depth

By comparing the curves reported in Figure 108a it can be noted that stiffer columns do not influence appreciably the results in ultimate conditions. In fact, although the maximum displacement reached is of about 4.7 cm against the values of 6.5 cm reached with the standard case, the vertical reaction reached in ultimate condition the same, about -300 kN.

Similar conclusions can be found by comparing the trend of the axial force in the beams. No appreciable differences of behaviour can be highlighted between the beams of the different levels.

Figure 109a shows the influence of different bracing systems on the variation of vertical reaction, Figure 109b, 109c and 109d show the trend of the axial force in the beams for all the solutions.

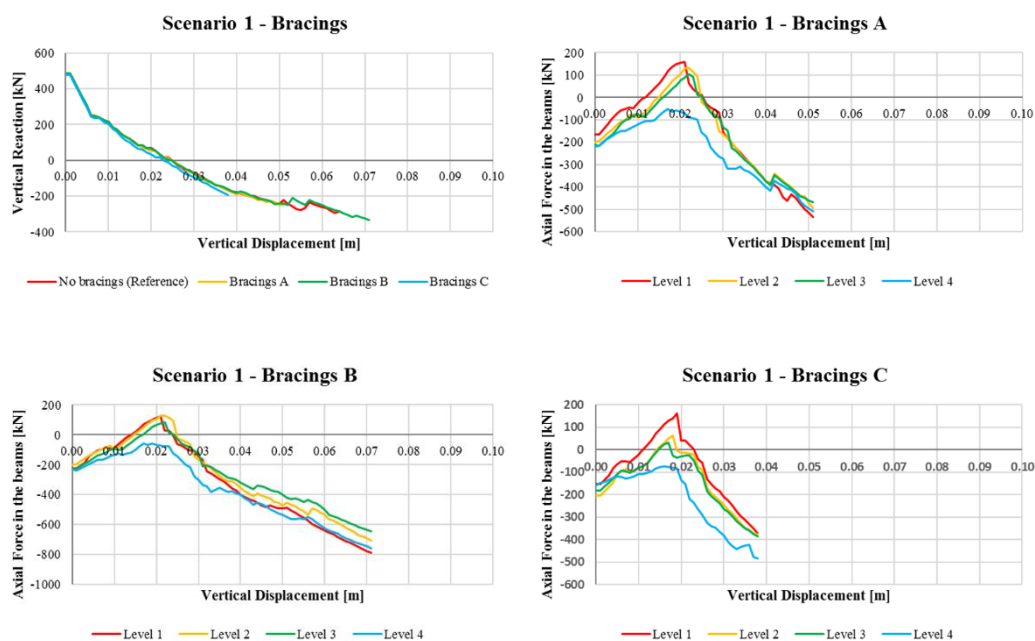


Figure 109: Collapse scenario 1 - Influence of bracings

By comparing the curves reported in Figure 109a it can be noted that the worse results are given by the bracing systems A and C with a maximum vertical reaction respectively of -200 and -220 kN against the ultimate values reached in the other cases, with -250 kN and -270 kN respectively. In terms of displacements the solution C is the worst with a maximum displacement of only 3.7 cm while the better results are shown by solution B with a maximum value of 7 cm.

By analysing the trend of the axial force in the beams, it can be noted that the global behaviour is similar to the reference one for all the solutions. No appreciable differences of behaviour can be highlighted between the beams of the different levels. Table 17 summarises the results obtained for scenario 1. Any cases in which the structure was not able to resist the removal of the column are highlighted in red.

Table 17: Collapse scenario 1 (Slab) – Summary of the results

Floor System	Scenario	Parameter tested	VR _i [kN]	δ(VR ₀) [cm]	VR _u [kN]	δ(VR _u) [cm]	
Floor System - Slab	1	Primary Beam depth	H=50cm (L/16) (RT)	485	-2.5	-287	-6.5
			H=40cm (L/20)	474	-2.7	-197	-6.1
			H=65cm (L/12)	500	-1.8	-380	-5.1
		Column depth	H=40cm (RT)	485	-2.5	-287	-6.5
			H=60cm	467	-2.2	-272	-4.7
		Bracing system	No Bracing (RT)	485	-2.5	-287	-6.5
			A	484	-2.5	-250	-5.1
			B	485	-2.5	-333	-7.1
			C	485	-2.3	-193	-3.8

(RT) = Reference Test; VR_i = Initial Vertical Reaction; δ(VR₀) = Vertical Displacement for Vertical Reaction = 0; VR_u = Ultimate Vertical Reaction; δ(VR_u) = Vertical Displacement for Ultimate Vertical Reaction.

6.2.2 Collapse scenario 1 – Floor system: Joists with collaborating slab

Figure 110a shows the trend of the vertical reaction measured in correspondence of the column removed, for increasing vertical displacements. For zero vertical displacement it can be observed a positive vertical reaction of about +350 kN which represents the axial force acting on the column before its removal. This value is lower than the one measured with slab solution due to the different floor system used. By progressively increasing the vertical displacement, the reaction decreases progressively until it reaches a zero value, this condition identifies the vertical displacement which unloads the column. This condition is reached for vertical displacement of about 6.5 cm versus the 2.5 cm necessary with slab solution.

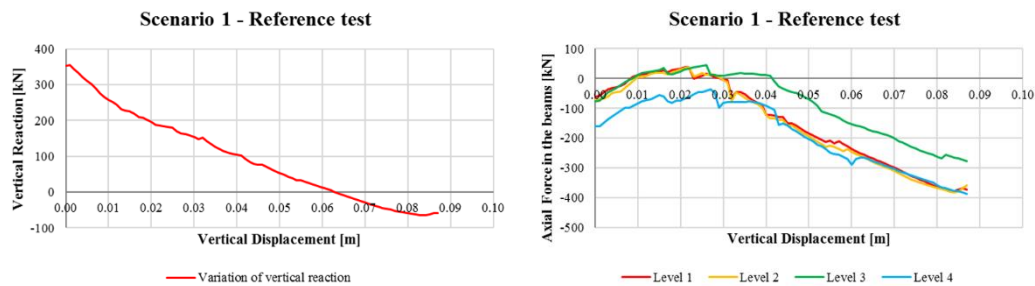
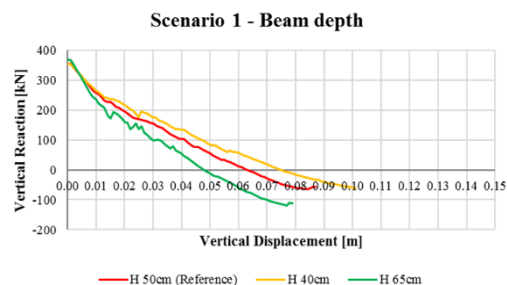


Figure 110: Collapse scenario 1 - Reference test

Further increasing the displacement, the ultimate condition is reached for a value of about 8.8 cm, in correspondence of this displacement the vertical reaction is equal to about -60 kN, smaller than the value of about -300 kN measured in slab solution, this means that the extra resistance resources are rather limited.

Figure 110b shows, the trend of the axial force in primary beams. It can be noted that at the beginning of the analysis all the beams are subjected to a negative axial force of about -80 kN, except for beam of level 4 that has an initial compression of about -180 kN. Increasing the applied displacement, the compression decreases progressively in all the elements, reaching negligible tension values in beams of level 1, 2 and 3, while the level 4 one remains in compression. Proceeding with the test all the beams return to compression, reaching a maximum value of -380 kN at the end of the analysis, except for level 3 beam that reaches a value of -280 kN.

Figure 111a shows the influence of beam depth on the variation of vertical reaction, Figure 111b and 111c show the trend of the axial force in the beams for both the solutions.



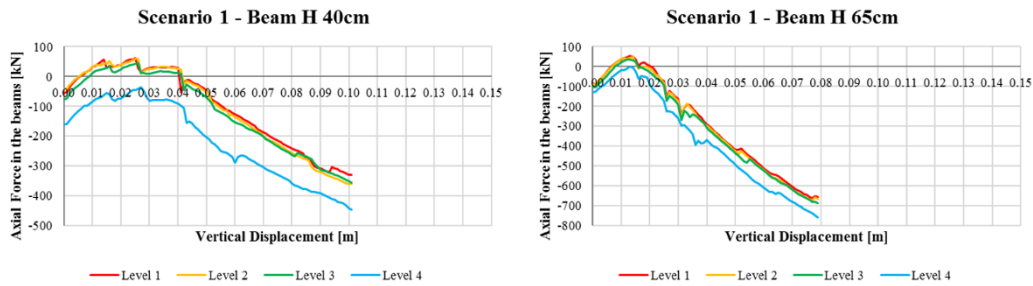


Figure 111: Collapse scenario 1 – Influence of primary beams depth

By comparing the curves reported in Figure 111a it can be noted that H 65 cm beam gives better results in ultimate conditions than the standard test or the one with the highest span/depth ratio. In fact, although with this solution is reached a maximum displacement of 7.9 cm against the values of 8.8 cm reached with the other cases, the vertical reaction reached in ultimate condition is the highest (-110 kN) if compared with the others (-60 kN).

By analysing the trend of the axial force in the beams it can be noted that both the solutions show a response similar to the reference one from a qualitative point of view. However, the solution with H 65 cm beams reaches a maximum compression between -650 ÷ -750 kN, while H 40 cm beams reach values between -320 ÷ -430 kN. No appreciable differences can be highlighted between the beams of the different levels.

Figure 112a shows the influence of a different column depth on the variation of vertical reaction, Figure 112b shows the trend of the axial force for H 60 cm columns solution.

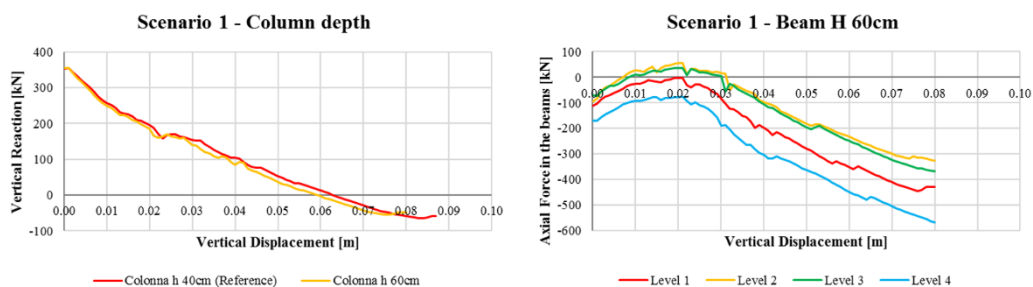


Figure 112: Collapse scenario 1 – Influence of columns depth

By comparing the curves reported in Figure 112a it can be noted that stiffer columns do not influence appreciably the results in ultimate conditions. Similar conclusions can be found by comparing the trend of the axial force in the beams. No appreciable differences of behaviour can be highlighted between the beams of the different levels.

Figure 113a shows the influence of different bracing systems on the variation of vertical reaction, Figure 113b, 113c and 113d show the trend of the axial force in the beams for all the solutions.

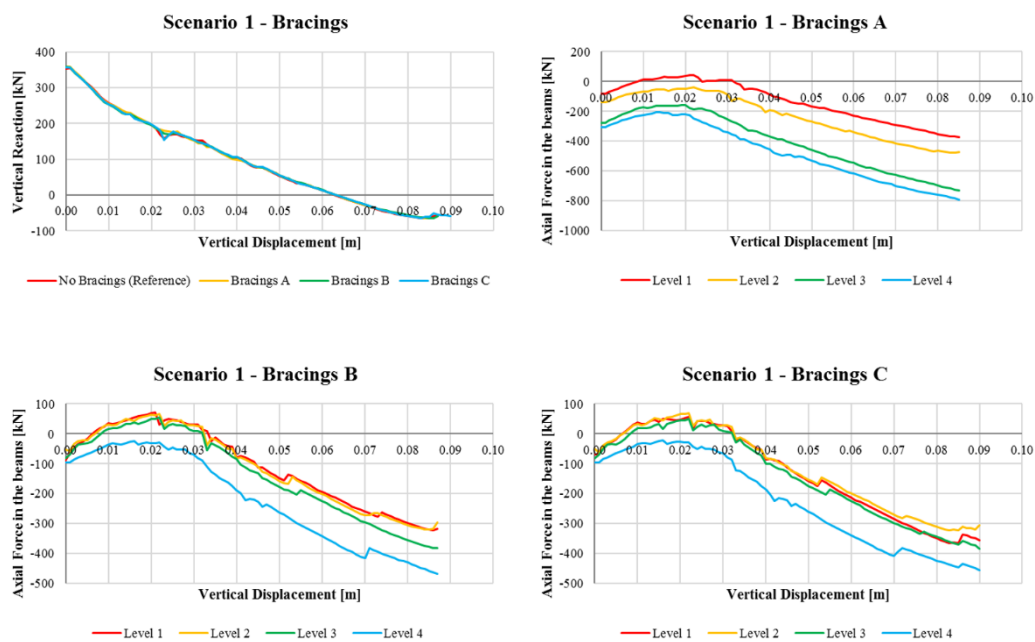


Figure 113: Collapse scenario 1 – Influence of bracing system

By comparing the curves reported in Figure 113a it can be noted all the bracing systems shown a similar response from a qualitative point of view. By comparing these results with the reference ones, the main difference is given by bracing system A that shows maximum compression values for all the beams, with a peak represented by -800 kN for level 4 element.

Figure 114a shows the response, in terms of variation of vertical reaction, obtainable by considering a limited amount of continuous reinforcement (compared with the reference test) but in line with Eurocodes provisions. Figure 114b, 114c and 114d show the trend of the axial force in the beams for all the solutions.

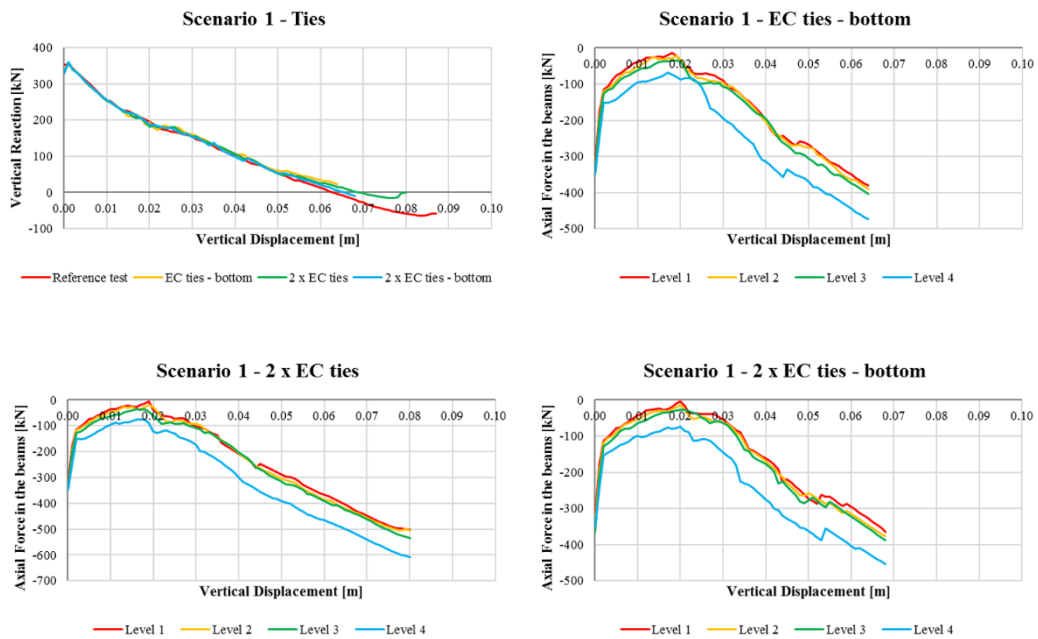
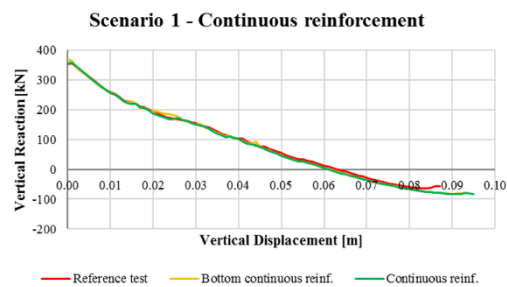


Figure 114: Collapse scenario 1 - Influence of minimum tying

By comparing the curves reported in Figure 114a it can be noted that by providing the minimum amount of continuous reinforcement defined by Eurocodes, the structure is not able to withstand the element removal. Slightly better results can be obtained by providing twice the minimum amount defined by the European standards. However, the strength resources are fairly limited. Figure 114b, 114c and 114d do not highlight significant changes in behaviour compared with the reference test.

Figure 115a shows the influence of continuous reinforcement on the variation of vertical reaction, Figure 115b and 115c show the trend of the axial force in the beams for both the solutions.



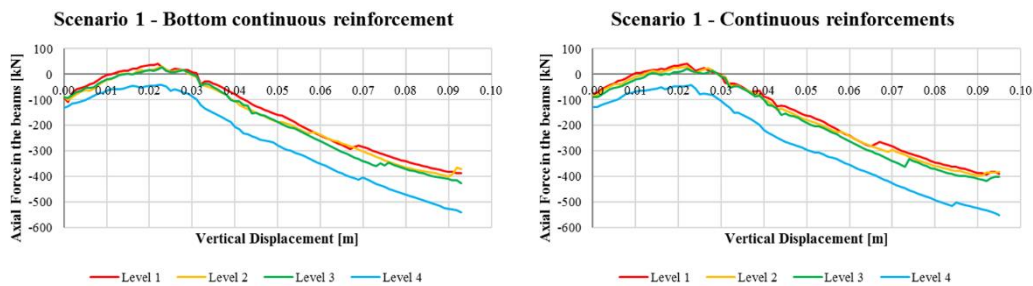


Figure 115: Collapse scenario 1 - Influence of continuous reinforcement

By comparing the curves reported in Figure 115a it can be noted that by arranging continuous top and bottom bars it can be obtained slightly better results in ultimate conditions than the standard test. However, the improvement in terms of structural response is negligible and above all economically unsuitable. Figure 115b and 110c do not highlight significant changes in behaviour.

Figure 116a shows the influence of seismic detailing on the variation of vertical reaction, Figure 116b shows the trend of the axial force of model designed to withstand the seismic action.

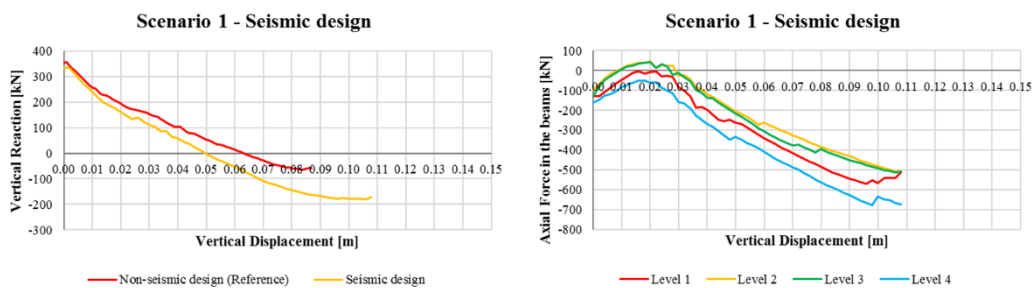


Figure 116: Collapse scenario 1 - Influence of seismic detailing

By comparing the curves reported in Figure 116a it must be highlighted that seismic detailing produces a noticeable improvement in terms of both ultimate vertical reaction (-190 kN against -60 kN) that maximum displacement (-10.8 cm against -8.8 cm). Therefore, seismic design greatly influences the overall structure response. Figure 116b instead does not show significant changes respect to the reference test. No appreciable differences of behaviour can be highlighted between the beams of the different levels. Table 18 summarises the results obtained for scenario 1. Any cases in which the structure was not able to resist the removal of the column are highlighted in red.

Table 18: Collapse scenario 1 (Joists + Collaborating Slab) – Summary of the results

Floor System	Scenario	Parameter tested	VR _i [kN]	δ(VR ₀) [cm]	VR _u [kN]	δ(VR _u) [cm]	
Floor System - Joists + collaborating slab	1	Primary Beam depth	H=50cm (L/16) (RT)	353	-6.3	-58	-8.7
			H=40cm (L/20)	352	-7.5	-61	-10.1
			H=65cm (L/12)	368	-4.8	-113	-7.9
		Column depth	H=40cm (RT)	353	-6.3	-58	-8.7
			H=60cm	355	-5.9	-48	-8.0
		Bracing system	No Bracing (RT)	353	-6.3	-58	-8.7
			A	358	-6.3	-64	-8.5
			B	358	-6.3	-58	-8.7
			C	357	-6.3	-58	-9.0
		Tyings	No Min EC (RT)	353	-6.3	-58	-8.7
			Min EC Bottom	330	-	24	-6.4
			2·Min EC Top&Bot	330	-6.9	-16	-8.0
			2·Min EC Bottom	329	-6.8	-9	-6.8
		Continuous Reinforcements	RT	353	-6.3	-58	-8.7
			Bottom	370	-6.1	-82	-9.3
			Top&Bottom	356	-6.1	-83	-9.5
		Detailing	Standard (RT)	353	-6.3	-58	-8.7
			Seismic	334	-2.5	-173	-5.4

(RT) = Reference Test; VR_i = Initial Vertical Reaction; δ(VR₀) = Vertical Displacement for Vertical Reaction = 0; VR_u = Ultimate Vertical Reaction; δ(VR_u) = Vertical Displacement for Ultimate Vertical Reaction.

6.3 Collapse scenario 2 analysis

The collapse scenario 2 concerns the removal of an edge column, Figure 117 illustrates the position of the element.

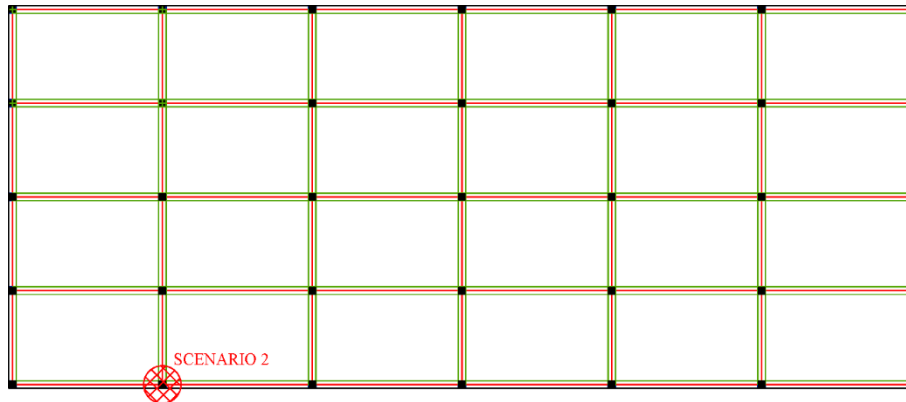


Figure 117: Collapse scenario 2

As mentioned, the column removal was simulated by imposing a vertical linearly increasing displacement of the node placed in correspondence of the top of the column removed.

6.3.1 Collapse scenario 2 – Floor system: slab

Figure 118a shows the trend of the vertical reaction measured in correspondence of the column removed, for increasing vertical displacements. For zero vertical displacement it can be observed a positive reaction of about +300 kN which represents the axial force acting on the column before its removal. By progressively increasing the displacement, the reaction decreases progressively until it reaches a zero value, this condition identifies the vertical displacement which unloads the column and is reached for vertical displacement of about 5 cm.

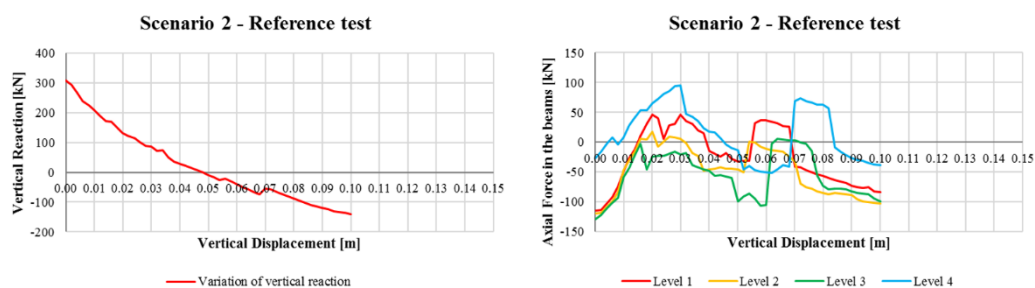


Figure 118: Collapse scenario 2 - Reference test

Further increasing the displacement, the ultimate condition is reached for a vertical displacement of about 10 cm, in correspondence of this displacement the vertical reaction is equal to about -130 kN.

Figure 118b shows, the trend of the axial force in primary beams. It is not possible to define a clear trend, in all situations it can be noted a fluctuation between tensile and compressive stresses, in any case the values are quite limited, between $-125 \div +95$ kN. At the beginning of the analysis all the beams are subjected to a negative axial force of about -125 kN, except for beam of level 4 that has an initial compression of about -25 kN.

Figure 119a shows the influence of beam depth on the variation of vertical reaction, Figure 119b and 119c show the trend of the axial force in the beams for both the solutions.

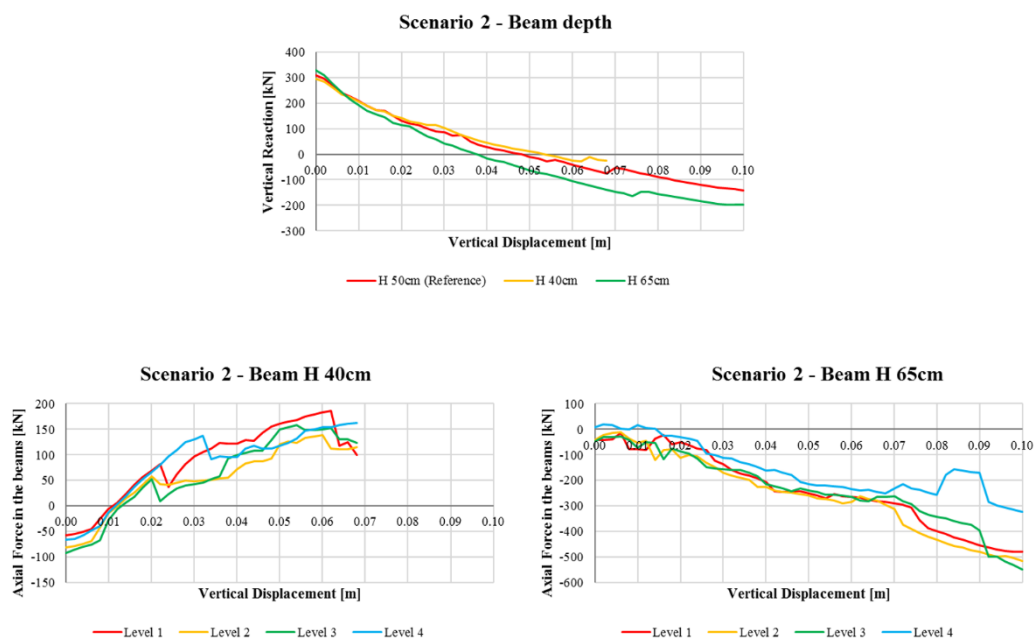


Figure 119: Collapse scenario 2 - Influence of primary beams depth

By comparing the curves reported in Figure 119a it can be noted that H 65 cm beams produce better results in ultimate conditions than the standard test or the one with the highest span/depth ratio. In fact, the vertical reaction reached in ultimate condition is the highest (-200 kN) if compared with the reference test (-125 kN). With regard to H 40 cm beams, it should be noted that in this case the reaction measured at the end of the analysis is of -10 kN, then the extra-resistance resources are virtually null.

By comparing the trend of the axial force in the beams there is a totally different behaviour between the tested solutions. In H 40 cm beams in fact, the compression decreases progressively, starting from a compressive value of about $-50 \div -100$ kN, until it becomes tension and then continues to grow until it reaches maximum values between +115 and +180 kN, after this point, it seems that the trend begins a decreasing phase, however the analysis is stopped so no further considerations can be done. H 65 cm beams instead start from negligible compressive values and remain in compression for all the test, reaching maximum values between $-315 \div -550$ kN. In both cases no appreciable behavioural differences can be highlighted between the beams of the different levels.

Figure 120a shows the influence of a different column depth on the variation of vertical reaction, Figure 120b shows the trend of the axial force for H 60 cm columns solution.

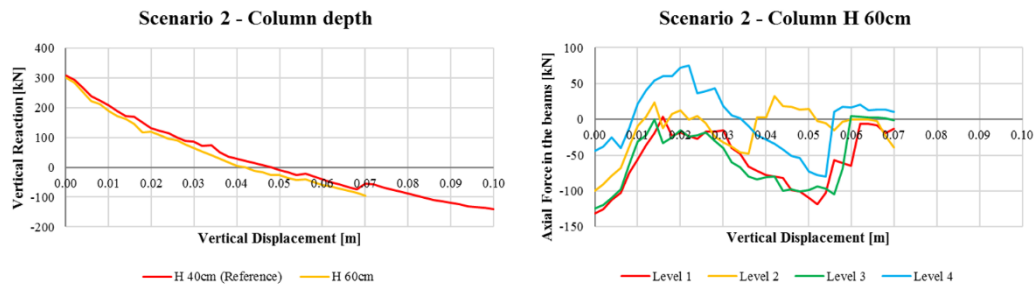
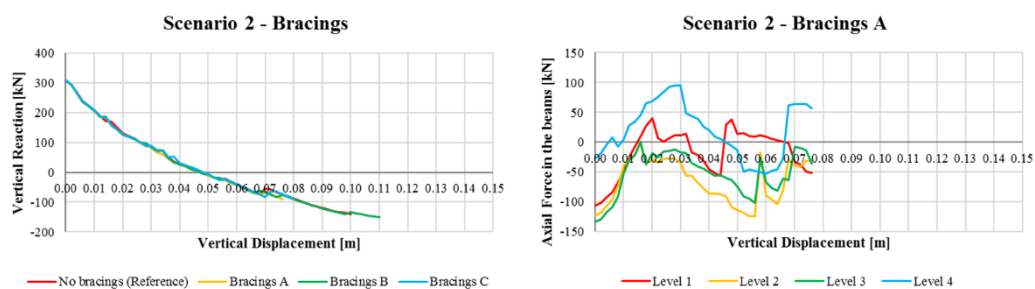


Figure 120: Collapse scenario 2 – Influence of columns depth

By comparing the curves reported in Figure 120a it can be noted that stiffer columns give slightly worse results in terms of vertical reaction, -100 kN against -130 kN. A greater difference is noted in terms of ultimate displacement, 7 cm against 10cm.

About the trend of the axial force, it can be noted a similar response to the reference one.

Figure 121a shows the influence of different bracing systems on the variation of vertical reaction, Figure 121b, 121c and 121d show the trend of the axial force in the beams for all the solutions.



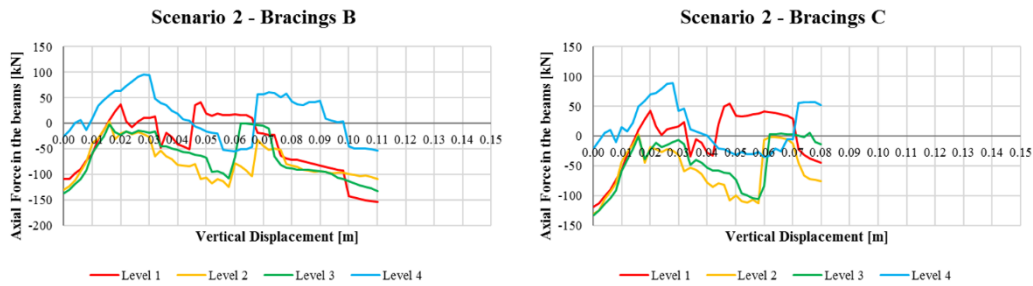


Figure 121: Collapse scenario 2 – Influence of bracing system

By comparing the curves reported in Figure 121a it can be noted all the bracing systems tested shown a similar response from a qualitative point of view. Thus, in this case the presence of bracing system and the type of bracing seem to play a marginal role. Table 19 summarises the results obtained for scenario 2. Any cases in which the structure was not able to resist the removal of the column are highlighted in red.

Table 19: Collapse scenario 2 (Slab) – Summary of the results

Floor System	Scenario	Parameter tested	VR_i [kN]	$\delta(VR_0)$ [cm]	VR_u [kN]	$\delta(VR_u)$ [cm]	
Floor System - Slab	2	Primary Beam depth	H=50cm (L/16) (RT)	308	-4.8	-141	-10
			H=40cm (L/20)	296	-5.4	-26	-6.8
			H=65cm (L/12)	327	-3.6	-197	-10
		Column depth	H=40cm (RT)	308	-4.8	-141	-10
			H=60cm	301	-4.2	-96	-7
		Bracing system	No Bracing (RT)	308	-4.8	-141	-10
			A	306	-4.8	-90	-7.6
			B	307	-4.8	-151	-11
			C	308	-4.8	-88	-8

(RT) = Reference Test; VR_i = Initial Vertical Reaction; $\delta(VR_0)$ = Vertical Displacement for Vertical Reaction = 0; VR_u = Ultimate Vertical Reaction; $\delta(VR_u)$ = Vertical Displacement for Ultimate Vertical Reaction.

6.3.2 Collapse scenario 2 – Floor system: joist with collaborating slab

Figure 122a shows the trend of the vertical reaction measured in correspondence of the column removed, for increasing vertical displacements. For zero vertical displacement it can be observed a positive vertical reaction of about +155 kN which represents the axial force acting on the column before its removal. By progressively increasing the vertical displacement, the reaction decreases progressively until it reaches a zero value, this condition identifies the vertical

displacement which unloads the column. This condition is reached for vertical displacement of about 7 cm.

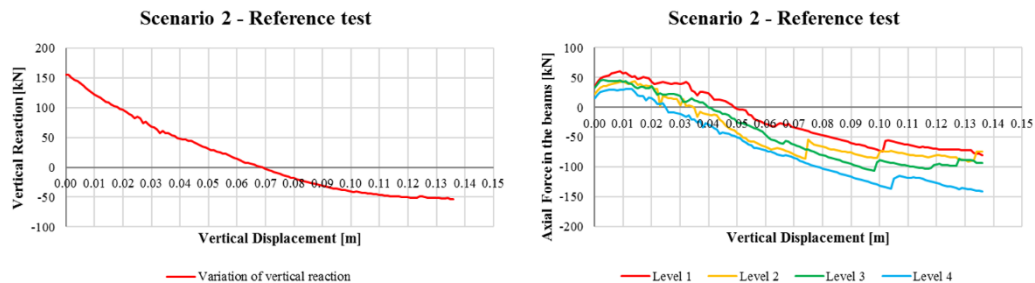
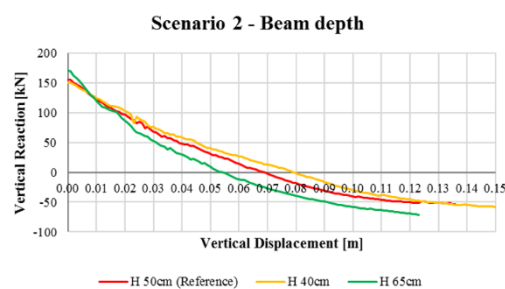


Figure 122: Collapse scenario 2 – Reference test

Further increasing the displacement, the ultimate condition is reached for a vertical displacement of about 13.5 cm, in correspondence of this displacement the vertical reaction is equal to about -50 kN. Thus, in this condition the structure is capable of great displacement if compared with the other scenarios. Despite of this, the ultimate reaction remains quite limited, as seen for scenario 1.

Figure 122b shows, the trend of the axial force in primary beams. All beams are initially subjected to a positive axial force, even though negligible. Proceeding with the analysis it is noted that the tension gradually decreases until it becomes compression and reaches maximum values between $-75 \div -145$ kN.

Figure 123a shows the influence of beam depth on the variation of vertical reaction, Figure 123b and 123c show the trend of the axial force in the beams for both the solutions.



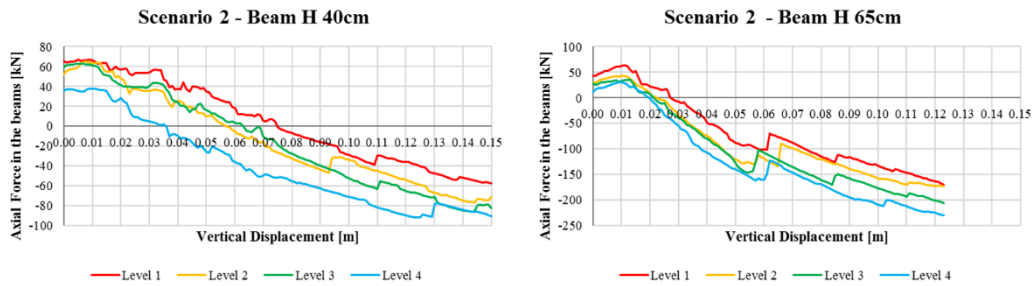


Figure 123: Collapse scenario 2 – Influence of primary beams depth

By comparing the curves reported in Figure 123a it can be noted that H 65 cm beam gives slightly better results in ultimate conditions than the other tests. In fact, the vertical reaction reached in ultimate condition is the highest (-75 kN) if compared with the reference test and H 40 cm beam test (-50 kN). By analysing the ultimate displacement, it can be noted that H 40 cm beams show a better behaviour, reaching a final displacement of 15 cm.

About the trend of the axial force in the beams, it can be noted that both the solutions shown a response similar to the reference one. In both cases no appreciable differences of behaviour can be highlighted between the beams of the different levels.

Figure 124a shows the influence of a different column depth on the variation of vertical reaction, Figure 124b shows the trend of the axial force for H 60 cm columns solution.

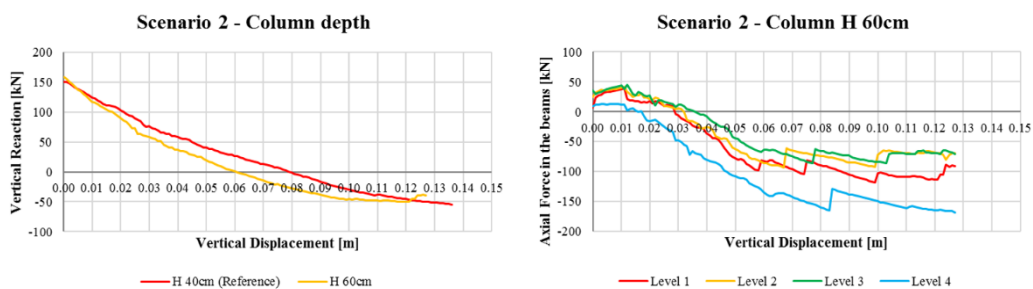


Figure 124: Collapse scenario 2 - Influence of beams depth

By comparing the curves reported in Figure 124a it can be noted that stiffer columns do not influence appreciably the results in ultimate conditions. Similar conclusions can be found by comparing the trend of the axial force in the beams.

No appreciable differences can be highlighted between the beams of the different levels. About the trend of the axial force, it can be noted a similar response to the reference one.

Figure 124a shows the influence of different bracing systems on the variation of vertical reaction, Figure 124b, 124c and 124d show the trend of the axial force in the beams for all the solutions.

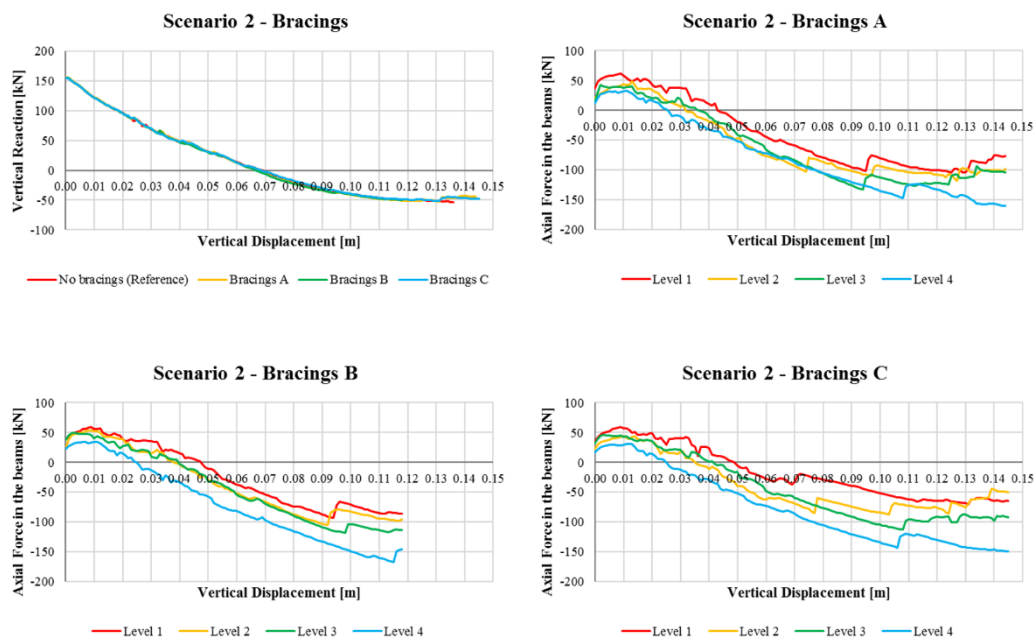


Figure 125: Collapse scenario 2 - Influence of bracings system

By comparing the curves reported in Figure 125a it can be noted all the bracing systems shown a similar response from a qualitative point of view. Thus, in this case the presence of bracing system and the type of bracing seem to play a marginal role.

Figure 126a shows the response, in terms of variation of vertical reaction, obtainable by considering a limited amount of continuous reinforcement (compared with the reference test) but in line with Eurocodes provisions. Figure 126b, 126c and 126d show the trend of the axial force in the beams for all the solutions.

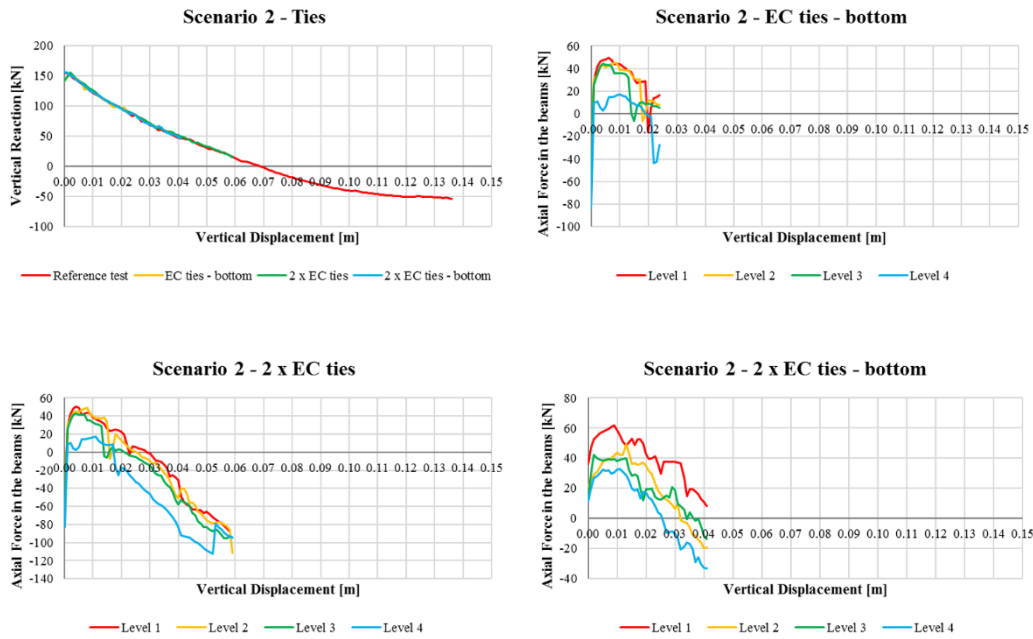
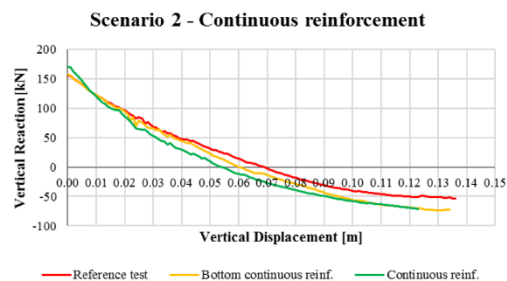


Figure 126: Collapse scenario 2 - Influence of minimum tying

By comparing the curves reported in Figure 126a it can be noted that by providing the minimum amount of continuous reinforcement defined by Eurocodes, the structure is not able to withstand the element removal. Unlike the scenario 1, the response does not improve even by doubling the minimum tying. Figure 126b, 126c and 126d report significant fluctuation in the trend of axial force in the beams, confirming the difficulties faced by the structure in seeking an equilibrium condition.

Figure 127a shows the influence of continuous reinforcement on the variation of vertical reaction, Figure 127b and 127c show the trend of the axial force in the beams for both the solutions.



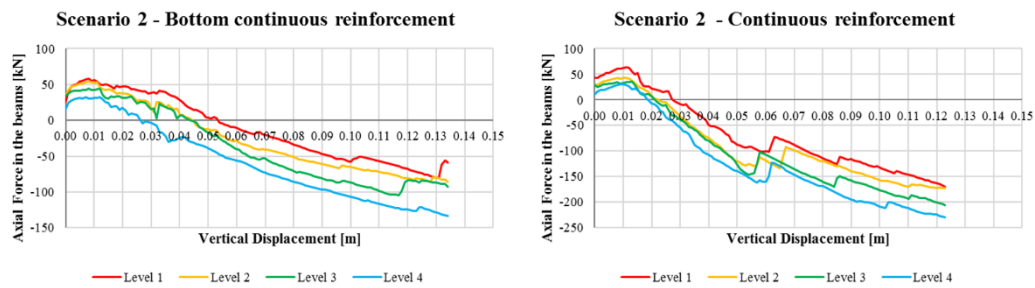


Figure 127: Collapse scenario 2 - Influence of continuous reinforcement

By comparing the curves reported in Figure 127a it can be noted that by arranging all the bars continuous it can be obtained better results in ultimate conditions than the standard test. The same improvement has been achieved by providing only bottom bars continuous. Therefore, the latter solution could be adopted to improve the response. Figure 127b and 127c do not highlight significant changes in behaviour.

Figure 128a shows the influence of seismic detailing on the variation of vertical reaction, Figure 128b shows the trend of the axial force of model designed to withstand the seismic action.

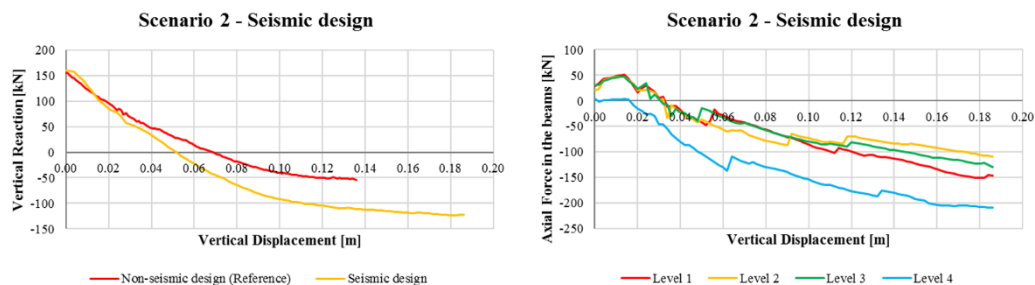


Figure 128: Collapse scenario 2 - Influence of seismic detailing

By comparing the curves reported in Figure 128a it must be highlighted that seismic detailing produces a noticeable improvement in terms of both ultimate vertical reaction (-120 kN against -50 kN) that maximum displacement (-13.5 cm against -18.6 cm). Therefore, seismic design greatly influences the overall structure response. Figure 128b instead does not show significative changes respect to the reference test. Table 20 summarises the results obtained for scenario 2. Any cases in which the structure was not able to resist the removal of the column are highlighted in red.

Table 20: Collapse scenario 2 (Joists + Collaborating slab) – Summary of the results

Floor System	Scenario	Parameter tested	VR _i [kN]	δ(VR ₀) [cm]	VR _u [kN]	δ(VR _u) [cm]	
Floor System - Joists + collaborating slab	2	Primary Beam depth	H=50cm (L/16) (RT)	155	-6.9	-54	-13.6
			H=40cm (L/20)	151	-7.9	-58	-15.0
			H=65cm (L/12)	170	-5.4	-71	-12.3
		Column depth	H=40cm (RT)	155	-6.9	-54	-13.6
			H=60cm	158	-6	-39	-12.7
		Bracing system	No Bracing (RT)	155	-6.9	-54	-13.6
			A	157	-6.7	-44	-14.4
			B	155	-6.7	-50	-11.8
			C	155	-6.9	-48	-14.5
		Tyings	No Min EC (RT)	155	-6.9	-54	-13.6
			Min EC Bottom	142	-	87	-2.4
			2·Min EC Top&Bot	142	-	15	-5.9
			2·Min EC Bottom	157	-	46	-4.1
		Continuous Reinforcements	RT	155	-6.9	-54	-13.6
			Bottom	158	-6	-73	-13.5
			Top&Bottom	170	-5.4	-71	-12.3
		Detailing	Standard (RT)	155	-6.9	-54	-13.6
			Seismic	160	-2.6	-122	-9.3

(RT) = Reference Test; VR_i = Initial Vertical Reaction; δ(VR₀) = Vertical Displacement for Vertical Reaction = 0; VR_u = Ultimate Vertical Reaction; δ(VR_u) = Vertical Displacement for Ultimate Vertical Reaction.

6.4 Collapse scenario 3 analysis

The collapse scenario 3 concerns the removal of a corner column, Figure 129 illustrates the position of the element.

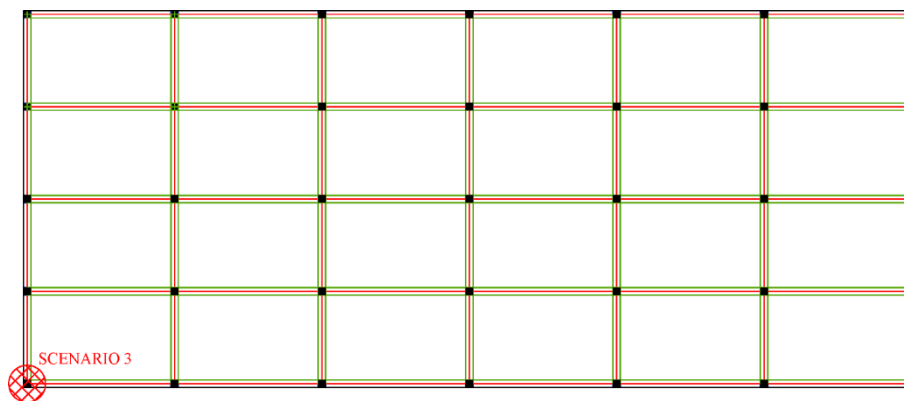


Figure 129: Collapse scenario 3

As mentioned, the column removal was simulated by imposing a vertical linearly increasing displacement of the node placed in correspondence of the top of the column removed.

6.4.1 Collapse scenario 3 – Floor system: slab

Figure 130a shows the trend of the vertical reaction measured in correspondence of the column removed, for increasing vertical displacements. For zero vertical displacement it can be observed a positive vertical reaction of about +165 kN which represents the axial force acting on the column before its removal. By progressively increasing the displacement, the reaction decreases progressively until it reaches a zero value, this condition identifies the vertical displacement which unloads the column. This condition is reached for vertical displacement of about 4.8 cm.

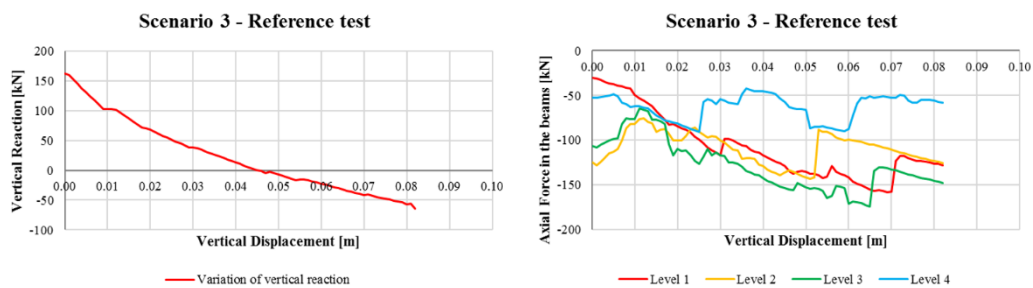


Figure 130: Collapse scenario 3 - Reference test

Further increasing the displacement, the ultimate condition is reached for a vertical displacement of about 8.2 cm, in correspondence of this displacement the vertical reaction is equal to about -55 kN.

Figure 130b shows, the trend of the axial force in primary beams. It can be noted that, although it is not possible to define a clear trend especially for level 2 and level 4 elements, in all situations the beams are subjected to compressive stresses.

Figure 131a shows the influence of beam depth on the variation of vertical reaction, Figure 131b and 131c show the trend of the axial force in the beams for both the solutions.

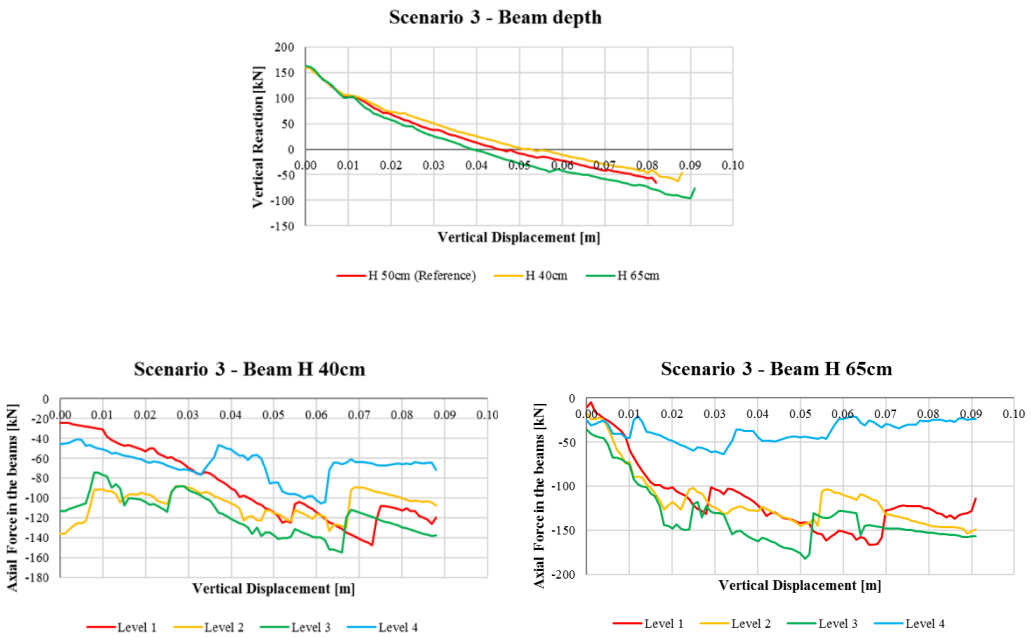


Figure 131: Collapse scenario 3 - Influence of primary beams depth

By comparing the curves reported in Figure 131a it can be noted that H 65 cm beam gives better results in ultimate conditions than the standard test or the one with the highest span/depth ratio. In fact, the vertical reaction reached in ultimate condition is the highest (-100 kN) if compared with the other tests (-60 kN).

By analysing the trend of the axial force in the beams it can be noted that both the solutions show a response similar to the reference one from a qualitative point of view.

Figure 132a shows the influence of a different column depth on the variation of vertical reaction, Figure 132b shows the trend of the axial force for H 60 cm columns solution.

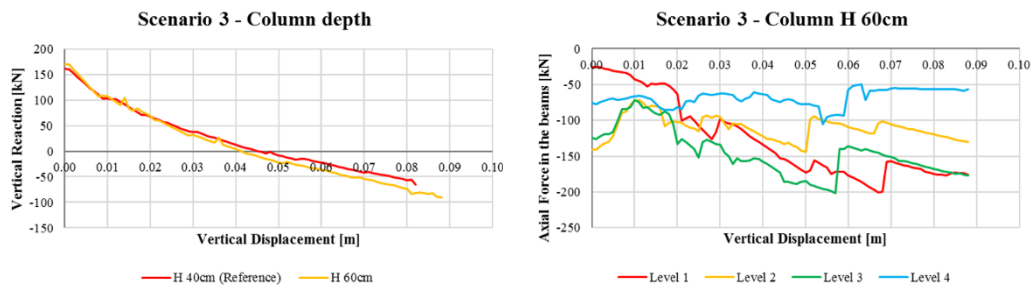


Figure 132: Collapse scenario 3 - Influence of columns depth

By comparing the curves reported in Figure 132a it can be noted that by using stiffer columns it is possible to achieve slightly better results in terms of vertical reaction, -90 kN against -60 kN. Similar considerations can be done in terms of ultimate displacement, 8.8 cm against 8.2 cm.

About the trend of the axial force, it can be noted a similar response to the reference one.

Figure 133a shows the influence of different bracing systems on the variation of vertical reaction, Figure 133b, 133c and 133d show the trend of the axial force in the beams for all the solutions.

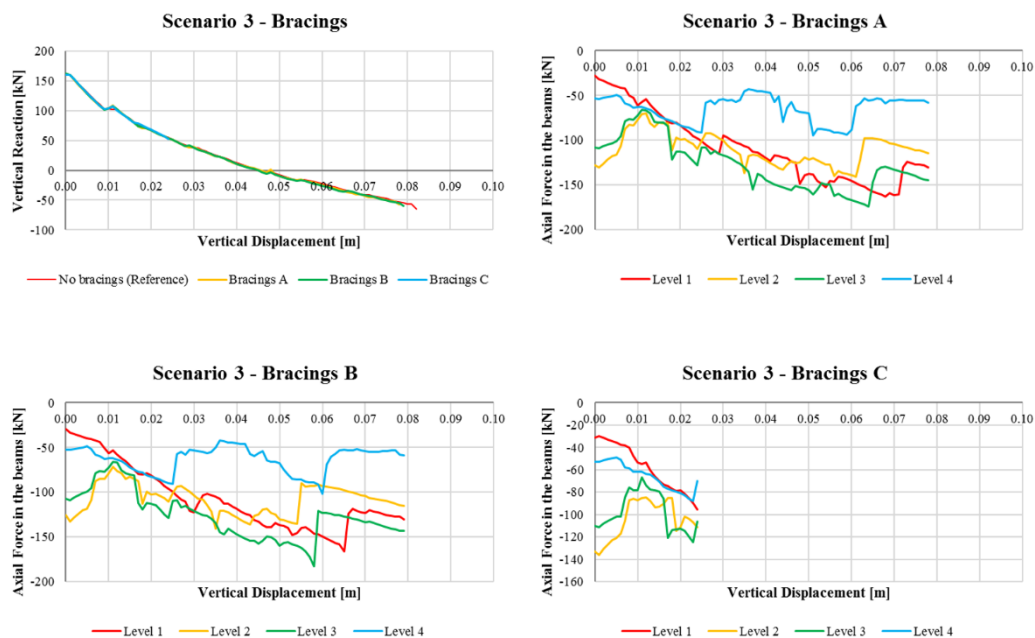


Figure 133: Collapse scenario 3 - Influence of bracing systems

By comparing the curves reported in Figure 133a it can be noted that bracing systems A and B shown a similar response from a qualitative point of view to the reference one. The same consideration can be done for bracing system C, however in this case the analysis stopped after only 2.5 cm. Table 21 summarises the results obtained for scenario 3. Any cases in which the structure was not able to resist the removal of the column are highlighted in red.

Table 21: Collapse scenario 3 (Slab) – Summary of the results

Floor System	Scenario	Parameter tested	VR _i [kN]	δ(VR ₀) [cm]	VR _u [kN]	δ(VR _u) [cm]	
Floor System - Slab	3	Primary Beam depth	H=50cm (L/16) (RT)	162	-4.5	-65	-8.2
			H=40cm (L/20)	158	-	39	-6.8
			H=65cm (L/12)	162	-9	-7	-10
		Column depth	H=40cm (RT)	162	-4.5	-65	-8.2
			H=60cm	170	-4.1	-90	-8.8
		Bracing system	No Bracing (RT)	162	-4.5	-65	-8.2
			A	161	-4.6	-57	-7.8
			B	161	-4.5	-59	-7.9
			C	160	-	52	-2.4

(RT) = Reference Test; VR_i = Initial Vertical Reaction; δ(VR₀) = Vertical Displacement for Vertical Reaction = 0; VR_u = Ultimate Vertical Reaction; δ(VR_u) = Vertical Displacement for Ultimate Vertical Reaction.

6.4.2 Collapse scenario 3 – Floor systems: joists with collaborating slab

Figure 134a shows the trend of the vertical reaction measured in correspondence of the column removed, for increasing vertical displacements. For zero displacement it can be observed a positive vertical reaction of about +78 kN which represents the axial force acting on the column before its removal. By progressively increasing the vertical displacement, the reaction decreases progressively until it reaches a zero value, this condition identifies the displacement which unloads the column. This condition is reached for vertical displacement of about 7 cm.

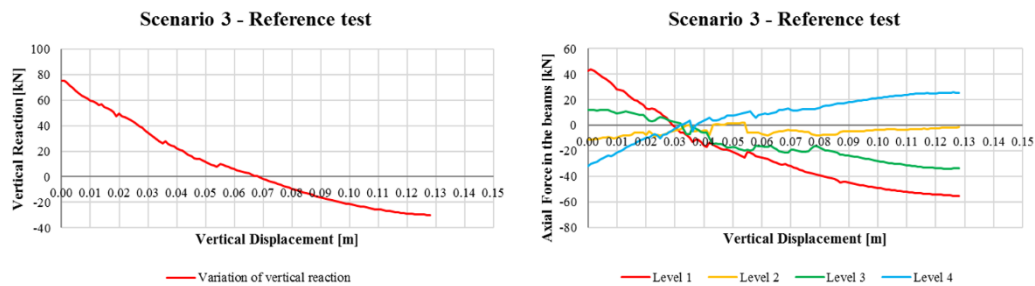
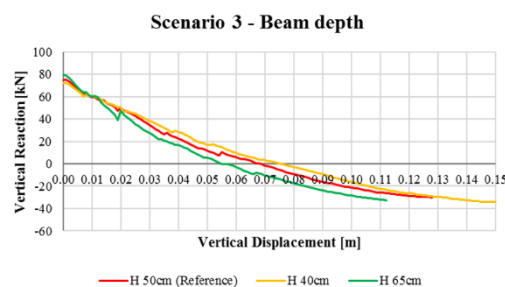


Figure 134: Collapse scenario 3 - Reference test

Further increasing the displacement, the ultimate condition is reached for a vertical displacement of about 12.8 cm, in correspondence of this displacement the vertical reaction is equal to about -30 kN. Thus, the structure is capable of greater displacement if compared with the other scenarios. Despite of this, the ultimate reaction remains quite limited, as seen for scenario 1.

Figure 134b shows, the trend of the axial force in primary beams. In this case it can be noted a particular response in beams of different levels. In fact, beams of levels 1 and 3 start with a positive axial force (between $15 \div 40$ kN) that decreases progressively until it becomes compression (between $-27 \div -57$ kN). Vice versa beams of levels 2 and 4 at the beginning exhibit a negative axial force (in the range $-17 \div -35$ kN) that decreases progressively until it becomes tension (ranging from 0 kN to +23 kN).

Figure 135a shows the influence of the beam depth on the variation of the vertical reaction. Figure 135b and 135c show the trend of the axial force in the beams for both the solutions.



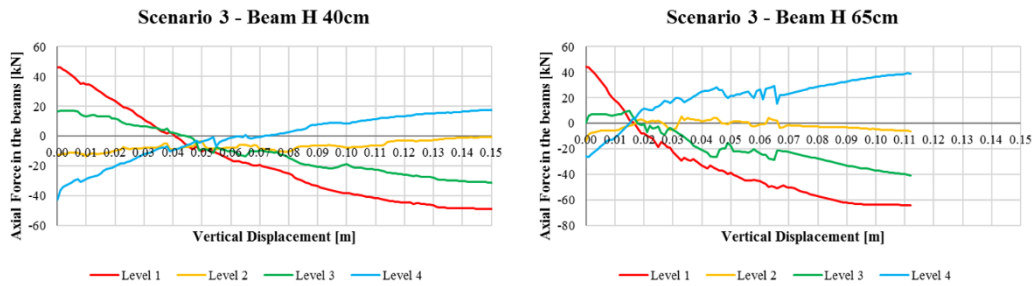


Figure 135: Collapse scenario 3 - Influence of primary beam depths

By comparing the curves reported in Figure 135a it can be noted that both the solutions give the same result in terms of vertical reaction, about -30 kN. By analysing the ultimate displacement, it can be noted that H 40 cm beams show a better behaviour, reaching a final displacement of 15 cm.

About the trend of the axial force in the beams, it can be noted that both the solutions show a response similar to the reference one.

Figure 136a shows the influence of a different column depth on the variation of vertical reaction, Figure 136b shows the trend of the axial force for H 60 cm columns solution.

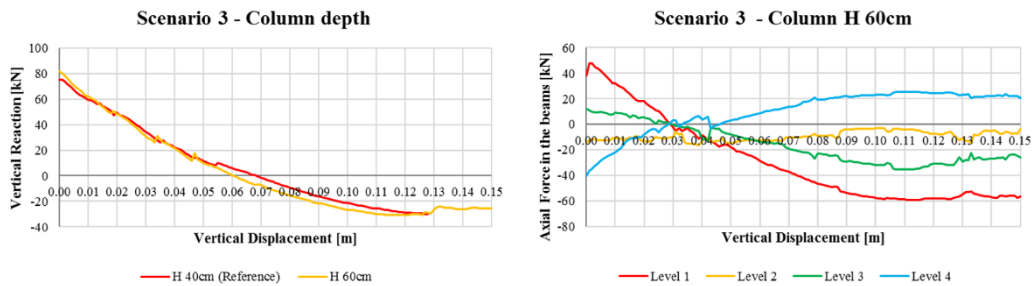


Figure 136: Collapse scenario 3 - Influence of columns depth

By comparing the curves reported in Figure 136a it can be noted that stiffer columns do not influence appreciably the results in ultimate conditions, although the ultimate displacement reached is of 15 cm against the value of 12.8 cm recorded during the reference test. Similar conclusions can be found by comparing the trend of the axial force in the beams.

Figure 137a shows the influence of different bracing systems on the variation of vertical reaction, Figure 137b, 137c and 137d show the trend of the axial force in the beams for all the solutions.

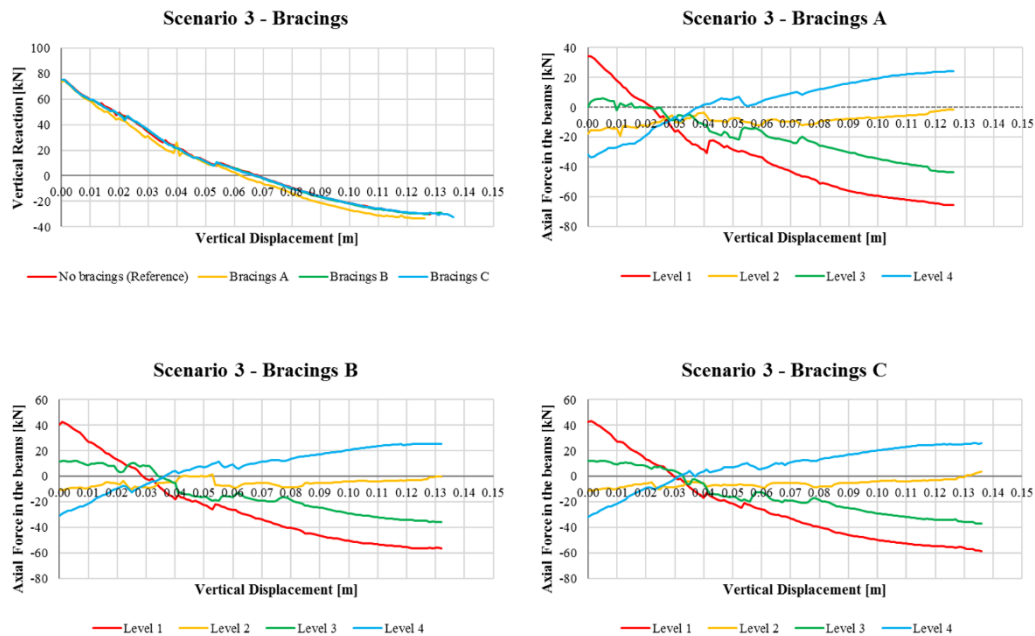


Figure 137: Collapse scenario 3 - Influence of bracing systems

By comparing the curves reported in Figure 137a it can be noted all the bracing systems exhibit a similar response from a qualitative point of view. Thus, in this case the presence of bracing system and the type of bracing seem to play a marginal role.

Figure 138a shows the response, in terms of variation of vertical reaction, achievable by considering a limited amount of continuous reinforcement (compared with the reference test) but in line with Eurocodes provisions. Figure 138b, 138c and 138d show the trend of the axial force in the beams for all the solutions.

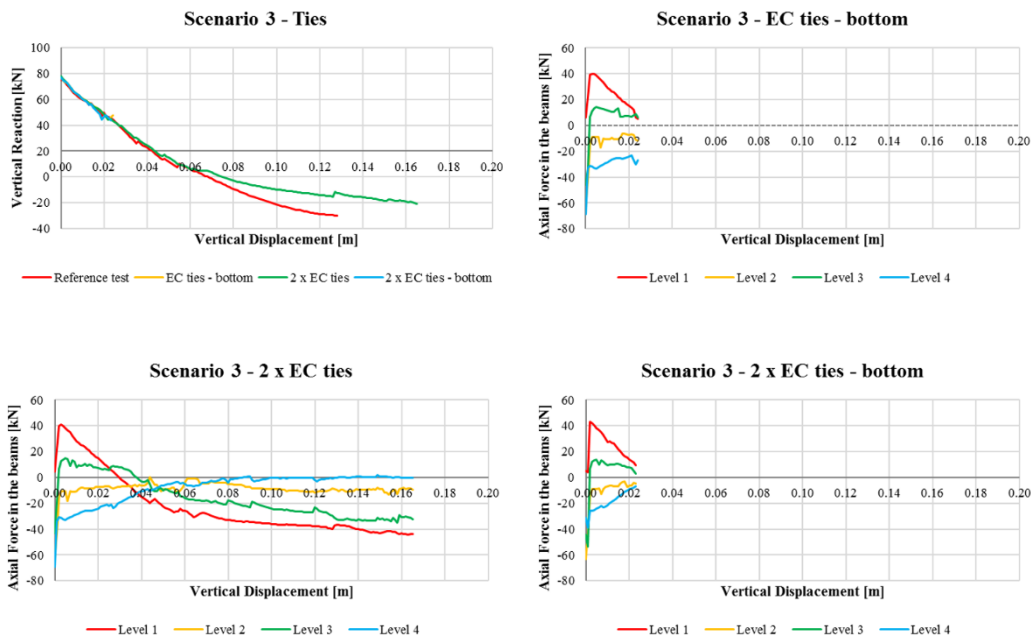


Figure 138: Collapse scenario 3 - Influence of minimum tying

By comparing the curves reported in Figure 138a it can be noted that by providing the minimum amount of continuous reinforcement defined by Eurocodes, the structure is not able to withstand the element removal. Unlike the scenario 1, the response does not improve even by doubling the minimum tying. In fact, although doubling the reinforcement it is possible to apply a greater displacement, the ultimate vertical reaction is smaller than the one achieved with the reference test. Figure 138c does not show significant changes in beam response compared to the reference test. The trends shown in Figure 138b and 138d cannot be considered significant.

Figure 139a shows the influence of continuous reinforcement on the variation of vertical reaction, Figure 139b and 139c show the trend of the axial force in the beams for both the solutions.

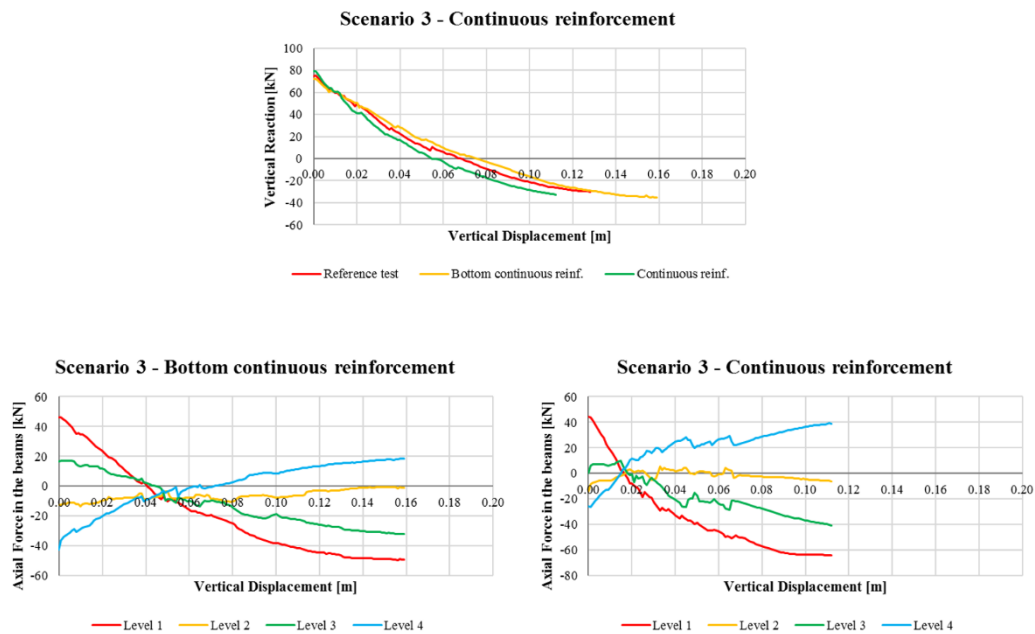


Figure 139: Collapse scenario 3 - Influence of continuous reinforcement

By comparing the curves reported in Figure 139a it can be noted that by arranging continuous top and bottom bars it can be obtained slightly better results in ultimate conditions than the standard test. However, the improvement in terms of structural response is negligible and above all economically unsuitable. Figure 139b and 139c do not highlight significant changes in behaviour compared to the reference test.

Figure 140a shows the influence of seismic detailing on the variation of vertical reaction, Figure 140b shows the trend of the axial force of model designed to withstand the seismic action.

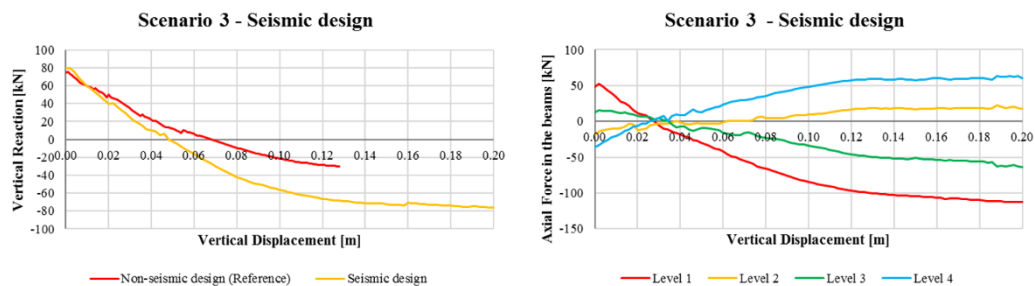


Figure 140: Collapse scenario 3 - Influence of seismic detailing

By comparing the curves reported in Figure 140a it must be highlighted that seismic detailing produces a remarkable improvement in terms of both ultimate vertical reaction (-80 kN against -30 kN) that maximum displacement (-12.8 cm against -20.0 cm). Therefore, seismic design greatly influences the overall structural response. Figure 140b instead does not show significative changes respect to the reference test. Table 22 summarises the results obtained for scenario 3. In red are highlighted the cases in which the structure was not able to withstand the column removal.

Table 22: Collapse scenario 3 (Joists + Collaborating slab) – Summary of the results

Floor System	Scenario	Parameter tested	VR _i [kN]	δ(VR ₀) [cm]	VR _u [kN]	δ(VR _u) [cm]	
Floor System - Joists + collaborating slab	3	Primary Beam depth	H=50cm (L/16) (RT)	75	-6.8	-30	-12.8
			H=40cm (L/20)	72	-7.5	-35	-15.9
			H=65cm (L/12)	79	-5.5	-33	-11.2
		Column depth	H=40cm (RT)	75	-6.8	-30	-12.8
			H=60cm	82	-6	-23	-15.7
		Bracing system	No Bracing (RT)	75	-6.8	-30	-12.8
			A	74	-6.2	-34	-12.6
			B	75	-6.7	-29	-13.2
			C	75	-6.8	-32	-13.6
		Tyings	No Min EC (RT)	75	-6.8	-30	-12.8
			Min EC Bottom	64	-	48	-2.4
			2·Min EC Top&Bot	64	-7.5	-21	-16.5
			2·Min EC Bottom	64	-	44	-2.3
		Continuous Reinforcements	RT	75	-6.8	-30	-12.8
			Bottom	72	-7.5	-35	-15.9
			Top&Bottom	79	-5.5	-33	-11.2
		Detailing	Standard (RT)	75	-6.8	-30	-12.8
			Seismic	80	-2.4	-76	-10.0

(RT) = Reference Test; VR_i = Initial Vertical Reaction; δ(VR₀) = Vertical Displacement for Vertical Reaction = 0; VR_u = Ultimate Vertical Reaction; δ(VR_u) = Vertical Displacement for Ultimate Vertical Reaction.

6.5 Collapse scenario 4 analysis

The collapse scenario 4 concerns the removal of an internal column. However, unlike scenario 1, the element directly involved by the failure is placed closer to the edges of the building, therefore the boundary conditions are different. Figure 141 illustrates the position of the element.

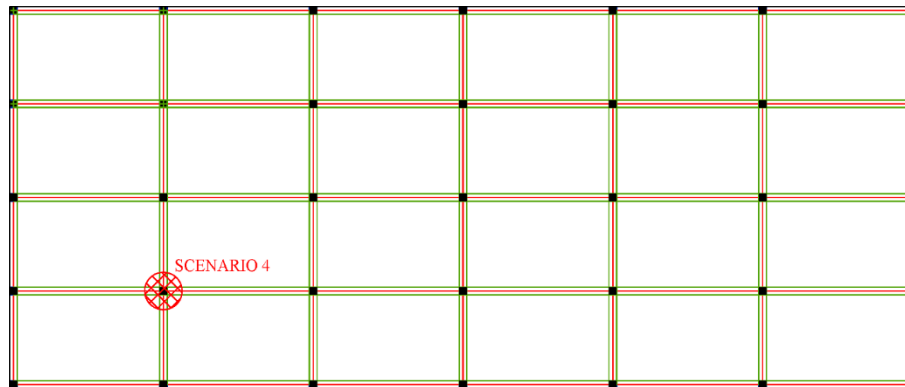


Figure 141: Collapse scenario 4

As mentioned, the column removal was simulated by imposing a vertical linearly increasing displacement of the node placed in correspondence of the top of the column removed.

6.5.1 Collapse scenario 4 – Floor system: slab

Figure 142a shows the trend of the vertical reaction measured in correspondence of the column removed, for increasing vertical displacements. For zero vertical displacement it can be observed a positive vertical reaction of about +530 kN which represents the axial force acting on the column before its removal. By progressively increasing the vertical displacement, the reaction decreases progressively until it reaches a zero value, this condition identifies the vertical displacement which unloads the column and is reached for vertical displacement of about 3.4 cm.

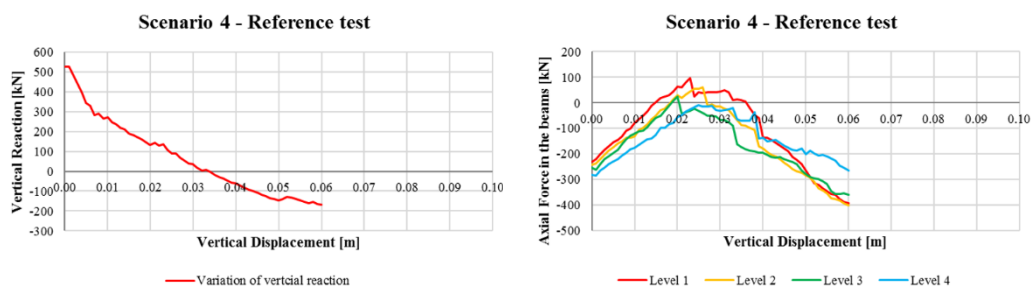


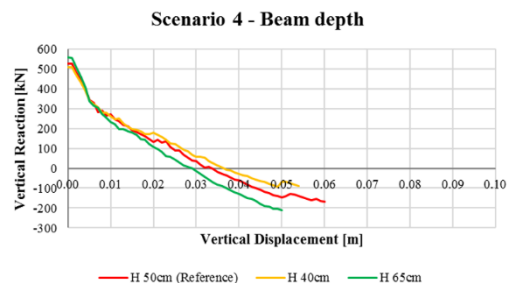
Figure 142: Collapse scenario 4 - Reference test

Further increasing the displacement, the ultimate condition is reached for a vertical displacement of about 6.0 cm, in correspondence of this displacement the vertical reaction is equal to about -175 kN.

It can be noted that at the beginning of the analysis all the beams are subjected to a negative axial force ranging from -225 kN to -280 kN, increasing the applied displacement the compression decreases progressively in all the elements. However, while the axial force of beams of levels 1 and 2 switches to tension, for imposed vertical displacement of the column between 1.5 ÷ 3.5 cm, reaching a peak value of about +100 kN, beams of level 3 and 4 remain in compression. By proceeding with the test all the beams return to compression, reaching a maximum value of -400 kN at the end of the analysis, except for beams of level 4 that reach an ultimate value of -260 kN.

By comparing the curves reported in Figure 143a it can be noted that beams with great depth give better results in ultimate conditions than the standard test or the one with the highest span/depth ratio. In fact, although with this solution is reached a maximum displacement of 3 cm against the values of 6 cm reached in the reference test, the vertical reaction recorded in ultimate condition is the highest if compared with the others, respectively -200 kN versus -175 kN for standard beams and -100 kN for beams with a depth of 40 cm.

By analysing the trend of the axial force in the beams it can be noted that the solution with H 40 cm beams shows a response close to the standard one, while with the solution with H 65 cm beams the elements remain in compression for all the analysis, reaching a maximum value of about -650 kN. No appreciable differences of behaviour can be highlighted between the beams of the different levels.



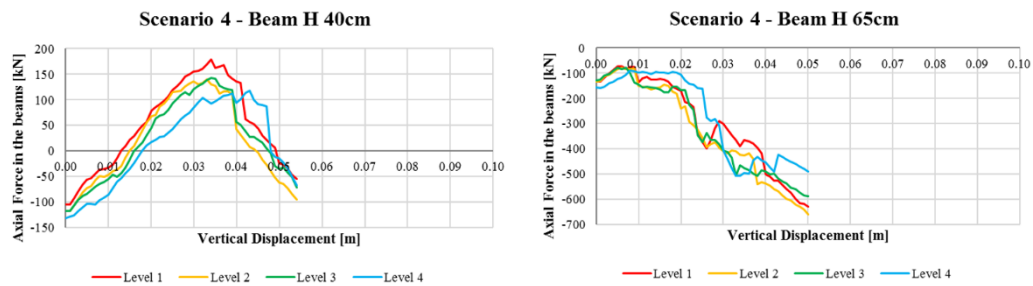


Figure 143: Collapse scenario 4 - Influence of primary beams depth

Figure 144a shows the influence of a different column depth on the variation of vertical reaction, Figure 144b shows the trend of the axial force for H 60 cm columns solution.

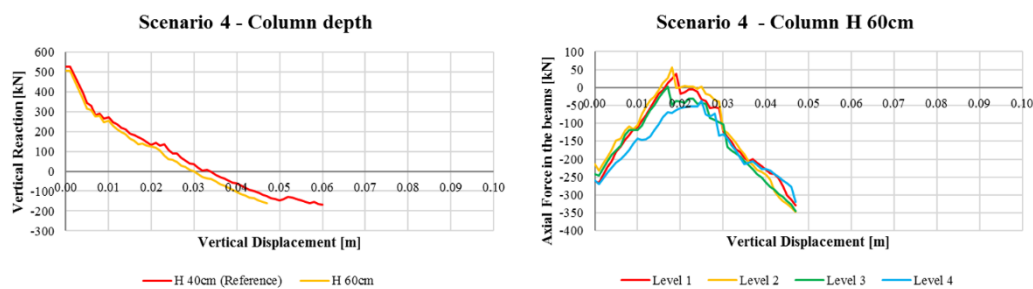


Figure 144: Collapse scenario 4 - Influence of columns depth

By comparing the curves reported in Figure 145a it can be noted that stiffer columns give the same results in terms of vertical reaction. In terms of ultimate displacement instead, the alternative solution gives worse results 4.7 cm against 6 cm.

About the trend of the axial force, it can be noted a similar response to the reference one.

Figure 145a shows the influence of different bracing systems on the variation of vertical reaction, Figure 145b, 145c and 145d show the trend of the axial force in the beams for all the solutions.

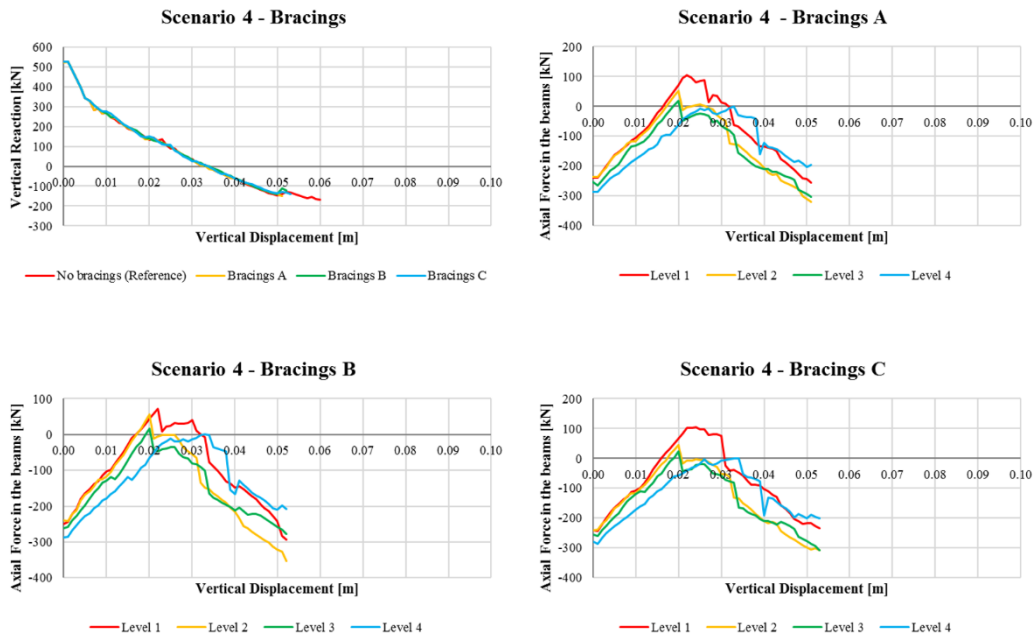


Figure 145: Collapse scenario 4 - Influence of bracing systems

By comparing the curves reported in Figure 145a it can be noted that all bracing systems shown a similar response from a qualitative point of view to the reference one. Table 23 summarises the results obtained for scenario 4. In red are highlighted the cases in which the structure was not able to withstand the column removal.

Table 23: Collapse scenario 4 (Slab) – Summary of the results

Floor System	Scenario	Parameter tested	VR_i [kN]	$\delta(VR_0)$ [cm]	VR_u [kN]	$\delta(VR_u)$ [cm]	
Floor System - Slab	4	Primary Beam depth	H=50cm (L/16) (RT)	509	-3.6	-90	-5.4
			H=40cm (L/20)	558	-2.9	-209	-5
			H=65cm (L/12)	524	-3.4	-170	-6
		Column depth	H=40cm (RT)	504	-3	-161	-4.7
			H=60cm	524	-3.4	-170	-6
			No Bracing (RT)	523	-3.3	-149	-5.1
		Bracing system	A	524	-3.4	-120	-5.2
			B	24	-3.4	-138	-5.3
			C	160	-	52	-2.4

(RT) = Reference Test; VR_i = Initial Vertical Reaction; $\delta(VR_0)$ = Vertical Displacement for Vertical Reaction = 0; VR_u = Ultimate Vertical Reaction; $\delta(VR_u)$ = Vertical Displacement for Ultimate Vertical Reaction.

6.5.2 Collapse scenario 4 – Floor system: joists with collaborating slab

Figure 146a shows the trend of the vertical reaction measured in correspondence of the column removed, for increasing vertical displacements. For zero displacement it can be observed a positive vertical reaction of about +425 kN which represents the axial force acting on the column before its removal. By progressively increasing the vertical displacement, it is noted that the reaction decreases but, unlike the previous cases, the analysis is stopped before the reaction reaches the 0 value. This means that in this scenario the structure does not have sufficient strength resources to withstand the column removal with collapsing.

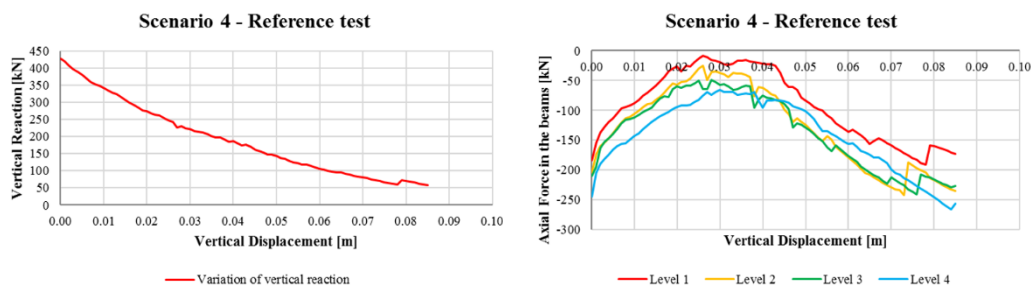
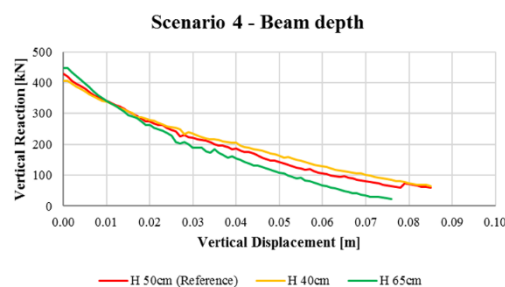


Figure 146: Collapse scenario 4 - Reference test

Figure 146b shows, the trend of the axial force in primary beams. It can be noted that the beams remain in compression for all the test. No appreciable differences of behaviour can be highlighted between the beams of the different levels.

Figure 147a shows the influence of beam depth on the variation of vertical reaction, Figure 147b and 147c show the trend of the axial force in the beams for both the solutions.



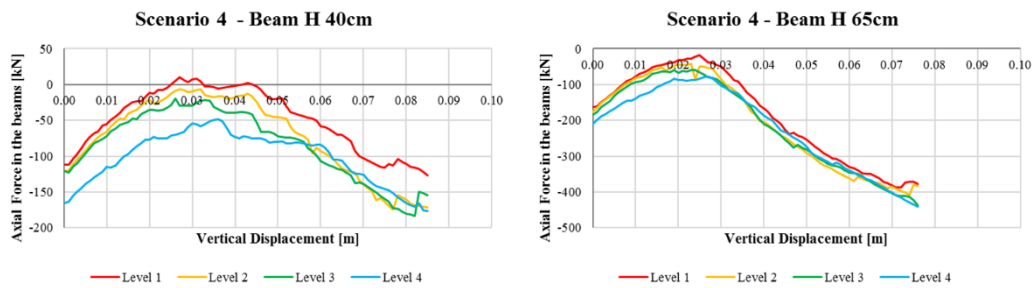


Figure 147: Collapse scenario 4 - Influence of primary beams depth

By comparing the curves reported in Figure 147a it can be noted that, although the H 65 cm beams solution gives slightly better results, no solution allows the structure to withstand the column removal.

About the trend of the axial force in the beams, it can be noted that both the solutions shown a response similar to the reference one.

Figure 148a shows the influence of a different column depth on the variation of vertical reaction, Figure 148b shows the trend of the axial force for H 60 cm columns solution.

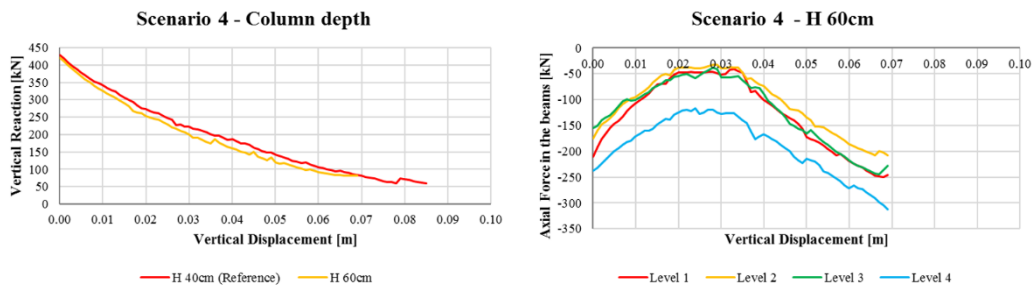


Figure 148: Collapse scenario 4 - Influence of columns depth

By comparing the curves reported in Figure 149a it can be noted that even by using stiffer columns the structure can withstand the column removal. Also in this case, the trend of the axial force is similar to the reference one.

Figure 149a shows the influence of different bracing systems on the variation of vertical reaction, Figure 149b, 149c and 149d show the trend of the axial force in the beams for all the solutions.

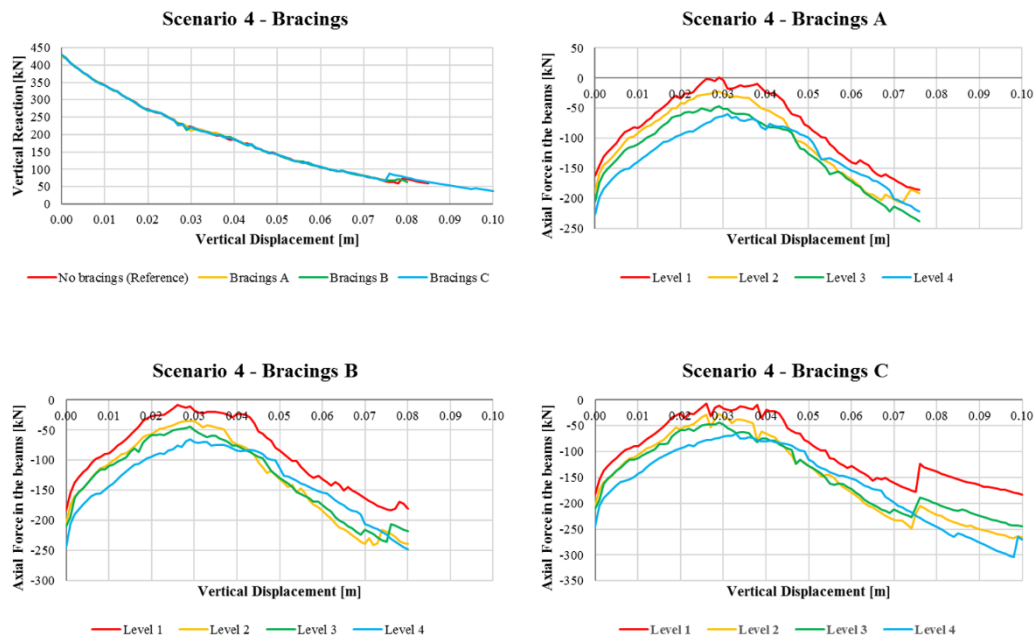
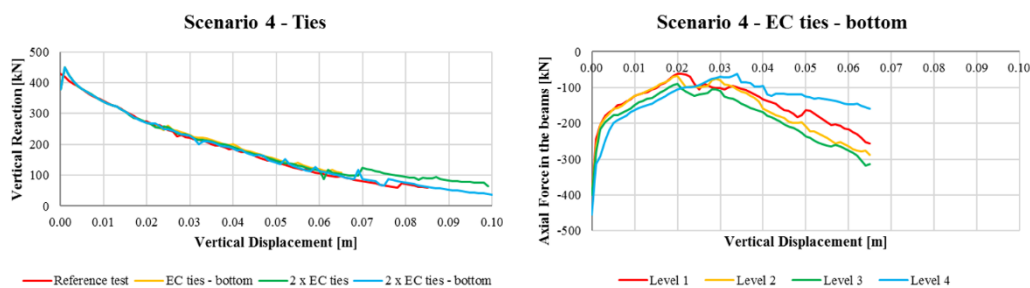


Figure 149: Collapse scenario 4 - Influence of bracing systems

By comparing the curves reported in Figure 149a it can be noted that although bracing system C allows to reach larger vertical displacements, under any circumstances the structure is able to withstand the column removal. Thus, the presence of bracing system seems to play a marginal role.

Figure 150a shows the response, in terms of variation of vertical reaction, obtainable by considering a limited amount of continuous reinforcement (compared with the reference test) but in line with Eurocodes provisions. Figure 150b, 150c and 150d show the trend of the axial force in the beams for all the solutions.



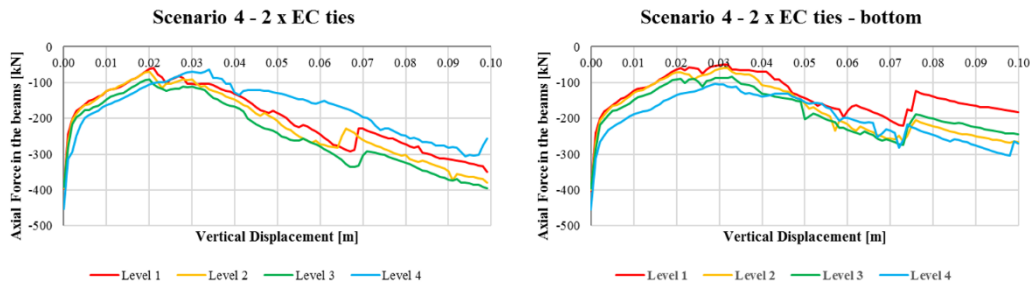
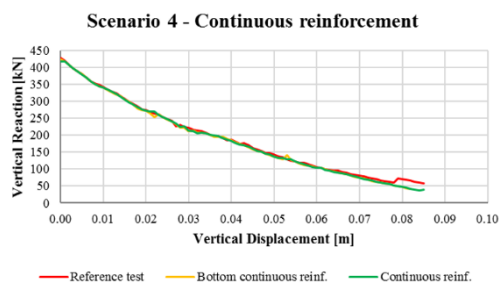


Figure 150: Collapse scenario 4 - Influence of minimum tying

By comparing the curves reported in Figure 150a it can be noted that by providing the minimum amount of continuous reinforcement defined by Eurocodes, the structure is not able to withstand the element removal. Comparable results were also achieved with the previous solutions, determining the inadequacy of the measures adopted up to now. The response does not improve even by doubling the minimum tying. In fact, although doubling the reinforcement it is possible to apply a greater displacement, the ultimate vertical reaction is the same achieved with the reference test. Figure 150c does not show significant changes in beam response compared to the reference test. The trends shown in Figure 150b and 150d cannot be considered significant.

Figure 151a shows the influence of continuous reinforcement on the variation of vertical reaction, Figure 151b and 151c show the trend of the axial force in the beams for both the solutions.



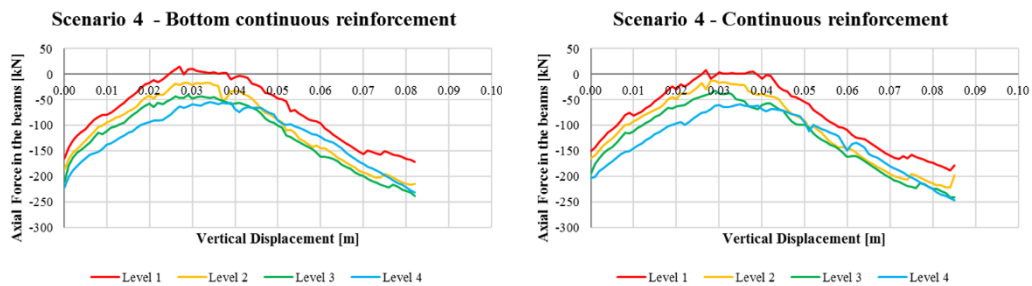


Figure 151: Collapse scenario 4 - Influence of continuous reinforcement

By comparing the curves reported in Figure 151a it can be noted that even the use of continuous reinforcement in the beams is not sufficient to improve the structural response. These results indicate therefore that to ensure an improvement in terms of robustness is necessary to adopt complementary measures to the beam reinforcement increasing. Figure 151b and c do not highlight significant changes in behaviour compared to the reference test.

Figure 152a shows the influence of seismic detailing on the variation of vertical reaction, Figure 152b shows the trend of the axial force of model designed to withstand the seismic action.

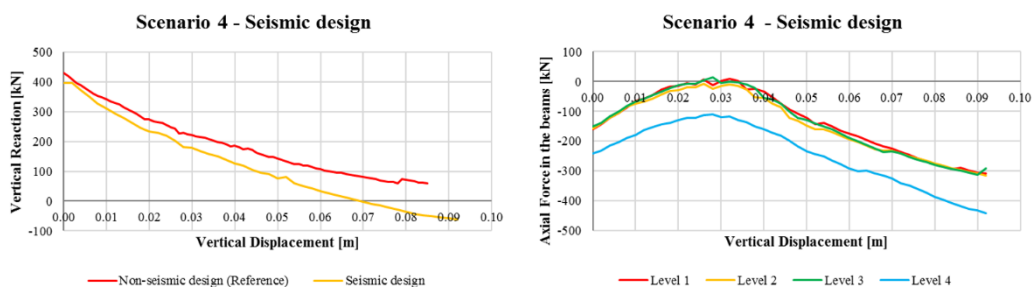


Figure 152: Collapse scenario 4 - Influences of seismic detailing

By comparing the curves reported in Figure 152a it must be highlighted that seismic detailing produces a crucial improvement in terms of ultimate vertical reaction. It can be noted that unlike the measures test up to now, seismic design allows the structure to withstand the column removal, even though with limited resisting resources, reaching an ultimate reaction of about -50 kN. Therefore, seismic design greatly influences the overall structure response. Figure 152b instead does not show significative changes respect to the reference test. Table 24

summarises the results obtained for scenario 4. Any cases in which the structure was not able to resist the removal of the column are highlighted in red.

Table 24: Collapse scenario 4 (Joists + Collaborating slab) – Summary of the results

Floor System	Scenario	Parameter tested	VR _i [kN]	δ(VR ₀) [cm]	VR _u [kN]	δ(VR _u) [cm]	
Floor System - Joists + collaborating slab	4	Primary Beam depth	H=50cm (L/16) (RT)	428	-	59	-8.5
			H=40cm (L/20)	405	-	65	-8.5
			H=65cm (L/12)	447	-	23	-7.6
		Column depth	H=40cm (RT)	428	-	59	-8.5
			H=60cm	421	-	82	-6.9
		Bracing system	No Bracing (RT)	428	-	59	-8.5
			A	423	-	67	-7.6
			B	428	-	64	-8.0
			C	428	-	38	-10.0
		Tyings	No Min EC (RT)	428	-	59	-8.5
			Min EC Bottom	378	-	108	-6.5
			2·Min EC Top&Bot	378	-	65	-9.9
			2·Min EC Bottom	378	-	80	-7.3
		Continuous Reinforcements	RT	428	-	59	-8.5
			Bottom	424	-	42	-8.2
			Top&Bottom	418	-	40	-8.5
		Detailing	Standard (RT)	428	-	59	-8.5
			Seismic	397	-3.5	-61	-4.6

(RT) = Reference Test; VR_i = Initial Vertical Reaction; δ(VR₀) = Vertical Displacement for Vertical Reaction = 0; VR_u = Ultimate Vertical Reaction; δ(VR_u) = Vertical Displacement for Ultimate Vertical Reaction.

Chapter 7

Conclusions and Recommendations for Future Works

7.1 Introduction

The main aim of this work was to develop simplified FE models to investigate the post-collapse behaviour of cast in situ reinforced concrete frames following a column removal due to abnormal loading conditions. This was done by defining numerical models and a parametric investigation to analyse the overall structural behaviour and the efficiency of current provisions, prescribed by main structural codes and recognised by the scientific community.

The study of structural robustness and of the mechanisms that govern it is a vast subject whose complexity makes it necessary to develop numerical analysis techniques as a tool to support and to complete the experimental campaigns. Currently, several laboratory tests are being developed with the aim of increasing the degree of knowledge on the structural behaviour following collapse scenarios involving the removal of a main bearing element.

These studies have highlighted a close relation between the structural response and the design criteria adopted, which in turn depends by the building features (i.e. span length, dead loads, live loads, beam and column depth, floor system typology, etc...).

Currently, most experimental studies concern isolated structural portions (i.e. beam-column assemblies, beam-column-slab assemblies) and especially two-dimensional frames. However, they have shown the considerable increase in resistance capacity achievable by considering the 3D structural behaviour and the slab contribution.

The main conclusions were reported in the following paragraphs, each covering distinct aspects and purposes of the study.

7.2 Finite element software validation and calibration

This procedure was necessary in the preliminary stages to choose the software to be used, the types of analysis to be developed, to optimize the definition of the models and to identify any critical issues inherent the work.

The main aim in this stage was to assess the reliability of commercial nonlinear finite element codes in the evaluation of the structural response after an element removal.

The initial simulations concerned simple structures (i.e. 2D frames, or scaled slab-beam-column assemblies), whose behaviour was previously studied through specific experimental investigations. The analyses were nonlinear, both static and dynamic.

Nonlinearity is a fundamental aspect to consider the evolutionary behaviour of the structural response, above all considering the extent of the displacements and deformations caused by the element removal that overcome the load-bearing capacity associated with a purely flexural mechanism and activate the catenary action.

The choice to simulate the removals both statically that dynamically was determined by the dependence of the structural response on the element removal mode (e.g. dynamic amplification factor, reinforced concrete response under dynamic conditions, etc...).

In actual conditions, the element removal assume characteristics closer to a static one rather than a dynamic one, or vice versa, depending on the cause that led to its collapse. As an example, in case of a collision or an explosion it is likely that the localised collapse occurs quickly and therefore with not negligible dynamic effects, while if the collapse is caused by a progressive deterioration of the element properties, as could happen in case of fire, a quasi-static removal probably better simulates the actual failure mode.

Simulations concerned both 2D frames subjected to static and dynamic column removal, and slab-beams assemblies subjected to static removal. In all cases the tested software correctly reproduced the experiments, capturing the structural

behaviour evolution and the response improvements achievable by considering 3D frames and the slab contribution. Furthermore, they successfully reproduced displacements and ultimate loads. The major uncertainties, as expected, were recorded in the case of dynamic removal tests. However, the software simulated properly the experimental results qualitatively, correctly estimating the order of magnitude of the monitored parameters.

The analysis results highlighted the high degree of correspondence between the experimental investigations and the numerical simulations, thus justifying the use of this analysis tool. The FE models accurately reproduced both the ultimate loads that the corresponding displacements reached during the experimental tests, capturing the markedly nonlinear evolution, both qualitatively that quantitatively. In this phase, the fundamental and certainly not negligible contribution offered by the decks was also highlighted.

Several software were tested, in order to define different modelling levels to evaluate the sensitivity of these tools and to identify the optimal solution for future analyses.

At the end of this phase, considering the results obtained, the pre-processing speed of the input data, the solving times and the ease of extraction and post-processing of the results, it was decided to use the software SeismoStruct.

Regarding this initial phase of the study it can be concluded that the objectives set have been reached, this has allowed to proceed with the second stage of the work.

7.3 Simplified numerical models to consider slab contribution

The studies cited as a reference highlighted the non-negligible contribution offered by the slab contribution on the structural response in the post-removal phase. These findings, confirmed by the numerical simulations, suggested to focus the research on the identification of effective solutions to simplify the floor-system modelling. This was the aim of the second stage of this work.

Generally, the structural analysis of a building does not contemplate the slab modelling, it considers only the planar stiffness contribution, by dimensioning the floor system separately to guarantee the correct transfer of vertical loads to the

beams. This happens because the modelling of the decks would require a large number of finite elements, resulting in an increase of the degrees of freedom of the structure. This means longer analysis times as well as the need to have adequate tools to pre-process the input data and to post-process the results.

To this scope, several solutions were tested, each of them characterized by distinct approximation levels. From this study emerged that, for the typical spans of reinforced concrete structures (4-8 m), it is sufficient to discretise the floor fields into three parts for each direction in which the load-bearing elements work (one direction in case of joists, two directions in case of bidirectional slab), to obtain reliable results both from a quantitative that a qualitative point of view. This led to a considerable reduction of the computational burdens keeping the reliability of the models.

Among the tested solutions there was also one based on the use of linear elastic springs to simulate the slab behaviour. This approach involved to calibrate the springs stiffness to replicate the actual one of the replaced elements. Although this solution showed encouraging results, it was not being further developed because the linearity of the element did not allow the correct reproduction of the actual nonlinear behaviour. A more complex calibration would have been necessary to calibrate nonlinear springs, but this would have led to an excessive increase in modelling times, contrasting with the original purpose of simplification behind this work.

7.4 Simplified numerical models to consider slab contribution

The third part of the work consisted of a parametric study aimed at investigating the influence of different factors on the global response. A reference structure, having common features with most of the reinforced concrete buildings, it was chosen and designed for this scope. In particular, the same structure was designed twice changing the floor system: a bidirectional slab in the first case, unidirectional joists in the second one.

Moreover, about the joists-solution, two distinct design were assumed: in the first case the seismic action was neglected, while in the second case it was developed a response spectrum analysis and the frames were designed to withstand the earthquakes expected, by referring to the design criteria defined by the Eurocodes for anti-seismic structures (i.e. capacity design).

The parametric investigation involved the following parameters: primary beams depth, columns depth, presence of bracing systems, minimum tying amount defined by Eurocodes, presence of continuous reinforcements in the beams, seismic detailing.

After a sensitivity analysis, four distinct scenarios were assumed. Each of these considered that the removed element was located at the ground floor. In particular, the removed elements were: two internal columns, one side column and a corner column.

The analyses developed provided clear indications: by comparing the buildings not directly designed to withstand an earthquake, the best results were obtained by the ones equipped with the slab. The ability to transfer the loads in two directions affects the overall response, providing greater resistance resources than the joist solution (by comparing the reference tests, it was recorded an improvement in the range $+80\% \div +400\%$). Therefore, the latter shown a reduced load-bearing capacity, even if they were able to withstand larger ultimate displacement (improvements in the range $+35\% \div +60\%$).

The attempts to increase the structural stiffness against the horizontal displacements (i.e. by increasing the columns cross section or by applying bracings system) to provide a constraint to support the development of the catenary action produced negligible improvements. Therefore, these measures alone were not sufficient to improve the structural response.

The response was instead improved by using higher beams. Especially with regard to scenarios 2 and 3, it was possible to reach greater ultimate loads if compared with the reference tests (improvements in the range $+50\% \div +80\%$).

Among all the parameters, the most influencing was definitively the seismic detailing. The criteria imposed by the capacity design involve several aspects including the reinforcement amount arranged, the rotational capacity of the beams (i.e. ductility), the nodes confinement and the shear strength of beams and columns. These parameters modify not only the behaviour in case of an earthquake but also the global post-removal response. The anti-seismic buildings have shown to be able to withstand not only greater ultimate displacements (and therefore larger beam rotations), but also higher ultimate loads with respect to the same structures without seismic details. It was recorded an improvement in the range $+140\% \div +220\%$ in

terms of ultimate reaction, and between +10% ÷ +55% in terms of ultimate displacement.

The structural behaviour recorded for the scenario 4, about buildings equipped with joists, deserves specific mention: it was found that the reference test was not able to withstand the element removal. No other modification among those proposed led to an improvement of the results except the seismic design which allowed a clear improvement of the response, allowing the structure to resist local damage without collapsing.

A further consideration concerns the minimum continuous reinforcements currently defined by the Eurocodes to ensure a correct structural response. All tests performed according to the European standard indications failed, revealing that these measures were not sufficient to guarantee a proper post-removal behaviour.

Finally, it must be emphasised that excluding modest tensile stresses recorded in the beams during the analyses, there was not a clear development of the catenary action. In most cases, in fact, the structure reached the ultimate conditions when the vertical displacements were rather modest, and the bearing mechanism was still flexural. These results contrast with what the ones found during the experimental tests in which the ultimate displacements reached larger values (up to twice the main beam depth) and the load-bearing mechanism evolved from a flexural one to catenary action. These results can be justified by the influence that the initial structural design has on the post-removal response. Especially, the design of those factors crucial in determining the ductility of the beams and their ability to transfer tensile stresses (i.e. nodes confinement by means of stirrups and continuous reinforcement amounts in the beams, especially the lower one).

7.5 Recommendations for future works

The results achieved can be helpful to design structures able to withstand a column removal without exhibiting a disproportionate collapse. However, as also confirmed by other studies, there is not a clear understanding about post-collapse behaviour and the mechanism of development of catenary action. Therefore, research in this area still has to take important steps.

In the experimental field it should be set up investigative campaigns to create a solid basis for future studies and to extend it also to other structural typologies. In

this sense, the influence of non-structural elements on the overall response, such as the infills, should also be assessed.

Similar remarks can be done also for FE studies which proved to be fundamental for highlighting critical issues in structural behaviour and to identify structural typologies less sensitive to the problem and targeted solutions to improve the response case-by-case.

A future advancement certainly concerns the development of techniques allowing to study only limited structural portions, to reduce the analysis and modelling times.

Finally new measures, complementary and/or alternative to those already present in the main structural codes, must be defined to guarantee an appropriate structural response with regard to structural robustness.

References

- Bunton, D. (2002). Generic moves in PhD thesis introductions. In J. Flowerdew, *Academic discourse* (p. 57-75). London: Pearson Education Limited.
- Kwan, B. S. (2009). Reading in preparation for writing a PhD thesis: Case studies of experiences. *Journal of English for Academic Purposes*, pages 180-191.
- American Concrete Institute (ACI) (2002). Building code requirements for structural concrete and commentary. ACI 318-02 and ACI 318R-02, Farmington Hills, MI.
- American Society of Civil Engineers (ASCE) (2002). Minimum design loads for buildings and other structures. SEI/ASCE 7-02, Reston, VA.
- Bao Y., Main, J. A., and Noh S. Y. (2017). Evaluation of Structural Robustness against Column Loss: Methodology and Application to RC Frame Buildings. *Journal of Structural Engineering*, ASCE, American Society of Civil Engineers, 143(8).
- Bertagnoli, G., Giordano, L., La Mazza, D. and Mancini, G. (2016). Use of different numerical models to evaluate the robustness of reinforced concrete frame structures. *Proceedings of World Multidisciplinary Civil Engineering-Architecture-Urban Planning Symposium 2016* (WMCAUS, Prague 13-17 June 2016). In *Procedia Engineering*, 161(2016), pp. 1013-1017.
- Bertagnoli, G., Gino, D., Giordano, L., La Mazza, D. and Mancini, G. (2016). Robustness of reinforced concrete framed buildings: A comparison between different numerical models. *Proceedings of ITALIAN CONCRETE DAYS - Giornate AICAP 2016* (CTE Congress, Rome 27-28 October 2016), pp. 1-8.

-
- British Standard BS 8110-11. (1997). The structural use of concrete in building - Part 1: Code of practice for design and construction. London, U.K.
- Canisius, T. D. G., Baker, J., Diamantidis, D., Ellingwood, B., Faber, M., Holicky, M., Markova, J., Maitra, A., Narasimhan, H., Sørensen, J. D., Vogel T., and Vrouwenvelder A. (2011). Structural robustness design for practicing engineers. Proceedings of COST Action TU0601: Robustness of structures.
- Chang, G. A., and Mander, J.B. (1994). Seismic energy based fatigue damage analysis of bridge columns: Part 1 - Evaluation of seismic capacity, NCEER Technical Report No. NCEER-94-0006. State University of New York, Buffalo, New York.
- Comité Européen du Béton (CEB) (1993). CEB-FIP model code 1990. CEB, Lausanne, Switzerland.
- Computers and Structures, Inc. (CSI) (2016). Sap2000 v18.2.0, Walnut Creek, California, U.S.A.
- Correia, A. A., and Virtuoso, F. B. E. (2006). Nonlinear Analysis of Space Frames, *Proceedings of the Third European Conference on Computational Mechanics: Solids, Structures and Coupled Problems in Engineering*, Mota Soares et al. (Eds.), Lisbon, Portugal.
- Department of Defense (DoD) Unified Facilities Criteria (UFC-04-023-03) (2005). Design Building to Resist Progressive Collapse. Washington, D.C.
- Department of Defense (DoD) Unified Facilities Criteria (UFC-04-023-03) (2013). Design Building to Resist Progressive Collapse. Washington, D.C.
- DIANA (2008). Finite element analysis. Release 9.3. TNO Building and Construction Research, Delft, Netherlands.
- DIANA (2016). Finite element analysis. Release 10.1. TNO Building and Construction Research, Delft, Netherlands.
- Ellingwood, B. R, Smilowit R, Donald O. D, Duthinh D, Nicholas J. C. (2007). Best Practices for Reducing the Potential for Progressive Collapse in Buildings. U.S. Department of Commerce, Technology Administration, National Institute of Standards and Technology.

-
- European Committee for Standardisation (CEN) (2002). EN 1990. Eurocode 0 - Basis of structural design. CEN, European Standard, Brussels, Belgium.
- European Committee for Standardisation (CEN) (2003). EN 1991-1-3:2003. Eurocode 1 - Actions on structures. Part 1-3: General actions – Snow loads. CEN, European Standard, Brussels, Belgium.
- European Committee for Standardisation (CEN) (2004). EN 1992-1-1:2004. Eurocode 2 - Design of concrete structures - Part 1-1: General rules and rules for buildings. CEN, European Standard, Brussels, Belgium.
- European Committee for Standardisation (CEN) (2005). EN 1991-1-4:2005. Eurocode 1 - Actions on structures. Part 1-4: General actions – Wind actions. CEN, European Standard, Brussels, Belgium.
- European Committee for Standardisation (CEN) (2005b). EN 1998-1:2005 - Eurocode 8 - Design of structures for earthquake resistance - Part 1: General rules, seismic actions and rules for buildings. CEN, European Standard, Brussels, Belgium.
- European Committee for Standardisation (CEN) (2006). EN 1991-1-7:2006. Eurocode 1 - Actions on structures. Part 1-7: General actions - Accidental actions. CEN, European Standard, Brussels, Belgium.
- GSA, General Service Administration (2003). Progressive collapse analysis and design guidelines for new federal office buildings and major modernization projects. U. S. General Services Administration, Washington, D. C., U.S.A.
- Hallquist, J. (2007). LS-DYNA keyword user's manual. Livermore, CA: Livermore Software Technology Corporation.
- International Code Council (ICC) (2003). International Building Code, Falls Church, VA.
- Izzuddin, B. A., Vlassis, A. G., Elghazouli, A. Y., and Nethercot D. A. (2007). Progressive collapse of multi-storey buildings due to sudden column loss - Part I: Simplified assessment framework. *Engineering Structures*, 30(5):1308-1318.
- La Mazza, D., Giordano, L., Castaldo, P. and Gino, D. (2017). Assessment of the efficiency of seismic design for structural robustness of rc structures.

Ingegneria Sismica – International Journal of Earthquake Engineering, 34(2017): 63-77.

- Lew, H. S., Bao, Y., Sadek, F., Main, J. A., Pujol, S. and Sozen, M. (2011). An Experimental and Computational Study of Reinforced Concrete Assemblies under a Column Removal Scenario, NIST Technical Note - 1720.
- Li, H., and El-Tawil, S. (2011). Three-dimensional effects in progressive collapse modeling. *Proceedings of the Structures Congress 2011*, pp. 2829-2839.
- Li, Y., Lu, Z., Guan, H., and Ye., L. (2014). Progressive collapse resistance demand of reinforced concrete frames under catenary mechanism. *ACI Structural Journal*, 111: 433-439.
- Longinow, A., and Ellingwood, B. R. (1998). The impact of the Ronan Point collapse—25 years after. *Structural Engineering World Wide*, Paper Reference P312-2, Elsevier Science, New York.
- Mander, J. B., Priestly, M. J. N., and Park, R. (1988). Theoretical stress-strain model for confined concrete. *Journal of Structural Engineering*, ASCE, 114(8): 1804-1826.
- Meacham, B. J. and Matthew, A. J. (2006). Extreme Event Mitigation. In *Building: Analysis and Design*. National Fire Protection Association, p. 559.
- Merola, R. (2009). Ductility and Robustness of Concrete Structures under Accident and Malicious Load Cases. PhD Thesis. School of Civil Engineering, University of Birmingham, U.K.
- Ned, M. (2008). Structural Integrity and Progressive Collapse in Large-Panel Concrete Structural system. *PCI Journal*, July- August-pp. 55-61.
- Neuenhofer, A., and Filippou, F. C. (1997). Evaluation of nonlinear frame finite-element models, *Journal of Structural Engineering*, 123(7): 958-966.
- Nurhuda, I., and Lie, H. A. (2004). Three dimensionally analysis of flat plate structures by equivalent grid method. In *29th Conference on our world in concrete and structures*, 25-26 August 2004, Singapore.

-
- Pearson, C., and Delatte, N. (2005). Ronan point apartment tower collapse and its effect on building codes. *Journal of Performance of Constructed Facilities*, ASCE: 19(5):172–7.
- Petrone, F., Shan, L., and Kunnath S. K. (2016). Modeling of RC Frame Buildings for Progressive Collapse Analysis. *International Journal of Concrete Structures and Materials*, 10(1): 1-13.
- Pham, A. T., and Tan, K. H. (2017). Experimental study on dynamic responses of reinforced concrete frames under sudden column removal applying concentrated loading, *Engineering Structures* 139: 31-45.
- Pillai, U. S., Menon, D. (2005). Reinforced concrete design – second edition. Tata McGraw-Hill Publishing Company Limited, New Delhi, India.
- Portland Cement Association (PCA) (1975). Loading Conditions. Design and Construction of Large-Panel Concrete Structures, report 1.
- Qian K., Li, B., and Ma, J. X. (2014). Load-carrying mechanism to resist progressive collapse of RC buildings. *Journal of Structural Engineering*, ASCE, American Society of Civil Engineers, 141(2).
- Qian, K., Bing, L., and Zhang, Z. W. (2015). Testing and simulation of 3D effects on progressive collapse resistance of RC buildings. *Magazine of Concrete Research*, ICE Publishing 67(4): 163-178.
- Sasani, M., Kazemi, A., Sagioglu, S., and Forest, S. (2011). Progressive collapse resistance of an actual 11-story structure subjected to severe initial damage. *Journal of Structural Engineering*, ASCE, 137(9): 893-902.
- Saunders, O., Griffiths, H., Griffiths, B., and Pugsley, A. Bunton, D. (2002). Generic moves in PhD thesis introductions. In J. Flowerdew, *Academic discourse* (p. 57-75). London: Pearson Education Limited.
- Kwan, B. S. (2009). Reading in preparation for writing a PhD thesis: Case studies of experiences. *Journal of English for Academic Purposes*, pages 180-191.
- Seismosoft Ltd. (2016). SeismoStruct 2016. Chalkida, Greece.

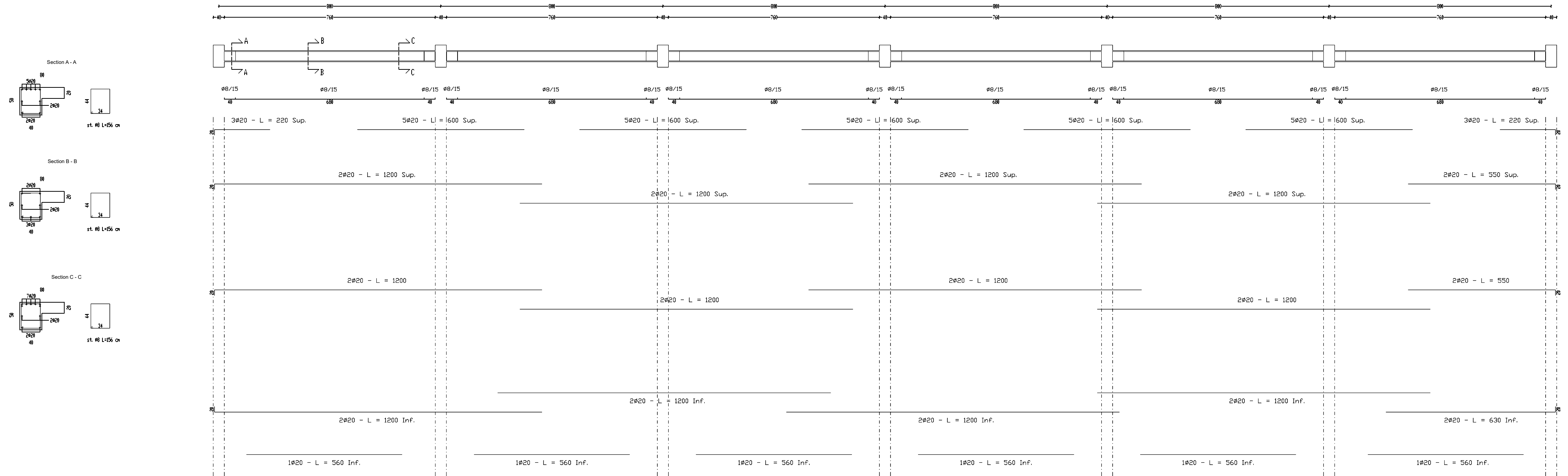
- Selby, R. G., and Vecchio, F. J. (1993). Three-dimensional Constitutive Relations for Reinforced Concrete. Department of Civil Engineering, University of Toronto, Toronto, Ontario, Canada, Publication No. 93-02.
- Spacone, E., Ciampi, V., and Filippou, F. C. (1996). Mixed formulation of nonlinear beam finite element *Computers & Structures*, 58(1): 71-83.
- Starossek, U. (2007). Typology of Progressive Collapse. *Engineering Structures* Vol. 29, No. 9, pp. 2302-2307.
- Tian, Y., Chen, J., Said, A., and Zhao, J. (2012). Nonlinear modeling of flat-plate structures using grid beam elements. *Computers and Concrete*, 10(5):489-505.
- Vecchio, F. J., and Collins, M. P. (1986). The modified compression field theory for reinforced concrete elements subjected to shear. *ACI Journal* 83(22):219-231.
- Way, A. G. J. (2011). Structural robustness of steel framed buildings. SCI, Silwood Park, Ascot, Berkshire, U. K.
- Yi, W. J., He, Q. F., Xiao, Y., and Kunnath, S. K. (2008). Experimental study on progressive collapse-resistant behavior of reinforced concrete frame structures. *ACI Structural Journal*, 105(4): 433-439.
- Yi, W. J., Zhang, F. Z., and Kunnath, S. K. (2014). Progressive collapse performance of RC flat plate frame structures. *Journal of Structural Engineering*, 140(9)

Appendix A

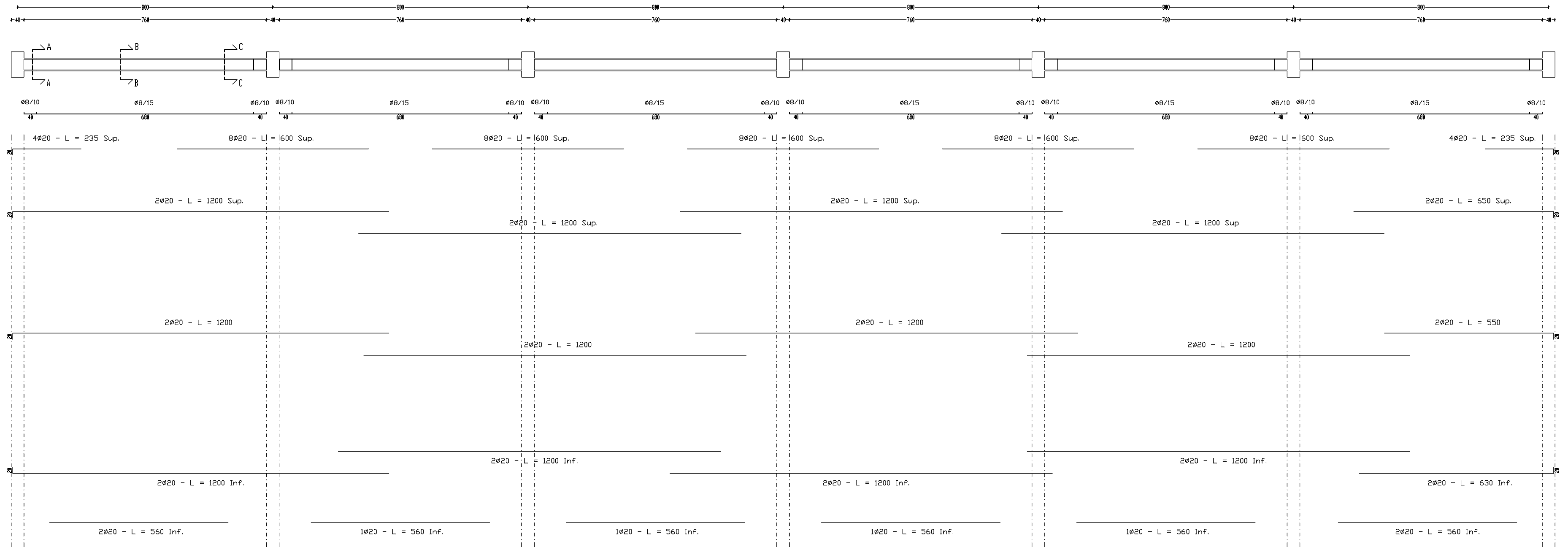
Building with slab

Structural drawing

PRIMARY BEAMS - FRAMES 1,5 Scale 1:100



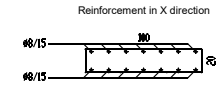
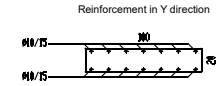
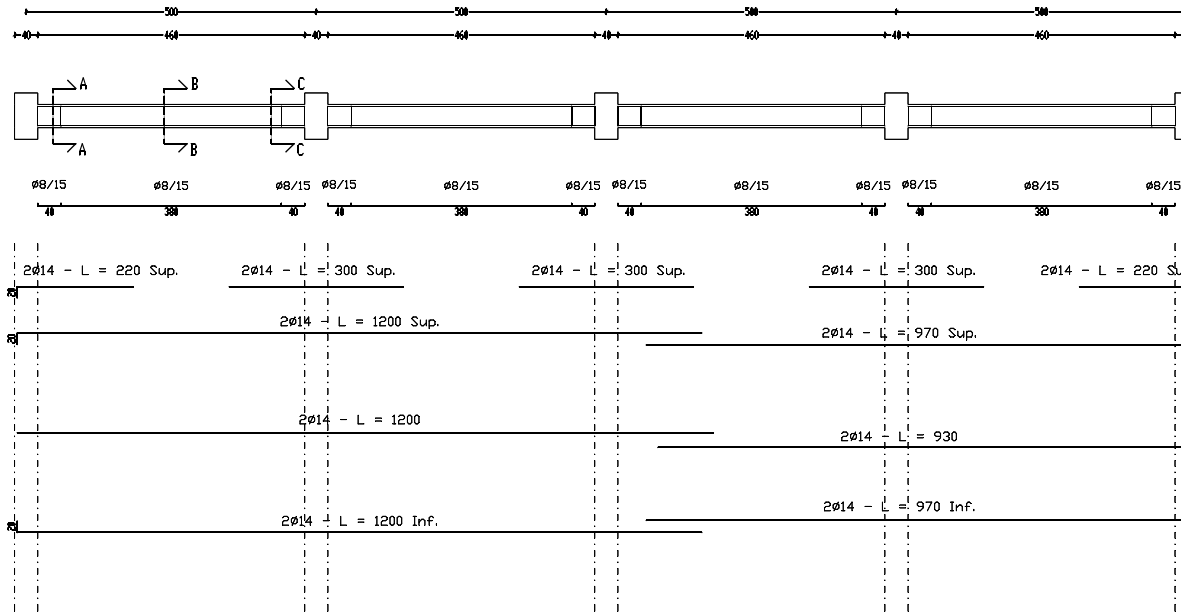
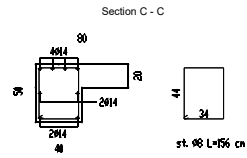
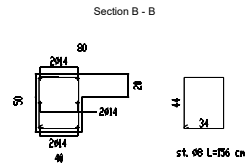
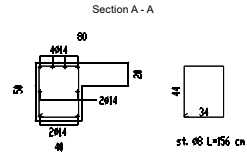
PRIMARY BEAMS - FRAMES 2,3,4 Scale 1:100



SECONDARY BEAMS - FRAMES A,G

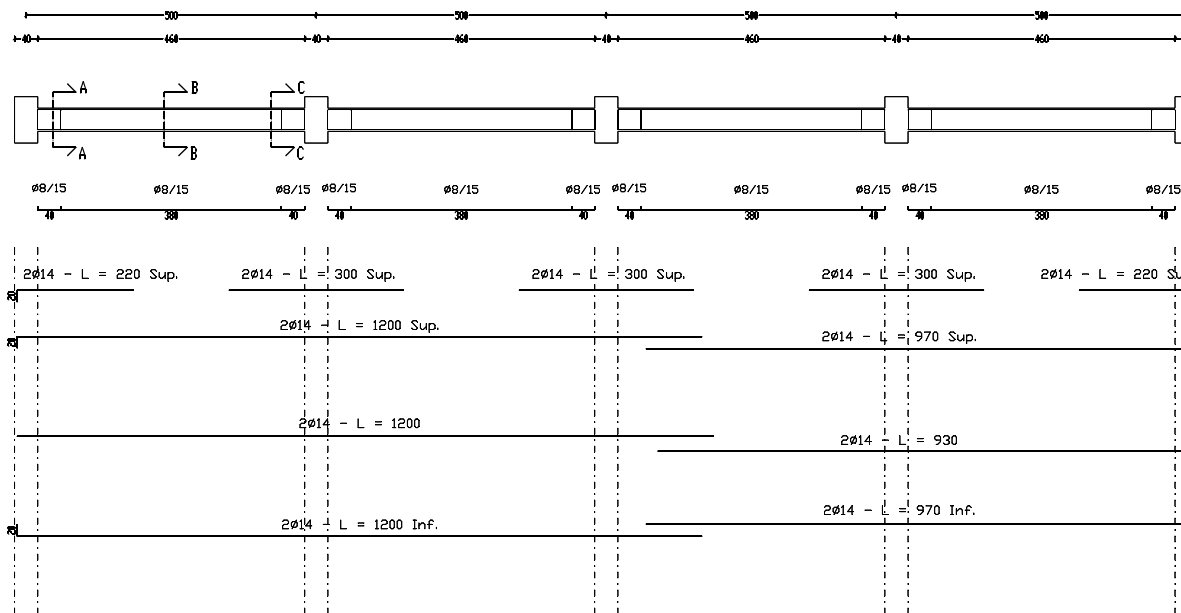
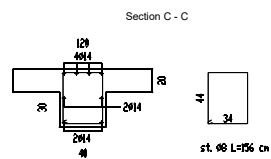
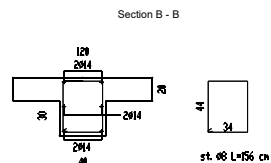
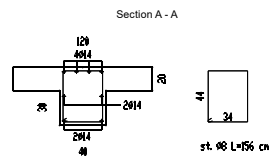
Scale 1:100

SLAB Scale 1:100



SECONDARY BEAMS - FRAMES B,C,D,E,F

Scale 1:100



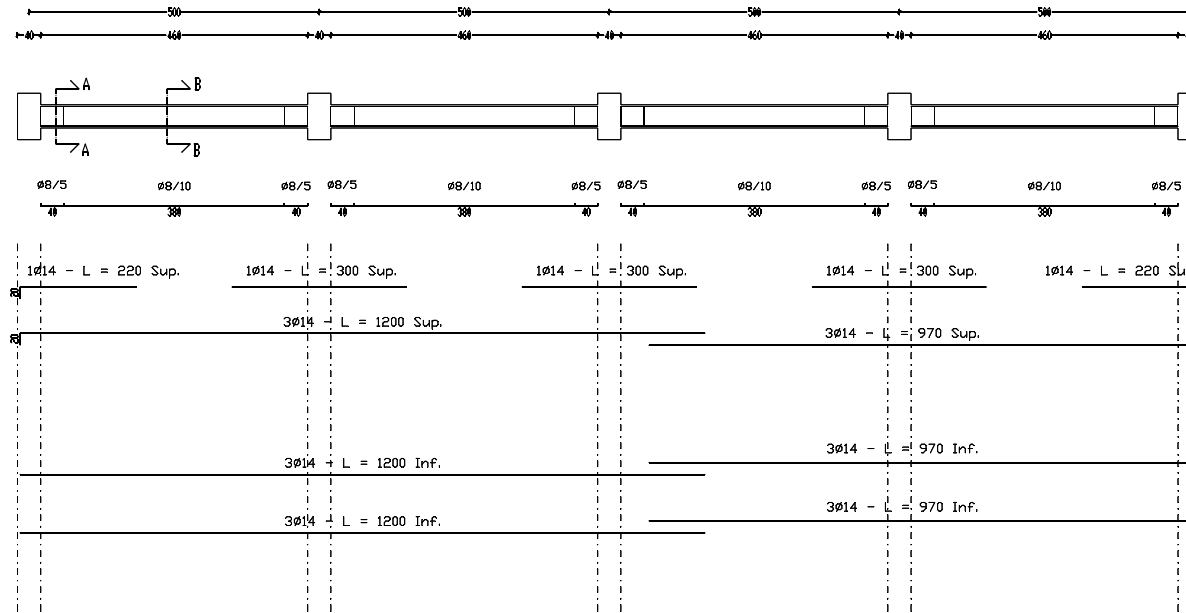
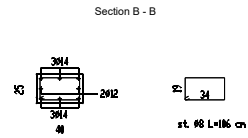
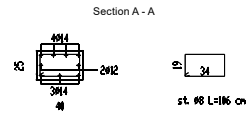
Appendix B

Building with joists

Structural drawings

SECONDARY BEAMS - FRAMES A,G

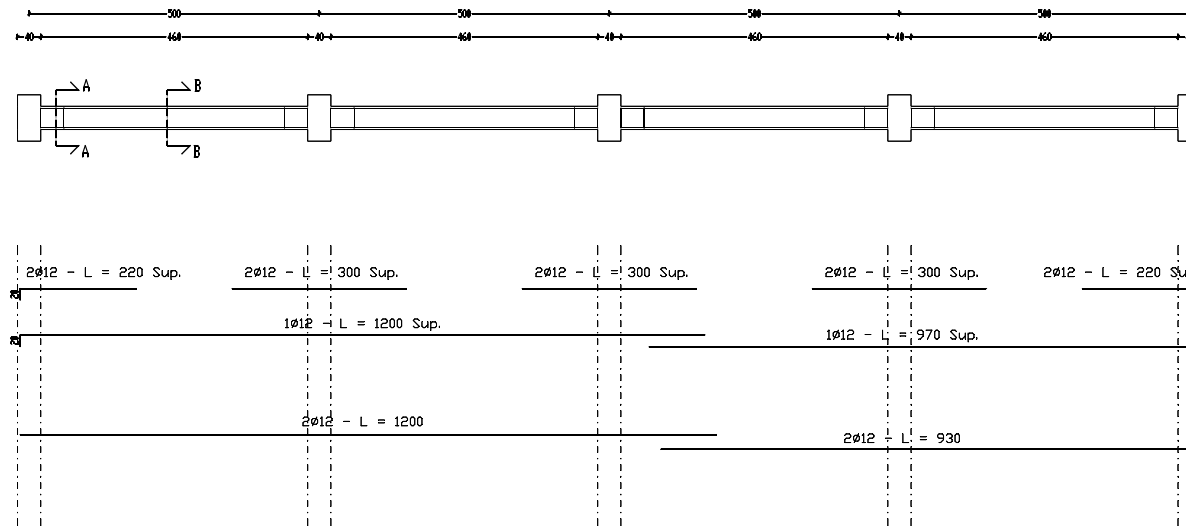
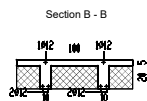
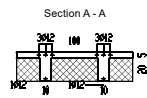
Scale 1:100



JOISTS Scale 1:100

SECONDARY BEAMS - FRAMES B,C,D,E,F

Scale 1:100

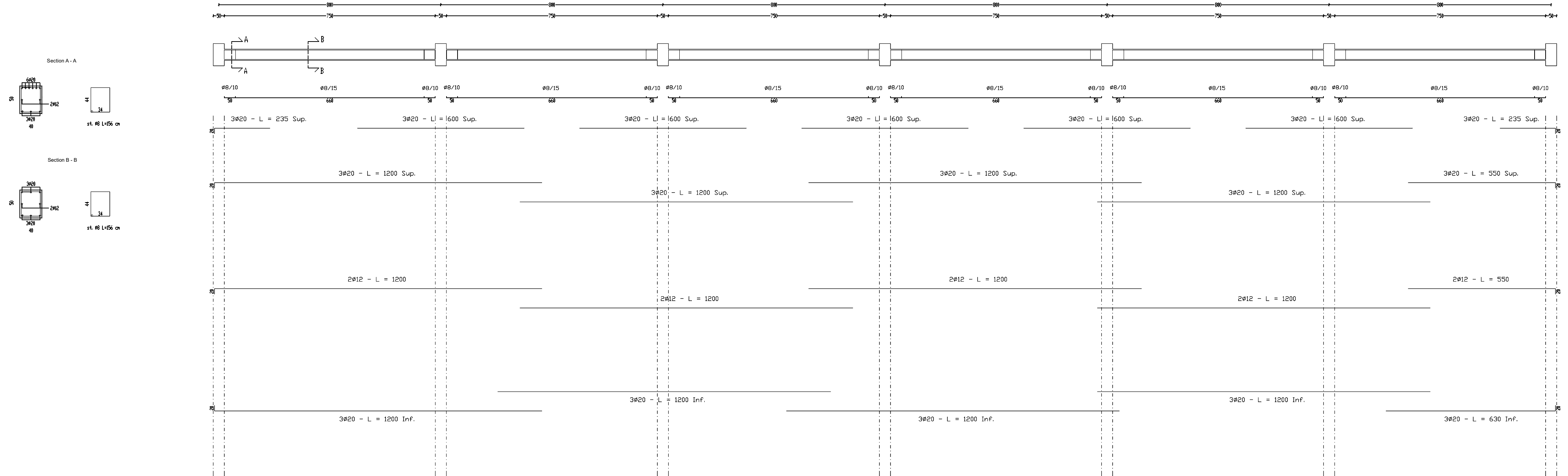


Appendix C

Building with joists in seismic zone

Structural drawings

PRIMARY BEAMS - FRAMES 1,5 Scale 1:100



PRIMARY BEAMS - FRAMES 2,3,4 Scale 1:100

